Modified Biopolymer Sorbents for the Uptake of Naphthenic Acid Fraction Components (NAFCs) from Aqueous Solutions

A Thesis Submitted to the College of

Graduate and Postdoctoral Studies and Research

In Partial Fulfillment of the Requirements

For the Degree of Doctor of Philosophy

In the Department of Chemistry

University of Saskatchewan

Saskatoon

By

Inimfon Abner Udoetok

Permission to Use

In presenting this thesis in partial fulfillment of the requirements for a Postgraduate degree from the University of Saskatchewan, I agree that the Libraries of this University may make it freely available for inspection. I further agree that permission for copying of this thesis in any manner, in whole or in part, for scholarly purposes may be granted by Professor L. D. Wilson and Dr. J. V. Headley who supervised my thesis work or, in their absence, by the Head of the Department or the Dean of the College in which my thesis work was done. It is understood that any copying or publication or use of this thesis or part thereof for financial gain shall not be allowed without my written permission. It is also understood that due recognition shall be given to me and to the University of Saskatchewan in any scholarly use which may be made of any material in my thesis. Requests for permission to copy or to make other use of material in this thesis in whole or part should be addressed to:

Head of Department of Chemistry

University of Saskatchewan

Saskatoon, SK (S7N 5C9)

Canada

College of Graduate and Postdoctoral Studies

University of Saskatchewan

Saskatoon, SK (S7N 5C9)

Canada

Acknowledgements

I hereby express my profound gratitude to **GOD ALMIGHTY**, the giver of life and protection, who against all odds kept me alive and provided the strength and inspiration that made the commencement and completion of this PhD study a reality. May glory and honor be to His name alone in Jesus name, Amen!

Special thanks to my supervisors, Drs. Lee Wilson and John Headley, whose encouragement, mentorship and support on an exceptional level provided a serene platform for the achievement of the results reported in this thesis. I also acknowledge the members of my advisory committee: Drs. Joe Boison, Steve Reid, Ed Krol, Alam Shafiq and Jean Duhamel for their constructive criticisms which enhanced the quality of this thesis. My appreciation also goes to Total E & P, Nigeria for initial funding, University of Saskatchewan, Government of Canada for partial support through the Natural Sciences and Engineering Research Council of Canada (Discovery Grant Number: RGPIN 2016-06197), Government of Saskatchewan through the Innovation & Opportunity Scholarship and the Agriculture Development Fund (PROJECT#: 20110162), Chemistry Department of the University of Saskatchewan for the Graduate Teaching Fellowship and Environment and climate change Canada for facilitating the achievement of the various successes recorded during the course of my PhD study.

I am grateful to Drs. Keith Brown, Ken Thoms, Jason Maley, Alexandra Bartole-Scott, Valerie Mackenzie, and Adrian Clark who were also helpful. I acknowledge the contributions of Jonathan Bailey and Kerry Peru through mass spectrometry analyses. I am thankful to previous and current members of the Wilson group; Mohamed Mohamed, Jae Kwon, Abadalla Karoyo, Louis Poon, Leila Dehabadi, Shaguftah Younus, Mohammad Mahaninia, Kong Dexu, Asghar

Dolatkhah, Chen Xue, Savi Bhalkaran, Henry Agbovi and Michael Danquah for being good colleagues.

Worthy of mention here are my parents; Elder Abner Udoetok and Deaconess Elizabeth Udoetok who sacrificially made sure I had the best they could afford, Mother In-law; Alice Afangideh and siblings; Uboko, Ndibekobong, Nkaiso and Ekemini for their understanding and support throughout my educational sojourn from high school to this point. The bible in Proverbs 18: 22 says "*He who finds a wife finds a good thing, and obtains favor from the Lord*" This has been the case concerning my beloved wife and family, I am sincerely indebted to my dear wife and perfect match: Idorenyin Udoetok as well as my kids; UbongAbasi and IfiokAwasi for their show of love, understanding, support, and endurance especially when I had to deny them that early morning cuddling due to leaving for the University before they were awake. May God continue to keep us together in love. I also sincerely appreciate Dr. Michael Udo, Mr. Koko Abia as well as friends in Canada and Nigeria who I cannot mention here for want of space, for their support and prayers throughout the period of my PhD study.

May the good Lord reward your efforts of love abundantly in Jesus name, Amen!

Dedication

This thesis is dedicated to my wife and daughters; Idorenyin, UbongAbasi and IfiokAwasi.

To my parents; Abner Jonathan Udoetok (father) and Elizabeth Abner Udoetok (mother)

To my siblings; Uboko, Ndibekobong, Nkaiso and Ekemini;

To my in-laws; Peter Afangideh of blessed memory (father in-law), Alice Afangideh (mother in-law), Joseph Afangideh (brother in-law), Uduak, Barbara (Uwakmfon), Idara, Mfon and Mary (sisters in-law)

I will forever remain grateful your love and support.

Abstract

The uncontrolled release of contaminants into the aquatic environment relates to industrial activities such as the extraction of bitumen from oil sands. This is a key challenge facing global water security due to reports on the toxicity of naphthenic acid fraction components (NAFCs). The overall objective of my thesis research concerns the development of biopolymer sorbent materials for the removal of NAFCs from aqueous solution. The research is further divided into various sub-themes as follows: *i)* synthesis of cellulose and chitosan based biopolymers through cross-linking reaction, *ii)* modification of cellulose via surface functionalization, *iii)* development of composite materials based on cellulose and chitosan and *iv*) sorption of NAFCs using cellulose and chitosan biopolymers.

In the first theme (chapters 2 - 4), chitosan (CH) and cellulose (C) were cross-linked with glutaraldehyde (GL) and epichlorohydrin (EP), respectively, using variable cross-linker ratios. The effects of sonication on the cross-linking of cellulose with EP/aqueous ammonia was also studied. The polymer structure and physicochemical properties were characterized via Fourier transform infrared (FTIR) and CP-MAS ^{13}C solids NMR spectroscopy, thermogravimetric analysis (TGA), elemental analysis (CHN), nitrogen adsorption, particle size analysis, differential scanning calorimetry (DSC), scanning electron microscopy (SEM), transmission electron microscopy (TEM), swelling studies and a dye-based (*p*-nitrophenol; PNP, and phenolphthalein; phth) sorption method in aqueous solution. The characterization results provided complementary confirmation of the structural modification of the biopolymers as evidenced by the variable morphology and thermal stability of the cross-linked polymers. The adsorption capacity of the cross-linked chitosan and cellulose (**CH-GL**, **C-EP** and **C-EP sonication/heating**) biopolymers with NAFCs and phenolic dyes were greater when compared to the unmodified cellulose and chitosan. Uptake of

adsorbates increased with greater cross-linker feed ratio except for **C-EP** polymers where the polymer with the medium feed ratio exhibited the highest sorption capacity. The **CH-GL** polymers displayed favorable uptake of model naphthenates as the hydrogen deficiency (*z*) decreased; whereas, the opposite trend was observed for the **C-EP** polymers. The molecular selectivity displayed by the **CH-GL** and **C-EP** polymers was due to steric hindrance as well as electrostatic repulsion between the negatively charged adsorbates and the negatively charged surface of the polymers.

In the second theme (Chapter 5), cellulose was modified via cross-linking with EP and/or surface functionalization with glycidyl trimethyl ammonium chloride (GTAC) to form materials that behave like hydrogels. The successful modification of cellulose was confirmed via characterization by CHN analysis, TGA, and FTIR/^{13}C solids NMR spectroscopy, where enhanced thermal stability and sorption capacity were observed for the hydrogels. Equilibrium sorption studies with naphthenates extracted from oil sands process affected water (OSPW) and a model naphthenic acid compound (2-naphthoxy acetic acid; **S6**) revealed that the cross-linked/surface functionalized hydrogel (**C-EP-G**) exhibited greater sorption capacity than the surface functionalized hydrogel. **C-EP-G** had similar binding affinity for the various OSPW naphthenate species in aqueous solution. Kinetic uptake of **S6** at variable temperature, pH and adsorbent dosage showed that an increased temperature and adsorbent dosage favored the sorption process, while pH had negligible effects. Thermodynamic parameters obtained from the kinetic studies revealed that the sorption process was favored by enthalpy-driven electrostatic interactions.

In the third theme (chapters 6 – 7), composite materials containing chitosan and cellulose biopolymers were prepared in order to evaluate the effects of cross-linking with glutaraldehyde and introduction of iron (III) species on the adsorption properties of the composites. The composite

materials were characterized by various techniques: FTIR spectroscopy, CHN, ^{13}C solid state NMR spectroscopy, powder X-ray diffraction (PXRD), TGA, SEM, equilibrium swelling, nitrogen adsorption and inductively coupled plasma-optical emission spectrophotometry (ICP-OES). The characterization techniques provided supportive evidence of composite formation between the biopolymers including cross-linking with glutaraldehyde. In chapter six, the chitosan-cellulose composite materials (**CH-GL-C**) displayed greater sorption capacity with phenolic dyes, OSPW and single component naphthenates relative to the **CH-GL** and **C-EP** polymers. The sorption results revealed that uptake of the adsorbates increased with cross-linker feed ratio, where the composite with the highest cross-linker ratio (**CH-GL3-C**) displayed greater uptake selectivity for naphthenates with lower double bond equivalence (DBE) values. Suspected charge screening at alkaline pH values may have attenuated the sorption capacity of the **CH-GL-C** composites. To overcome the related effects of charge screening observed in chapter 6, quaternary (**CH-GL-CC-Fe**) and ternary (**CH-CC-Fe**) composite materials with variable iron (Fe) contents were prepared from chitosan (CH) and carboxymethyl cellulose (CC) (see chapter 7). Equilibrium uptake studies with equimolar mixed and OSPW naphthenates in aqueous solution indicated that **CH-GL-CC-Fe** surpassed the sorption capacity of **CH-CC-Fe** and **CH-GL3-C**. According to high resolution electrospray ionization mass spectrometry (HR ESI-MS) analysis, the quaternary and ternary composite materials displayed little or no selectivity for OSPW naphthenates, irrespective of the double bond equivalence (DBE) or carbon number of the species, contrary to results obtained in chapter 6.

Table of Contents

List of Schemes

List of Figures

List of Tables

List of Abbreviations

β-CD …… Beta Cyclodextrin

ΔG ……... Change in Standard Gibbs Free Energy

ΔH……... Change in Standard Enthalpy

ΔS ……..... Change in Standard Entropy

AC ……..... Activated Carbon

ACS …….. American Chemical Society

AGU ……..Anhydroglucose Unit

Amu ……..... Atomic Mass Unit

BET ……..... Brunauer-Emmett-Teller

BJH …….....Barret–Joyner–Halenda

C …….....Cellulose

CC …….....Carboxymethyl Cellulose

CH …….....Chitosan

CHN……..Carbon, Hydrogen, Nitrogen

CNC …….....Cellulose Nanocrystal

CPMAS ……...Cross Polarization Magic Angle Spinning

CTAB ……..Cetyl Trimethylammonium Bromide

DRIFT ……Diffuse Reflectance Infrared Fourier Transform

DSC …….Differential Scanning Calorimetry

EP ……Epichlorohydrin

EPA …….Environmental Protection Agency

HR ESI-MS ……High Resolution Electrospray Ionization Mass Spectrometry

ESI-MS ……...Electrospray Ionization Mass Spectra

FTIR …….Fourier Transform Infra Red

FWHM ……Full Width Half Maximum

GTAC ……Glycidyl Trimethylammonium Chloride

GL …….Glutaraldehyde

HLB ……...Hydrophile Lipophile Balance

IL ……...Ionic Liquid

IUPAC ……International Union of Pure and Applied Chemists

LDH ……Lactate Dehydrogenase

NA ……..Naphthenic Acid

NAFCs ……..Naphthenic Acid Fraction Components

NMR ……...Nuclear Magnetic Resonance

NPRI ……...National Pollutant Release Inventory

ONPAA ……...Ortho Nitro Phenyl Acetic Acid

OSPW ……Oil Sands Process Water

PFO ……..Pseudo First Order

PSO ……Pseudo Second Order

Phth ……Phenolphthalein

PNP ……...Para-Nitrophenol

PSD ……...Particle Size Distribution

PZC ……..Point of Zero Charge

SA ……Surface Area

S ……Surrogate

SSE ……...Sum of Squares of Errors

SEM ……Scanning Electron Microscopy

TEM ……...Transmission Electron Microscopy

TGA ……Thermogravimetric Analysis

UV-vis ……...Ultra Violet Visible

WHO ……..World Health Organization

XRD ……..X-ray Diffraction

Z ……..Hydrogen Deficiency

CHAPTER 1

1. Introduction

1.1 Knowledge gaps and Research hypotheses

This thesis research was designed to bridge the following knowledge gaps according to the hypotheses that will be highlighted in the subsequent section.

1.1.1 Knowledge gaps

1. The effects of cross-linking of cellulose and chitosan at incremental cross-linker content on their sorption properties towards Naphthenic acid fraction components (NAFCs).

2. The effects of sonication on the efficiency of cross-linking cellulose with epichlorohydrin.

3. The effects of cross-linking and/or surface functionalization of cellulose on its sorption affinity towards NAFCs.

3. The effects of composite formation between chitosan and cellulose as well as cross-linking with glutaraldehyde on the sorption properties of their composite materials.

4. The evaluation of the effects of cross-linking and /or doping of iron III species with carboxymethyl cellulose-chitosan composite on the sorption properties of the composite materials.

1.1.2 Research Hypotheses

The thesis research was driven by the following hypotheses which were conceived during various stages of the Ph.D. thesis research as summarized below:

1. The cross-linking of chitosan with glutaraldehyde can occur at incremental cross-linker levels and results in an increase of the sorption properties of chitosan toward NAFCs.

2. The cross-linking of cellulose with epichlorohydrin can occur at incremental levels and contributes to the *pillaring* of the fibril structure of cellulose, with a consequent increase in the surface area and sorption properties of cellulose.

3. The cross-linking of cellulose with the aid of sonication can increase the yield of the cross-linking reaction.

4. The cross-linking and/or surface functionalization of cellulose can increase the sorption affinity of cellulose for NAFCs

5. Composite formation between cellulose and chitosan and cross-linking with glutaraldehyde can enhance the sorption properties of the composite materials.

6. The cross-linking and /or doping of iron III species on to carboxymethyl cellulose-chitosan composites can improve the sorption properties of the composite materials.

1.2 Research Objectives

The overall objective of this research work was to develop biopolymer sorbent materials from chitosan and cellulose for the uptake of naphthenic acids from aqueous solution. The overall objective is divided into four short term objectives as follows; *i*) cross-linking of cellulose and chitosan, *ii*) surface functionalization of cellulose, iii) composite formation between cellulose and chitosan based biopolymers and *iv*) sorption of NAFCs using cellulose and chitosan biopolymer materials.

The first part of the thesis research relates to the modification of chitosan and cellulose by cross-linking with glutaraldehyde (GL) and epichlorohydrin (EP) at variable linker ratios, respectively. The effects of ultra-sonication on cross-linking of cellulose with epichlorohydrin/ aqueous ammonia was also studied. This project also involved evaluation of the sorption properties

of the synthesized polymers with phenolic dyes and NAFCs. The research was conceived due to the need for low-cost sorbent materials for the removal of NAFCs from aqueous solution. Cellulose and chitosan were chosen herein for study, apart from being the most abundant biopolymers from nature, they are also non-toxic biopolymers. The cross-linked chitosan and cellulose polymers were characterized using a variety of methods such as Fourier Transform Infrared spectroscopy (FTIR), CP-MAS ^{13}C solids NMR spectroscopy, thermogravimetric analysis (TGA), elemental analysis (CHN), nitrogen adsorption, particle size analysis, differential scanning calorimetry (DSC), scanning electron microscopy (SEM) transmission electron microscopy (TEM), swelling studies and a dye-based (*p*-nitrophenol; PNP, and phenolphthalein; phth) sorption method. Modification of these biopolymers at variable cross-linker levels was anticipated to tune the physicochemical and sorption properties of the cross-linked polymers according to the level of cross-linking. The application of sonication in the cross-linking process was expected to improve the extent of cross-linking and consequently the yield of the resulting polymers. Sorption studies with phenolic dyes and model naphthenic acid compounds was deployed to elucidate the proposed variation in the physicochemical properties of the cross-linked polymers.

The second aspect of the thesis research was designed to bridge the knowledge gaps of the first part, where it was revealed that the strong intra/intermolecular hydrogen bonding in cellulose impeded greater pillaring of its fibril structure. This resulted in cross-linked polymers that display low surface area and porosity. Another finding from the first part of the thesis research was the negative surface charge of the cross-linked polymers at alkaline pH conditions. In view of the above, the first hydrogel (**C-EP-G**) was synthesized by cross-linking cellulose with EP/aqueous ammonia followed by surface functionalization with glycidyl trimethyl ammonium chloride

(GTAC). Another hydrogel (**C-G**) was prepared by direct grafting of GTAC on cellulose. Cross-linking and surface functionalization was expected to address the challenge of negative surface charge of cellulose at alkaline pH conditions. The hydrogels were characterized using CHN analysis, TGA, and FTIR/^{13}C solids NMR spectroscopy and their sorption properties evaluated with **S6** as the adsorbate. The modified hydrogels exhibited greater sorption affinity for naphthenate anions relative to the **C-EP** polymers prepared in the first part of the thesis project.

The third part of the Ph.D. thesis research involved the preparation of composite materials based on cellulose and chitosan. This project was anticipated to address the challenge of limited pillaring of the cellulose fibril structure, as well as the collapse of the pore structure of cross-linked chitosan polymers. It was also meant to address the challenge of charge repulsion between the polymers and anions at alkaline pH conditions. To achieve this goal, two types of composite materials containing chitosan and cellulose were prepared. The first composite material (**CH-GL-C**) was made from chitosan and cellulose with further cross-linking with glutaraldehyde at incremental biopolymer monomer/ cross-linker mole ratio. Another composite material (**CH-GL-CC-Fe**) of carboxymethyl cellulose and chitosan was cross-linked with glutaraldehyde, followed by doping of iron III species. The composite materials were characterized by various techniques such as FTIR/^{13}C solid state NMR spectroscopy, CHN, XRD, TGA, SEM, equilibrium swelling, nitrogen adsorption and ICP-OES studies. To achieve the anticipated goal of the project, sorption studies were performed using phenolic dyes, single component and OSPW naphthenates. The results revealed that cross-linking with glutaraldehyde and doping of iron III species into the composite materials further improved the sorptive affinity of the composite materials for naphthenate anions, relative to the single component cross-linked polymers.

1.3 Extraction of Bitumen from Oil Sands

Oil sands, also referred to as bituminous sands or tar sands are deposits of sand saturated with bitumen. One of the methods of extracting bitumen from the oil sands is the Clark hot water extraction (CHWE) process.[1-2] This method of bitumen extraction is a two-step process that involves liberation and aeration. The liberation process involves mixing of the ores that were mined via the open pit surface mining technology. The mined ores were crushed to break the lumps and mixed with a hot caustic aqueous solution, followed by agitation to enhance the separation of bitumen from the oil sands. This separation is driven by the alkalinity of the mixture as well as the repulsive force between the negatively charged bitumen droplets and the oil sands. The second step is the aeration process, where air is blown into the flotation system. Air bubbles become attached to the bitumen which rises to the top and forms a froth while the heavy solids sink to the bottom. The froth recovered from the aeration process is sent to the froth treatment plant for further processing, where the following processes take place; addition of suitable amount of a light hydrocarbon and thorough mixing, separation of the water/solids (tailings stream) from the bitumen/hydrocarbon mixture (product stream), recovery of hydrocarbons from the product and tailing streams and the upgrading of the clean bitumen to crude oil.[3-4] The tailing stream consists of water, sand, fine silts, clay, residual bitumen and light hydrocarbons, inorganic salts along with water-soluble organic compounds[5]. The trapping of large volumes of water by fine silts and the toxicity of the water-soluble organic fraction of OSPW known as the naphthenic acid fraction components (NAFCs) makes tailing ponds reclamation very challenging.[6-9]

1.4 Naphthenic Acid Fraction Components (NAFCs)

Naphthenic acid fraction components (NAFCs) are components of the tailings stream obtained from the extraction of bitumen from oil sand. They are a broad range of polar alkyl-substituted acyclic, monocyclic and polycyclic carboxylic acids that may be either saturated or aliphatic. Classical naphthenic acids are defined by the conventional formula, $C_nH_{2n+z}O_2$, where "*z*" represents the "hydrogen deficiency" and is a negative even integer.[10-14] A broader definition for NAFCs recognize the presence of extractable organic compounds that possess aromatic functional groups, nitrogen and sulphur atoms as well as unsaturated groups (*cf.* Figure 1.1).[15-18] Generally, the carboxylic acid groups of NAFCs are not directly attached to a ring, but through a $–CH_2-$ group or an alkyl chain (*cf.* Figure 1.1). Similar to other homologous series, the NAFCs differ by the mass of 2 hydrogen atoms (H2) between *z*-series and 14 mass units (CH_2) between *n*-series. Within the same homologous series, isomers exist where the number of possible NAFCs bearing the same molecular composition, within *n* values ranging from 6 to 30, containing 0 to 6 saturated rings may be up to 134.[19]

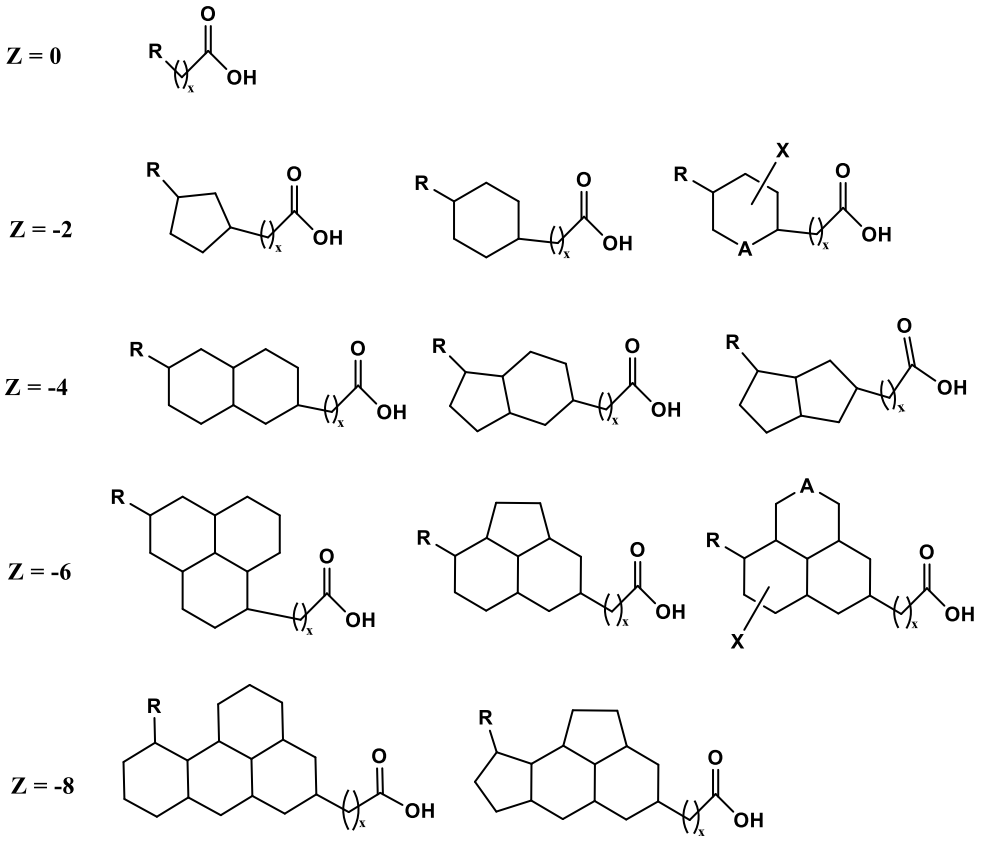

Figure 1.1: Representative structural forms of NAFCs in OSPW showing z values (0 to -8) and heteroatoms. *R* = alkyl group, *X* = COOH, R, OH, SO_x, NO_x, SH and *A* = C, S, N. (where x is a variable integer value)

1.4.1 Physical and Chemical Properties of Naphthenic Acids

Naphthenic acids are highly polar viscous liquids with a characteristic odor, largely attributed to the presence of phenolic and sulfur impurities. Their colors range from pale yellow to dark amber with a boiling point in the range of 250–350 ºC. They have limited solubility in water but are completely soluble in organic solvents and oils. NAFCs are chemically similar to conventional carboxylic acids, where their acid strengths are comparable with those of higher fatty acids. Their dissociation constants in the order of 10^{-5} to 10^{-6} reveal that their acid strength are slightly weaker than low molecular weight carboxylic acids like acetic acid, but are stronger than phenol and cresylic acid.[20] NAFCs have found applications such as the production of metal salts.

These metals salts are used industrially as emulsifying agents, additives for fuel, catalysts, wood preservatives, curing agents, adhesion promoters and corrosion inhibitors in oil-well and petroleum refinery applications. Other properties of NAFCs are summarized in Table 1.1.

Table 1.1: Summary of the physical and chemical properties of NAFCs.[20-24]

Parameter	**General Characteristics**
Color	Pale yellow, dark amber, yellowish brown, black
Odor	Primarily imparted by the presence of phenol and sulphur impurities; musty hydrocarbon odor
State	Viscous liquid
Molecular weight	Generally between 140 and 450 amu
Solubility	< 50 mg/L at pH 7 in water
	Completely soluble in organic solvents
Density	0.97 – 0.99 g/cm^3
Refractive index	~ 1.5
pK_a	5 – 6
Log K_{ow} (octanol water partition coefficient)	~ 4 at pH 1
	~ 2.4 at pH 7
	~ 2 at pH 10
Boiling point	250 – 350 ^oC
Acid dissociation constant	10^{-5} - 10^{-6}

1.4.2 Toxicity of Naphthenic Acids

The challenges posed by the presence of NAFCs in the environment ranges from their recalcitrant nature to toxicity concerns. NAFCs are suspected to be toxic to both aquatic and terrestrial organisms, where they are reported to function as endocrine disruptors and may be potential carcinogens. However, their mutagenicity is yet to be established. The toxicity of NAFCs is likely a consequence of their surfactant properties[25] at alkaline pH conditions, where there are

able to partition into the water phase. The complex composition of NAFCs has made it difficult for the tagging of its toxicity to a specific class of the compounds, however, the low molecular weight NAFC compounds tend to be more toxic. Narcosis and seizure have been reported as the likely mode of acute and sub-chronic toxicity from NAFCs,[9, 26-28] while their endocrine disruption capabilities relate to their ability to mimic and activate estrogen and androgen receptors.[29] One of the outstanding toxicity challenges posed by the presence of high concentrations of NAFCs in the environment is their ability to attenuate the phytoplankton and aquatic invertebrate community diversity, thus disrupting natural remediation processes.[30-31] A recent study on the toxicity of NAFCs using the absorption, distribution, metabolism, excretion and toxicity (ADMET) predictor™ confirmed their carcinogenic but not mutagenic potentials, where the TD50 value of >50 mg/kg/d was estimated for non-aromatic NAFCs and 19-85 mg/kg/d for the aromatic species.[9] Other studies have shown that NAFCs at concentrations above 25 mg/L can inhibit fathead minnow spawning, decrease testosterone and secondary sex characteristics in males while in females, the levels of 17β-estradiol was depleted.[9, 32] The available studies on the toxicity of NAFCs to mammals show that the human lethal dosage was estimated as 1 L,[21, 33] where the enzyme lactate dehydrogenase (LDH) in the liver was the most affected.[9] Further studies on NAFCs toxicity on other mammals such as rats, dogs, and rabbits indicated a variety of effects not limited to the difficulty in the formation of red and white blood cells and platelets, where the liver was the target organ in both acute and sub-chronic dosing experiments.[28]

1.4.3 Methods of Removing Naphthenic Acids from Water

The removal of naphthenic acids from OSPW has attracted much attention from researchers, thus resulting in different approaches being adopted to address the challenges posed by the presence of these pollutants in the environment. Various methods include sorption,[34-41]

biodegradation,[24, 39, 42-45] photolysis, [40, 46-49] ozonation[50-53] and filtration.[54] None of the aforementioned methods have proven to be sustainable or cost effective and reveal the need for the development of a more effective approach for achieving greater success in NAFCs removal from OSPW. The objective of this thesis research is based on the development of a sustainable and low-cost sorption approach for the removal of NAFCs from water. Therefore, subsequent sections will discuss the sorption of NAFCs in greater detail.

1.4.3.1 Sorption of Naphthenic Acids

Adsorption (*cf.* Scheme 1.1) refers to the accumulation of molecules at an interface, where the nature of the interface may be *solid-liquid, gas-liquid, liquid-liquid* or *solid-gas*. This process is quite different from absorption since the later involves the permeation of the absorbent by the adsorbate. Another difference between these processes is that adsorption is a surface-based process while absorption involves partitioning within the whole volume of the material. However, both processes may take place concurrently and the term sorption is used to express their dual occurrence. The favorable interactions at the interface determine the type of sorption that occurs, physical or chemical in nature. When the prominent driving force for the sorption process is chemical, irreversible, and chemical bonds are formed between the adsorbate and adsorbent, the phenomenon is called chemisorption. On the other hand, if the process is reversible and is driven by physical interactions such as van der Waals and electrostatic interactions as well as hydrogen bonding, it is called physisorption.

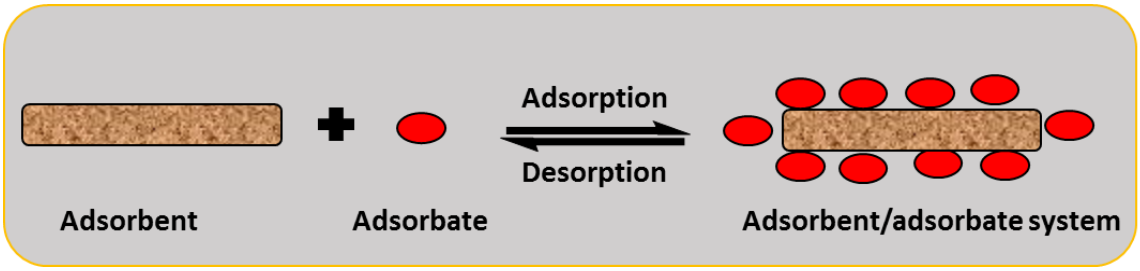

Scheme 1.1: Schematic presentation of a physical adsorption (physisorption) process.

The removal of NAFCs from OSPW via an adsorption-based technique has been widely studied and dates back to the earlier works of Gaikar and Maiti[55] and Wong *et al.*[12] Sorptive removal of NAFCs is an interesting technique because it is a feasible approach with low energy, low input cost, and it allows for high throughput and wide-ranging removal of NAFCs in most cases. Several sorbent materials have been employed in the sorption of NAFCs from OSPW, however, a cost effective sorbent material with optimum sorption properties is yet to be developed. Table 1.2 presents a summary of the sorbent materials that have been reported for the removal of NAFCs from OSPW. From the Table 1.2, it is evident that the most widely used sorbent material for the sorption of NAFCs are various forms of activated carbon and petroleum coke, while there are limited or no studies on the use of cellulose, chitosan, carboxymethyl cellulose and their modified forms.

Table 1.2: Sorbent materials used for the uptake of Naphthenic acids

Sorbent Materials	Reference	Year
Activated carbon / Granular activated carbon	Wong *et al.*;[12] Niasar *et al.*;[56] Martinez-Iglesias *et al.*;[57], Iranmanesh *et al.*;[58] *Islam et al.*;[59]	1996 2013 - 2016
Synthetic resins	Gaikar and maiti[55]	1996
Clay	Li *et al.*[60] Zou *et al.*[61]	1997, 2017
Ion exchange resins	Saab *et al.*[62]	2005
Organic rich soils/soils	Janfada *et al.*[63]	2006
β-cyclodextrin-polyurethanes, goethite, magnetite, cellulose, activated carbon (AC), biochar, polyaniline	Mohamed *et al.*[35-36, 41, 64-65]; Headley *et al.*[66] Wilson *et al.*[67]	2008–2009, 2011, 2013 - 2015
Petroleum coke	Gama El-din et. al.;[38] Pourrezaei *et al.*;[68] Zubot *et al.*;[69]	2011 - 2012, 2014
Mineral surfaces	Keleşoğlu *et al.*[70]	2012
Nickel-Alumina/activated alumina	Azad *et al.*[71]	2013
Magnetite	Balmasova *et al.*[72]	2015
Silica-supported ionic liquid	Shah *et al.*[73]	2015
Toluene-water interface	Teklebrhan *et al.*[74]	2016
Nitrogen-coordinated transition-metal embedded graphene	Ma *et al.*[75]	2016
Biochar-biofilm	Frankel *et al.*[39]	2016
Modified keratin PMKB and GMKB)	Arshad *et al.*[76]	2016
Biomass based biochar	Bhuiyan *et al.*[77]	2016
Molecular sieves	Nascimento *et al.*[78]	2016
Quaternized chitosan beads	Quinlan *et al.*[37]	2017

1.5 Biopolymers for the Sorption of Naphthenic Acids

Biopolymers are renewable and biodegradable polymer materials that are either synthesized by animals, plants and microorganisms or produced via modification of precursor biomaterials. They can be classified into polynucleotides, polypeptides and polysaccharides. Biopolymers have gained wide interest due to the availability of reactive functional groups that support their modification and subsequent usage in a wide range of fields, from biomedical to food sciences. The interest for the use of biopolymers for sorption of naphthenic acids is a consequence of their unique properties such as non-toxicity, abundance, amenability, low-cost, eco-friendliness, sustainability as well as biodegradability.[79] The two most abundant polysaccharides are cellulose and chitosan. Chitosan and cellulose have similar structure, where the differences between them occur at the position C-2 of the glucopyranose ring where a replacement of the amine (-NH_2 or –$NHCOCH_3$) group in chitosan with a hydroxyl (-OH) group may occur. In terms of their origin, chitosan can be obtained from fungi, it is mainly obtained from crustaceans (animal-based) while cellulose is plant-based. The properties of cellulose and chitosan are further discussed in the subsequent sections below.

1.5.1 Chitosan

Chitosan (CH) (*cf.* Figure 1.2) is derived from a naturally occurring polysaccharide chitin after deacetylation by acid-base hydrolysis. Chitin is a naturally abundant mucopolysaccharide, inherent in a wide range of organisms such as crustaceans, fungi, insects and some algae.[80-81] Chitosan is an *N*-deacetylated form of chitin after treatment with strong alkali such as NaOH, where partial deacetylation occurs from 50 – 99 %.[82-85] Therefore, chitosan is a biopolymer composed of glucosamine and *N*-acetylglucosamine units linked by the β-1, 4-glycosidic bonds. Its physical properties are dependent on parameters such as the molecular weight, degree of

deacetylation (50 – 99 %), arrangement of the amino and acetamido groups, along with the purity of the product.[86-87] Chitosan is soluble in organic acids such as acetic acid and some inorganic acids such as HCl and HNO_3 at pH values below the pK_a of chitosan (~ 6.5). Chitosan is generally not soluble in water in its non-protonated form when pH lies above the pK_a. The amine groups of chitosan are protonated at acidic pH, thus affording it the binding affinity toward negatively charged species at such conditions.[88-89] The foregoing makes chitosan a good sorbent material for the removal of NAFCs from water. Also, the presence of amine groups in chitosan affords chemical modification of its textural, morphological and chemical functionality, where the modification enhances the sorption properties of the resulting modified polymer. As a result, chitosan has attracted significant interest for use as a sorbent material for water treatment technologies.

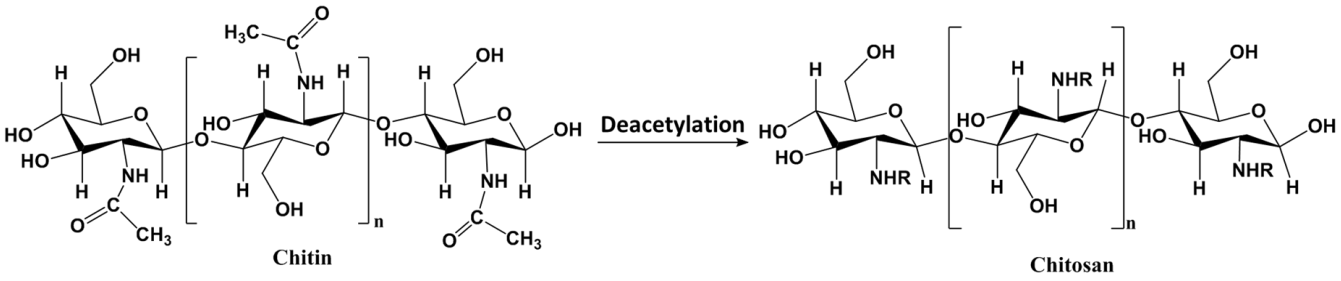

Figure 1.2: Structure of chitin and chitosan (where n represent the number of repeating units and R represent H or acetyl groups according to the level of deacetylation).

1.5.2 Cellulose

Cellulose (C) (*cf.* Figure 1.3) is one of the most abundant, biodegradable, non-toxic and renewable biopolymers on earth.[90-91] It is composed of D-anhydroglucose units linked by β-l, 4-glucosidic bonds that exist between the carbon atoms C1 and C4 of adjacent glucose units. The molecular structure of cellulose supports its hydrophilicity, degradability, and amenability which is initiated by the reactivity of the OH groups.[92] The presence of extensive intra/intermolecular

hydrogen bond networks of cellulose biopolymers result in the formation of partially crystalline fiber structure and morphology.[93] However, the intramolecular hydrogen bonding contributes significantly to its mechanical strength and high tendency to crystallize and form fibrils, making it insoluble in most conventional solvents. However, the use of mixed solvent systems ranging from alkali/urea solutions[94-96] to ionic liquids (ILs)[97-99] has enhanced its usage in a wide range of industrial applications. The textural and morphological properties of cellulose can be modified via a range of methods such as mercerization, enzymatic treatment, acid hydrolysis as well as cross-linking reactions.[100-101]

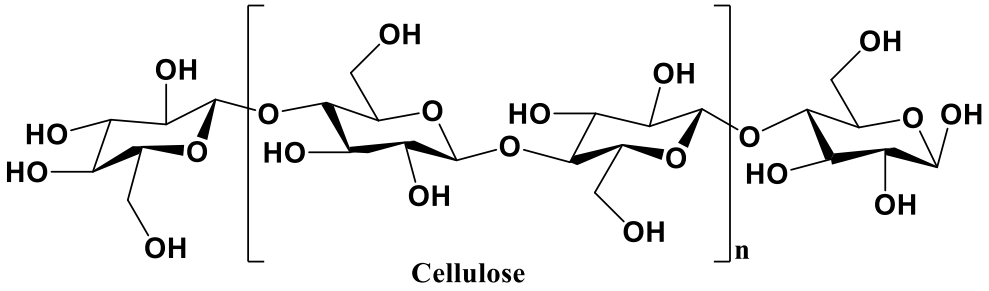

Figure 1.3: Molecular structure of cellulose (where n represent the number of repeating units).

1.5.3 Carboxymethyl Cellulose

Carboxymethyl cellulose (CC) is a soluble derivative of cellulose obtained through the chemical modification of the -OH groups of cellulose with -CH_2COONa group derived from sodium monochloroacetate, $ClCH_2COONa$. The backbone of carboxymethyl cellulose consists of hydrophobic D-glucose oligomers linked by the β-l,4-glucosidic, and many hydrophilic carboxyl groups, thus exhibiting amphiphilic characteristics (*cf.* Figure 1.4).[102] The consequence of the replacement of the H-atom on the OH-groups with -CH_2COONa is a possible loss of the parallel alignment of the CC chains.[103] The foregoing results in noticeable changes of the properties of cellulose as evidenced by the solubility, swelling properties as well as the anionic nature of the

biopolymer. In solution, polysaccharides tend to favor the coiled conformations due to the extensive intramolecular hydrogen bonding, and a consequent reduction in the hydrodynamic volume of the biopolymer.[104] On the contrary, the electrostatic repulsion between the carboxymethyl groups of CC in solution traverses the biopolymer backbone, disrupting the coiled conformation, due to loss of hydrogen bonding relating to defects introduced by the substitution of carboxymethyl groups, resulting in a greater hydrodynamic volume, relative to native cellulose.[104] The aforementioned properties of CC has afforded its application in several industrial applications.

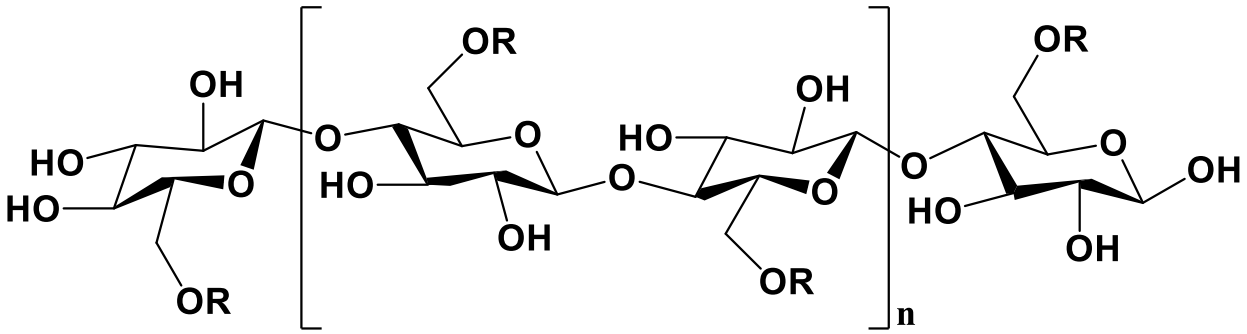

Carboxymethyl Cellulose, R = CH_2COONa

Figure 1.4: Molecular structure of carboxymethyl cellulose (where n represent the number of repeating units).

1.5.4 Modification of Biopolymers

An efficient sorbent material is a material that exhibits all or many of the following properties: High sorption capacity and efficiency, good affinity for the targeted adsorbate, high surface area, good mechanical and structural integrity, good regeneration properties and low cost.[93] Though biopolymers exhibit many of the aforementioned properties, modification via a variety of methods is required to tune these intrinsic properties to their optimum level. The three methods of

modification of biopolymers used in this thesis research (*cf.* Scheme 1.2) are i) cross-linking, ii) surface functionalization and iii) composite formation, as discussed below:

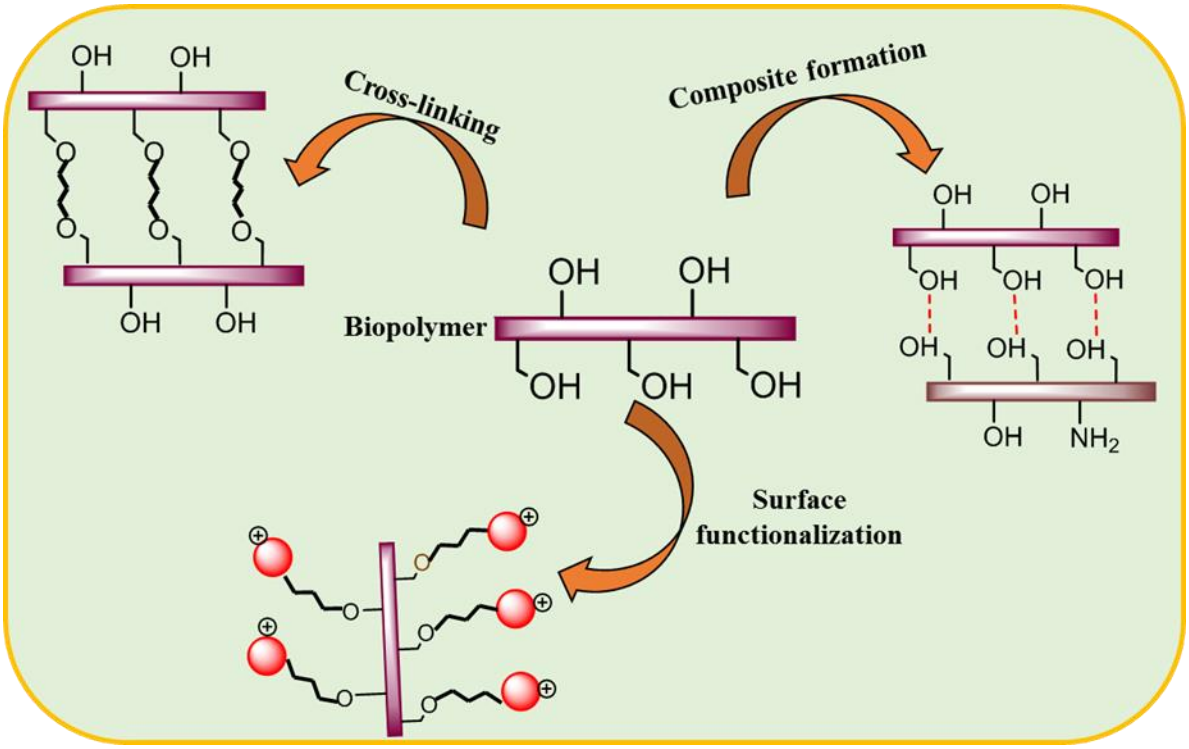

Scheme 1.2: Schematic presentation of the various forms of biopolymer modification (where the red spheres and pendant groups represent surface functionalization groups and cross-linkers respectively).

1.5.4.1 Cross-linking

Cross-linking is one synthetic approach used for modifying the physicochemical properties of biopolymers.[105-106] It is a method of modification that involves merging two or more species through the formation of covalent bonds with a cross-linker. It also refers to the *pillaring* of the fibril structure of biopolymers. Pillaring refers to the introduction of cross-linkers as intermolecular bridges within the fibril structure of biopolymers that result in changes in the biopolymer structure and morphology. This *pillaring effect* results in alteration of the surface chemistry, morphology, mechanical properties and chemical stability of the biopolymer due to the introduction or cleavage of target chemical groups.[107-108] Various cross-linkers and synthetic

methods have been used for the modification of biopolymers, according to the nature and extent of modification required. A report by Chang et al.[101] revealed that the use of epichlorohydrin for the cross-linking of cellulose and polyvinyl alcohol resulted in greater porosity and decreased crystallinity of the cross-linked polymer. Cross-linking of biomaterials with carboxylic acids was reported to result in better hemocompatibility, greater mechanical and thermal stability, improved bio-conjugation, decreased solubility and water vapor transmission rate.[109-110] Glutaraldehyde is another cross-linker that is widely used due to its ability to enhance the mechanical and textural properties of biopolymers. However, there exists contradictory evidence concerning the cytotoxicity of cross-linked polymers containing glutaraldehyde,[111-115] where it has been reported that amniotic membrane treated at <0.03 mmol glutaraldehyde per mg membrane exhibited good cytocompatibility with human corneal epithelial cells.[113] The aforementioned studies provide support that cross-linking is an effective tool for biopolymer modification.

1.5.4.2 Surface Functionalization

Surface functionalization is another method for tuning the surface properties of biomaterials by introducing new desired properties that depend on the intended end-use application. These properties range from morphology, hydrophilicity, surface charge, biocompatibility and reactivity.[116] The advantages of this technique stem from the fact that it is environmentally friendly and allows the modification of the surface properties of biomaterials without destroying the inherent favorable bulk characteristics of the precursor biomaterial.[116] Though there are various methods for the surface functionalization of biomaterials[117], this thesis research is focused on the grafting of new functional groups on the surface of the biomaterial with the aim of changing the surface functionality and textural properties of the resulting grafted biopolymer. Previous studies on surface functionalization of biopolymers like cellulose via

grafting of quaternary amine groups reveal that the grafted cellulose is relatively versatile and less sensitive towards pH changes.[118] Xu *et al*.[119] reported that saturation of the surface of modified wheat residue was achieved within 10 – 15 minutes during the kinetic studies of the uptake of phosphate from aqueous solution. Abitbol *et al.*[120] observed that modification of cellulose nanocrystals (CNC) with cetyltrimethylammonium bromide (CTAB) did not alter the particle size and morphology, but resulted in an enhanced thermal stability and hydrophobicity of the CTAB-modified CNCs. Cellulose nanofibrils were reported to demonstrate ultrahigh water absorbency, high surface cationic charge density and high anionic dye adsorption capacity due to treatment with GTAC.[121] Other studies[122-124] show that surface grafted biomaterials find applications as controlled-release agents for poorly water-soluble drugs, or antimicrobial and flocculation agents.

1.5.4.3 Composite Formation

Another method for modifying biopolymer structure for the efficient sorption of contaminants from aqueous solution is composite formation. The process involves blending of two similar or dissimilar biopolymer materials with the aim of improving the structural, textural and morphological properties of the resulting composite.[125] Formation of biopolymer composites is advantageous because the blended polymers exhibit variable properties according to composition, relative to the precursors in several aspects. Composite materials can be made from synthetic polymers and biopolymers,[126] two synthetic polymers[127] and two biopolymers.[128] This thesis research is focused on composite formation between two different types of biopolymers to be discussed further in chapters 6 and 7. Composite formation between two polysaccharides usually occur due to their biocompatibility.[129] All polysaccharides are composed of similar anhydroglucose units with minor differences in their chemical functionalization. For example, cellulose has a hydroxyl group at the C2 of the anhydroglucose unit while chitosan possesses an

amine or N-acetyl group. Similarly, cellulose has a hydroxyl group at C6 while for carboxymethyl cellulose, the protons of some of the C6 hydroxyl groups are substituted by carboxymethyl groups. These structural and functional similarities along with their similar hydrophile-lipophile balance (HLB) makes blending different forms of polysaccharides a facile process. Previous studies on biopolymer composites show that blending of cellulose with other polysaccharides like chitin, chitosan, starch, alginates and hyaluronic acid gave rise to composite materials that provide good biocompatible adsorbents and raw materials for tissue engineering.[130-132] In other reports, hydroxyethyl cellulose-sodium alginate blend beads were used as a controlled-release agents, cellulose-sodium alginate hydrogels exhibited macroporous structure, excellent mechanical strength, and high equilibrium swelling ratio in water while chitosan/carboxymethyl chitosan hydrogel displayed greater mechanical strength relative to chitosan/carboxymethyl cellulose hydrogel.[129, 133-134]

1.6. Structural and Physicochemical Characterization of Biopolymers Sorbents

Structural and physicochemical techniques are used to detect and evaluate the extent of biopolymer modification since different synthetic strategies impact the structure and composition of biopolymers differently. For example, cross-linking results in the pillaring of the fibril structure of the biopolymers that alter the morphology and structure of the biopolymer.[107-113] Elucidation of changes in the structure, chemical composition and physicochemical properties are important since it provides support that successful modification of the biopolymers is achieved. In this thesis, a variety of techniques were used for the systematic characterization of the precursor and modified biopolymers. An overview of these characterization methods are discussed in subsequent sections.

1.6.1 Spectroscopic Methods

Infrared (IR) and nuclear magnetic resonance (NMR) spectroscopy are the spectroscopic techniques that were used for the characterization of both precursor and modified biopolymers and are described in this section. IR spectroscopy is a very common analytical tool for the characterization of biomaterials.[135-142] It is a very rapid and cheap method that is widely available and provides unique spectral fingerprints characteristic of the biopolymer.[136] IR spectroscopy relies on the discrimination of variable functional groups of biopolymers to absorb radiation at different spectral frequencies that exhibit specific molecular vibrations according to their respective functionalities. These vibrations may result in changes in bond length and are referred to stretching vibrations, while others involve changes in the bond angle are known as bending vibrations.[143] These vibrations enable the detection of changes in the structure of biopolymers due to cross-linking, surface functionalization and composite formation. For example, chapters 2 – 5 describe the characterization of the biopolymers via FTIR spectroscopy for changes in the C–O–C / C–N–H bands of cellulose and chitosan between 1000 – 1200 cm^{-1}. It also highlighted changes in the spectral bands between 1600 – 1720 cm^{-1} due to cross-linking and surface functionalization effects. In chapters 6 and 7, IR spectroscopy provided support of composite formation between the biopolymers by highlighting changes in the O–H / N–H (3310 - 3370 cm^{-1}), C–H (2000 - 2300 cm^{-1}), C=O (1701-1715 cm^{-1}), C–O–C and C–N–H (1000 – 1200 cm^{-1}) bands of the biopolymers.

NMR spectroscopy is a very useful technique for the study of the structure of biopolymers. It exploits the magnetic properties of certain nuclei due to the application of an external magnetic field with a specific radio frequency. In NMR spectroscopy, changes in the resonance frequency of atoms in a molecule due to the magnetic field acting on it provides information about the nuclear and electronic structure of the molecule as well as the functional groups in their proximity. NMR

spectroscopy study of biomaterials can be done in the solution or the solid state, where nuclei with spin, I= ½ such as ^{1}H, ^{13}C, ^{19}F, ^{31}P, and ^{15}N are among the most widely studied. However, in this thesis, the insolubility of the modified biopolymers in conventional solvents, according to their composition, warranted their characterization using solids NMR spectroscopy via cross-polarization with magic angle spinning (MAS), where ^{13}C nuclei were the focus of interest. CP-MAS solids NMR is a technique that affords high-resolution NMR spectra with characteristics that resemble spectral results obtained using NMR in the solution phase. The technique involves a combination of sample spinning at the magic angle ($\theta = 54.74^{o}$) with respect to the direction of the magnetic field and polarization transfer from abundant spins such as ^{1}H or ^{19}F to dilute spins (less abundant) such as ^{13}C or ^{15}N.[144-145] The CP-MAS ^{13}C NMR spectra of the respective biopolymers provide evidence of the structural modification of the biopolymers judging by the appearance of new ^{13}C resonance lines, as well as attenuation/or increase of their line intensity. For instance, in chapter 5, the NMR spectra of the cross-linked/surface functionalized cellulose hydrogels display resonance lines that were absent in the spectra of pristine cellulose, thus providing evidence of the successful grafting of quaternary amine groups onto cellulose. Also in chapter 6, the broadening of existing ^{13}C resonances and appearance of new spectral lines at ~28.0 and 41.0 ppm, ~100 ppm, ~129/125 ppm, ~142/144 ppm and ~180 ppm provide support that composite formation and cross-linking with glutaraldehyde occurs between the biopolymers.

1.6.2 Swelling Studies

Solvent swelling of a materials in a medium refers to an increase in the volume due to the uptake of a liquid or gas species. This usually results in the modification of the mechanical properties of the resulting swollen material. The measurement of swelling phenomena provide a simple technique for elucidating variation in the sorption properties of biopolymers due to

synthetic modification.[146-147] Biopolymer modification is expected to alter the physicochemical properties since cross-linking or surface modification may contribute to *pillaring* of the fibril structure of the material. The consequence of *pillaring effects* relate to an increase in the surface area (SA) of the modified biopolymer relative to its native form. For example, a biopolymer that was initially soluble in aqueous solution may become insoluble due to modification and vice-versa. Also, modification of biopolymers may lead to an increase or decrease in the water sorption capacity of the biopolymer. In chapters 3 to 6, the modified biopolymers displayed greater degree of swelling in water relative to the unmodified biopolymers.

1.6.3 Thermal Analyses

Thermal analyses collectively refers to a group of techniques where the properties of a sample such as mass, enthalpy, deformation and pressure are studied as a function of its temperature through heating or cooling in a regulated manner.[148-149] It provides information on the stability, composition and phase changes occurring in the sample especially upon modification. The properties of materials measured through thermal analyses in this thesis relate to mass and enthalpy, hence thermogravimetric analyses (TGA) and differential scanning calorimetry (DSC) are discussed below:

Thermogravimetric analysis is a thermal analysis method that monitors the change in mass of a sample according to changes in temperature. The variation in mass may arise due to processes such as decomposition, degradation, sublimation, vaporization, adsorption, desorption, oxidation, and reduction. These processes are dependent on the structure and composition of the material under study.[150] The results of the analyses are often presented as a plot of the change in mass (Δm) versus temperature (T) or first derivative plots to provide information on the thermal stability and composition of the sample. Pristine biopolymers such as cellulose, chitosan and carboxymethyl

cellulose reported in this thesis usually exhibit one or two thermal events, depending on the presence of bound water in their structure.[151-155] On the other hand, the modified forms of such biopolymers display a variable number of thermal events that depend on the nature of the modification.

DSC is a thermal analysis technique that measures changes in the heat flow to a sample and a reference material due to phase transitions or chemical reactions. The change in heat flow is measured against temperature where the temperature of both the sample and reference are controlled.[149] For example, if the sample undergoes an endothermic change, the heat flow to the sample is increased to compensate for the heat consumed, whereas, for exothermic processes, the heat flow to the reference material is increased.[156-158] Since the pressure of the system is constant during the analysis, it implies that changes in heat flow is equivalent to changes in the enthalpy of the system and can be represented by the equation below:

$$\left(\frac{dq}{dT}\right)_p = \left(\frac{dH}{dT}\right)_p \qquad \text{Equation 1.1}$$

Where $\frac{dH}{dT}$ is related to the heat flow (provided the heat capacity is constant over the temperature scan of interest, i.e. $dH = C_p dT$), hence the difference between the heat flow to the sample and reference can be calculated according to the equation below:

$$\Delta\left(\frac{dH}{dT}\right)_p = \left(\frac{dH}{dT}\right)_{p,sample} - \left(\frac{dH}{dT}\right)_{p,reference} \qquad \text{Equation 1.2}$$

Previous studies indicate that the thermophysical properties of biopolymers such as heat capacity, melting temperature, enthalpy and crystallization temperature can vary due to modification.[159-163] Therefore, the above affirms that DSC is a potentially viable technique for evaluating the effects due to synthetic modification in biopolymers, such as cross-linking, surface functionalization and

composite formation. For example in chapter 2, DSC studies of cross-linked chitosan polymers affirmed that the different cross-linked polymers have tunable physicochemical properties. The DSC results revealed variable dehydration transitions and decomposition temperatures, according to the cross-linker feed ratio, when they were hydrated in a solution of a model NAFC compound. Also in chapter 4, DSC studies provided support that variations in the properties of cross-linked cellulose polymers occurred upon modification via different synthetic routes. According to the results (*cf.* chapter 4), the polymer cross-linked via heating and stirring (**C-EP heating**) exhibited an endothermic melting process while the polymer cross-linked with the aid of sonication (**C-EP sonication**) displayed an exothermic melting event.

1.6.4 Elemental Analysis

Elemental analysis is another physicochemical method of analysis that is widely used for evaluation of the level of modification of biopolymers.[162, 164-166] This technique involves the determination of the weight composition (%) for elements such as carbon, hydrogen and nitrogen, along with other heteroatoms like sulphur and halogens. This is done through a complete combustion of the sample in air or oxygen followed by quantification of the oxides of the constituent elements produced. For instance, for a biopolymer whose major component elements are carbon, hydrogen and nitrogen, the carbon is quantified as carbon dioxide, hydrogen as water and nitrogen as nitric oxide. This technique is a very feasible method for evaluation of the modification of biopolymers because cross-linking, surface functionalization and composite formation results in the introduction of new or similar elements into the biopolymers. These methods of biopolymer modification afford an increase in the weight of existing elements as well as the introduction of new elements that were absent in the pristine biopolymer. For instance in

chapters 3 and 6, cross-linking as well as composite formation resulted in an increase in the content (%) of carbon, hydrogen and nitrogen in the cross-linked polymers and composites, respectively.

1.6.5 Solid-gas and Solid-solution Adsorption

Solid-gas and solid-solution adsorption is a physicochemical characterization method that employs the use of adsorption studies to analyze the SA and porosity of modified biopolymers relative to their pristine forms. In this technique, the adsorbent (solid) is exposed to the adsorbate (gas, solution of a dye) and the uptake of the adsorbate is evaluated under controlled conditions. In general, porous materials will display greater uptake of the adsorbate at the chosen experimental condition, hence the application of this technique for the estimation of the surface area and pore structure characteristics of sorbent materials.[167-168]

The solid-gas adsorption technique usually employs molecular nitrogen (T = 77 K and cross-sectional area of 16.2 $Å^2$ /molecule) as the adsorptive probe, where it is exposed to a sample under investigation. The adsorption isotherms are usually reported as a plot of relative pressure (p/p_o) versus volume of nitrogen adsorbed, and the subsequent amount that is desorbed. The adsorption of nitrogen depends on the textural (pore structure and surface area) properties of the sorbent. According to the guidelines set by the International Union of Pure and Applied Chemistry (IUPAC),[167] these isotherms are classified into six types, where four common types I – IV (*cf.* Figure 1.5) are discussed below:

The type I isotherm describes the sorption properties of microporous solids (pore widths ≤ 2 nm) where the external surface area is relatively small. The isotherm is concave to the p/p_o axis and uptake of the adsorbate is limited by the accessible micropore volume rather than by the internal SA of the sorbent material. It is also characterized by filling of the micropores of the

sorbent at low p/p_o. The Langmuir isotherm model provides the best description for adsorption processes where the monolayer of the sorbent material undergoes saturation. For these sorbent materials, it is assumed that the material is made up of relatively uniform adsorption sites, where no further sorption occurs upon saturation of the monolayer. Granular activated carbon, molecular sieves, zeolites and certain porous oxides are examples of sorbent materials that exhibit this type of adsorption behavior.[167-168]

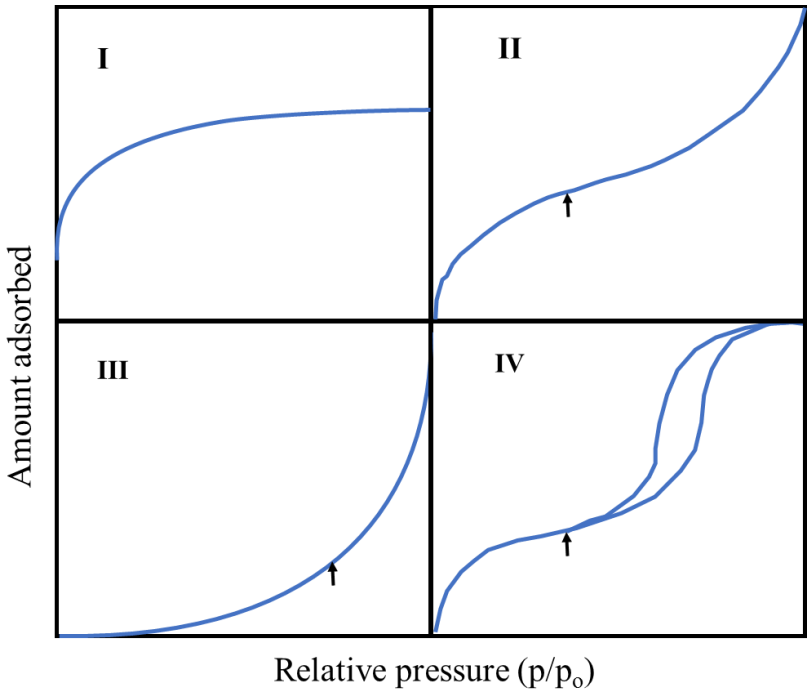

Figure 1.5: Types of adsorption isotherms, where the arrows represent regions of complete monolayer coverage.

Another type of isotherm displayed by sorbent materials is represented by the type II isotherm (*cf.* Figure 1.5). This isotherm type is exhibited by non-porous or macroporous sorbent materials with pore widths that exceed 50 nm. Unlike the type I isotherm where there is no further adsorption after the completion of the monolayer as indicated by the arrow in Figure 1.5, further adsorption occurs that results in the formation of a multilayer.[167-168]

Type III isotherm (*cf.* Figure 1.5) behavior is exhibited by non-porous sorbent materials whose interaction with the adsorbate is weak. It describes a multilayer sorption facilitated by stronger adsorbate-adsorbate interaction relative to the adsorbate-adsorbent interaction.

In the case of the type IV isotherm (*cf.* Figure 1.5), a similar profile is seen relative to the type II system where the difference relates to the presence of a hysteresis loop. The hysteresis loop occurs due to capillary condensation and evaporation in the mesopores at different relative pressures. The type IV isotherm is the outcome of adsorption by materials with mesoporous character (pore widths between 2 – 50 nm).

The solid-solution adsorption isotherm method is another technique that is used to estimate the SA of biopolymers.[169-170] In this method, the accessible SA is determined using the uptake parameters obtained from the sorption of dyes such as *p*-nitrophenol (**PNP**) and methylene blue (MB), according to the equation 1.3 below:

$$\text{SA}\ (\text{m}^2/\text{g}) = \frac{\text{Q}_\text{m} \times \text{N} \times \sigma}{\text{Y}} \qquad \text{Equation 1.3}$$

Q_m is the monolayer adsorption capacity (mol/g) obtained from the best fit adsorption isotherm model, N is Avogadro's number (6.02214×10^{23} mol^{-1}), σ is the cross-sectional molecular area of the adsorbate (m^2) and Y is the coverage factor (Y =1 for **PNP** and Y =2 for MB).[169, 171-173] Determination of the coverage factor is based on the number of layers of dye species adsorbed at the surface of a sorbent material. For PNP, the molecular area (σ) is 52.5 Å^2 when it is adsorbed in a co-planar orientation and 25.0 Å^2 for an orthogonal arrangement with a planar surface.[174] This method is considered relatively simple since it can be carried out both in aqueous media or inorganic solvents and can be used for studying porous and non-porous sorbent materials. However, the method is limited by the following factors: i) variations in the coverage factor to due

to potential dimerization and trimerization of adsorbates, ii) differences in the cross-sectional molecular area of the adsorbate based on its orientation on the adsorbent, iii) formation of multilayer adsorption due to potential micellization of the adsorbates, and iv) errors in SA estimates due to size screening at micropores of the adsorbent.[170] The aforementioned limitations may be inconsequential when it relates to comparing structurally similar materials such as the ones reported in this study.

1.7 Sorption Studies

During sorption (*cf.* Scheme 1.3), the adsorbent and the adsorbate are allowed to be in contact for an appropriate time to establish equilibrium between the amount of the sorbate bound by the sorbent and the amount of unbound sorbate in solution. Sorption studies relate to the use of various isotherm models to understand the equilibrium binding of sorbates to the sorbents.

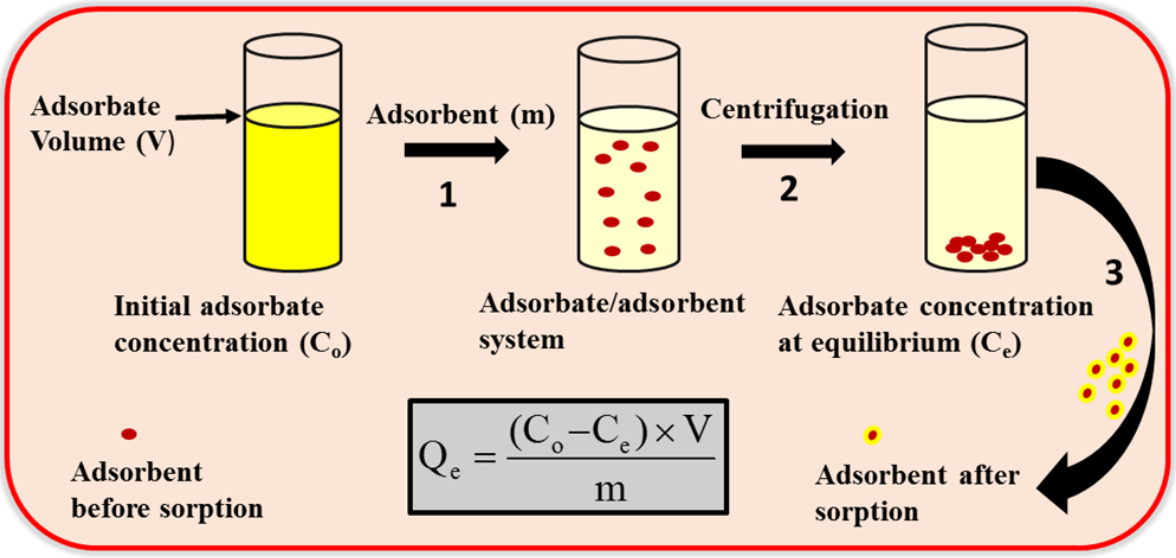

Scheme 1.3: Step-wise process of the determination of the quantity of adsorbate removed from solution during an adsorption process.

The adsorption isotherm *(cf.* Scheme 1.4) is a plot of the quantity of the adsorbate removed from the solution by the adsorbent at equilibrium (Q_e; mmol/g or mg/g) versus equilibrium concentration (C_e; mmol/L or mg/L) of the unbound adsorbate. The isotherm parameters provide information that describe the adsorption affinity between the adsorbate and the adsorbent as well as the maximum adsorption capacity (Q_m) of the sorbent material under the conditions employed. Q_e is usually determined from the equation 1.4 while C_e is determined from spectroscopic studies or some suitable analytical method such as mass spectrometry.

$$Q_e = \frac{(C_o - C_e) \times V}{m} \qquad \text{Equation 1.4}$$

C_o refers to the initial concentration of the adsorbate prior to sorption, *m* is the mass (g) of adsorbent, and *V* is the volume (L) of the adsorbate solution.

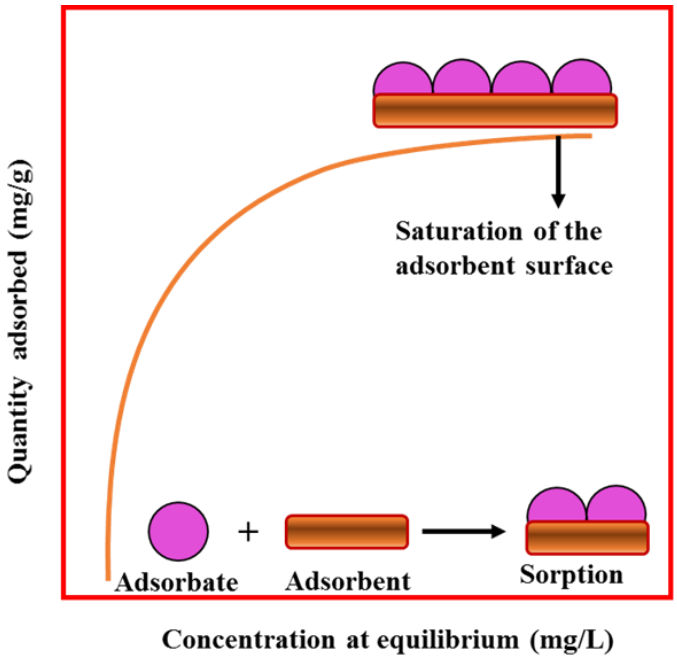

Scheme 1.4: Schematic presentation of an adsorption isotherm depicting the adsorbent surface upon saturation of the monolayer surface sites in the plateau region.

1.7.1 Isotherm Studies on Biopolymer-NAFC Systems

As previously stated in Section 1.7, isotherm models are used to provide an understanding of the nature and efficacy of the sorption process. The isotherm models that provide the best-fit (*cf.* Equation 1.5) to the experimental profile enable the interpretation of the nature of the adsorption process. The various isotherm models are discussed in Section 1.7.2

$$\mathrm{SSE} = \sum\sqrt{\frac{\left(Q_{e,i} - Q_{f,i}\right)^2}{N}} \qquad \text{Equation 1.5}$$

1.7.2 Sorption Isotherm Models

The Langmuir, Freundlich and Sips sorption isotherm models were used in the different studies and are discussed in the following section.

1.7.2.1 Langmuir Model

The investigations of Irving Langmuir regarding surface chemistry, which resulted in his being awarded the Nobel Prize in 1932, gave birth to the Langmuir isotherm model.[175] This isotherm model which describes the adsorption of an adsorbate onto the surface of an adsorbent was established based on the following three assumptions; *i)* the surface of the adsorbent possesses uniform and equivalent adsorption sites, *ii)* at equilibrium, only a monolayer adsorption (*cf.* Scheme 1.6) at the surface of the adsorbent takes place and *iii)* the adsorption of a molecule of the adsorbate does not influence the uptake of other molecules at other adsorption sites. The foregoing implies that this model accounts for homogeneous adsorption sites of an adsorbent, where the adsorbate displays a similar affinity for all sorption sites. This isotherm model is similar to the type I isotherm discussed earlier on in Section 1.6.5. and is described by Equation 1.6, where Q_m

is the monolayer surface coverage of the adsorbate on the sorbent material, and K_L is the equilibrium adsorption constant. For modified biopolymers such as the ones reported in this thesis, the Langmuir isotherm model may not be valid since they are likely to exhibit at least two sorption sites (cross-linker and biopolymer domains, see Scheme 1.2). The only exception may be the surface functionalized biopolymers where adsorption at the grafted sites may be of greater abundance and/or much greater binding affinity. Also for hydrophobic molecules like the naphthenates which are anionic at alkaline pH conditions, some of the assumptions of the Langmuir isotherm model may be invalid since they possess two potential adsorption sites (the hydrophobic tail and the anionic head) which would confer two potential modes of binding via the apolar fragment or the polar carboxylate group (*cf.* Scheme 1.5).

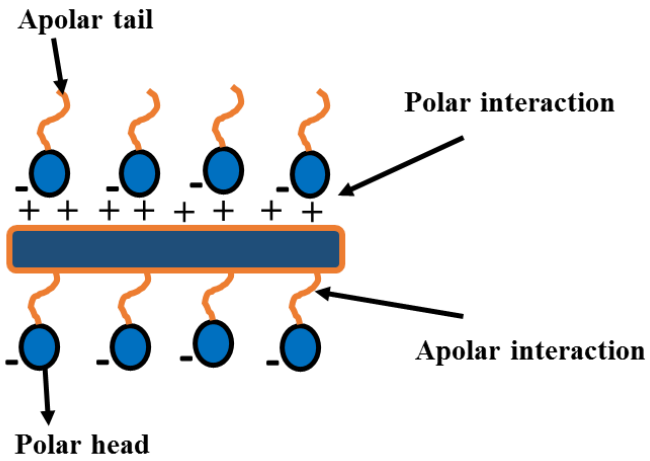

Scheme 1.5: Schematic presentation of polar versus apolar interactions exhibited by NAFCs.

$$Q_e = \frac{K_L Q_m C_e}{1 + K_L C_e}$$ Equation 1.6

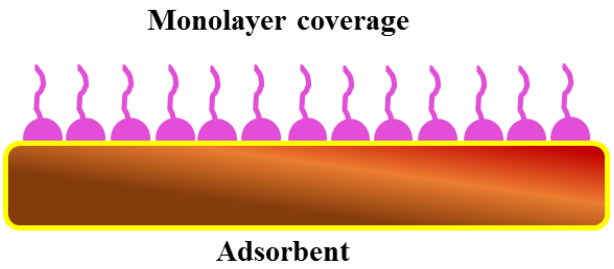

Scheme 1.6: Schematic presentation of the monolayer coverage portrayed by the Langmuir isotherm model.

1.7.2.3 Freundlich Model

The Freundlich isotherm model describes non-ideal and reversible sorption that is not restricted to formation of the monolayer.[176] The model is suitable for describing adsorption on sorbent materials with heterogeneous surfaces and sorption sites. This implies that the model is well suited for adsorption processes where multilayer adsorption (*cf.* Scheme 1.7) with non-uniform distribution of heats of adsorption and binding affinity occur. For the Freundlich model, the adsorbed amount of species is a sum of all occupied sites, where binding sites are occupied according to the relative adsorbent-adsorbate binding affinity. This isotherm model is described by Equation 1.7, where parameters K_F and n_F, are the Freundlich constants that relate to the binding constant and intensity of adsorption, respectively. The $1/n_F$ values are usually in the range of 0 and 1 and serve as a measure of adsorption intensity or surface heterogeneity, where values above 1 indicate cooperative adsorption.[177] The Freundlich model may describe the sorption of NAFCs by the modified biopolymers since the NAFCs and the modified biopolymers possess at least two potential sorption sites (*cf.* Scheme 1.5). However, the inability to obtain direct Q_m estimates from this model poses a limitation, since Q_m is one of the key thermodynamic parameters of adsorbents that determine its efficiency.

$$Q_e = K_F C_e^{1/n_f}$$ Equation 1.7

1.7.2.4 Sips Model

The Sips isotherm model was put forward by R. J. Sips during his seminal studies on the distribution of adsorption energies of the active sites on catalyst surfaces.[178] This model combines the attributes of the Langmuir and Freundlich models.[177-178]

$$Q_e = \frac{Q_m (K_S C_e)^{n_s}}{1 + (K_S C_e)^{n_s}}$$ Equation 1.8

According to Equation 1.8, K_s is the Sips equilibrium constant while n_s indicates the heterogeneity of the adsorption process. The Sips isotherm model is useful for the prediction of adsorption on heterogeneous adsorbents, where it is able to overcome the limitations of the Freundlich model. In cases where $n_s > 1$, the Sips model indicates that the sorbent material is made up of heterogeneous sorption sites. Also when $n_s < 1$, it describes Freundlich model behavior while monolayer behavior is described when $n_s = 1$, according to the Langmuir model. The latter implies that the sorbent material is characterized by homogeneous surface sites. The strength of the Sips model lies in its ability to describe sorption processes at both high and low adsorbate concentrations. The above description of the Sips isotherm model implies that it is a valid model for the study of biopolymer/NAFC systems.

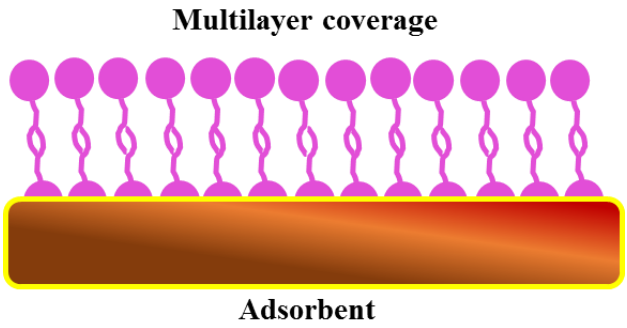

Scheme 1.7: Multilayer coverage inferred by the Freundlich isotherm model.

1.7.3 Sorption of Model Naphthenic Acid Compounds and OSPW Naphthenates

Model compounds to represent naphthenic acids from OSPW were used to establish a sorption protocol and understand the sorption mechanism of the modified biopolymers due to the limited availability of OSPW extracts. OSPW is generally not available in large quantities due to dependence on industrial oil sands partners for supply, whereas the extracts are available in limited quantities due to the laborious nature of the extraction process.[179] The model naphthenic acid compounds were carefully selected to properly represent the structural complexity of the naphthenates present in OSPW. Previous studies[19, 36, 180] have shown that the most prominent naphthenates in OSPW are monocarboxylic acids with *z* values between 0 to -6. In line with the above, model compounds that are monocarboxylic acids with DBE values from 1 to 4 or *z* values from 0 to -6 (*cf.* Scheme 1.8) were selected. Sorption studies of the modified biopolymers with the model compounds provided insights on their sorption affinity for the OSPW naphthenates in terms of selectivity. The established sorption protocol[35, 181] for the model naphthenic acid compounds was applied for studies related to the OSPW naphthenates which are more complex in terms of their variable composition and mixture of congeners. The application of modified biopolymers for the sorption of OSPW naphthenates shall demonstrate the suitability of the materials for the

treatment of more complex NAFC mixtures. Details of these studies are reported in chapters 5, 6 and 7.

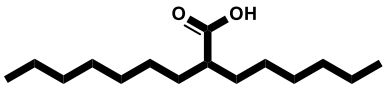

S1, 2 Hexyl decanoic acid

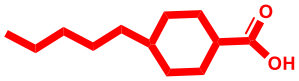

S2, Trans-4-pentyl cyclohexane carboxylic acid

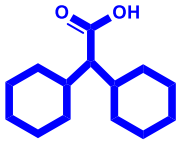

S3, Dicyclohexyl acetic acid

S4, Adamantane carboxylic acid

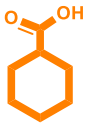

S5, Cyclohexane carboxylic acid

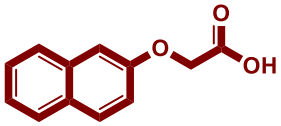

S6, 2 Naphthoxy acetic acid

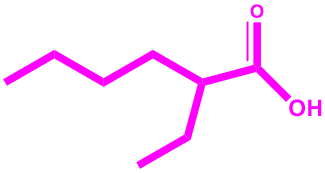

S7, 2 Ethyl hexanoic acid

Scheme 1.8: Structure of single component carboxylic acids (**S1** – **S7**).

The sorption processes were performed at equilibrium and kinetic uptake conditions, where the studies are discussed in sections 1.7.3.1 and 1.7.3.2.

1.7.3.1 Equilibrium Studies

Equilibrium sorption studies usually provide information on the sorption capacity as well as the nature of the interaction between the modified biopolymers and the adsorbates.[41, 55, 182-184] Equilibrium adsorption studies also provide information on some thermodynamic parameters of

the sorption process such as the standard Gibbs free energy change ($\Delta_{ads}G^o$), enthalpy change ($\Delta_{ads}H^o$) and entropy change ($\Delta_{ads}S^o$).[182, 185-186] These parameters are usually obtained from the dependence of the sorption equilibrium constant (K_{ads}) on temperature according to the following relationships:

$$\Delta_{ads}G^\circ = -RT\ln K_{ads} \qquad \text{Equation 1.9}$$

$$\ln K_{ads} = -\frac{\Delta_{ads}H^o}{RT} + \frac{\Delta_{ads}S^o}{R} \qquad \text{Equation 1.10}$$

Where K_{ads} is the equilibrium constant, obtained from the sorption isotherm, R is the gas constant (8.314 J/ (mol K), and T is absolute temperature (K).

In this thesis, equilibrium studies were carried out using the batch and one pot[181] systems. Gaikar and Maiti[55] in their studies reported that macroporous weak anionic ion-exchange resins were better sorbents for the removal of naphthenic acids from petroleum oil, relative to strong anionic-exchange resins with isoporous structure. The authors[55] also reported that the strong anion-exchange resin exhibited greater interaction with naphthenic acids, where the rate of uptake of NAFCs by the sorbent materials was governed by the resistance to internal diffusion. Through sorption studies at equilibrium and kinetic conditions, Mohamed *et. al.*[184] discovered that various sorbent materials displayed similar sorption capacity but possess variable selectivity for the NAFC species in OSPW extract, and for raw/treated wetland samples. Another study[183] on the uptake of NAFCs from water revealed that chemically and physically treated activated carbons (ACs) displayed variable affinities for NAFCs, where one gram of the chemically treated AC removed up to 35 mg of NAFCs. Peng *et. al.*[187] after their study on the sorption of single-ring model naphthenic acids on soils reported that the interaction between the adsorbate and the soils was a

predominantly physical process, where pH and the presence of inorganic salts significantly influenced the sorption process.

1.7.3.2 Kinetic Studies

Sorption kinetic studies provide information on the rate at which the adsorption process occurs. Kinetic studies provide a greater understanding of the non-equilibrium process with respect to the time required for equilibrium to become established.[188-189] Kinetic isotherm profiles are usually presented as a plot of uptake (Q_t) vs. time (t) according to Equation 1.11:

$$Q_t = \frac{(C_o - C_t) \times V}{m} \qquad \text{Equation 1.11}$$

These plots are usually analyzed using kinetic models such as the pseudo-first order (PFO) and the pseudo-second order (PSO) models respectively (*cf.* Equations 1.12 – 1.13 respectively).

$$Q_t = Q_e (1 - e^{-k_1 t}) \qquad \text{Equation 1.12}$$

$$Q_t = \frac{Q_e^{\,2} k_2 t}{1 + k_2 t Q_e} \qquad \text{Equation 1.13}$$

These kinetic models were established based on the following assumptions: *i*) sorption takes place at specific sites, where there are no interactions between the adsorbates *ii*), the surface coverage does not affect the adsorption energy, *iii*) adsorption on the surface of the adsorbent is at a maximum after monolayer coverage is achieved, *iv*) there is no variation in the concentration of the adsorbate and *v*) uptake of the adsorbate is governed by a first-order rate equation for the PFO model and second-order rate equation for the PSO model.[188]

Through the kinetic isotherm analyses, parameters such as the activation energy, standard enthalpy of activation ($\Delta_{ads}H^*$), entropy of activation ($\Delta_{ads}S^*$), and free energy of activation ($\Delta_{ads}G^*$) of the sorption process can be obtained. The activation energy (E_a) is usually obtained by plotting *ln* k_i versus 1/T according to the Arrhenius equation 1.14. $\Delta_{ads}H^*$ and $\Delta_{ads}S^*$ are obtained as the slope and intercept of the plot of ln k_i/T versus 1/T, according to the linear relationship displayed in Equation 1.15, and $\Delta_{ads}G^*$ is computed from Equation 1.16

$$lnk = lnA + \frac{E_a}{R}\left(\frac{1}{T}\right) \qquad \text{Equation 1.14}$$

$$\frac{\ln k}{T} = \ln\frac{k_B}{h} + \frac{\Delta_{ads}S^*}{R} - \frac{\Delta_{ads}H^*}{RT} \qquad \text{Equation 1.15}$$

$$\Delta_{ads}G^* = \Delta_{ads}H^* - T\Delta_{ads}S^* \qquad \text{Equation 1.16}$$

k_i is the adsorption rate constant, A is the pre-exponential factor, E_a is the activation energy for the process leading to adsorption, T is the temperature (K), k_B is the Boltzmann constant (1.3807×10^{-23} J K^{-1}), h is Planck's constant (6.6261×10^{-34} J s), and R is the ideal gas constant (8.314 $J.mol^{-1}K^{-1}$). Saha *et. al.*[190] reported that kinetic parameters can be effectively used for the determination of the thermodynamic adsorption parameters, in agreement with other studies.[191-193] Further details of similar results are reported in chapters 2, 5 and 6.

1.8. Thermodynamic Parameters that Influence Sorption

Thermodynamic parameters for adsorption processes describe the relationship between the adsorbate and adsorbent relative to variables such as pressure (P), temperature (T) and composition or chemical potential (μ_i). The information provided by adsorption parameters from thermodynamic studies facilitate a greater understanding of the contributions to the standard Gibbs

free energy, standard enthalpy and standard entropy to the adsorption process. However, it is limited by its inability to predict molecular-level details. Thermodynamic studies at equilibrium also fail to provide information related to activation energies and chemical kinetics.[194-195] The relationship between changes in the Gibb's surface energy and the change in Gibbs free energy during a sorption process is shown by Equation 1.17.

$$dG^{o} = Vdp - S^{\circ}dT + \gamma dA + \sum \mu_i \, dn_i \qquad \text{Equation 1.17}$$

Where A is the surface area, γ is the surface tension, T is the temperature, μ is the chemical potential, V is the volume and S is the entropy. For sorption processes, the surface tension [N/m] at the adsorbent/solvent interface represents the surface energy [Nm/m^2], which is the driving force for the process. Other parameters that affect sorption processes include the temperature (T), standard enthalpy ($\Delta_{ads}H^{o}$) and entropy ($\Delta_{ads}S^{o}$) and are related to $\Delta_{ads}G^{o}$ according to equation 1.18, where $\Delta_{ads}G^{o}$ must be negative for the sorption process to be spontaneous. From equation 1.18, it implies that $\Delta_{ads}G^{o}$ is negative under the following conditions:

i) $\Delta_{ads}H^{o} < 0$ and $\Delta_{ads}S^{o} > 0$ at all temperatures,

ii) $\Delta_{ads}H^{o} < 0$ and $\Delta_{ads}S^{o} < 0$ at low temperatures,

iii) $\Delta_{ads}H^{o} > 0$ and $\Delta_{ads}S^{o} > 0$ at high temperatures.

$$\Delta_{ads}G^{o} = \Delta_{ads}H^{o} - T\Delta_{ads}S^{o} \qquad \text{Equation 1.18}$$

The magnitude of $\Delta_{ads}H^{o}$ (heat transfer during the sorption process) provides useful information concerning the type of interactions driving the sorption process. These interactions may be physical (physisorption) or chemical (chemisorption). Physisorption is reversible and is characterized by low enthalpy and activation energy values due to weak interaction between the

adsorbate and the adsorbent. On the contrary, the strong interactions between the adsorbate and adsorbent during chemisorption makes the process irreversible and gives rise to high enthalpy and activation energy values.[196] Some of the intermolecular interactions that drive sorption processes are discussed in the following section.

1.8.1 Intermolecular Interactions

1.8.1.1 Hydrogen Bonding

A hydrogen bond is a moderately strong (~ 50 kJ/mol) interaction that occurs between two species due to the formation of a link such as X–H-----O, where X and O are strongly electronegative and O has lone pair of electrons (*cf.* Scheme 1.9). These bonds are generally stronger than typical dipole-dipole and dispersion forces, but weaker than covalent and ionic bonds. For polysaccharide biopolymers with many hydroxyl groups, the formation of hydrogen bonds with neutral carboxylic molecules and their anionic forms is likely one of the major forms of interaction that drives the sorption process involving them along with apolar and polar contributions.

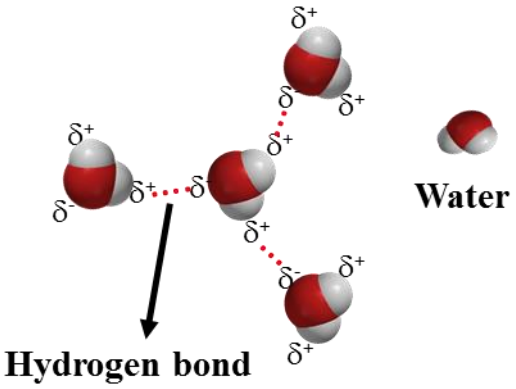

Scheme 1.9: Intermolecular hydrogen bonding between water molecules.

1.8.1.2 van der Waals Interactions

van der Waals interactions are driven by induced dipole moments between two or more atoms or molecules in close proximity to each other (*cf.* Scheme 1.10). It is the weakest of all intermolecular attractions between molecules but may become cooperatively stronger in assemblies such as micelles or polymer aggregates.[197] These interactions play a fundamental role in various fields such as supramolecular chemistry, polymer science, nanotechnology and surface science. Though the interior atoms of large biopolymer molecules like polysaccharides are not in contact with the solvent during adsorption, van der Waals interactions may be favored. Such types of favorable interactions between the species lower the Gibbs energy of the system and consequently improve their sorption affinity for neutral and charged molecules.[198-199]

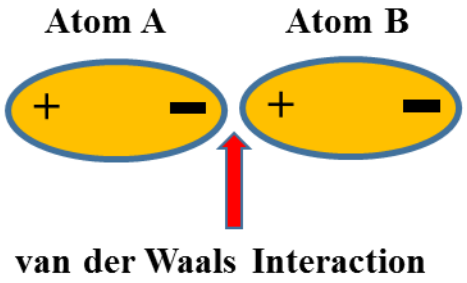

Scheme 1.10: van der Waals interaction between two gaseous atoms A and B.

1.8.1.3 Electrostatic Interactions

Electrostatic interactions refer to non-covalent interaction that are non-directional and originate from the electric charges and dipoles of atoms or group of atoms. They enable the stability, molecular recognition and assembly of macromolecules. For instance, electrostatic attraction exists between oppositely charged molecules whereas electrostatic repulsion occurs in

the presence of molecules that are similarly charged (*cf.* Scheme 1.10). The energy of an electrostatic interaction is described by the relationship in Equation 1.19:

$$\Delta E = {}^{Kaq_1q_2}/_{\varepsilon\, r} \qquad \text{Equation 1.19}$$

where E is the potential energy, q_1 and q_2 are the charges on the two species, a is Avogadro's number, ε is the dielectric constant of the medium r is the distance between the charged species and k is a proportionality constant (*Coulomb's law constant*). However for ion-dipole interaction, the distance dependence of potential energy is given by ${}^{1}/_{r^2}$ relative to ${}^{1}/_{r}$ for ion-ion interactions. This implies that ion-dipole interactions possess much weaker strength when compared to ion-ion interactions.[200] Biopolymers such as polysaccharides in this study possess the intrinsic ability to be neutral or charged according to the type of synthetic modification. The charge is dependent on their isoelectric point and pH of the solution. At pH values above their isoelectric point, the surface of the biopolymers are often negatively charged and they interact with positively charged molecules via electrostatic interaction. On the contrary, at pH values below their isoelectric point, their surface is positively charged and electrostatic interaction with negatively charged species become predominant. In this study, the surface of the biopolymers are characterized by a negative charge at alkaline pH conditions that vary according to cross-linking, surface functionalization and composite formation. Synthetic modification was necessary to enhance the uptake of negatively charged naphthenates at alkaline pH conditions.

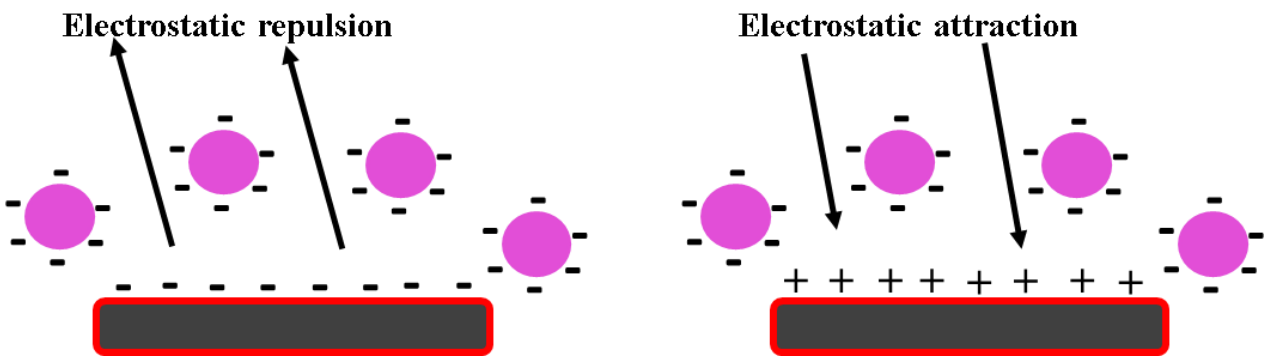

Scheme 1.11: Electrostatic interaction between oppositely and similarly charged species.

1.8.1.4 Hydrophobic Effects

The tendency of nonpolar molecules to stick together with the aim of reducing their interaction with the aqueous solution gives rise to the attractive force known as hydrophobic effects.[201,202] It is a solvent-induced attractive force between apolar molecules in aqueous solution such that the solvent avoids entropically unfavorable interactions with apolar molecules. This interaction is the driving force for the removal of hydrophobic molecules from aqueous solutions as well as the aggregation or formation of micelles by amphiphilic molecules.[201] Hydrophobic effects are important because it drives *in vivo* and adsorption processes, enzyme-substrate interactions and lipids assembly in biomembranes.[202] Thermodynamically, the transfer of a hydrophobic molecule to a polar solvent is an exothermic process. The exothermic nature of the process relates to the formation of a solvent cage around the hydrophobic species as a result of the formation of new hydrogen bonds among the solvent molecules. The initial stage of the process leads to a decrease in entropy of the system due to the formation of a very large number of small solvent cages. However, as the hydrophobic molecule begin to cluster, some of the solvent cages are destroyed and more solvent molecules become free to move (*cf.* Scheme 1.12). The outcome of the formation of large aggregates of hydrophobic molecules is an increase in entropy of the

system due to a decrease in the ordering of the solvent molecules.[203] The entropy increase and exothermic nature of the process makes $\Delta_{ads}G^{o}$ negative, and according to equation 1.18, a negative $\Delta_{ads}G^{o}$ affords a spontaneous process.

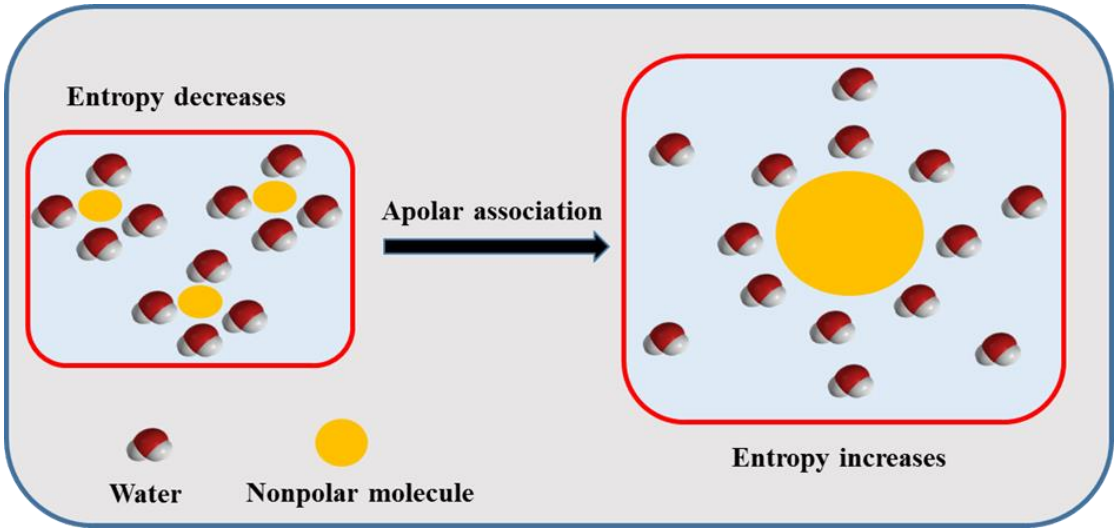

Scheme 1.12: Illustration of apolar association due to hydrophobic effects

The hydrophobicity of biopolymers may be evaluated using their hydrophile-lipophile balance (HLB). HLB is a numerical system used to express the relative amounts of hydrophilic (polar) and lipophilic (apolar) groups in a biopolymer. The HLB concept was proposed by Griffin in 1949 and is a good method for the selection of suitable surfactants for applications such as emulsion formation.[204] Though it is mostly applied for surfactants, it may also be used for biopolymers based on the nature of the functional groups available in the biopolymer. For instance, a biopolymer whose dominant functional groups are hydrophilic is expected to exhibit greater hydration in water relative to a biopolymer with more apolar groups. The biopolymers used in this study possess abundant hydroxyl groups on the surface while the hydrophobic domains may reside within the biopolymer depending on its tertiary structure, hence they are considered to be very hydrophilic. The hypothesis used in this study relate to methods of modification such as cross-

linking, surface functionalization and composite formation that will alter the HLB of the polymers toward apolar domains to favor the removal of naphthenates with greater lipophile (apolar) character from water.

1.9 Organization and Scope

The main objective of this Ph.D. thesis research concern the development of biopolymer sorbent materials for the removal of NAFCs from aqueous solution. Modification of the biopolymers was based on the following themes: *i)* modification of cellulose and chitosan based biopolymers through cross-linking, *ii)* modification of cellulose via surface functionalization, *iii)* development of composite materials based on cellulose and chitosan and *iv*) sorption of NAFCs using cellulose and chitosan based polymers. The thesis is divided into 8 chapters. Chapter 1 is the introduction, chapters 2 – 6 consist of formatted and edited published articles and manuscript in preparation, while chapter 8 consist of integrated discussion of manuscript chapters, concluding remarks and proposed future research work. The published articles and manuscript in preparation are outlined below:

1. Mohamed, M. H; **Udoetok**, **I. A;** Wilson, L. D; Headley, J. V. Fractionation of Carboxylate Anions from Aqueous Solution using Chitosan Cross-linked Sorbent Materials. *RSC Adv*, **2015**, 5, 82065-82077. **(Chapter 2).**
2. **Udoetok**, **I. A;** Dimmick, R. M; Wilson, L. D; Headley, J. V. Adsorption Properties of Cellulose-Epichlorohydrin Copolymers in Aqueous Solution. *Carbohyd Polym*, **2016**, 136, 329-340 **(Chapter 3)**.
3. **Udoetok**, **I. A;** Wilson, L. D; Headley, J. V. Ultra-Sonication Assisted Synthesis of Cross-linked Cellulose Polymers. *Ultrason Sonochem* **2018**, 42, 567-576 **(Chapter 4).**

4. **Udoetok, I. A;** Wilson, L. D; Headley, J. V. Quaternized Cellulose Hydrogels as Sorbent Materials for the Uptake of Naphthenic Acids from Aqueous Solution. *Materials,* **2016***,* 9(8):645 **(Chapter 5).**
5. **Udoetok, I. A**; Wilson, L. D; Headley, J. V. Self-Assembled and Cross-Linked Animal and Plant-Based Polysaccharides: Chitosan–Cellulose Composites and Their Anion Uptake Properties. *ACS Appl. Mater. Interfaces*, **2016**, 8 (48), 33197–33209 (**Chapter 6)**.
6. **Udoetok, I. A;** Wilson, L. D; Headley. Amphiphilic Iron Doped Chitosan- Carboxymethyl Cellulose Composites for Anion Uptake. Manuscript in preparation **(Chapter 7)**.

A short summary of the research work and a description of the contributions of each author are presented in each chapter. Additionally, the justification of the completion of the general objectives of the Ph.D. thesis are also included.

Chapter 1 provides an overview of the various concepts used in the Ph. D. thesis as well as the knowledge gaps, hypotheses and objectives of the thesis. The literature review of the concepts in the thesis are presented within the chapters.

Chapter 2 presents the modification of chitosan via cross-linking. Chitosan was cross-linked with glutaraldehyde and the cross-linked polymers characterized using FTIR spectroscopy and TGA. The results revealed that the cross-linked chitosan (**CH-GL**) polymers exhibited tunable properties according to the cross-linker feed ratio, where the polymer with highest cross-linker feed ratio displayed the optimum sorption capacity. However, the sorption affinity of the **CH-GL** polymers was suspected to attenuate due to the collapse of the pore structure as well as charge screening at alkaline pH conditions.

Chapter 3 reports the cross-linking of cellulose in an effort to overcome the shortcomings of cross-linking that was reported in chapter 2. The collapse of the pore structure and charge screening at alkaline pH conditions attenuated the sorption properties of the C-EP polymers. Cellulose was cross-linked with EP at variable levels from low to high, in order to determine the effects of cross-linking on the morphology, textural and absorption properties of the cross-linked cellulose (**C-EP**) polymers. The **C-EP** polymers were characterized by TGA and FTIR spectroscopy, pH at the point of zero charge (pH_{pzc}), water swelling, and dye-adsorption methods that employ two types of dyes [phenolphthalein (phth) and *p*-nitrophenol (PNP)]. The results revealed that the **C-EP** polymers displayed tunable morphology and adsorption properties in accordance with the level of cross-linking, where the surface of the biopolymers were negatively charged at alkaline pH conditions. The uptake properties of the **C-EP** polymers reported in this chapter were lower than that of **CH-GL** polymers reported in chapter 2. This was attributed to inefficient pillaring of cellulose due to strong inter-/intra-molecular hydrogen bonding in the biopolymer and the negative surface charge of the **C-EP** polymers at alkaline pH conditions.

Chapter 4 presents the cross-linking of cellulose with EP/aqueous ammonia via the conventional heating and stirring method as well as the application of sonication. It was designed to overcome the challenge of inefficient *pillaring* of cellulose due to strong inter-/intra-molecular hydrogen bonding within the biopolymer. The modified cellulose materials, **C-EP heating** and **C-EP sonication**, were characterized via FTIR and ^{13}C solids NMR spectroscopy, differential scanning calorimetry (DSC) and TGA studies. The results revealed cross-linked cellulose with variable modification according to the synthetic procedure. The different synthetic routes produced modified biopolymers with different morphology, equilibrium swelling and adsorption

properties. These polymers exhibited greater sorption affinity with NAFCs at both alkaline and acidic pH conditions, relative to the **C-EP** polymers reported in chapter 3.

Chapter 5 reports the grafting of quaternary ammonium ions on the surface of cellulose, to overcome the challenge of charge repulsion between anions and the biopolymer surface of systems reported in chapters 2 and 3. Cellulose hydrogels were prepared by cross-linking cellulose with EP and/or functionalization with glycidyl trimethyl ammonium chloride (GTAC). The hydrogels were characterized via CHN analysis, TGA, and FTIR/^{13}C solids NMR spectroscopy. The results indicated that the hydrogels exhibited enhanced thermal stability and sorption properties relative to native cellulose. An improved sorption capacity of the hydrogels relative to **C-EP**, **C-EP heating** and **C-EP sonication** polymers reported in chapters 3 and 4 support the claim that the adsorption properties of **C-EP** polymers were limited by a negative surface charge at alkaline pH conditions.

Chapter 6 presents the preparation of cross-linked chitosan/cellulose glutaraldehyde composite materials (**CH-GL-C**). The chapter builds on the findings from chapters 1 and 2, where the collapse of the pore structure of cross-linked chitosan and inefficient pillaring of cellulose attenuated the sorption properties of the **CH-GL** and **C-EP** polymers. It was hypothesized that the mechanical strength of cellulose may support the pore structure of cross-linked chitosan when a composite of the two biopolymers undergoes cross-linking. The composite materials were characterized using physicochemical parameters related to the adsorption properties. The results obtained indicated that the composite materials display variable morphology and adsorption properties according to the cross-linker feed ratio, where the composite with higher cross-linker feed ratio (**CH-GL3-C**) revealed optimum sorption properties. The results reported in this chapter support the earlier hypothesis that the mechanical strength of cellulose due to its rigidity may

support the pore structure of cross-linked chitosan. This is evidenced by greater sorption capacity of the **CH-GL-C** composites relative to single component **CH-GL** and **C-EP** polymers. Though the composite materials showed greater sorption properties than their precursors, **CH-GL** and **C-EP** polymers, the role of charge screening was inferred and may have attenuated the sorption affinity for NAFCs at alkaline pH conditions.

In chapter 7, quaternary (**CH-GL-CC-Fe**) and ternary (**CH-CC-Fe**) composite materials were prepared from carboxymethyl cellulose (CC), chitosan (CH), glutaraldehyde (GL) and iron (III) species (Fe). Iron (III) doping of materials was executed to bridge the knowledge gap from the study reported in chapter 6, where the negative surface charge of **CH-GL-C** polymers attenuated their sorption affinity for NAFCs at alkaline pH conditions. Characterization of the composites through FTIR and TGA studies provided support that successful composite formation between the anionic and cationic polysaccharides occurred with Fe (III) species. ICP-OES and SEM results provided further evidence of a variable iron doping and morphology for the composite materials. The results presented in this chapter reveal that the introduction of Lewis acid species onto the composite materials enhanced the sorption capacity of the composites, and supports the claim that charge screening may have attenuated the sorption capacity of the **CH-GL-C** composite materials. The **CH-GL-CC-Fe** composite had the highest sorption capacity with **S6** and OSPW naphthenates relative to the other polymers reported in this thesis.

Chapter 8 presents integrated discussion of manuscript chapters, concluding remarks and proposed future work.

1.10 References

1. Masliyah, J.; Zhou, Z. J.; Xu, Z. H.; Czarnecki, J.; Hamza, H. *Can. J. Chem. Eng.* **2004,** *82* (4), 628-654.
2. Clark, K. A.; Pasternack, D. S. *Ind. Eng. Chem.* **1932,** *24*, 1410-1416.
3. Rao, F.; Liu, Q. *Energy Fuels* **2013,** *27* (12), 7199-7207.
4. Allen, E. W. *J. Environ. Eng. Sci.* **2008,** *7* (2), 123-138.
5. Nix, P. G.; Martin, R. W. *Environ. Toxicol. Water Qual.* **1992,** *7* (2), 171-188.
6. Giesy, J. P.; Anderson, J. C.; Wiseman, S. B. *Proc. Natl. Acad. Sci.* **2010,** *107* (3), 951-952.
7. Leishman, C.; Widdup, E. E.; Quesnel, D. M.; Chua, G.; Gieg, L. M.; Samuel, M. A.; Muench, D. G. *Chemosphere* **2013,** *93* (2), 380-387.
8. Bartlett, A. J.; Frank, R. A.; Gillis, P. L.; Parrott, J. L.; Marentette, J. R.; Brown, L. R.; Hooey, T.; Vanderveen, R.; McInnis, R.; Brunswick, P.; Shang, D.; Headley, J. V.; Peru, K. M.; Hewitt, L. M. *Environ. Pollut.* **2017,** *227*, 271-279.
9. Scarlett, A. G.; West, C. E.; Jones, D.; Galloway, T. S.; Rowland, S. J. *Sci. Total Environ.* **2012,** *425*, 119-127.
10. Dzidic, I.; Somerville, A. C.; Raia, J. C.; Hart, H. V. *Anal. Chem.* **1988,** *60* (13), 1318-1323.
11. Fan, T. P. *Energy Fuels* **1991,** *5* (3), 371-375.
12. Wong, D. C. L.; van Compernolle, R.; Nowlin, J. G.; O'Neal, D. L.; Johnson, G. M. *Chemosphere* **1996,** *32* (8), 1669-1679.
13. St. John, W. P.; Rughani, J.; Green, S. A.; McGinnis, G. D. *J. Chromatogr. A* **1998,** *807* (2), 241-251.
14. Hsu, C. S.; Dechert, G. J.; Robbins, W. K.; Fukuda, E. K. *Energy Fuels* **1999,** *14* (1), 217-223.
15. Grewer, D. M.; Young, R. F.; Whittal, R. M.; Fedorak, P. M. *Sci. Total Environ.* **2010,** *408* (23), 5997-6010.
16. Headley, J. V.; Barrow, M. P.; Peru, K. M.; Derrick, P. J. *J. Environ. Sci. Health., Part A* **2011,** *46* (8), 844-854.
17. Headley, J. V.; Peru, K. M.; Janfada, A.; Fahlman, B.; Gu, C.; Hassan, S. *Rapid Commun. Mass Spectrom.* **2011,** *25* (3), 459-462.

18. Headley, J. V.; Peru, K. M.; Barrow, M. P. *Mass Spectrom. Rev.* **2009,** *28* (1), 121-134.

19. Headley, J. V.; Peru, K. M.; Mohamed, M. H.; Frank, R. A.; Martin, J. W.; Hazewinkel, R. R. O.; Humphries, D.; Gurprasad, N. P.; Hewitt, L. M.; Muir, D. C. G.; Lindeman, D.; Strub, R.; Young, R. F.; Grewer, D. M.; Whittal, R. M.; Fedorak, P. M.; Birkholz, D. A.; Hindle, R.; Reisdorph, R.; Wang, X.; Kasperski, K. L.; Hamilton, C.; Woudneh, M.; Wang, G.; Loescher, B.; Farwell, A.; Dixon, D. G.; Ross, M.; Pereira, A. D. S.; King, E.; Barrow, M. P.; Fahlman, B.; Bailey, J.; McMartin, D. W.; Borchers, C. H.; Ryan, C. H.; Toor, N. S.; Gillis, H. M.; Zuin, L.; Bickerton, G.; McMaster, M.; Sverko, E.; Shang, D.; Wilson, L. D.; Wrona, F. J. *J. Environ. Sci. Health., Part A* **2013,** *48* (10), 1145-1163.

20. Brient, J. A.; Wessner, P. J.; Doyle, M. N., Naphthenic Acids. **2000**.

21. Headley, J. V.; McMartin, D. W. *J. Environ. Sci. Health., Part A* **2004,** *39* (8), 1989-2010.

22. Clemente, J. S.; Prasad, N. G.; MacKinnon, M. D.; Fedorak, P. M. *Chemosphere* **2003,** *50* (10), 1265-1274.

23. Headley, J. V.; Peru, K. M.; McMartin, D. W.; Winkler, M. *J. AOAC Int.* **2002,** *85* (1), 182-187.

24. Herman, D. C.; Fedorak, P. M.; MacKinnon, M. D.; Costerton, J. W. *Can. J. Microbiol.* **1994,** *40* (6), 467-477.

25. Mohamed, M. H.; Wilson, L. D.; Peru, K. M.; Headley, J. V.*J. Colloid Interface Sci.* **2013,** *395*, 104-110.

26. Headley, J. V.; McMartin, D. W. *J. Environ. Sci. Health A Tox. Hazard Subst. Environ. Eng.* **2004,** *39* (8), 1989-2010.

27. Roberts, D. W. *Sci. Total Environ.* **1991,** *109-110*, 557-568.

28. Rogers, V. V. *Toxicol. Sci.* **2002,** *66* (2), 347-355.

29. Rowland, S. J.; West, C. E.; Jones, D.; Scarlett, A. G.; Frank, R. A.; Hewitt, L. M. *Environ. Sci. Technol.* **2011,** *45* (22), 9806-9815.

30. Leung, S. S.-C.; MacKinnon, M. D.; Smith, R. E. H. *Environ. Toxicol. Chem.* **2001,** *20* (7), 1532-1543.

31. Nero, V.; Farwell, A.; Lee, L. E. J.; Van Meer, T.; MacKinnon, M. D.; Dixon, D. G. *Ecotoxicol. Environ. Saf.* **2006,** *65* (2), 252-264.

32. Kavanagh, R. J.; Frank, R. A.; Oakes, K. D.; Servos, M. R.; Young, R. F.; Fedorak, P. M.; MacKinnon, M. D.; Solomon, K. R.; Dixon, D. G.; Van Der Kraak, G. *Aquat. Toxicol.* **2011,** *101* (1), 214-220.

33. Rockhold, W. T. *Arch. Indust. Health* **1955,** *12* (5), 477-482.

34. Mohamed, M. H.; Wilson, L. D.; Headley, J. V. *J. Phys. Chem. B* **2013,** *117* (13), 3659-3666.

35. Mohamed, M. H.; Wilson, L. D.; Headley, J. V.; Peru, K. M. *J. Colloid Interface Sci.* **2011,** *356* (1), 217-226.

36. Mohamed, M. H.; Wilson, L. D.; Headley, J. V.; Peru, K. M. *Chemosphere* **2015,** *136*, 252-258.

37. Quinlan, P. J.; Grishkewich, N.; Tam, K. C. *Can. J. Chem. Eng.* **2017,** *95* (1), 21-32.

38. Gamal El-Din, M.; Fu, H.; Wang, N.; Chelme-Ayala, P.; Pérez-Estrada, L.; Drzewicz, P.; Martin, J. W.; Zubot, W.; Smith, D. W. *Sci. Total Environ.* **2011,** *409* (23), 5119-5125.

39. Frankel, M. L.; Bhuiyan, T. I.; Veksha, A.; Demeter, M. A.; Layzell, D. B.; Helleur, R. J.; Hill, J. M.; Turner, R. J. *Bioresour. Technol.* **2016,** *216*, 352-361.

40. Kannel, P. R.; Gan, T. Y. *J. Environ. Sci. Health., Part A* **2012,** *47* (1), 1-21.

41. Mohamed, M. H.; Wilson, L. D.; Headley, J. V.; Peru, K. M. *Phys. Chem. Chem. Phys.* **2011,** *13* (3), 1112-1122.

42. Del Rio, L. F.; Hadwin, A. K.; Pinto, L. J.; MacKinnon, M. D.; Moore, M. M. *J Appl Microbiol* **2006,** *101* (5), 1049-1061.

43. Yue, S.; Ramsay, B. A.; Wang, J.; Ramsay, J. A. *Sci. Total Environ.* **2016,** *572*, 273-279.

44. Xue, J.; Zhang, Y.; Liu, Y.; Gamal El-Din, M. *RSC Adv.* **2017,** *7* (29), 17670-17681.

45. Quesnel, D. M.; Oldenburg, T. B. P.; Larter, S. R.; Gieg, L. M.; Chua, G. *Environ. Sci. Technol.* **2015,** *49* (21), 13012-13020.

46. Mishra, S.; Meda, V.; Dalai, A. K.; McMartin, D. W.; Headley, J. V.; Peru, K. M. *J. Water Resource Prot.* **2010,** *02* (07), 644-650.

47. McMartin, D. W.; Headley, J. V.; Friesen, D. A.; Peru, K. M.; Gillies, J. A. *J. Environ. Sci. Health., Part A* **2004,** *39* (6), 1361-1383.

48. Afzal, A.; Drzewicz, P.; Pérez-Estrada, L. A.; Chen, Y.; Martin, J. W.; Gamal El-Din, M. *Environ. Sci. Technol.* **2012,** *46* (19), 10727-10734.

49. Leshuk, T.; Wong, T.; Linley, S.; Peru, K. M.; Headley, J. V.; Gu, F. *Chemosphere* **2016,** *144*, 1854-1861.

50. Al jibouri, A. K. H.; Wu, J. *Environ. Sci. Pollut. Res.* **2015,** *22* (4), 2558-2565.

51. Klamerth, N.; Moreira, J.; Li, C.; Singh, A.; McPhedran, K. N.; Chelme-Ayala, P.; Belosevic, M.; Gamal El-Din, M. *Sci. Total Environ.* **2015,** *506-507*, 66-75.

52. Pérez-Estrada, L. A.; Han, X.; Drzewicz, P.; Gamal El-Din, M.; Fedorak, P. M.; Martin, J. W. *Environ. Sci. Technol.* **2011,** *45* (17), 7431-7437.

53. Wang, N.; Chelme-Ayala, P.; Perez-Estrada, L.; Garcia-Garcia, E.; Pun, J.; Martin, J. W.; Belosevic, M.; Gamal El-Din, M. *Environ. Sci. Technol.* **2013,** *47* (12), 6518-6526.

54. Aher, A.; Papp, J.; Colburn, A.; Wan, H.; Hatakeyama, E.; Prakash, P.; Weaver, B.; Bhattacharyya, D. *Chem. Eng. J.* **2017,** *327*, 573-583.

55. Gaikar, V. G.; Maiti, D. *React. Funct. Polym.* **1996,** *31* (2), 155-164.

56. Niasar, H. S.; Li, H.; Kasanneni, T. V. R.; Ray, M. B.; Xu, C. *Chem. Eng. J.* **2016,** *293*, 189-199.

57. Martinez-Iglesias, A.; Niasar, H. S.; Xu, C.; Ray, M. B. *Adsorpt. Sci. Technol.* **2015,** *33* (10), 881-894.

58. Iranmanesh, S.; Harding, T.; Abedi, J.; Seyedeyn-Azad, F.; Layzell, D. B *J. Environ. Sci. Health A Tox. Hazard Subst. Environ. Eng.* **2014,** *49* (8), 913-922.

59. Islam, M. S.; Zhang, Y.; McPhedran, K. N.; Liu, Y.; Gamal El-Din, M. *J. Environ. Manage.* **2015,** *152*, 49-57.

60. Yan, L. X. M. R. H. F. L. *China Pet. Process Pe.* **2017,** *19* (1), 123-134

61. Zou, L.; Han, B.; Yan, H.; Kasperski, K. L.; Xu, Y.; Hepler, L. G. *J. Colloid Interface Sci.* **1997,** *190* (2), 472-475.

62. Saab, J.; Mokbel, I.; Razzouk, A. C.; Ainous, N.; Zydowicz, N.; Jose, J. *Energy Fuels* **2005,** *19* (2), 525-531.

63. Janfada, A.; Headley, J. V.; Peru, K. M.; Barbour, S. L. *J. Environ. Sci. Health., Part A* **2006,** *41* (6), 985-997.

64. Mohamed, M. H.; Wilson, L. D.; Headley, J. V.; Peru, K. M. *Process Saf. Environ. Prot.* **2008,** *86* (4), 237-243.

65. Mohamed, M. H.; Wilson, L. D.; Headley, J. V.; Peru, K. M. *Rapid Commun. Mass Spectrom.* **2009,** *23* (23), 3703-3712.

66. Headley, J. V.; Peru, K. M.; Mohamed, M. H.; Wilson, L.; McMartin, D. W.; Mapolelo, M. M.; Lobodin, V. V.; Rodgers, R. P.; Marshall, A. G. *Energy Fuels* **2013,** *27* (4), 1772-1778.

67. Wilson, L. D.; Mohamed, M. H.; Headley, J. V. *Rev. Environ. Health* **2014**, 29(1-2):5-8.

68. Pourrezaei, P.; Alpatova, A.; Chelme-Ayala, P.; Perez-Estrada, L. A.; Jensen-Fontaine, M.; Le, X. C.; Gamal El-Din, M. Int. J. Environ. Sci. Te. **2013,** *11* (7), 2037-2050.

69. Zubot, W.; MacKinnon, M. D.; Chelme-Ayala, P.; Smith, D. W.; Gamal El-Din, M. *Sci. Total Environ.* **2012,** *427-428*, 364-372.

70. Keleşoğlu, S.; Volden, S.; Kes, M.; Sjöblom, J. *Energy Fuels* **2012,** *26* (8), 5060-5068.

71. Azad, F. S.; Abedi, J.; Iranmanesh, S. *J. Environ. Sci. Health., Part A* **2013,** *48* (13), 1649-1654.

72. Balmasova, O. V.; Ramazanova, A. G.; Korolev, V. V. *Russ. J. Phys. Chem. A* **2015,** *89* (3), 487-490.

73. Shah, S. N.; Lethesh, K. C.; Abdul Mutalib, M. I.; Mohd Pilus, R. B *Chem. Prod. Process Model* **2015,** *10* (4).

74. Teklebrhan, R. B.; Jian, C.; Choi, P.; Xu, Z.; Sjöblom, J. *J. Phys. Chem. B* **2016,** *120* (50), 12901-12910.

75. Ma, L. L.; Chen, X. *Russ. J. Phys. Chem. B* **2016,** *10* (6), 1027-1031.

76. Arshad, M.; Khosa, M. A.; Siddique, T.; Ullah, A. *Chemosphere* **2016,** *163*, 334-341.

77. Bhuiyan, T. I.; Tak, J. K.; Sessarego, S.; Harfield, D.; Hill, J. M. *Chemosphere* **2017,** *168*, 1337-1344.

78. Nascimento, G. E. D.; Duarte, M. M. M. B.; Sales, D. C. S.; Barbosa, C. M. B. D. M. *Chem. Eng. Commun.* **2016,** *204* (1), 105-110.

79. Kaith, B. S.; Mittal, H.; Bhatia, J. K.; Kalia, S., Polysaccharide Graft Copolymers – Synthesis, Properties and Applications. In *Biopolymers*, John Wiley & Sons, Inc.: 2011; pp 35-57.

80. Pillai, C. K. S.; Paul, W.; Sharma, C. P. *Prog. Polym. Sci.* **2009,** *34* (7), 641-678.

81. Kumar, M. N. V. R., *A review of chitin and chitosan applications*. Elsevier Science B.V.: 2000.

82. Islam, S.; Bhuiyan, M. A. R.; Islam, M. N. *J. Polym. Environ.* **2016,** *25* (3), 854-866.

83. Qaroush, A. K.; Assaf, K. I.; Bardaweel, S. K.; Al-Khateeb, A.; Alsoubani, F.; Al-Ramahi, E.; Masri, M.; Bruck, T.; Troll, C.; Rieger, B.; Eftaiha, A. F. *Green Chemistry* **2017,** *19* (18), 4305-4314.

84. Qinna, N.; Karwi, Q.; Al-Jbour, N.; Al-Remawi, M.; Alhussainy, T.; Al-So'ud, K.; Omari, M.; Badwan, A. *Marine Drugs* **2015,** *13* (4), 1710-1725.

85. Younes, I.; Rinaudo, M. *Marine Drugs* **2015,** *13* (3), 1133-1174.

86. Rinaudo, M. *Polym. Int.* **2008,** *57* (3), 397-430.

87. Khor, E.; Lim, L. Y. *Biomaterials* **2003,** *24* (13), 2339-2349.

88. Sahoo, D.; Nayak, P. L., Chitosan: The Most Valuable Derivative of Chitin. In *Biopolymers*, John Wiley & Sons, Inc.: 2011; pp 129-166.

89. Patashnk, S.; Rabinovich, L.; Golomb, G. *J. Drug Target* **2009,** *4* (6), 371-380.

90. Qiu, X.; Hu, S. *Materials* **2013,** *6* (3), 738-781.

91. Yamazawa, A.; Iikura, T.; Shino, A.; Date, Y.; Kikuchi, J. *Molecules* **2013,** *18* (8), 9021-9033.

92. Klemm, D.; Heublein, B.; Fink, H.-P.; Bohn, A. *Angew. Chem. Int. Ed.* **2005,** *44* (22), 3358-3393.

93. Boufi, S.; Alila, S., Modified Cellulose Fibres as a Biosorbent for the Organic Pollutants. **2011**, 483-524.

94. Cai, J.; Zhang, L. *Macromol. Biosci.* **2005,** *5* (6), 539-548.

95. Qin, X.; Lu, A.; Zhang, L. *J. Appl. Polym. Sci.* **2012,** *126* (S1), E470-E477.

96. Zhou, J.; Zhang, L. *Polym. J.* **2000,** *32* (10), 866-870.

97. Wang, H.; Gurau, G.; Rogers, R. D. *Chem. Soc. Rev.* **2012,** *41* (4), 1519.

98. Swatloski, R. P.; Spear, S. K.; Holbrey, J. D.; Rogers, R. D. *J. Am. Chem. Soc.* **2002,** *124* (18), 4974-4975.

99. Moulthrop, J. S.; Swatloski, R. P.; Moyna, G.; Rogers, R. D. *Chem. Commun.* **2005,** (12), 1557-1559.

100. Siqueira, G.; Bras, J.; Dufresne, A. *Polymers* **2010,** *2* (4), 728-765.

101. Chang, C.; Lue, A.; Zhang, L. *Macromol. Chem. Phys.* **2008,** *209* (12), 1266-1273.

102. Metodiev, A., Electric Properties of Carboxymethyl Cellulose. **2013**.

103. Sen, G.; Sharon, A.; Pal, S., Grafted Polysaccharides: Smart Materials of the Future, Their Synthesis and Applications. In *Biopolymers*, John Wiley & Sons, Inc.: 2011; pp 99-127.

104. Kalia, S.; Avérous, L., *Biopolymers: Biomedical and Environmental Applications*. Wiley: 2011.

105. Martinez, A. W.; Caves, J. M.; Ravi, S.; Li, W.; Chaikof, E. L. *Acta Biomater.* **2014,** *10* (1), 26-33.

106. Koide, T.; Daito, M. *Dent. Mater. J.* **1997,** *16* (1), 1-9,109.

107. Reddy, N.; Reddy, R.; Jiang, Q. *Trends Biotechnol.* **2015,** *33* (6), 362-369.

108. Rimdusit, S.; Somsaeng, K.; Kewsuwan, P.; Jubsilp, C.; Tiptipakorn, S. *Eng. J.* **2012,** *16* (4), 15-28.

109. Coma, V.; Sebti, I.; Pardon, P.; Pichavant, F. H.; Deschamps, A. *Carbohydr. Polym.* **2003,** *51* (3), 265-271.

110. Mao, Z.; Gao, C.; Wang, D.; Ma, L.; Shen, J. *J. Bioact. Compat. Polym.* **2016,** *19* (5), 353-365.

111. Hennink, W. E.; van Nostrum, C. F. *Adv. Drug Deliv. Rev.* **2012,** *64*, 223-236.

112. Jiang, Q.; Reddy, N.; Zhang, S.; Roscioli, N.; Yang, Y.*J. Biomed. Mater. Res. A* **2013,** *101A* (5), 1237-1247.

113. Umashankar, P. R.; Kumari, T. V.; Mohanan, P. V. *Toxicol Int.* **2012,** *19* (1), 51.

114. Lai, J.Y. *RSC Adv.* **2014,** *4* (36), 18871-18880.

115. Meng, L.; Arnoult, O.; Smith, M.; Wnek, G. E. *J. Mater. Chem.* **2012,** *22* (37), 19412.

116. Bazaka, K.; Jacob, M. V.; Crawford, R. J.; Ivanova, E. P., *Acta Biomater.* **2011,** *7* (5), 2015-2028.

117. Tallawi, M.; Rosellini, E.; Barbani, N.; Cascone, M. G.; Rai, R.; Saint-Pierre, G.; Boccaccini, A. R. *J. R. Soc. Interface* **2015,** *12* (108), 20150254.

118. Gruber, E.; Granzow, C.; Ott, T., Cationization of Cellulose Fibers in View of Applications in the Paper Industry. **1998,** *688*, 94-106.

119. Xu, X.; Gao, B.; Wang, W.; Yue, Q.; Wang, Y.; Ni, S. *Colloids Surf. B Biointerfaces* **2009,** *70* (1), 46-52.

120. Abitbol, T.; Marway, H.; Cranston, E. D. *Nord. Pulp Pap. Res. J.* **2014,** *29* (1), 46-57.

121. Chaker, A.; Boufi, S. *Carbohydr. Polym.* **2015,** *131*, 224-232.

121. Song, Y.; Zhang, L.; Gan, W.; Zhou, J.; Zhang, L. *Colloids Surf. B Biointerfaces* **2011,** *83* (2), 313-320.

123. Saini, S.; Yücel Falco, Ç.; Belgacem, M. N.; Bras, J. *Carbohydr. Polym.* **2016,** *135*, 239-247.

124. Yan, L.; Tao, H.; Bangal, P. R. *Clean* **2009,** *37* (1), 39-44.

125. Chang, C.; Zhang, L. *Carbohydr. Polym.* **2011,** *84* (1), 40-53.

126. Marcasuzaa, P.; Reynaud, S.; Ehrenfeld, F.; Khoukh, A.; Desbrieres, J. *Biomacromolecules* **2010,** *11* (6), 1684-1691.

127. El-Hag Ali, A.; Abd El-Rehim, H. A.; Hegazy, E.-S. A.; Ghobashy, M. M. *Radiat. Phys. Chem.* **2006,** *75* (9), 1041-1046.

128. Hebeish, A.; Higazy, A.; El-Shafei, A.; Sharaf, S. *Carbohydr. Polym.* **2010,** *79* (1), 60-69.

129. Shang, J.; Shao, Z.; Chen, X. *Polymer* **2008,** *49* (25), 5520-5525.

130. Long, D. D.; Luyen, D. V. *J. Macromol. Sci., Pure Appl. Chem.* **1996,** *33* (12), 1875-1884.

131. Işiklan, N. *J. Appl. Polym. Sci.* **2006,** *99* (4), 1310-1319.

132. Sannino, A.; Madaghiele, M.; Conversano, F.; Mele, G.; Maffezzoli, A.; Netti, P. A.; Ambrosio, L.; Nicolais, L. *Biomacromolecules* **2004,** *5* (1), 92-96.

133. Chang, C.; Duan, B.; Zhang, L. *Polymer* **2009,** *50* (23), 5467-5473.

134. Krishna Rao, K. S. V.; Subha, M. C. S.; Vijaya Kumar Naidu, B.; Sairam, M.; Mallikarjuna, N. N.; Aminabhavi, T. M. *J. Appl. Polym. Sci.* **2006,** *102* (6), 5708-5718.

135. Brugnerotto, J.; Lizardi, J.; Goycoolea, F. M.; Argüelles-Monal, W.; Desbrières, J.; Rinaudo, M. *Polymer* **2001,** *42* (8), 3569-3580.

136. KacurÃ¡kovÃ¡, M. *Carbohydr. Polym.* **2001,** *44* (4), 291-303.

137. Kizil, R.; Irudayaraj, J.; Seetharaman, K. *J. Agric. Food. Chem.* **2002,** *50* (14), 3912-3918.

138. Lawrie, G.; Keen, I.; Drew, B.; Chandler-Temple, A.; Rintoul, L.; Fredericks, P.; Grøndahl, L. *Biomacromolecules* **2007,** *8* (8), 2533-2541.

139. Zhu, T.; Tan, S.-c.; Tong, L.-b.; Wang, Y.-q.; Wang, R.-n. 2014 Sixth International Conference on Measuring Technology and Mechatronics Automation (2011) Shangshai, China, IEEE Computer Society, **2011**, 700-703.

140. Černá, M.; Barros, A. S.; Nunes, A.; Rocha, S. l. M.; Delgadillo, I.; Čopíková, J.; Coimbra, M. A., *Carbohydr. Polym.* **2003,** *51* (4), 383-389.

141. Kacuráková, M. *Carbohydr. Polym.* **2000,** *43* (2), 195-203.

142. Kačuráková, M.; Wellner, N.; Ebringerová, A.; Hromádková, Z.; Wilson, R. H.; Belton, P. S. *Food Hydrocolloids* **1999,** *13* (1), 35-41.

143. Stuart, B. H., *Infrared Spectroscopy: Fundamentals and Applications*. Wiley: 2004.

144. Bai, S.; Wang, W.; Dybowski, C. *Anal. Chem.* **2010,** *82* (12), 4917-4924.

145. Laws, D. D.; Bitter, H. M. L.; Jerschow, A., Solid-state NMR spectroscopic methods in chemistry. *Angew. Chem. Int. Ed.* **2002,** *41* (17), 3096-3129.

146. Sienkiewicz, A.; Krasucka, P.; Charmas, B.; Stefaniak, W.; Goworek, J. *J. Therm. Anal. Calorim.* **2017**,130 (1), 85-93

147. Guvendiren, M.; Burdick, J. A.; Yang, S. *Soft Matter* **2010,** *6* (9), 2044-2049.

148. Principles of Thermal Analysis and Calorimetry Edited by P. J. Haines (Oakland Analytical Services, Farnharm, U.K.). Royal Society of Chemistry: Cambridge. 2002. xiv + 220 pp. *J. Am. Chem. Soc.* **2002,** *124* (42), 12629-12629.

149. Lever, T.; Haines, P.; Rouquerol, J.; Charsley, E. L.; Van Eckeren, P.; Burlett, D. J. *Pure Appl. Chem.* **2014,** *86* (4).

150. Vyazovkin, S., Thermogravimetric Analysis. Characterization of Materials. **2012,** 1-12.

151. Leal, G. F.; Ramos, L. A.; Barrett, D. H.; Curvelo, A. A. S.; Rodella, C. B. *Thermochim. Acta* **2015,** *616*, 9-13.

152. Loof, D.; Hiller, M.; Oschkinat, H.; Koschek, K. *Materials* **2016,** *9* (6), 415.

153. Moussout, H.; Ahlafi, H.; Aazza, M.; Bourakhouadar, M. *Polym. Degrad. Stab.* **2016,** *130*, 1-9.

154. Weng, R.; Chen, L.; Lin, S.; Zhang, H.; Wu, H.; Liu, K.; Cao, S.; Huang, L. *Polymers* **2017,** *9* (4), 116.

155. Zengin Kurt, B.; Uckaya, F.; Durmus, Z. *Int. J. Biol. Macromol.* **2017,** *96*, 149-160.

156. Gregorova, A., Application of Differential Scanning Calorimetry to the Characterization of Biopolymers. In *Applications of Calorimetry in a Wide Context - Differential Scanning Calorimetry, Isothermal Titration Calorimetry and Microcalorimetry*, Elkordy, A. A., Ed. InTech: Rijeka, 2013; DOI: 10.5772/53822.

157. Bruylants, G.; Wouters, J.; Michaux, C. *Curr. Med. Chem.* **2005,** *12* (17), 2011-2020.

158. Jelesarov, I.; Bosshard, H. R. *J. Mol. Recognit.* **1999,** *12* (1), 3-18.

159. Teramoto, Y. *Molecules* **2015,** *20* (4), 5487-5527.

160. Tongdeesoontorn, W.; Mauer, L. J.; Wongruong, S.; Sriburi, P.; Rachtanapun, P. *Chem. Cent. J.* **2011,** *5* (1), 6.

161. Xu, B.; Malik, N. S.; Ahmad, M.; Minhas, M. U. *Plos One* **2017,** *12* (2), e0172727.

162. Kamal, H.; Abd-Elrahim, F. M.; Lotfy, S. *J. Radiat. Res. Appl. Sci.* **2014,** *7* (2), 146-153.

163. Barros, S. C.; da Silva, A. A.; Costa, D. B.; Costa, C. M.; Lanceros-Méndez, S.; Maciavello, M. N. T.; Ribelles, J. L. G.; Sentanin, F.; Pawlicka, A.; Silva, M. M. *Cellulose* **2015,** *22* (3), 1911-1929.

164. Hashem, M.; Hauser, P.; Smith, B. *Text. Res. J.* **2016,** *73* (9), 762-766.

165. Monteiro, O. A. C.; Airoldi, C. *Int. J. Biol. Macromol.* **1999,** *26* (2-3), 119-128.

166. Qu, X.; Wirsén, A.; Albertsson, A. C. *Polymer* **2000,** *41* (12), 4589-4598.

167. Thommes, M. *Chem. Ing. Tech.* **2010,** *82* (7), 1059-1073.

168. Alothman, Z. *Materials* **2012,** *5* (12), 2874-2902.

169. Giles, C. H.; MacEwan, T. H.; Nakhwa, S. N.; Smith, D. *J. Chem. Soc. (Resumed)* **1960**, 3973.

170. Inel, O.; Tumsek, F. *Turk. J. Chem.* **2000,** *24* (1), 9-19.

171. Lynam, M. M.; Kilduff, J. E.; Weber, W. J. *J. Chem. Educ.* **1995,** *72* (1), 80.

172. Guo, R.; Wilson, L. D. *J. Colloid Interface Sci.* **2012,** *388* (1), 225-234.

173. Wilson, L. D.; Mohamed, M. H.; Headley, J. V. *J. Colloid Interface Sci.* **2011,** *357* (1), 215-222.

174. Allen, T., Other methods for determining surface area. In *Particle Size Measurement*, Springer Netherlands: Dordrecht, 1990; pp 597-623.

175. Langmuir, I. *J. Am. Chem. Soc.* **1916,** *38* (11), 2221-2295.

176. Freundlich, H. M. F. *J. Phys. Chem.* **1906,** *57A*, 385-470.

177. Foo, K. Y.; Hameed, B. H. *Chem. Eng. J.* **2010,** *156* (1), 2-10.

178. Sips, R. *J. Chem. Phys.* **1948,** *16* (5), 490-495.

179. Zhao, B. C., R.; Mian, H. *Catalogue of Analytical Methods for Naphthenic Acids Related to Oil Sands Operations.*; OSRIN Report No. TR-2.

180. Noestheden, M. R.; Headley, J. V.; Peru, K. M.; Barrow, M. P.; Burton, L. L.; Sakuma, T.; Winkler, P.; Campbell, J. L. *Environ. Sci. Technol.* **2014,** *48* (17), 10264-10272.

181. Mohamed, M.; Wilson, L. *Nanomaterials* **2015,** *5* (2), 969-980.

182. Ata, S.; Imran Din, M.; Rasool, A.; Qasim, I.; Ul Mohsin, I. *J. Anal. Methods Chem.* **2012,** *2012*, 1-8.

183. Iranmanesh, S.; Harding, T.; Abedi, J.; Seyedeyn-Azad, F.; Layzell, D. B. *J. Environ. Sci. Health., Part A* **2014,** *49* (8), 913-922.

184. Mohamed, M. H.; Peru, K. M.; Headley, J. V.; Wilson, L. D. *J. Geosci. Environ. Protect.* **2017,** *05* (06), 214-225.

185. Liu, X.; Lee, D.-J. *Bioresour. Technol.* **2014,** *160*, 24-31.

186. Raja, S.; Yaccone, F. S.; Ravikrishna, R.; Valsaraj, K. T. *J. Chem. Eng. Data* **2002,** *47* (5), 1213-1219.

187. Peng, J.; Headley, J. V.; Barbour, S. L. *Can. Geotech. J.* **2002,** *39* (6), 1419-1426.

188. Tan, K. L.; Hameed, B. H. *J. Taiwan Inst. Chem. Eng. (DNLM)* **2017,** *74*, 25-48.

189. Largitte, L.; Pasquier, R. *Chem. Eng. Res. Des.* **2016,** *109*, 495-504.

190. Saha, P.; Chowdhury, S., Insight Into Adsorption Thermodynamics. **2011**.

191. Al-Rashed, S. M.; Al-Gaid, A. A. *J. Saudi Chem. Soc.* **2012,** *16* (2), 209-215.

192. Mobasherpour, I.; Salahi, E.; Ebrahimi, M. *J. Saudi Chem. Soc.* **2014,** *18* (6), 792-801.

193. Lu, X.; Shao, Y.; Gao, N.; Ding, L. *J. Chem. Eng. Data* **2015,** *60* (5), 1259-1269.

194. Bartell, F. E.; Thomas, T. L.; Fu, Y. *J. Phys. Chem.* **1951,** *55* (9), 1456-1462.

195. Myers, A. L., Thermodynamics of adsorption. In Chemical Thermodynamics for Industry ; Letcher, T. M., Ed.; Royal Society of Chemistry: Cambridge, UK, 2004 **2007**, 243-253.

196. Berger, A. H.; Bhown, A. S. *Energy Procedia* **2011,** *4*, 562-567.

197. Leckband, D.; Israelachvili, J. *Q Rev Biophys* **2001,** *34* (02), 105.

198. Jones, O. G.; McClements, D. J. *Compr. Rev. Food Sci. Food Saf. (DNLM)* **2010,** *9* (4), 374-397.

199. Pitera, J. W.; van Gunsteren, W. F. *J. Am. Chem. Soc.* **2001,** *123* (13), 3163-3164.

200. Adamczyk, Z., Electrostatic Interactions. In *Encyclopedia of Colloid and Interface Science*, Tadros, T., Ed. Springer Berlin Heidelberg: Berlin, Heidelberg, 2013; pp 362-362.

201. Meyer, E. E.; Rosenberg, K. J.; Israelachvili, J. *Proc. Natl. Acad. Sci.* **2006,** *103* (43), 15739-15746.

202. Blokzijl, W.; Engberts, J. B. F. N. *Angew. Chem. Int. Ed.* **1993,** *32* (11), 1545-1579.

203. Atkins, P.; de Paula, J., *Atkins' Physical Chemistry*. OUP Oxford: 2010.

204. Genot, C.; Kabri, T. H.; Meynier, A. **2013**, 150-193.

Chapter 2

(Manuscript 1)

Description

In chapter 2, a study on the cross-linking of chitosan (CH) with glutaraldehyde (GL) at incremental mole ratios is presented. The structure and physicochemical properties of cross-linked polymers were characterized using FTIR, TGA, DSC and nitrogen adsorption studies. The sorption affinity of the **CH-GL** polymers was tested using single component carboxylate anions as well as an equimolar solution containing mixtures of carboxylate anions.

Authors' contribution

I performed the entire synthesis and characterization of the polymers except for particle size analysis, DSC and regeneration studies where M. H. Mohamed assisted along with data analysis. Lee D. Wilson conceived the project and secured funding and John V. Headley contributed mass spectrometry (MS) analysis tools; I wrote the first draft of the manuscript with extensive editing by M. H. Mohammed, Lee D. Wilson and John V. Headley prior to submission for publication. Permission was obtained from all contributing authors before the inclusion of the manuscript in this thesis.

Relation of Manuscript 1 to Overall Objective of this Project

The objective of this project relates to the synthesis and characterization of chitosan-based polymers at incremental cross-linker feed ratios, from low to high values. Another aim of the study was to elucidate the sorption affinity of the synthesized polymers for model naphthenic acid

compounds. These objectives coincide with the first and fourth themes (cross-linking of chitosan and cellulose and sorption studies of NAFCs using these biopolymers) of the thesis objectives.

Graphical Abstract

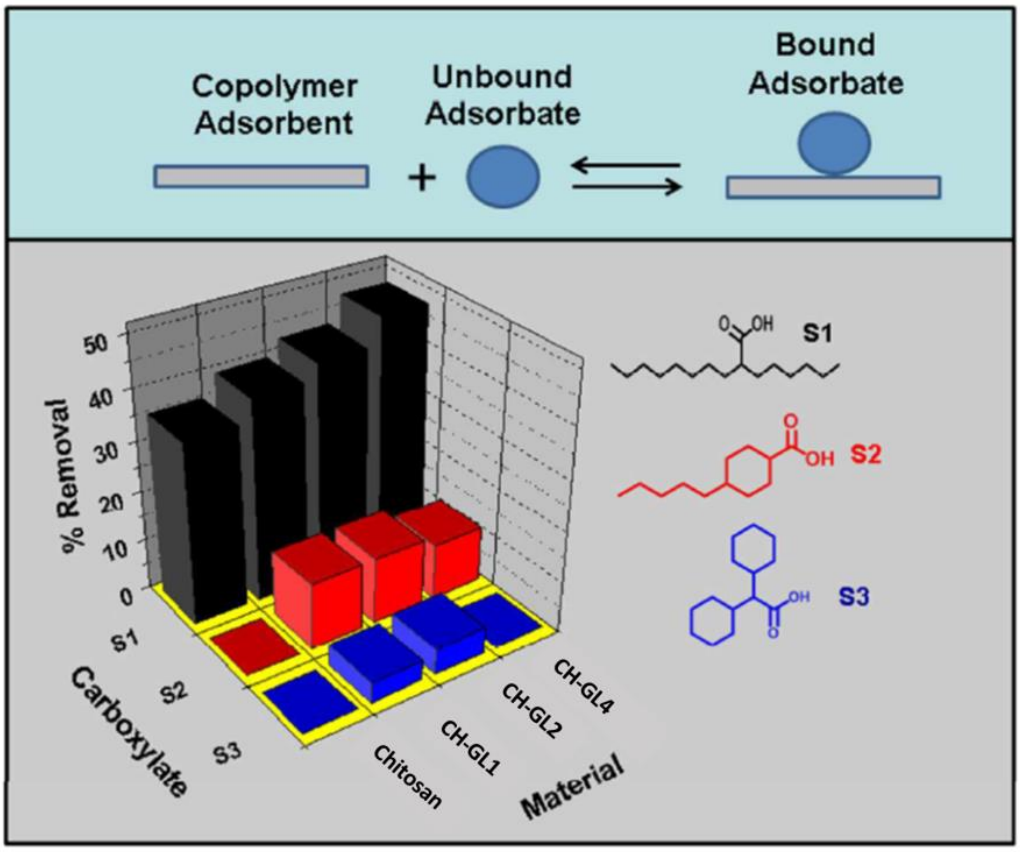

Research Highlights

- Chitosan was cross-linked at incremental glutaraldehyde feed ratio.
- The cross-linked polymers have tunable properties according to the cross-linker feed ratio.
- The sorption affinity of the cross-linked polymers for naphthenate anions was greater than that of the precursors.
- **CH-GL4** with the highest GL feed ratio displayed the best anion recognition properties.

2. Fractionation of Carboxylate Anions from Aqueous Solution Using Chitosan Cross-Linked Sorbent Materials

M. H. Mohamed[1]; I. A. Udoetok[1]; L. D. Wilson[1*] and J. V. Headley[2]

[1]Department of Chemistry, University of Saskatchewan, 110 Science Place, Saskatoon, Saskatchewan, S7N 5C9

[2]Water Science and Technology Directorate, Environment Canada, 11 Innovation Boulevard, Saskatoon, Saskatchewan, S7N 3H5

***Corresponding Author**: L. D. Wilson, Tel. +1-306-966-2961, Fax. +1-306-966-4730,

Email: lee.wilson@usask.ca

2.1 Abstract

The sorptive uptake properties are reported for chitosan and cross-linked chitosan-glutaraldehyde (**CH-GL**) polymers with single component carboxylic acids (surrogates; **Si**, i=1-3 and 7). The single component surrogates are treated as model compounds to represent traditional naphthenic acids (NAs) with variable hydrogen deficiency (*z*) and carbon number (C), as follows: 2-hexyldecanoic acid (*z* = 0 and C = 16; **S1**), *trans*-4-pentylcyclohexanecarboxylic acid (*z* = -2 and C = 12; **S2**), dicyclohexylacetic acid (*z* = -4; C = 14; **S3**) and 2 ethyl hexanoic acid (*z* = 0 and C = 8; **S7**). Cross-linked polymers were synthesized at variable CH: GL mole ratios (i.e. 1:1, 1:2, and 1:4) and characterized using FTIR and TGA. The uptake studies were demonstrated at pH 6.00 and 9.00 in aqueous solution. Corresponding equilibrium uptake parameters were evaluated by several isotherm models (Sips and Freundlich). The Freundlich model provided the "best-fit" for **S1**, **S2** and **S3**. The Sips isotherm model gave the "best-fit" results for **S7**. The Freundlich sorption affinity constant (K_F; $L.mg \cdot g^{-1}$) and the Sips monolayer adsorption capacity (Q_m; $mg \cdot g^{-1}$) for the sorbent systems were estimated. The parameters for each **Si** vary as the CH: GL mole ratio increases (K_F, **S1**: 0.00800 ± 0.03 – 6.65 ± 0.35, **S2**: 1.41 ± 0.12 – 2.45 ± 0.20, **S3**: 1.29 ± 0.11 –

2.93 ± 0.34 and Q_m, **S7**: 28.4 ± 2.63 – 33.5 ± 4.88). Differences in the uptake of **Si** species by the sorbents were attributed to steric effects between **Si** with ring systems (z<0) *versus* linear alkyl fragments (z=0). Fractionation of equimolar mixture of **Si** reveals that the sorbents display unique and variable binding affinity with remarkable molecular selective uptake (given in parentheses; $mg \cdot g^{-1}$): **S1** (4-30) > **S2** (4-10) > **S3** (3-9). The fractionation efficacy of **Si** species is attributed to *molecular sieving effects* due to the tunable micropore sites of the cross-linked polymer, in accordance with the variable cross-linker content of the chitosan framework. Regeneration studies revealed the utility of these materials in cyclic adsorption-desorption processes.

Keywords: Alkyl carboxylates; adsorption; molecular sieving; isotherm; fractionation; chitosan; mass spectrometry

2.2. Introduction

Aquatic environments are exposed to anthropogenic activities that result in the uncontrolled production and release of wastewater effluent. [1, 2] This has resulted in environmental regulations by various bodies such as the World Health Organization (WHO), Environmental Protection Agency (EPA) and the Government of Canada in attempts to control the release of deleterious substances into aquatic environments.[3] In Northern Alberta, Canada, persistent organic pollutants known as naphthenic acids represent a class of chemical by-products that are enriched from the processing of bitumen from the oil sands extraction *via* the Clark hot water extraction process.[4]

The resulting saline wastewater stream obtained from the Clark process (oil sands process water, OSPW) contains a complex mixture of organic compounds. OSPW contains an organic acid fraction referred to as naphthenic acids (NAs), comprised of a broad range of polar organics which

include classical NAs defined by the conventional formula, $C_nH_{2n+z}O_2$, where "z" represents the "hydrogen deficiency" and is a negative even integer value.[5-9] For the classical NAs, many isomers exist for a given *z*-value and the carboxylic acid group is often linked to an aliphatic side chain, rather than directly to the alicyclic ring. The molecular weights differ by 14 *amu* (CH_2) between *n*-series and by 2 *amu* (2H) between z-series.[10] Naphthenic acids ($C_nH_{2n+z}O_2$) may exist as naphthenate anions at alkaline conditions and are known to be toxic to aquatic organisms, algae, and mammals.[7, 11-16] Reports indicate that exposure of fish to mixtures of NAs, either commercially sourced or diluted levels ($0.3 - 9.0$ mg L^{-1}) of OSPW, cause changes in the blood components and carbon metabolism. NAs are known to have toxicological effects that lead to the disruption of cell membrane function, spinal deformations, tissue haemorrhaging, reduction in testosterone and estradiol levels, and growth reduction. OSPW levels (25 mg L^{-1}) result in impaired reproduction. Changes in gill and liver histopathology occur at $0.9-1.7$ mg L^{-1}; whereas, levels between $1.4-7.5$ mg L^{-1} cause developmental toxicity. Endocrine disruption and modulation of the normal endocrine processes in fish and amphibians are associated with exposure to mixtures containing NAs, according to recent studies.[17-19] These results emphasize the need to develop an understanding of the relative toxicity of NAs and suitable processes for the controlled removal of NAs to environmentally safe levels.

The sorptive removal of waterborne contaminants using organic polymer materials was reviewed by Crini *et al*. for a wide range of organic dyes.[20] The host-guest chemistry of β-cyclodextrin (β-CD) and its polymeric forms are relatively unique when compared with conventional organic polymers, as evidenced in a recent review by Wilson *et al*.[21] However, the incorporation of β-CD into cross-linked polymers afford materials with unique molecular selective uptake properties because the inclusion site of β-CD acts as the principal sorption site of the

polymer framework, while the cross-linker domains represent secondary sorption sites.[22-24] Alternative polysaccharides such as chitosan and cellulose are of considerable interest as sorbent materials for large-scale and industrial applications due to their low cost, relative abundance, and sustainable supply. Cellulose and chitosan differ according to their chemical reactivity due to the functionalization at carbon-2 (OH versus NHR where R = H or $COCH_3$) of the glucopyranosyl moiety. Chitosan contains a mixture of D-glucosamine and N-acetyl D-glucosamine units of variable composition depending on the hydrolysis reaction conditions employed for chitin. In contrast to β-CD polymers, there are sparse reports of the adsorption behaviour of chitosan with carboxylic acids or their anions.[25-28] A novel series of cross-linked chitosan polymers were developed by Wilson and Xue as sorbent materials for uptake studies of urea,[29] along with some binary and ternary chitosan-based polymers for the removal of arsenate anions.[30, 31] A unique feature of chitosan-glutaraldehyde (**CH-GL**) polymer materials is their enhanced uptake properties toward diverse hydrophilic adsorbates such as urea, arsenate, and *p*-nitrophenolate, as compared with unmodified chitosan.[30, 31] To address the need for development of alternative biopolymer materials for the uptake of organic anions such as NAs, modified chitosan represents a promising material due to its synthetic versatility and tunable properties.[29-31] There are reports[20, 32-35] describing the sorption of chitosan with dyes and other organic species. However, there are sparse examples for the sorption of carboxylate anions with chitosan or its modified polymers. Herein, we report the preparation and characterization of chitosan-glutaraldehyde (**CH-GL**) polymers and a systematic study describing their adsorption properties with a series of single-component naphthenic acids in aqueous solution at two pH values (pH = 6 and 9). The results of this study highlight the *first example* of chitosan and its cross-linked materials for the fractionation of single components and complex mixtures of alkyl carboxylates in aqueous solution. This study

contributes to the greater understanding of the molecular details of the adsorption properties for chitosan and its cross-linked materials. An improved understanding of cross-linking effects will contribute to the development of alternative low-cost sorbent materials which are suitable for large-scale controlled sequestration of NAs in aquatic environments.

2.3. Experimental

2.3.1 Materials

Low molecular weight chitosan with ~75%-85% deacetylation, sodium hydroxide, aqueous ammonia, glutaraldehyde, 2-hexyldecanoic acid (**S1**), *trans*-4-pentylcyclohexylcarboxylic acid (**S2**), 2, 2-dicyclohexylacetic acid (**S3**) and 2 ethyl hexanoic acid (**S7**), were obtained from Sigma-Aldrich Canada Ltd. (Oakville, ON). HPLC grade methanol was obtained from Fisher scientific, NJ, USA, whereas, ACS grade glacial acetic acid was obtained from EMD chemicals, NJ, USA. Samples were stored in 2 mL HPLC amber vials with screw-cap perforated Teflon-lined septa from Canadian Life Sciences. All the materials used for the synthesis were used as received without further purification.

2.3.2 Synthesis of Cross-linked Chitosan

The synthesis of the polymeric material (chitosan-glutaraldehyde, **CH-GL2**) was adapted from a previous study[36] as follows: 6 g of low molecular weight chitosan was stirred in 600 mL of 5% v/v glacial acetic acid in a 1 L beaker until complete dissolution was achieved. To the resulting light yellow chitosan solution at pH 3.8, 6.3 mL of glutaraldehyde was added drop-wise over a one minute period with stirring at 550 rpm. The initial yellow solution gradually turned to dark yellow after stirring for 12 h. Complete gelation was achieved as evidenced by the gel inversion test.[37] 1 M NaOH solution was gradually added to the gel with vigorous stirring using a

spatula initially followed by magnetic stirring, until the gel was mechanically broken and the mixture was raised to pH 7 where a brown coloured precipitate was formed. The precipitate was separated from the supernatant by vacuum filtration and washed with several generous portions of cold Millipore water, followed by drying at ~50^{o}C with intermittent grinding using a mortar and pestle. The resulting product was washed in a Soxhlet extractor with HPLC grade methanol followed by drying in a vacuum oven at 56^{o}C for 12 h. The polymer was ground in a mortar and pestle and then passed through a 40-mesh sieve. A similar procedure was adopted for the synthesis of other polymeric materials prepared with variable amounts of glutaraldehyde (*cf*. Table 2.1). Each material was synthesized at least 3 times during the research project and characterization results affirmed the repeatability of the synthetic procedure.

Table 2.1 Mass of chitosan *versus* volume of glutaraldehyde in cross-linked **CH-GL** materials

Reaction Conditions	**CH-GL1**	**CH-GL2**	**CH-GL4**
Glutaraldehyde content (mL)	3.80	6.30	9.00
Mass of chitosan (g)	6.00	6.00	6.00

2.3.3 Characterization

2.3.3.1 Thermal Gravimetric Analysis (TGA)

Thermal gravimetric analysis (TGA) of the polymeric materials was performed using a TA Instruments Q50 TGA system operating with a heating rate of 5°C min^{-1} to a maximum temperature of 500°C using nitrogen as the carrier gas. Thermal stability of the respective components of the polymer material was examined using first derivative (DTG) plots of weight with temperature (%/$^{\circ}$C) against temperature ($^{\circ}$C).

2.3.3.2 FTIR Spectroscopy

IR spectra of the polymer materials were obtained using a Bio-RAD FTS-40 spectrophotometer. Powdered polymer samples were mixed with pure spectroscopic grade KBr in a weight ratio of 1:10 followed by grinding in a small mortar and pestle. The DRIFT (Diffuse Reflectance Infrared Fourier Transform) spectra was operated in reflectance mode at room temperature with a resolution of 4 cm^{-1} over the 400–4000 cm^{-1} spectral range. Multiple scans were recorded and corrected relative to a background of pure KBr.

2.3.3.3 SEM

The surface morphology of chitosan and the cross-linked polymers was studied using scanning electron microscopy (SEM; Model JSM-6010, JEOL/EO). Images form gold coated samples were collected under the following instrument conditions; accelerating voltage-10 kV, 9 mm working distance (WD), magnification-2000× and spot size-50

2.3.3.4 Gas Adsorption Studies

Nitrogen adsorption measurements were made using a Micromeritics ASAP 2020 (Norcross, GA) to obtain the surface area and pore structure properties with an accuracy of ±5%. Briefly, a 1.0 g sample was degassed at an evacuation rate of 5 mm Hg/s in the sample chamber until the outgas rate became stabilized (<10 mmHg/min). The degassing temperature for the samples was maintained at ~ 100°C for 48 h. Alumina (Micromeretics) was used to calibrate the instrumental parameters. The BET surface area was calculated from the adsorption isotherm using 0.162 nm^2 as the surface area for gaseous molecular nitrogen.[38, 39] The micropore surface area was obtained using a t-plot (de Boer method).[40] The Barret–Joyner–Halenda (BJH) method was used

to estimate the pore volume and pore diameter from the adsorption isotherm. The BJH method uses the Kelvin equation and the assumption of slit-shaped pores.

2.3.3.5 Particle Size Analysis

The particle size of the pristine chitosan and polymers dispersed in Millipore water was measured in quadruple replicates by laser diffraction analysis using a Mastersizer 2000 (Malvern Instruments, U.K) equipped with a wet dispersion cell of the Mastersizer 2000 (Hydro 2000^{SM}).

2.3.3.6 Differential Scanning Calorimetry (DSC) Studies

DSC of **CH-GL4**, **CH-GL4**/$NH_{3(aq)}$ and various **CH-GL4**/carboxylate anion systems were acquired using a TA Q20 thermal analyzer over a temperature range of 40 − 400°C. A scan rate of 5°C/min and dry nitrogen gas was used to regulate the sample temperature and sample compartment gas purging. The air dried samples were analyzed in hermetically sealed aluminum pans with a sample mass ranged of 1.69 to 3.72 mg.

2.3.3.7 ***Regeneration Studies***

The sorption experiment was carried out by mixing 20 mg of **CH-GL4** polymer with 3 mL of 100ppm surrogate 7 (**S7**) aqueous solution in 2 dram vial. The Sample mixture was equilibrated at room temperature on a horizontal shaker for 24 h. The desorption of the adsorbate was achieved by washing the polymer/**S7** system with 7mL Millipore water and the water removed from the vial leaving only the polymer. This was followed by the addition of 7mL of acetone and agitation in a horizontal shaker for 30mins. The acetone-surrogate solution was removed from the vial and the polymer air-dried for 12 h. The analytical concentrations for the surrogates were measured before

(C_o) and after (C_e) uptake at equilibrium using a ThermoScientific LTQ Orbitrap Elite mass spectrometer. This procedure was repeated for two cycles of adsorption-desorption.

2.3.4 Sorption Studies

2.3.4.1. Sorption of Carboxylate Anions

A 100 mL stock solution at 100 ppm was prepared for the single component carboxylic acids (**S1**, **S2**, and **S3**) and 200 ppm for **S7**, respectively. This was done by dissolving appropriate amounts of the surrogates in an aqueous NH_3 solution with sonication, and subsequently stirred overnight until complete dissolution was achieved. Different concentrations between (1 – 120 ppm) of each of the surrogates were prepared by diluting the stock solution with Millipore water.

Fixed amounts (10 mg) of the powdered and sieved cross-linked polymers or chitosan (20 mg) were mixed with 3 mL of surrogate solutions in 3 dram vials at variable concentration. Samples were equilibrated at room temperature on a horizontal shaker table for 24 h. The analytical concentrations for the surrogates were measured before (C_o) and after (C_e) uptake at equilibrium using a ThermoScientific LTQ Orbitrap Elite mass spectrometer. The samples were centrifuged to remove any traces of the polymer material prior to ESI-MS analysis. Uptake of **S1**, **S2**, **S3 or S7** was determined from the difference between C_o and C_e values described by equation 2.1.

$$Q_e = \frac{(C_o - C_e) \times V}{m} \qquad \text{Equation 2.1}$$

Q_e is the quantity of adsorbate in the solid phase adsorbed at equilibrium (mg g^{-1}), C_o is initial concentration of adsorbate (mg L^{-1}) in solution, C_e is concentration of adsorbate at equilibrium (mg L^{-1}) in solution, V is volume of adsorbate solution, and m is mass (g) of sorbent material.

Batch uptake kinetics were studied for **S1** with the three polymers and pristine chitosan, respectively. Approximately 10 mg of cross-linked polymer or ~20 mg for chitosan was placed in 2 dram vials followed by addition of 5 mL of **S1**. Each vial was shaken for specific time intervals (2, 5, 10, 15, 20, 30, 40, 50 and 60 min). The aliquots were quantified using mass spectrometry after phase separation of the solid polymer, as described above. Uptake of **S1** at each time interval (t) were determined according to equation 2.2, where C_o and C_t refer to the surrogate concentration at t = 0 and variable t values respectively.

$$Q_t = \frac{(C_o - C_t) \times V}{m} \qquad \text{Equation 2.2}$$

2.3.4.2. Electrospray Ionization Mass Spectrometry Analysis

A ThermoScientific LTQ Orbitrap Elite mass spectrometer was used to monitor the electrospray ionization mass spectra (ESI-MS) and estimate the concentration of the acid species in aqueous solutions. The resolution setting of the spectrometer was 30,000 while a full-scan mass spectrum was collected between *m/z* 100 and 600. Samples were quantified by extracting the mass range of the analyte of interest. For example, **S3** was quantified by extraction of the mass range (*m/z* 223.16716 − 223.17398) and comparing the response area with a calibration standard. The electrospray ionization (ESI) interface was set to negative ionization mode. Mass spectrometer conditions were optimized by the transmission of *m/z* 112.98563. Parameters for the heated ESI interface (HESI) were as follows: source heater temperature (53 °C); spray voltage (2.86 kV); capillary temperature (275 °C); sheath gas flow rate (25 L h^{-1}); auxiliary gas flow rate (5 L h^{-1}); and spray current (5.25 μA).

2.3.4.3. Sorption Isotherms and Modeling

Sorption isotherms were obtained by plotting Q_e *vs* C_e (*cf*. Equation 2.1) that were subsequently analyzed using Langmuir [41], Freundlich [42] and Sips [43] isotherm models (*cf*. Equations 2.3-2.5). The Langmuir model assumes that the adsorbent surface is homogeneous, while the Freundlich and Sips models additionally account for surface heterogeneities. The binding constant is represented by an equilibrium parameter (K_i). The sum of square of errors (SSE) was used as a criterion of the "best fit" where a lower value of SSE (*cf*. Equation 2.6) indicates a better *goodness-of-fit*. Optimized data fitting was done by minimization of the SSE for all data across the range of experimental conditions. Q_{ei} is the experimental value, Q_{ef} is the calculated value from data fitting and N is the number of Q_e data points.

$$Q_e = \frac{K_L Q_m C_e}{1 + K_L C_e} \qquad \text{Equation 2.3}$$

$$Q_e = K_F C_e^{1/n_f} \qquad \text{Equation 2.4}$$

$$Q_e = \frac{Q_m (K_S C_e)^{n_s}}{1 + (K_S C_e)^{n_s}} \qquad \text{Equation 2.5}$$

$$SSE = \sqrt{\frac{(Q_{ei} - Q_{ef})^2}{N}} \qquad \text{Equation 2.6}$$

Equation 2.7 is the imprinting factor [44] and is defined according to the ratio of the K_F value (*cf*. Equation 2.3) obtained from data fitting of the cross-linked polymer relative to that of chitosan for a given adsorbate system.

$$IF = \frac{K_F(\text{copolymer})}{K_F(\text{chitosan})}$$ Equation 2.7

Kinetics isotherms were obtained by plotting Q_t vs t (*cf*. Equation 2.8) that were subsequently analyzed using the pseudo-first order (PSO) and the pseudo-second order (PSO) kinetics models (*cf*. Equations 2.8-2.9). Similar to the equilibrium isotherms, the SSE (*cf*. Equation 2.6) was used as a criterion of the "best-fit" between theoretical and experimental values.

$$Q_t = Q_e(1 - e^{-k_1 t})$$ Equation 2.8

$$Q_t = \frac{Q_e^2 k_2 t}{1 + k_2 t Q_e}$$ Equation 2.9

2.4. Results and Discussion

2.4.1 FTIR Characterization of Cross-linked Chitosan-Glutaraldehyde Polymers

The FTIR spectra of chitosan, **CH-GL1**, **CH-GL2**, **CH-GL4** and glutaraldehyde are shown in Figure. 2.1. The spectra show general features characteristic of different functional groups such as a broad band at ~3000 – 3500 cm^{-1} due to the stretching of OH groups, ~2800–3000 cm^{-1} attributed to C–H stretching. Others are a vibrational band ~1660 cm^{-1} indicative of adsorbed water, several bands ~1000 – 1200 cm^{-1} which indicate C–O–H, C–O–C and C–N–H asymmetric stretching, and N–H bending that correspond to bands ~1550 – 1640 cm^{-1}. The spectra of the polymer materials bear similar features, in agreement with other reports of cross-linked chitosan.[31, 45] Comparison of the vibrational bands present in chitosan and glutaraldehyde with those for the cross-linked materials indicate that the amine and aldehyde groups responsible for these vibrational bands undergo cross-linking, as evidenced by an attenuation of their peak intensities. The reduced IR band intensity for the glutaraldehyde signature confirms cross-linking

between glutaraldehyde and chitosan[45] due to the appearance of an imine bond (~1604 cm^{-1}). The vibrational bands ~1000 - 1200 cm^{-1} in the FT-IR spectrum for glutaraldehyde indicate that it may exist as a cyclic aldehyde form.[45, 46]

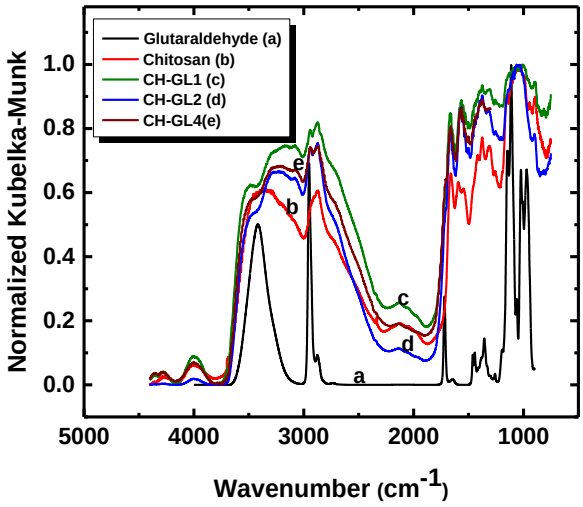

Figure 2.1. FTIR spectra of chitosan, glutaraldehyde, and cross-linked **CH-GL** polymers.

2.4.2 Thermal Gravimetric Analysis (TGA) Characterization

The TGA results for the polymers and chitosan are shown in Figure 2.2. The main thermal event is characterized by decomposition of the materials from 200 to 400°C; whereas, unmodified chitosan decomposes near 300°C. By contrast, the **CH-GL** polymers decompose at lower temperatures (< 300°C), in agreement with other reports.[29, 31] The attenuated decomposition temperature range for the polymers was attributed to the changes in thermal stability due to the cross-linking of chitosan and glutaraldehyde. The latter effect was affirmed by the attenuated peak intensities in the FTIR spectra, as described above. The event at ~ 460°C occurs within the thermal decomposition range anticipated for the glutaraldehyde cross-linker domains of the polymer

materials. Thermal transitions that occur below 100˚C are attributed to the loss of water and/or residual solvents.[29, 30]

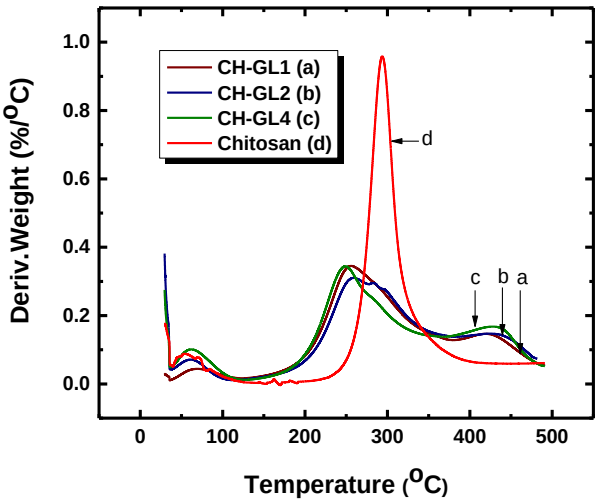

Figure 2.2. TGA of chitosan and its cross-linked **CH-GL** polymers.

2.4.3 Gas Adsorption Studies

Result of the nitrogen adsorption/desorption isotherm for the **CH-GL4** material is presented in Figure 2.3. The shape of the isotherm corresponds to type II system according to the International Union of Pure and Applied Chemistry (IUPAC) designation. Type II describes adsorption on non-porous powders or on powders with pore diameter larger than micropores.[47] The results obtained from this study show the completion of adsorbed monolayer at a relative pressure (p/p^o) ~ 0.2, with a BET surface area of 0.436 m^2/g and pore width in the range of 4 to 17 nm. The isotherm displays low uptake of nitrogen up to a p/p^o value ~ 0.8, however, at p/p^o values > 0.8, the polymer displays greater adsorption of nitrogen due to adsorption at the outer surface of the polymer.[48] [49] According to Figure 3, > 90% is adsorbed on the grain boundaries while

remainder occurs within the micropores of the solid polymer. The absence of hysteresis may be due to capillary evaporation and condensation which occurs reversibly at the same pressure.[50, 51] This may be due to the collapse of the polymer network which is magnified by the quantity of desorbed gas being lower than the quantity of adsorbed gas from $p/p^o < 0.6$.[48, 49]

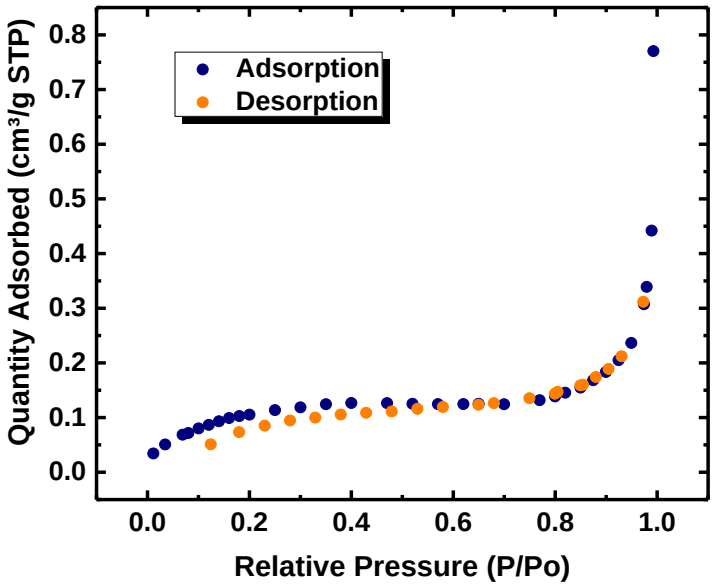

Figure 2.3. Nitrogen adsorption/desorption isotherm at 77 K for cross-linked chitosan **CH-GL4**.

2.4.4 Particle Size Distribution (PSD)

The particle size distribution (PSD) of chitosan and its cross-linked forms is presented in Figure 2.4 and Table 2.2, where d (4,3) represent volume mean diameter; d (3,2), area mean diameter; and d (0.1), d (0.5), and d (0.9) are number of particles in the materials that are smaller (i.e. 10%, 50%, and 90%) than the average particle size of the sample, respectively.[52]

Table 2.2. Particle size distribution/specific surface area of chitosan and cross-linked chitosan

Parameters	Chitosan	CH-GL1	CH-GL2	CH-GL4
Specific surface area (m^2/g)	0.2290	0.0280	0.0545	0.0484
Volume mean diameter (µm)	631	274	171	153
Surface mean diameter (µm)	262	214	110	124
d(0.1)	167	134	64	74
d(0.5)	548	252	147	138
d(0.9)	1229	450	315	255

The results in Table 2.2 show a decrease in the specific surface area, volume and surface mean diameters with increased level of cross-linking. The results also show that the respective percentage of particles (i.e. 10%, 50% and 90%) that are smaller than the average particle size of the samples also decrease as cross-linker content increases. However, the irregularity noticed in the trend of specific surface area may be due to higher crosslinking density for the **CH-GL4** polymer. The above results indicate that cross-linking of chitosan with glutaraldehyde results in an increased surface area and internal pore as the particle size decreases according to the level of cross-linking (*cf.* scheme 2.1).

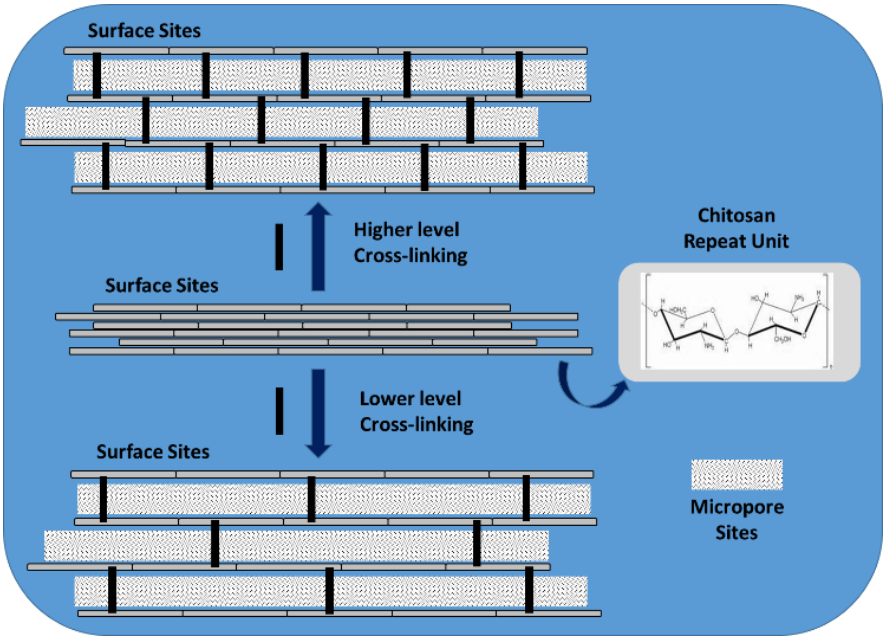

Scheme 2.1: High vs Low cross-linking level according to cross-linker content.

In Figure 2.4, a salient feature of the width of the band shapes at full width half maximum (fwhm) seen in the particle distribution plot are noted for cross-linked chitosan *versus* chitosan. The greater size distribution of chitosan is attributed to greater tendency of aggregation for chitosan relative to the cross-linked material. Therefore, the sharp *versus* broad size distribution may relate to differences in surface charge (zeta potential) of the polymer, colloidal stability and/or the tendency to aggregate in aqueous solution.

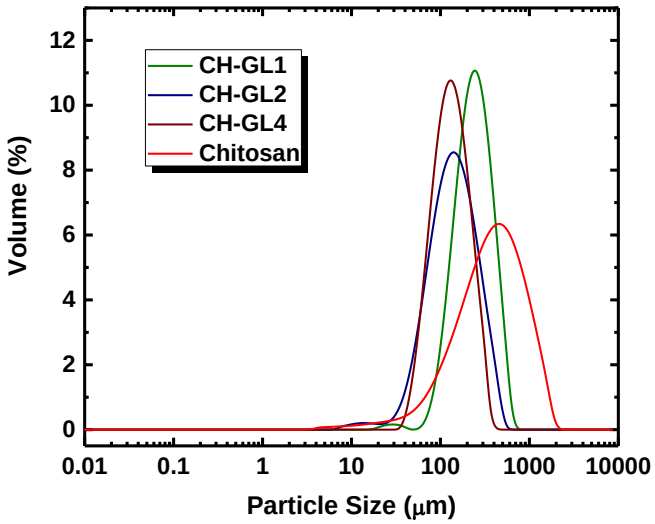

Figure 2.4. Particle size distribution profile of chitosan and cross-linked chitosan.

2.4.5 Scanning Electron Microscopy (SEM)

The SEM images of chitosan and one of the cross-linked polymers (**CH-GL2**) are presented in Figure 2.5. The images show that crosslinking of chitosan with glutaraldehyde results in increased smoothening of the surface of the polymer when compared to that of chitosan and is in agreement with similar studies.[53, 54]

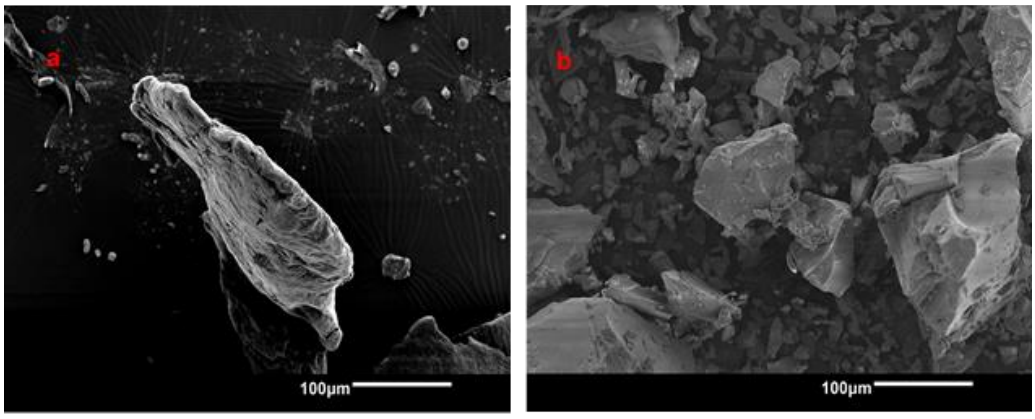

Figure 2.5. SEM images of (a) chitosan and (b) one of the cross-linked polymers (**CH-GL2**)

2.4.6 *Differential Scanning Calorimetry (DSC) Studies*

The DSC thermograms of **CH-GL4**, **CH-GL4**/$NH_{3(aq)}$ and various **CH-GL4**/carboxylate anion systems are presented in Figure 2.6.

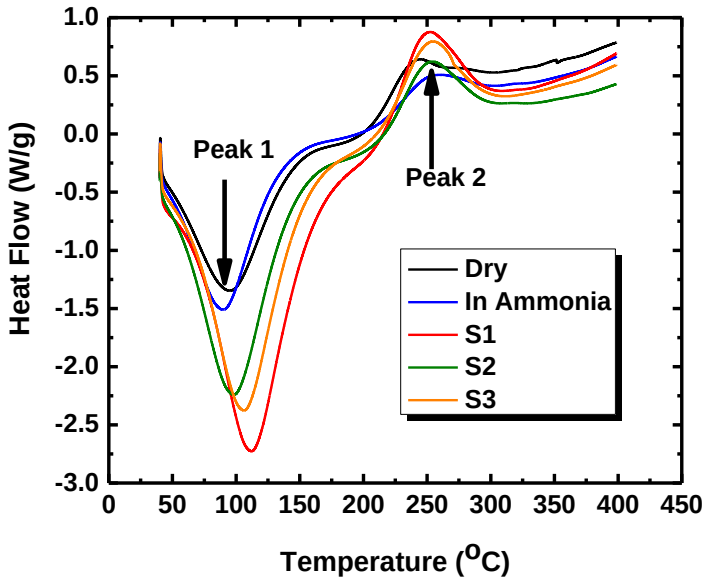

Figure 2.6. DSC thermograms of **CH-GL4** before and after adsorption with **S1-S3** at pH 9 and 295K

The DSC results show endothermic peaks (peak 1) at ~100°C attributed to the dehydration transitions and exothermic peaks (peak 2) at ~250°C attributed to the decomposition of the various **CH-GL4**/carboxylate anion systems. The thermograms display different dehydration and decomposition temperatures (T_{max}) (*cf.* Table 2.3) for the different systems with the non-incubated **CH-GL4** and **CH-GL4**/$NH_{3(aq)}$ displaying similar T_{max} values whereas the various **CH-GL4** /carboxylate anion systems show higher T_{max} values. Also the enthalpy changes associated with the decomposition of the various systems show that the various polymer/carboxylate anion systems displayed higher energies relative to that of **CH-GL4** and **CH-GL4**/$NH_{3(aq)}$ systems. The above

observations along with the decreased concentrations of the adsorbates in solution affirm the host-guest interaction between the adsorbates and the **CH-GL** polymers.

Table 2.3: DSC results showing the enthalpies and T_{max} of the two peaks for **CH-GL4** before and after adsorption with **S1-S3** at pH and 295K (*cf.* Fig. 2.6)

	Peak 1 (J/g), T_{max} (ºC)	**Peak 2 (J/g), T_{max} (ºC)**
Dry	345, 94.7	106, 244
In $NH_{3(aq)}$	489, 89.7	95.6, 260
S1	463, 112	126, 252
S2	472, 98.4	122, 254
S3	497, 107	141, 255

2.4.7 Sorption Studies

2.4.7.1. Sorption Isotherms of Single Component Carboxylates

The isotherm results for the sorption of various single-component surrogate species (i.e. **S1**, **S2**, **S3** and **S7**) with **CH-GLX** (X= 1, 2, and 4) polymers are shown in Figures 2.7a-d. It should be noted that the concentration range for each surrogate (S_i) used for all isotherms was maintained at levels below the CMC[55] to avoid contributions arising from competitive secondary equilibria, and to minimize the occurrence of colloidal aggregation phenomena. As seen in Figure 2.7, the value of Q_e increases nonlinearly as C_e increases where saturation of the isotherm is reached at higher values of C_e. As reported by Pratt et al. [31] the cross-linked polymers display greater sorption toward anion species as the glutaraldehyde content of the polymer increases. Cross-linking of chitosan contributes greater textural porosity due to the formation of micropore sites including decreased crystallinity of the materials. Cross-linking of chitosan leads to greater surface area and greater access to surface functional groups due to *pillaring* of the structure (*vide infra*). A decrease

in the crystallinity of cross-linked materials is supported by substantial line broadening in the PXRD spectra of cross-linked materials (not shown). The value of Q_e for each carboxylate anion species decreased as follows: **CH-GL4** > **CH-GL2** > **CH-GL1** > Chitosan. Among the various surrogates investigated, the highest sorptive uptake occurs for **S7** and **S1**, followed by **S2** and **S3**. In the case of **S1** (*cf*. Figure 2.7a), greater uptake is supported by the offset in magnitude of Q_e *vs*. C_e between pristine chitosan and the **CH-GL** polymer materials. In Figure 2.7a, the Freundlich model provided the "best-fit". The Freundlich constant (K_F) is an indicator of the uptake capacity for each sorbent with **S1**, as follows: chitosan (0.0800 ± 0.03), **CH-GL1** (3.42 ± 0.19), **CH-GL2** (4.46 ± 0.24) and **CH-GL4** (6.65 ± 0.35). The uptake values indicate an improved sorption of **S1** as the glutaraldehyde content of the polymers increased. The exponent term (*1/n*) in Equation 2.3 is a measure of the intensity of adsorption.[42] Based on the *1/n* value, the sorptive uptake is favoured for **S1** relative to the other surrogates. According to Table 2.4, the best-fit values of *1/n* are given in parentheses: chitosan (0.980 ± 0.09), **CH-GL1** (2.14 ± 0.02), **CH-GL2** (2.23 ± 0.02) and **CH-GL4** (2.30 ± 0.02). As the level of glutaraldehyde content increases, the sorptive uptake and the overall binding affinity for **S1** increased.

Table 2.4 Sorption isotherm parameters from the Langmuir, Sips and Freundlich models for pristine chitosan and **CH-GL** polymer materials with various carboxylate anions at pH 9.0 and 295 K.

Carboxylate	Isotherm Models	Parameters	Sorbent Materials Examined in this Study			
			Chitosan	CH-GL1	CH-GL2	CH-GL4
S1	**Freundlich**	**K_F (L.mg g^{-1})**	0.0800±0.03	3.42±0.19	4.46±0.24	6.65±0.35
		1/n_f	0.980±0.09	2.14±0.02	2.23±0.02	2.30±0.02
		SSE	1.12	1.61	1.93	2.54
S2	**Freundlich**	**K_F (L.mg g^{-1})**	N/A	1.41±0.12	1.93±0.019	2.45±0.20
		1/n_f		2.83±0.02	3.61±0.03	3.16±0.02
		SSE		1.11	1.07	1.26
S3	**Sips**	**Q_m (mg g^{-1})**	N/A	4.32±0.24	5.45±0.46	$9.25\pm6.85\times10^{-6}$
		K_S (L.mg^{-1})		0.331±0.03	0.244±0.04	$0.566\pm1.45\times10^{-6}$
		n_s		0.930±0.11	0.779±0.10	$1.10\pm2.45\times10^{-6}$
		SSE		1.07	1.13	0.613
S7 (pH 6)	**Freundlich**	**K_F (L.mg g^{-1})**	N/A	1.29±0.11	1.45±0.12	2.93±0.34
		1/n_f		3.06±0.03	2.98±0.03	3.01±0.04
		SSE		0.586	1.03	3.48
	Sips	**Q_m (mg g^{-1})**	N/A	N/A	N/A	28.4±2.6
		K_S (L.mg^{-1})				0.0357±0.008
		n_s				1.07±0.12
		SSE				0.527
S7 (pH 9)	**Sips**	**Q_m (mg g^{-1})**	N/A	N/A	N/A	33.5±4.9
		K_S (L.mg^{-1})				0.0272±0.009
		n_s				1.13±0.20
		SSE				0.691

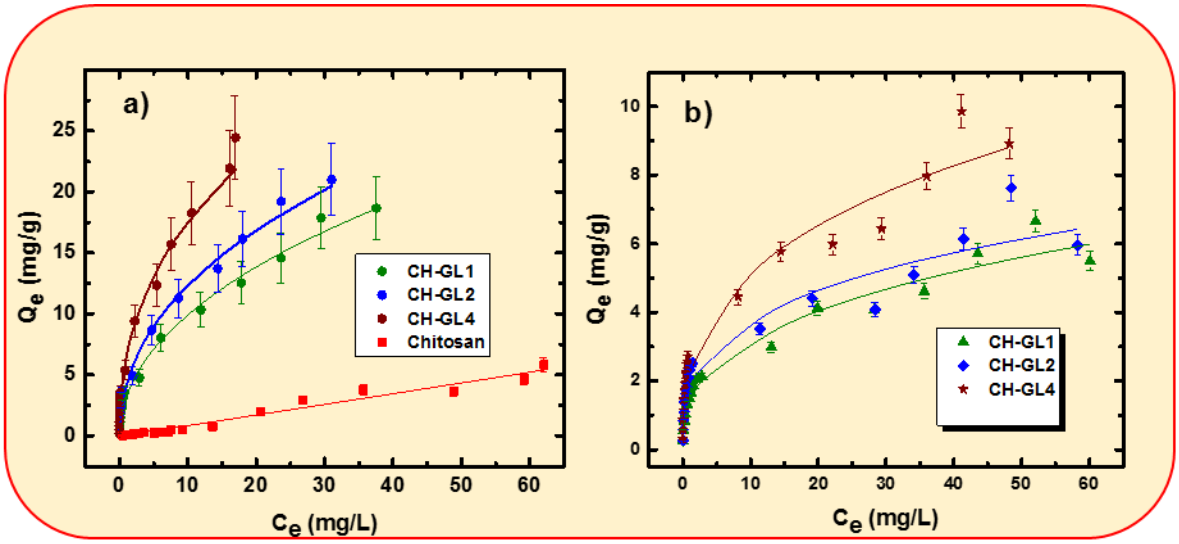

Figure 2.7. Equilibrium sorption isotherms of chitosan and cross-linked **CH-GL** polymers at pH 9 and 295 K with a) **S1** and b) **S2**

The sorptive uptake of **S2** (*cf.* Figure 2.7b) shows a more gradual increase between Q_e and C_e as compared with the observed result for **S1** (*cf.* Figurre 2.7a). The reduced binding affinity between the **CH-GL** polymers with **S2** is evidenced by the Freundlich isotherm constant (K_F) for each sorbent material in parentheses: **CH-GL1** (1.41± 0.12), **CH-GL2** (1.93 ± 0.19) and **CH-GL4** (2.45± 0.20). According to Table 2.4, the best-fit values for *1/n* are given in parentheses: **CH-GL1** (2.83± 0.02), **CH-GL2** (3.61± 0.03) and **CH-GL4** (3.16± 0.02). By comparison with the results for **S1**, the sorptive uptake of **S2** is lower for the **CH-GL** polymers even at the highest glutaraldehyde content. This effect may be due to the steric effects arising from the cyclohexyl ring unit (z = -2) as compared with surrogates such as **S1** or **S7** (z = 0) with linear alkyl fragments.

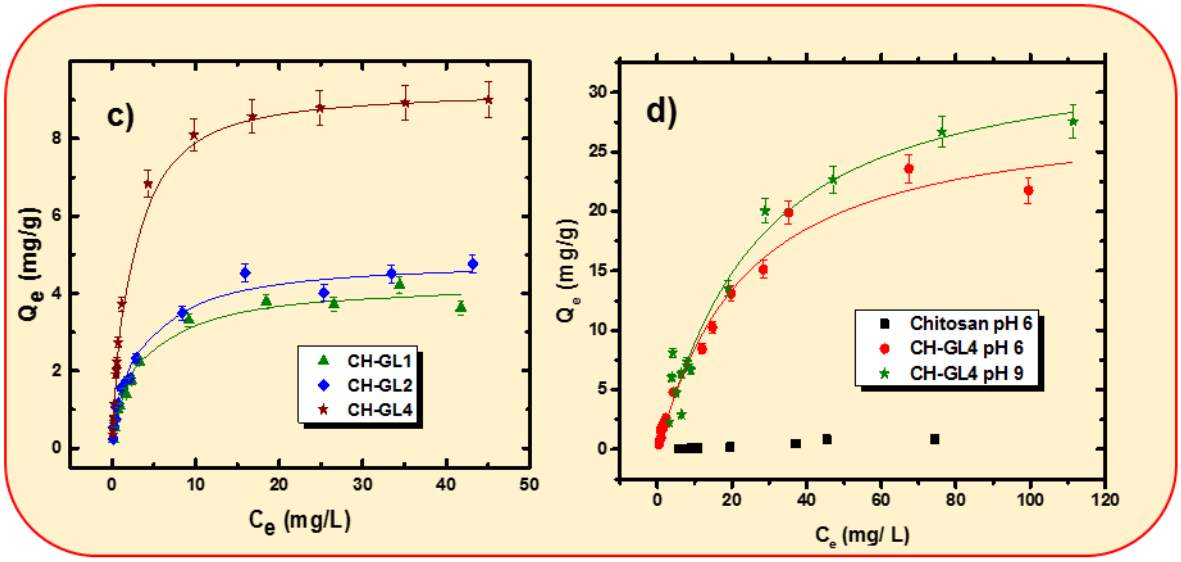

Figure 2.7. Equilibrium sorption isotherms of chitosan and cross-linked **CH-GL** polymers at pH 9 and 295 K with c) **S3** and d) **S7**

In the case of **S3** (*cf.* Figure 2.7c), the sorptive capacity falls in a similar range as for **S2**, however; the uptake of **S3** reaches saturation at lower concentration (~ 10 mg L^{-1}), and this trend may indicate the influence of steric effects on binding at the sorbent surface, especially at the micropore adsorption sites. Unlike **S1** and **S2**, the Langmuir isotherm model yields the "best-fit" for **CH-GL1** and **CH-GL2** while the Sips model provides a better description of the uptake behaviour for the **CH-GL4** polymer. The Langmuir and Sips models afford comparable best fit parameters due to the composite nature of the Sips isotherm. **S3** displays adsorption behaviour well-described by the Langmuir model which indicates that the **CH-GL** polymers display relatively homogeneous adsorption sites with relatively low uptake that compares with uptake observed for **S2**.

The sorption of **S7** by the cross-linked material at pH 9 (*cf.* Figure 2.7d) reveals uptake similar to **S1**. The comparable uptake of **S7** and **S1** may be related to reduced steric effects for surrogates when z=0, as supported by an independent study.[25] The isotherms for **S7** were studied

at pH 6 to evaluate surface charge effects on the adsorptive uptake for this system. Due to the solubilisation of chitosan at lower pH values (below pH 5.5), the results for chitosan and the cross-linked polymer (**CH-GL4**) are shown. The Sips model provided the "best-fit" with Q_m values of 28.4 ± 2.6 mg g^{-1} (pH 6) and 33.5 ± 4.9 mg g^{-1} (pH 9). A comparison of the results obtained pH 6 and pH 9 indicate that lower pH conditions do not contribute to significant variation in the uptake. It follows that van der Waals interactions and hydrophobic effects may provide the driving force for uptake of this polymer/surrogate system. The slightly greater value of K_s (0.0375 ± 0.008 $L \cdot mg^{-1}$) at pH 6 relative to the value (0.0272 ± 0.009 $L \cdot mg^{-1}$) at pH 9 may reflect secondary charge contributions due to potential protonation of amine groups of chitosan that contribute to favourable carboxylate interactions in the sorption process.

The sorption isotherm results for the surrogates show that the uptake properties of **S1** and **S7** are similar but exceed the uptake of **S2** and **S3**. The trend in uptake does not parallel the variation in relative lipophilic character of the various surrogates; however, there is a variation in uptake behaviour based on the degree of unsaturation (ring structures) of the surrogate species. According to the results in Figure 2.7, the uptake is greater for cross-linked chitosan relative to the pristine material, which further supports the important role of micropore domains in the uptake properties of chitosan materials. As well, variable uptake properties for the surrogates herein is related to the nature of alkyl fragments, aliphatic chains *versus* ring systems. The surrogates with ring systems (**S2** and **S3**) appear to have lower uptake relative to the aliphatic surrogates (**S1** and **S7**). Since the micropore domains are likely the principal adsorption sites, the difference in uptake among the surrogates investigated was attributed to steric effects since **S2** and **S3** have greater cross-sectional diameter than linear aliphatic surrogates (**S1** and **S7**). The trends in relative uptake according to the level of cross-linking of chitosan reveals the importance of micropore adsorption

sites, in agreement with the steric effects for surrogates with linear (z=0) versus ring systems (z<0) and the positive contribution of micropores to surface area of the sorbent. Based on the similar uptake values for saturated (**S1** and **S7**) *versus* unsaturated (**S2** and **S3**) surrogates, it is likely that van der Waals interactions and hydrophobic effects are the primary driving forces for the adsorptive interactions. The role of steric effects that result from differing numbers of ring systems and LSA values of the surrogates are supported by the results in Table 2.5. Ion-dipole interactions between the carboxylate head group and the hydrophilic domains of chitosan likely contribute to the sorptive uptake and binding affinity of the various $\mathbf{S_i}$ species; however, such electrostatic interactions appear to play a secondary role according to the results in Figure 2.4.

Table 2.5: LSA, dipole moment, and ΔG° of hydration for the surrogate carboxylate anion species investigated in this study

Carboxylate Anion	Lipophilic Surface Area (LSA)[a]	Dipole moment (Debye)[a]	ΔG°(hydration) (kJ mol^{-1})[a]	CMC (M)[b]
S1	327	5.99	-13.4	3.56×10^{-5}
S2	222	6.43	-17.2	5.45×10^{-4}
S3	233	5.24	-16.0	4.71×10^{-3}

[a]Lipophilic surface area, dipole moments and solvation energy values were obtained using Spartan '08 V1.2.0 from Hartree-Fock SCF calculation performed using Pulay DIIS + Geometric Direct Minimization. The basis set used was 3-21G(*).
[b]Critical micelle concentration (CMC) obtained from surface tension results (*cf.* Ref. 53)

2.4.7.2. Sorption Kinetics

To further understand the molecular details of the adsorption process, the rate of uptake was studied for **S1** with selected sorbents using batch kinetics. Figure 2.8 shows the dependence of q_t *versus* t data for the uptake of **S1** onto chitosan and the three cross-linked materials. The results obtained show that saturation of the monolayer was achieved within ~15 minutes. As was

the case with the equilibrium studies, the cross-linked chitosan displayed better uptake with **S1** than pristine chitosan as depicted by their respective Q_t values (chitosan: 3.84 ± 0.15 mg/g, **CH-GL1**: 22.5 ± 0.2 mg/g, **CH-GL2**: 25.2 ± 0.19 mg/g and **CH-GL4**: 27.0 ± 0.5 mg/g). As well, the rate of uptake (k_2; g mg^{-1} min^{-1}) listed in parentheses for **S1** parallels the behaviour for the Q_e values, as follows: (chitosan: 0.07836 ± 0.001; **CH-GL1**: 0.00957 ± 0.001; **CH-GL2**: 12.5 ± 5.71 $\times 10^{-4}$; and **CH-GL4**: 0.0022). The uptake properties for the systems are presented in Figure 2.8. The pseudo-first order (*cf.* PFO; Equation 2.8) and pseudo-second order (*cf.* PSO; Equation 2.9) kinetic models were used to evaluate the uptake results. The PSO model provided the best overall fit for the data in agreement with the presence of surface and micropore adsorption sites of the adsorbent.[56, 57] Based on the estimated k_2 values, pristine chitosan had the fastest rate of uptake while **CH-GL1** had the slowest. The attenuated rate of the cross-linked polymers relative to unmodified chitosan is attributed to uptake within the micropore domains of the sorbent. **CH-GL4** displayed the largest value of k_2 among the cross-linked materials and is related to the variable number of adsorption sites as a result of increased cross-linker content. The surface chemistry and textural properties of the materials varies according to the cross-linker content as supported by other studies.[36, 58]

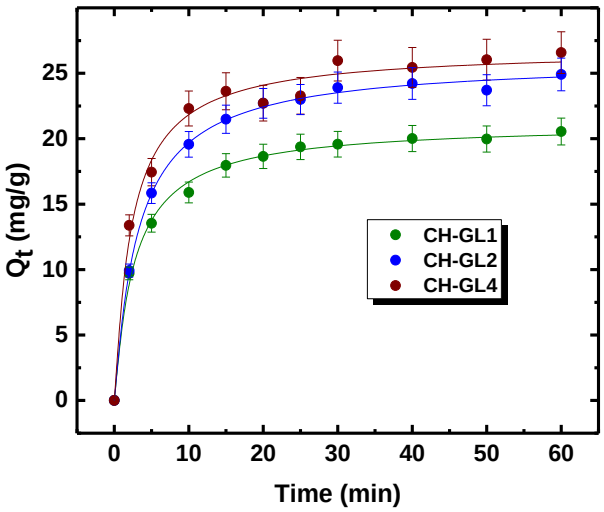

Figure 2.8. Kinetic uptake profiles for **CH-GL** polymers with **S1** in aqueous solution at pH 9 and 295 K using the batch method. The solid lines represent the "best-fit" using the PSO kinetic model

2.4.7.3. Sorptive Fractionation of the Surrogate Mixtures

The relative sorptive uptake of the various carboxylate anions in equimolar mixtures of surrogates (**S1**, **S2**, and **S3**) was studied at equilibrium. The relative uptake was evaluated using ESI-MS for the various sorbent materials as illustrated in Figure 2.9, where the removal (%) of surrogates from the 100 ppm mixture with a constant sorbent dosage (~3 mg/mL) is shown. In all cases, the uptake of **S1** is highly favored relative to either **S2** or **S3** for all sorbent materials, as noted in Figure 2.7. However; **CH-GL** polymers display greater sorption relative to chitosan due to the role of micropore adsorption *versus* surface sites due to cross-linking. The observed differences in uptake in Figure 2.9 are attributed to steric effects, as described for the kinetic uptake results in Figure 2.8. Hydrophobic effects are a major driving force for the sorptive uptake of chitosan materials in this study. Similar trends in uptake for cyclodextrin inclusion complexes have

been reported where *size-fit* between host and guest occur that parallel the molecular sieving effects for cross-linked chitosan herein.[55, 59]

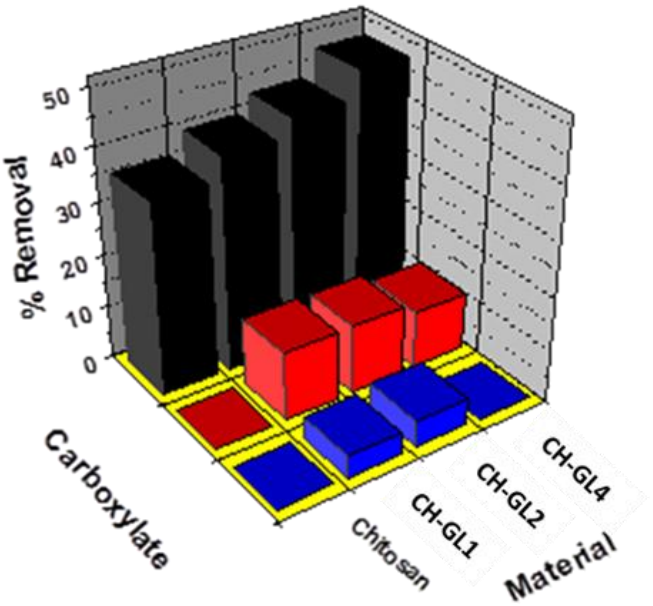

Figure 2.9. Percentage removal of 100 ppm mixture of **S1**, **S2** and **S3** using a sorbent dosage of ~3 mg/mL of pristine chitosan and the **CH-GL** polymers at pH 9 and 295 K.

Ion-dipole interactions between the carboxylate headgroup and the sorbent surface are likely of secondary importance for the systems studied herein, due to the strong hydration of the carboxylate head group[57] (*cf.* $\Delta G°$(hydration) in Table 2.5). The observed uptake results agree with the steric bulk of alicyclic *versus* aliphatic units of the surrogate due to the micropore adsorption sites, as described above. The role of ion-dipole interactions for chitosan-based materials is supported by anion recognition behaviour reported elsewhere.[60] Scheme 2.2 is a generalized illustration of the surface and micropore sorption sites of cross-linked chitosan that govern the uptake of the **Si** adsorbate species.

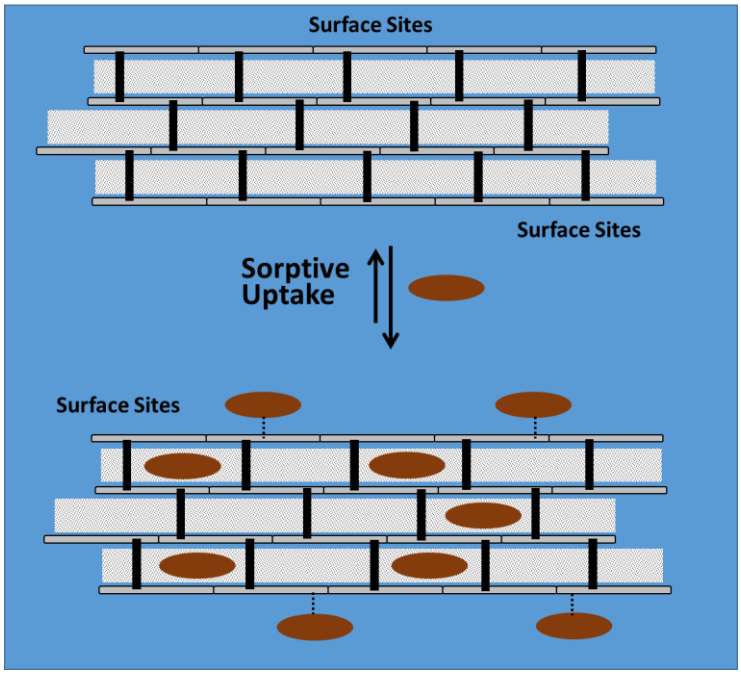

Scheme 2.2. Surface *versus* micropore binding of alkyl carboxylate anions (spheres) in cross-linked chitosan polymers.

2.4.7.4. Comparison of Sorptive Properties with Cyclodextrin Polymers

In a previous study, the sorptive uptake and fractionation behaviour of cross-linked cyclodextrin and cellulose polymers was reported for a homologous series of surrogates [22,62] along with chitosan materials and selected dyes (Table 2.6). The monolayer sorption capacity (Q_m) of the polymer materials was based on the Sips model (in parentheses), as follows: **S1** (32.0 mg g^{-1} and 4.27 mg g^{-1}), **S2** (34.9 mg g^{-1} and 0.816 mg g^{-1}) and **S3** (15.6 mg g^{-1} and 3.25 mg g^{-1}); originally reported as μmol g^{-1}.[22] Based on the sorption isotherms in section 2.4.7.1, β-CD polymers show slightly greater uptake, as compared with the **CH-GL** polymers herein. The similar uptake between β-CD and **CH-GL** polymers is remarkable if one considers that cross-linked chitosan does not possess a well-defined macrocycle binding site like cyclodextrin.[22] A recent

report of molecular imprinted polymer (MIP) films and their adsorption behaviour toward phenol yields imprinting factors (IF) that vary from 1.04 to 1.20 (*cf.* Table S2 in Ref. 41). By comparison, the IF value of the **CH-GL** polymers was calculated using Equation 2.7 and the Freundlich parameter (K_F) in Table 2.4. The IF value for chitosan materials with low to high levels of glutaraldehyde content vary from IF = 43 (**CH-GL1**) to IF = 83 (**CH-GL4**). The ability to tune the sorptive uptake of chitosan by controlled cross-linking with glutaraldehyde represents a unique *green strategy* for the design of micropore binding sites in modified biopolymers such as chitosan. The preparation of **CH-GL** polymers facilitate the formation of micropore domains that can be tuned for the "molecular sieving" of appropriate sized adsorbates. This approach represents a cost-effective method for the synthetic engineering of microporous adsorbent materials for the fractionation of amphiphilic organic anions such as NAs in oil sands process water (OSPW).

Table 2.6: Comparison of adsorption of selected dyes by chitosan materials

Sorbent	Dye/Dye form	Sorption pH	Sorption capacity (mg/g)	References
Chitosan powder	Reactive red 141	11	68	63
Chitosan flake	Reactive black 5	9	19.91	64
CH-GL polymers	Anionic PNP	9	0.306 - 0.572	65
Chitosan flake	Eosin Y	8	79	66

2.4.8 *Regeneration Studies*

Regeneration and reuse of the **CH-GL** polymers was studied by eluting the surrogate with Millipore water followed by acetone. The results obtained (Figure 2.10) demonstrates reusability of the **CH-GL** polymers (Q_e *vs* number of cycles). The above results affirm the cost and time effectiveness of these materials and their ability to be regenerated for reuse by simply exposing the incubated adsorbent to a small volume of water and acetone within 30 mins

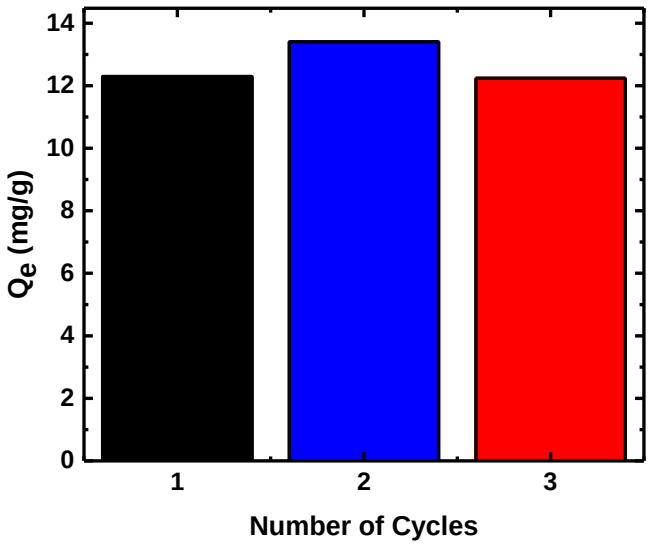

Figure 2.10. Regeneration efficiency of **CH-GL4** at pH 9 and 295 K using **S7**

2.5 Conclusion

Controlled cross-linking of chitosan with glutaraldehyde at variable cross-linker content produces sorbent materials with tunable textural properties and surface chemistry. The materials were characterized and their adsorption properties with several single components and mixtures of alkyl carboxylate anions were studied at pH 6 and 9 in aqueous solutions. The results reported herein highlight *the first example study* that highlight the use of chitosan and its cross-linked materials for the uptake of single components and complex mixtures of alkyl carboxylates in aqueous solution. Unique molecular selective uptake was observed for cross-linked chitosan according to the composition, in accordance with the formation of micropore sites. Variable binding affinity and uptake of single component surrogates depend on the *z*-value (hydrogen deficiency or the number of ring systems), as follows: **S7** ≈ **S1** > **S2** > **S3**. Variable uptake of the surrogates was attributed to steric effects due to the presence of ring systems *versus* aliphatic

chains due to “molecular sieving” effects. Cross-linking of chitosan enables molecular selective uptake (**S1** > **S2** > **S3**) of equimolar surrogate mixtures by preferential adsorption within the micropore sites of the polymer framework. In the case of the **CH-GL** polymer/ carboxylate anion systems, the imprinting factor ranges from *43- to 83-fold* relative to unmodified chitosan. Cross-linking of chitosan illustrates the role of imprinting and formation of preorganized binding sites (micropores) where the primary sorptive interactions are due to hydrophobic effects. Herein, we report a versatile green strategy for the design of chitosan-based materials with tunable adsorption properties for the fractionation of waterborne contaminants and chemical separations. This study will contribute to future advances in materials and environmental science as evidenced by the development of tunable biomaterial adsorbents for the controlled removal of waterborne pollutants from the environment.[61]

2.6 References

1. Council of Canadian Academies, *Water and Agriculture in Canada: Towards Sustainable Management of Water Resources. The Expert Panel on Sustainable Management of Water in the Agricultural Landscapes of Canada*, Ottawa, Canada, 2013.
2. Richardson, S. D.; Ternes, T. A., Water Analysis: Emerging Contaminants and Current Issues. *Anal. Chem.* **2011,** *83* (12), 4614-4648.
3. Ministry of Justice, Fisheries Act, http://laws.justice.gc.ca/eng/F-14/FullText.html, Accessed 13th February 2014, 2012.
4. Chastko, P. A., *Developing Alberta's Oil Sands: From Karl Clark to Kyoto*. University of Calgary Press: Calgary, 2004.
5. Dzidic, I.; Somerville, A. C.; Raia, J. C.; Hart, H. V. *Anal. Chem.* **1988,** *60* (13), 1318-1323.
6. Fan, T. P. *Energy Fuels* **1991,** *5* (3), 371-375.
7. Wong, D. C. L.; van Compernolle, R.; Nowlin, J. G.; O'Neal, D. L.; Johnson, G. M. *Chemosphere* **1996,** *32* (8), 1669-1679.

8. St. John, W. P.; Rughani, J.; Green, S. A.; McGinnis, G. D. *J. Chromatogr. A* **1998,** *807* (2), 241-251.

9. Hsu, C. S.; Dechert, G. J.; Robbins, W. K.; Fukuda, E. K. *Energy Fuels* **1999,** *14* (1), 217-223.

10. Herman, D.; Fedorak, P. M.; MacKinnon, M. D.; Costerton, J. W. *Can. J. Microbiol.* **1994,** *40* (6), 467-477.

11. Rogers, V. V.; Liber, K.; MacKinnon, M. D. *Chemosphere* **2002,** *48* (5), 519-527.

12. Headley, J. V.; Crosley, B.; Conly, F. M.; Quagraine, E. K. *J Environ Sci Health A Tox Hazard Subst Environ Eng.* **2005,** *40* (1), 1 - 27.

13. Quagraine, E. K.; Headley, J. V.; Peterson, H. G. *J Environ Sci Health A Tox Hazard Subst Environ Eng.* **2005,** *40* (3), 671-684.

14. Clemente, J. S.; Fedorak, P. M. *Chemosphere* **2005,** *60* (5), 585-600.

15. Nero, V.; Farwell, A.; Lee, L. E. J.; Van Meer, T.; MacKinnon, M. D.; Dixon, D. G. *Ecotoxicol. Environ. Saf.* **2006,** *65* (2), 252-264.

16. Peters, L. E.; MacKinnon, M.; Van Meer, T.; van den Heuvel, M. R.; Dixon, D. G. *Chemosphere* **2007,** *67* (11), 2177-2183.

17. Kannel, P. R.; Gan, T. Y. *J. Environ. Sci. Health., Part A* **2012,** *47* (1), 1-21.

18. Kavanagh, R. J.; Frank, R. A.; Oakes, K. D.; Servos, M. R.; Young, R. F.; Fedorak, P. M.; MacKinnon, M. D.; Solomon, K. R.; Dixon, D. G.; Van Der Kraak, G. *Aquat. Toxicol.* **2011,** *101* (1), 214-220.

19. Tollefsen, K. E.; Petersen, K.; Rowland, S. J. *Environ. Sci. Technol.* **2012,** *46* (9), 5143-5150.

20. Morin-Crini, N.; Crini, G. *Prog. Polym. Sci.* **2013,** *38* (2), 344-368.

21. Wilson, L. D.; Mohamed, M. H.; Headley, J. V. *Rev Environ Health.* **2014,** 29(1-2), 5-8

22. Mohamed, M. H.; Wilson, L. D.; Headley, J. V. *J. Phys. Chem. B* **2013,** *117* (13), 3659-3666.

23. Mohamed, M. H.; Wilson, L. D.; Headley, J. V.; Peru, K. M. *Phys Chemistry Chemical Physics* **2011,** *13* (3), 1112-1122.

24. Headley, J. V.; Peru, K. M.; Mohamed, M. H.; Wilson, L.; McMartin, D. W.; Mapolelo, M. M.; Lobodin, V. V.; Rodgers, R. P.; Marshall, A. G. *Energy Fuels* **2012,** *27* (4), 1772-1778.

25. Shamov, M. V.; Bratskaya, S. Y.; Avramenko, V. A. *J. Colloid Interface Sci.* **2002,** *249* (2), 316-321.

26. Sathivel, S.; Prinyawiwatkul, W. *J. Am. Oil Chem. Soc.* **2004,** *81* (5), 493-496.

27. Lee, M.Y.; Hong, K.J.; Kajiuchi, T.; Yang, J.W. *Int. J. Biol. Macromol.* **2005,** *36* (3), 152-158.

28. Gylienė, O.; Nivinskienė, O.; Vengris, T. *Carbohydr. Res.* **2008,** *343* (8), 1324-1332.

29. Wilson, L. D.; Xue, C. *J. Appl. Polym. Sci.* **2013,** *128* (1), 667-675.

30. Wilson, L. D.; Pratt, D. Y.; Kozinski, J. A. *J. Colloid Interface Sci.* **2013,** *393* (0), 271-277.

31. Pratt, D. Y.; Wilson, L. D.; Kozinski, J. A. *J. Colloid Interface Sci.* **2013,** *395* (0), 205-211.

32. Kumar, M. N. V. R.; Muzzarelli, R. A. A.; Muzzarelli, C.; Sashiwa, H.; Domb, A. J. *Chem. Rev.* **2004,** *104* (12), 6017-6084.

33. Vårum, K. M.; Smidsrød, O., Structure-Property Relationship in Chitosans. In *Polysaccharides*, CRC Press: 2004.

34. Wan Ngah, W. S.; Teong, L. C.; Hanafiah, M. A. K. M. *Carbohydr. Polym.* **2011,** *83* (4), 1446-1456.

35. Li, C. B.; Hein, S.; Wang, K. *Mater. Sci. Technol.* **2008,** *24* (9), 1088-1099.

36. Poon, L.; Wilson, L. D.; Headley, J. V. *Carbohydr. Polym.* **2014,** *109* (0), 92-101.

37. J. W. Steed, J. A. Atwood, *Supramolecular Chemstry 2nd Edition,* Wiley: West Sussex, UK, AZ, 2009, pp. 888-893.

38. T. Allen, *Particle Size Measurement: Volume 2: Surface Area and Pore Size Determination*, Springer, London, UK, 1997.

39. K. Sing, *Colloids Surf A Physicochem Eng Asp.*, 2001, 187–188, 3-9.

40. Broekhoff, J. C. P.; De Boer, J. H. *J. Catal.* **1968,** *10* (2), 153-165.

41. Langmuir, I. *J. Am. Chem. Soc.* **1918,** *40*, 1361-1402.

42. Freundlich, H. M. F. *J. Phys. Chem.* **1906,** *57A*, 385-470.

43. Sips, R. *J. Chem. Phys.* **1948,** *16* (5), 490-495.

44. Gryshchenko, A.; Bottaro, C. *Int. J. Mol. Sci.* **2014,** *15* (1), 1338-1357.

45. Knaul, J. Z.; Hudson, S. M.; Creber, K. A. M. *J. Polym. Sci., Part B: Polym. Phys.* **1999,** *37* (11), 1079-1094.

46. Kildeeva, N. R.; Perminov, P. A.; Vladimirov, L. V.; Novikov, V. V.; Mikhailov, S. N., *Russ J Bioorg Chem* **2009,** *35* (3), 360-369.

47. Karoyo, A. H., Sidhu, P. S., Wilson, L. D., Hazendonk, P. *J. Phys. Chem. B* **2013**, 117, 8269 -8282.

48. Lowell, S.; Shields, J. E.; Thomas, M. A.; Thommes, M., *Characterization of Porous Solids and Powders: Surface Area, Pore Size and Density*. Springer Netherlands: 201249.

49. Dehabadi, L.; Wilson, L. D. *Carbohydr. Polym.* **2014,** *113*, 471-479.

50. Kruk, M.; Jaroniec, M. *Chem. Mater.* **2001,** *13* (10), 3169-3183.

51. Gregg, S. J.; Sing, K. S. W., *Adsorption, surface area, and porosity*. Academic Press: London; New York, 1982.

52. Guo, Z.; Zeng, S.; Lu, X.; Zhou, M.; Zheng, M.; Zheng, B. *Food Chem.* **2015,** *186*, 223-230.

53. Shivashankar, M.; Mandal, B. K. *Trop J Pharm Res*, **2013,** *12* (1), 13-18.

54. Ostrowska-Czubenko, J.; Gierszewska, M.; Pierog, M. *J Polym Res* **2015,** *22* (8).

55. Mohamed, M. H.; Wilson, L. D.; Peru, K. M.; Headley, J. V. *J. Colloid Interface Sci.* **2013,** *395* (0), 104-110.

56. Xu, C.; Chen, H.; Jiang, F. *Colloids Surf A Physicochem Eng Asp.* **2015,** *479*, 60-67.

57. Gao, Q.; Zhu, H.; Luo, W.-J.; Wang, S.; Zhou, C.-G. *Micropor Mesopor Mat.* **2014,** *193*, 15-26.

58. Grundy, M.; Ye, Z. *J. Mater. Chem. A.* **2014,** *2* (47), 20316-20330.

59. Wilson, L. D.; Siddall, S. R.; Verrall, R. E. *Can. J. Chem.* **1997,** *75* (7), 927-933.

60. Wilson, L. D. in *Water Conditioning & Purification Magazine*, Tucson, AZ, 2014, 56 (12), 28-33.

61. Mohamed, M. H.; Wilson, L. D.; Headley, J. V.; Peru, K. M. *Energy Fuels* **2015,** *29* (6), 3591-3600.

62 Sakkayawong, N.; Thiravetyan, P.; Nakbanpote, W. *J Colloid Interface Sci* **2005**, 286, 36–42.

63 Saha, T. K.; Bhoumik, N. C.; Karmaker, S.; Ahmed, M. G.; Ichikawa, H.; Fukumori, Y. *Clean: Soil, Air, Wate*r, **2011**, 39, 984–993.

64 Poon, L.; Wilson, L. D.; Headley, J. V. *Carbohydr Polym* **2014**, 109, 92–101.

65 Chatterjee, S.; Chatterjee, S.; Chatterjee, B. P.; Das, A. R.; Guha, A. K. *J Colloid Interface Sci* **2005**, 288(1), 30–35.

Chapter 3

(Manuscript 2)

Description

This chapter highlights the effects of cross-linking cellulose with epichlorohydrin at incremental mole ratio on the sorption affinity of the cross-linked polymers for NAFCs and phenolic dyes. Characterization and sorption results revealed that the polymers exhibit tunable properties according to the cross-linker feed ratio, where the polymer with medium linker feed ratio (**C-EP- 2**), displayed optimum sorption capacity for both phenolic dyes and NAFCs.

Authors' contribution

Authors'contribution: I undertook the initial synthesis, characterization of the polymers, sorption studies with model naphthenic acid compounds and data analysis while R. M. Dimmick reproduced the polymers and performed **PNP** adsorption studies. I and Lee D. Wilson conceived the project, Lee D. Wilson secured funding and John V. Headley contributed analysis tools; I wrote the first draft of the manuscript with reviews by R. M. Dimmick and extensive editing by Lee D. Wilson and John V. Headley prior to submission of the paper for publication. Permission was obtained from all contributing authors before the inclusion of the manuscript in this thesis.

Relation of Manuscript 2 to Overall Objective of this Project

This study reported in this chapter relates to the first and fourth themes (cross-linking of chitosan and cellulose and sorption studies of NAFCs using cellulose and chitosan based polymers) of the general objective of the thesis research. It was designed to overcome to shortcomings of the

results reported in chapter 2, where collapse of the pore structure and charge screening at alkaline pH conditions attenuated the sorption properties of **CH-GL** polymers.

Graphical Abstract

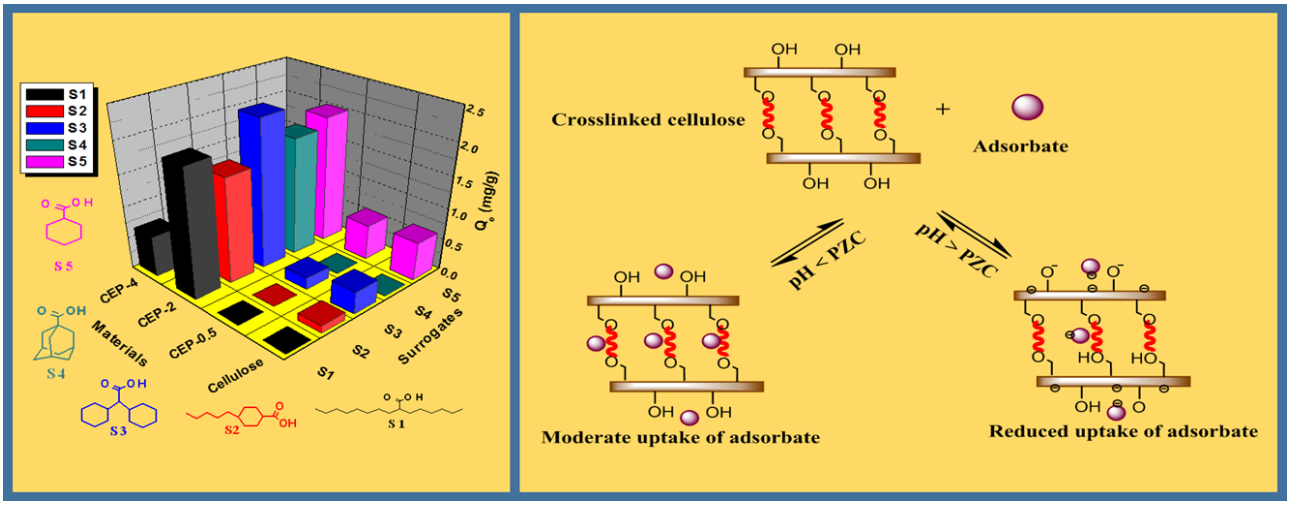

Research Highlights

- Cellulose was cross-linked with epichlorohydrin at variable composition.
- Tunable physical properties are evidenced by materials characterization methods.
- Cross-linked cellulose has greater uptake with carboxylate anions versus unmodified cellulose.
- Cross-linked polymers show molecular selective uptake in solution at equilibrium.
- Micropore domains of cross-linked polymers are active adsorption sites.

3. Adsorption Properties of Cross-linked Cellulose-Epichlorohydrin Polymers in Aqueous Solution

Inimfon A. Udoetok[1]; Raquel M. Dimmick[1]; Lee D. Wilson[1]; John V. Headley[2]

[1]Department of Chemistry, University of Saskatchewan, 110 Science Place, Saskatoon, Saskatchewan, S7N 5C9

[2]Water Science and Technology Directorate, Environment Canada, 11 Innovation Boulevard, Saskatoon, Saskatchewan, S7N 3H5

***Corresponding Author**: L. D. Wilson, Tel. +1-306-966-2961, Fax. +1-306-966-4730, Email: lee.wilson@usask.ca

3.1 Abstract

Cellulose was cross-linked with epichlorohydrin (EP) at variable levels (**C-EP-0.5**, **C-EP-2** and **C-EP-4)**, where **C-EP-i** denotes the cellulose to EP mole ratios. The cross-linked products were characterized by TGA and FTIR spectroscopy, pH at the point of zero charge (pHpzc), water swelling, and dye-adsorption methods employing two types of dyes [phenolphthalein (**phth**) and *p*-nitrophenol (**PNP**)]. The characterization methods provide evidence of cross-linking of cellulose in accordance with variations in surface area, point of zero charge (PZC), available surface hydroxyl groups, and thermal stability when compared against pristine cellulose. The pHpzc of the sorbent materials was ~6.50 indicating a negatively charged surface above pHpzc. The cross-linked polymers possess better swelling properties relative to pristine cellulose. Detailed adsorption studies were carried out at pH 9 for cellulose and **C-EP-i** with five single component carboxylate anions [2-hexyldecanoic acid (**S1**), *trans*-4-pentylcyclohexanecarboxylic acid (**S2**), 2-dicyclohexylacetic acid (**S3**), adamantane carboxylic acid (**S4**), and cyclohexane carboxylic acid (**S5**)] at 295 K. The uptake properties of **PNP** with cellulose and **C-EP-i** were also compared at

pH 5 and 9, respectively. **C-EP-2** had the highest uptake of **PNP** (Q_m= 1.22 ×10^{-1} mmol/g, pH 9) and **S1** (Q_m= 4.27 mg/g) while cellulose and **C-EP-4** had the strongest binding affinity (1.43 L/mmol and 5.90×10-2 L/mg), respectively. Uptake of **PNP** by **C-EP-0.5** at pH 5 (Q_m= 5.30×10^{-2} mmol/g) was higher than uptake at pH 9 (Q_m= 3.11 × 10^{-2} mmol/g). Sorption of **C-EP-4** with **S1**, **S2** and **S3** showed that relative uptake of the surrogates had the following the order: **S3**>**S2** >**S1**, where **S2** had the strongest binding affinity to **C-EP-i**. **C-EP-2** had the highest sorption capacity toward **Si** in an equimolar mixture with evidence of molecular selective uptake. At pH 9, low uptake was mainly related to electrostatic repulsion between the negatively charged sorbent surface and the carboxylate head groups of **Si**.

Keywords: aliphatic carboxylate anions; surrogates; isotherm; *p*-nitrophenolate; cellulose; cross-linking

3.2 Introduction

Unregulated industrial activities and resource extraction activities may contribute to the release of contaminants into aquatic environments, according to a recent review[1].The natural erosion and weathering of oil sands deposits, buildup of tailings deposits, along with industrial extraction of bitumen can lead to the introduction of naphthenic acid fraction components (NAFCs) to the aquatic environments. Different classes of waterborne contaminants such as dyes may result from activities such as the manufacture/processing of textile and paper.[2-5] This study examines the uptake of several representative examples of NAFCs to evaluate the sorptive properties of cellulose and its epichlorohydrin cross-linked polymers. NAFCs are chemically stable, persistent, non-volatile, highly viscous liquids with surfactant-like properties, especially at pH conditions above their pKa. NAFCs display toxicity to aquatic and mammalian life.[6] Their toxicity is due to a combination of their aggregation properties, endocrine disruption properties,

bio-concentration, and variable octanol-water partition coefficients (K_{ow} =10^2 to 10^4). NAFCs may undergo bio-concentration in fish and other aquatic organisms,[7-8] where toxicity studies indicate that organs such as liver, kidneys, heart, spleen, ovaries and lungs are adversely affected.[9] Contaminants such as phenolic dyes are highly mobile in aquatic environments as evidenced by high water solubility of phenol.[10] Phenolic species are ubiquitous contaminants in the environment and are of environmental concern due to their toxicity.[11] In particular, nitro phenol compounds are an important class of agrochemicals with known toxicity and high mobility in aquatic environments.[12] Phenols are toxic in aquatic environments at ppb levels due to their organoleptic properties.[13] Effluents containing phenols often originate from textile and chemical industries and are known to have carcinogenic and mutagenic properties.[14] Exposure to phenolic dyes cause skin irritation, necrosis, and damage to kidneys, liver, muscle and eyes. The fate and transport of such phenolic compounds can be modified by the adsorptive removal using cross-linked polysaccharide materials.[15]

The 2012 National Pollutant Release Inventory (NPRI) Facility reported data shows that about 3.5 million tonnes of toxic substances were released into water, air and land.[1] The scale of the release of contaminants outline the need for cost-effective methods for the removal of toxic substances from the environment. Sorption-based removal of pollutants using organic polymer materials represent a feasible technological approach, as evidenced by the utility of adsorption toward a wide range of inorganic and organic compounds.[16-18] Cellulose is among one of the most abundant renewable natural biopolymers that is non-toxic and exhibits favorable biodegradability.[19-20] The relative insolubility of cellulose in water and organic solvents pose limitations on its general application and technological applications.[21-22] Despite the insolubility of cellulose, it has utility due to its relatively low cost, biodegradability, high functionality, unique

morphology and amenability.[23] Recently, modified cellulose materials have been widely studied.[23-35] Synthetic modification has focused on the improvement of physicochemical properties such as the dispersability, hydrophobicity and biocompatibility of cellulose.

Cellulose is a linear biopolymer that possesses complex structure and function especially synthetically modified forms of cellulose.[23-24, 27-36] Cross-linking of biopolymers such as cellulose (*cf.* Scheme 3.1) offer a facile approach for modifying the adsorption and hydration properties of such materials due to alteration of the surface area and surface chemical properties.[25, 37] Chang et al.[38] reported that the cross-linking of cellulose and polyvinyl alcohol using EP as the linker resulted in the introduction of small and dense pores in the biopolymer. They also reported a decrease in the crystallinity of the material. Hu et. al.[39] reported an increase in the adsorption capacity of microcrystalline cellulose due to the surface grafting of quaternary amine groups. This was evidenced by the textural coarseness, increased porosity and decreased crystallinity of the adsorbent material. Cellulosic derivatives cross-linked with a polycarboxylic acid display decreased solubility and water vapour transmission rates.[40] The above studies collectively affirm that cross-linking is a versatile tool for tuning the surface chemistry, morphology and physicochemical properties of cellulose for a range of adsorption-based applications.

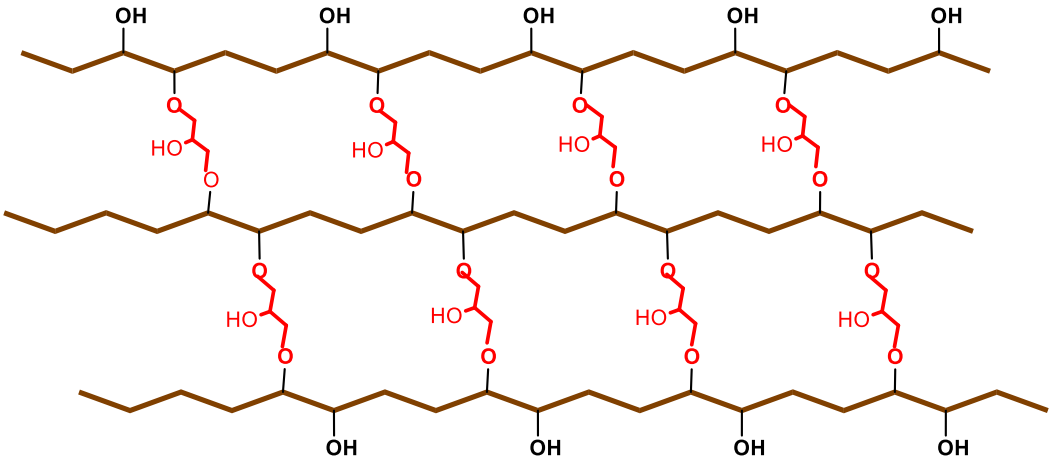

Scheme 3.1: Schematic representation of cellulose cross-linked with epichlorohydrin (red line segment).

There are sparse reports (*cf.* Table 3.1) concerning the use cellulose-epichlorohydrin polymers for the removal of waterborne contaminants. This study reports the preparation of cellulose and its modified forms *via* cross-linking with epichlorohydrin (*cf.* Scheme 3.1). It also reports characterization of the adsorption properties of these materials in aqueous solution with several dye probes [*p*- (**PNP**); phenolphthalein (**phth**)] along with several alkyl carboxylate anions (**Si**) that represent specific examples of NAFCs typically found in oil sands process water (OSPW).

Table 3.1: Summary of studies on uptake of dyes by cellulose cross-linked with epichlorohydrin (EP) and other modified cellulose materials

Sorbent	Dye specie	Sorption pH	Sorption capacity (mg/g)	References
Cellulose-EP	Anionic PNP	9	16.9	This work
Cellulose-EP	Neutral PNP	5	7.37	This work
Lyocell cellulose/NaOH	Anionic DB71	NR	15 – 30	Ibbett et al., 2007[41]*
Regenerated cellulose	Anionic DB 71	NR	2 – 6	Kreze et al., 2002[42]*
Cellulose	Cationic MG	7 – 9.8	2.4	Sekhar et al., 2009[43]*
Activated carbon	Cationic MB	Low	40 – 46	Ahmad and Kumar 2010[44]*
Biomass adsorbent (Aspergillus)	Cationic MB	High	3.4	Acemioglu et al., 2010[45]*
Beech sawdust/$CaCl_2$	Cationic MB, RB22	8	10, 20	Batzian and S., 2004[46]*
Beech sawdust/acid hydrolysis	Cationic MB, RB22	>8	1.6 – 3.1	Batzian and S., 2007[47]*
Cellulose-aminoethanethiol	Anionic RR RB	9	26.0	Silva et al., 2013
Cellulose-aminoethanethiol	Anionic RR RB	2	78.0	Silva et al., 2013
Activated carbon from mango seed	Anionic Alizarin	NR	0.962	Abdus-Salam and Buhari 2014[48]
Activated carbon from mango seed	Anionic Fluorescein	NR	1.11	Abdus-Salam and Buhari 2014[48]
Cellulose acetate/ phthalate–alumina NP	Neutral Catechol	8.2	66	Mukherjee and De, 2014[49]
Cellulose acetate/ phthalate–alumina NP	Neutral PNP	6.5	62	Mukherjee and De, 2014[49]
Cellulose acetate/ phthalate–alumina NP	Neutral OCP	6.6	57	Mukherjee and De, 2014[49]
Cellulose acetate/ phthalate–alumina NP	Neutral OCP	5.9	55	Mukherjee and De, 2014[49]
Cellulose acetate/ phthalate–alumina NP	Neutral OCP	5.7	51	Mukherjee and De, 2014[49]

*Adapted from Hubbe et al.,[50] PNP- *p*-nitrophenol, DB- Direct blue, MB- Methylene blue, RR- Reactive red, RB- Reactive blue, OCP- *o*-chloro phenol, NP - nanoparticle, NR- not reported in literature.

3.3 Experimental

3.3.1 Materials

Cellulose (medium fibre derived from cotton linters), epichlorohydrin (EP), HCl, NaOH, sodium bicarbonate, *p*-nitrophenol (**PNP**), phenolphthalein (**phth**), 2-hexyldecanoic acid (**S1**), *trans*-4-pentylcyclohexane carboxylic acid (**S2**), 2, 2-dicyclohexylacetic acid (**S3**), adamantine carboxylic acid (**S4**), and cyclohexane carboxylic acid (**S5**) were obtained from Sigma-Aldrich Canada Ltd. (Oakville, ON). HPLC grade acetone was obtained from Fisher Scientific, NJ, USA. Samples were stored in 2 mL HPLC amber vials with screw cap perforated Teflon-lined septa from Canadian Life Sciences. All the chemicals used were ACS grade unless specified otherwise and used as received without further purification.

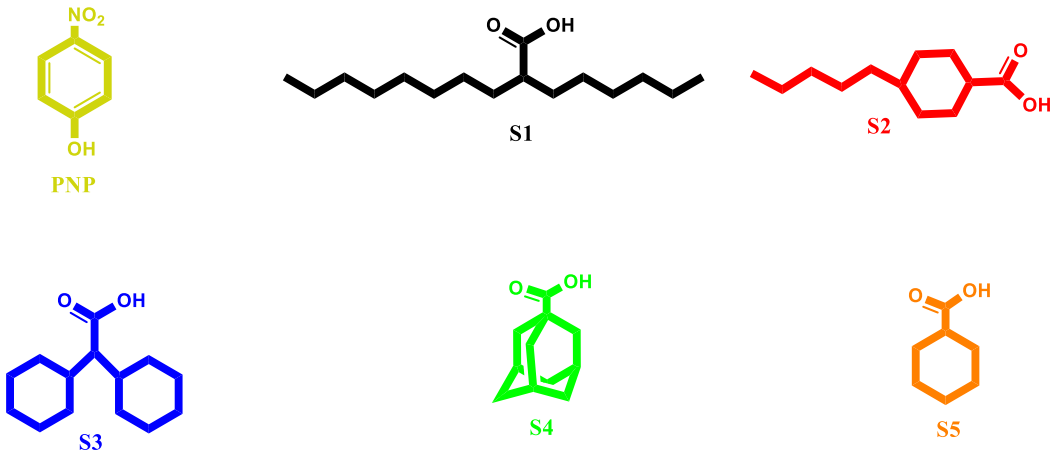

Scheme 3.2: Molecular structure of *p*-nitrophenol (**PNP**) and the single component carboxylic acids (**S1**-**S5**).

3.3.2. Synthesis of Cross-linked Cellulose (C-EP)

The synthesis of the polymers was adapted from previous reports[25, 51] with modification, as required. Briefly, cellulose was cross-linked using epichlorohydrin from low to high values (0.5 to 4 moles). 2 g of bulk cellulose was heated with stirring in 16 mL of 2 M NaOH in a 100 mL

volumetric flask in an inert atmosphere of Ar gas at 80 ºC for 3 h. To the resulting mixture at 80 ºC, requisite volumes of epichlorohydrin (ρ = 1.18 g/mL) corresponding to different cross-linker ratios (*cf.* Table 3.2) were added drop-wise for one minute with stirring. The resulting mixture was allowed to stir for 12 h before neutralization with 1 M HCl solution. The precipitate was separated from the supernatant by vacuum filtration and washed with several generous portions of cold Millipore water, followed by drying at ~50º C. The solid product was exhaustively washed in a Soxhlet extractor with HPLC grade acetone for 24 h followed by drying in a vacuum oven at 56º C for 12 h. The polymer was ground in a mortar and pestle and then passed through a 40-mesh sieve. The synthetic procedure and characterization was repeated atleast three times with no variations in the results obtained each time.

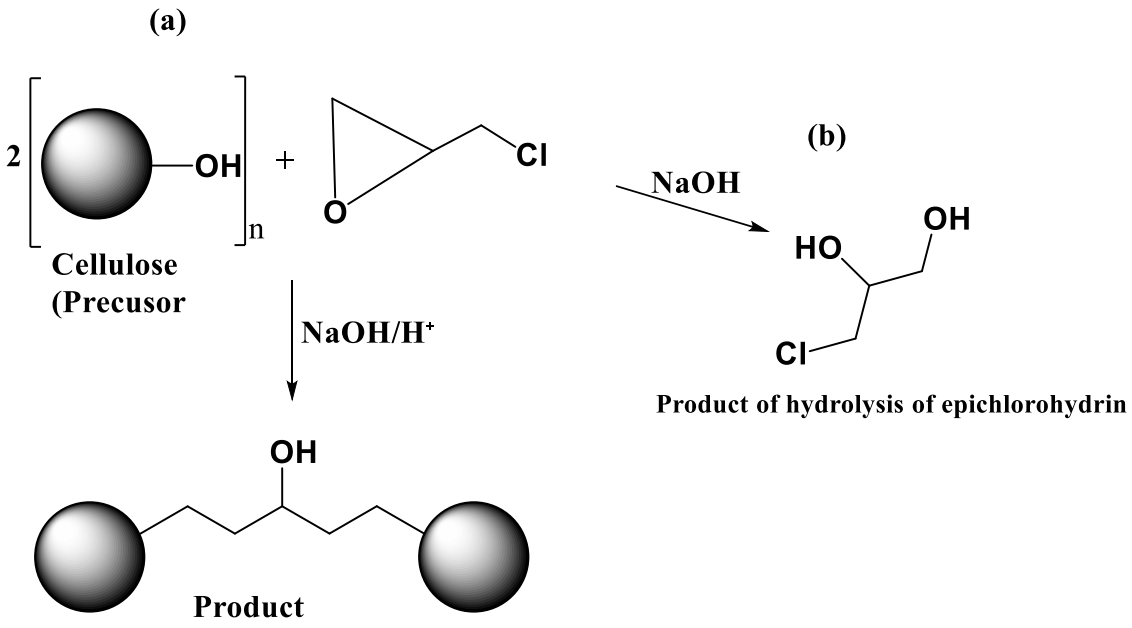

Scheme 3.3: (a) The cross-linking reaction between two cellulose units (the sphere denotes glucopyranose ring of cellulose) and epichlorohydrin in aqueous solution at alkaline conditions. (b) Hydrolysis of epichlorohydrin.

Table 3.2: Mass of cellulose and volume of epichlorohydrin for the preparation of cross-linked polymers.

Reaction conditions	C-EP-0.5*	C-EP-2*	C-EP-4*
Epichlorohydrin content (mL)	0.24	0.97	1.94
Mass of cellulose (g)	2.01	2.00	2.00

*Numerical descriptors in the copolymer names refer to the different number of moles of epichlorohydrin employed in the cross-linking of cellulose

3.3.3 Characterization of Cross-linked Cellulose Materials

3.3.3.1 Thermogravimetric Analysis (TGA)

Thermograms of the polymers were obtained using a Q50 (TA instruments) that operated with a heating rate of 5 °C min^{-1} to a maximum temperature of 500 °C with nitrogen as the carrier gas. Thermal stability of the respective components of the polymer materials is shown using first derivative plots (DTG) of weight with temperature (%/ °C) against temperature (°C).

3.3.3.2 FTIR Spectroscopy

FTIR spectra of the polymers were obtained using a Bio-RAD FTS-40 spectrophotometer. Powdered samples were obtained by mixing polymers with pure spectroscopic grade KBr in a polymer/KBr weight ratio of 1:10 followed by grinding in a small mortar and pestle. The Diffuse Reflectance Infrared Fourier Transform (DRIFT) spectra were obtained in reflectance mode at 295 K with a resolution of 4 cm^{-1} over the 400–4000 cm^{-1} spectral range. Multiple scans were recorded and corrected relative to a background of pure KBr.

3.3.3.3 Point of Zero Charge (PZC)

The point of zero charge of the sorbent materials was determined according to a method described by Singh et al.[52] A stock solution of NaCl (0.01 M) was prepared and 25 mL portions were transferred into five separate 125 mL Erlenmeyer flasks. The pH of the solutions was adjusted between 2 to 10 using NaOH/HCl such that each flask had a different pH value. Approximately 100 mg of the sorbent material was added to each solution and equilibrated for 48 h before the final pH was measured. A graph of final pH vs initial pH was plotted and the intersection point was recorded as the pH for point of zero charge (pHpzc) for each material.

3.3.3.4 Equilibrium Swelling Properties of Cellulose Materials

The swelling properties of the cellulose and its cross-linked forms were studied by equilibrating approximately 50 mg of the materials in 12 mL of Millipore water for 48 h. The weight of hydrated polymer (*ws*) was determined after tamping with a filter paper, while the dry weight (*wd*) was measured after further drying in an oven at 60 °C to a constant weight. The swelling ratio was calculated using Equation 3.1:

$$\mathrm{Sw}(\%) = \frac{\mathrm{Ws\text{-}Wd}}{\mathrm{Wd}} \times 100 \qquad \text{Equation 3.1}$$

3.3.3.5 *Phenolphthalein Decolorization*

The surface accessible hydroxyl groups of the cellulose materials was estimated according to the decolorization of phenolphthalein in aqueous solution; a method developed for the study of materials containing β-cyclodextrin.[53] A 50 mmol stock phenolphthalein in ethanol solution was diluted to 33 μmol by making up 66μL of the stock solution to 100 mL with sodium bicarbonate buffer (pH 10.5). All absorption measurements were carried out at λ_{max} =552 nm. 7 mL of aqueous

solution containing phenolphthalein (33 μmol) were added to vials containing variable mass of the sorbent materials and the mixtures shaken for 24 h, followed by centrifuging (Precision Micro-Semi Micro Centricone, Precision Scientific Co.) at 1550 rpm. The absorbance change was determined using a double beam spectrophotometer (Varian CARY 100) at room temperature (295 ± 0.5 K).

3.3.4 Sorption Studies

3.3.4.1 p-Nitrophenol (PNP) Sorption at pH 9 and 5

Fixed amounts (~20 mg) of the powdered sorbent were mixed with 7 mL of dye at variable concentration (0.1–10 mM) in 0.1 M bicarbonate buffer solution at pH 9 or potassium phosphate monobasic buffer solution at pH 5 with equilibration on a horizontal shaker table for 24 h. The initial **PNP** concentration (C_o) was determined before the sorption process using a blank solution (no sorbent) and the residual equilibrium concentration (C_e) was obtained after sorption (after phase separation) at 295 K. The uptake of the dye was determined with UV-vis absorbance spectrophotometry at λ_{max} = 400 nm and 317 nm respectively, according to Equation 3.2. The molar absorptivity (ε) value for PNP was estimated as 18,270 L $mol^{-1}cm^{-1}$ (pH 9; λ_{max} = 400 nm) and 10,260 L $mol^{-1}cm^{-1}$ (pH 5; λ_{max} = 317 nm) with the Beer–Lambert relation, in agreement with previous reports.[54-55]

$$Q_e = \frac{(C_o - C_e) \times V}{m} \qquad \text{Equation 3.2}$$

Q_e is the amount of adsorbate bound at equilibrium (mmol/g or mg/g), C_o and C_e are initial and equilibrium concentrations of adsorbate (mmol/L or mg/L), V is volume of solution, and m is mass of sorbent material. The surface area (SA; m^2/g) of the polymer sorbent was estimated from Equation 3.3 where Q_m is the maximum monolayer adsorption capacity at equilibrium (mol/g), N

is Avogadro's number (6.02214 ×1023 mol^{-1}), σ is the cross-sectional molecular area of the adsorbate (m^2), and Y is the coverage factor (Y = 1 for PNP).[56-57] The molecular area (σ) is 52.5 $Å^2$ for **PNP** when adsorbed in a co-planar orientation and 25.0 $Å^2$ when it adsorbs orthogonally relative to a planar adsorbent surface.[58]

$$SA = \frac{Q_m \times N \times \sigma}{Y}$$ Equation 3.3

3.3.4.2 UV-vis Spectroscopy

UV-vis absorbance spectra of the samples were obtained using a double beam Varian-Cary (Cary 100) spectrophotometer. Approximately 3 mL of the samples were added to quartz cuvettes and the absorbance value of the different samples were obtained.

3.3.4.3 Sorption of Carboxylate Anions

A 100 mL stock solution (100 ppm) was prepared for the single component carboxylate species (**S1**, **S2** and **S3**), hereafter referred to as **Si**. Adsorbates (**Si**) were dissolved in appropriate amounts of aqueous NH_4OH solution with sonication followed by stirring overnight. Variable stock solutions (1 – 80 ppm) of each **Si** were prepared by dilution with Millipore water. Fixed amounts (~10 mg) of the powdered and sieved polymers were mixed with 3 mL of **Si** solution in 2 dram vials at variable concentration and equilibrated at 295 K on a horizontal shaker table for 24 h. The concentration of **Si** before (C_o) and after sorption (C_e) at equilibrium was determined *via* electrospray ionization mass spectrometry (ESI-MS). The samples were centrifuged using a Beckman Coulter Microfuge 18 Centrifuge set to ambient temperature and 13,000 rpm for 1 h to

remove any traces of the sorbent prior to ESI-MS analysis. Uptake of **Si** was determined from the difference between C_o and C_e as described by Equation 3.2.

3.3.4.4 Sorption of Equimolar Concentration of Mixed Surrogates

To assess the level of sorption when competition for sorption sites occur, an equimolar mixture containing **Si** (**S1** to **S5**) was prepared by dissolving an appropriate level of the components in aqueous NH_3 solution with sonication and stirring overnight. Fixed amounts (~10 mg) of the powdered and sieved polymers were mixed with 3 mL of the equimolar aliquots of **Si** in 2 dram vials. Equilibration of sorbent/**Si** systems was done at 295 K on a horizontal shaker table for 24 h. The concentration values of **Si** before (C_o) and after sorption (C_e) at equilibrium was determined as described above; however, ESI-MS (see below) was used for measurement of concentration instead of UV-vis spectroscopy.

3.3.4.5 Electrospray Ionization Mass Spectrometry (ESI-MS) Analysis

A ThermoScientific LTQ Orbitrap Velos mass spectrometer was used to monitor the solution concentration of **Si**. The resolution setting of the spectrometer was 30 000 while a full-scan mass spectrum was collected between *m/z* 100 and 600 using a lock mass of *m/z* 112.98563. Samples were quantified by extracting the mass range of the **Si** specie of interest. For example, **S3** was quantified by extraction of the mass range (*m/z* 223.16716 − 223.17398) and comparing the response area with a five point calibration curve for this component. The electrospray ionization (ESI) interface was set to negative ion mode. Ionization with full scan MS conditions was optimized by calibrating the instrument with automated tuning to optimize the transmission of *m/z* 112.98563. Parameters for the heated ESI interface (HESI) were as follows: source heater

temperature (53 °C); spray voltage (2.86 kV); capillary temperature (275 °C); sheath gas flow rate (25 L h^{-1}); auxiliary gas flow rate (5 L h^{-1}); and spray current (5.25 μA).

3.3.4.6 Sorption Isotherms

Sorption isotherms were obtained by plotting Q_e *vs* C_e (*cf.* Equation 3.2). The isotherm results were fit using the Sips isotherm model (*cf.* Equation 3.4) which accounts for surface heterogeneities (n_s) and the sorptive equilibrium parameter (K_s).[59] The Sips isotherm model is preferred because it accounts for Langmuir or Freundlich isotherm behaviour, in accordance with the adjustable parameters (Q_m, n_s, and K_s).[54] The sum of square of errors (SSE) was used as a "best fit" criterion, where a lower value of SSE (*cf.* Equation 3.5) implies a better goodness-of-fit. The value of SSE was minimized across all data sets, where Q_{ei} is the experimental value, Q_{ef} is the fitted value and N is the number of Q_e data points.

$$Q_e = \frac{Q_m (K_S C_e)^{n_s}}{1 + (K_S C_e)^{n_s}} \qquad \text{Equation 3.4}$$

$$SSE = \sqrt{\frac{(Q_{ei} - Q_{ef})^2}{N}} \qquad \text{Equation 3.5}$$

3.4.0 Results and Discussion

3.4.1 Characterization of C-EP Polymers

3.4.1.1 FTIR Results

Fourier transform infrared (FTIR) spectroscopy is considered a reliable tool for general characterization of cross-linked polymers because it highlights spectral signatures arising from the

formation of new bonding arrangements or functional groups due to cross-linking.[17-18, 60] The FTIR spectra of cellulose, **C-EP-0.5**, **C-EP-2** and **C-EP-4** are shown in Figures 3.1a-b. The spectra show a broad band attributed to intermolecular bonded OH groups (~3000 – 3600 cm-1) C–H stretching (~2800–3000 cm-1), O–H and C–H bending (~1400 – 1300 cm-1), and C–O–H and C–O–C asymmetric stretching (~1000 – 1200 cm-1). These bands are approximately similar for the various cellulose materials aside from the respective signal intensities that increase and become sharper with greater epichlorohydrin content. An exception occurs for **C-EP-4** where attenuation of these bands may occur due to self-cross-linking of the hydroxyl (OH) group of epichlorohydrin at the C2 position and/or hydrolysis of epichlorohydrin (*cf.* Scheme 3.3) due to the stoichiometric excess of cross-linker. The potential self cross-linking of EP is more likely once the available OH groups of cellulose have reacted or become sterically inaccessible due to cross-linking or the fibrous nature of cellulose. The reduced intensity of the OH band (~2800–3000 cm^{-1}) for this polymer (*cf.* Figure 3.1a) when compared to **C-EP-2** is supported by this incremental cross-linking process. A useful IR signature band for the formation of **C-EP** polymers is the C–O band at ~1050 – 1200 cm^{-1}, where new peaks are evident due to the formation of new C–O bonds. The greater intensity of this band for the polymers (*cf.* Figure 3.1b) when compared to that of pristine cellulose provide additional support for the cross-linking reaction in Scheme 3.3. The similar IR spectra of pristine cellulose and the cross-linked materials suggest that the basic structural units are preserved, in agreement with an independent study.[55]

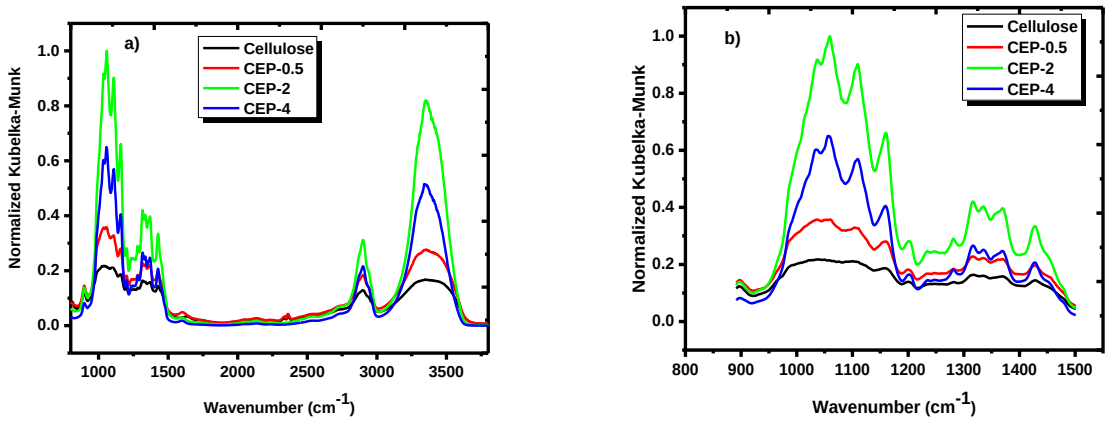

Figure 3.1: (a) FTIR spectra of cellulose and the **C-EP** polymers from 1000 to 5000 cm^{-1}, and (b) FTIR spectra of cellulose and the **C-EP** polymers from 800 to 1500 cm^{-1}.

3.4.1.2 Thermal Gravimetric Analysis (TGA) Characterization

TGA is a sensitive diagnostic tool for monitoring cross-linking reactions[61-64] due to the measureable differences in the thermal stability and heat capacity of pristine and cross-linked materials. The TGA results are shown in Figure 3.2 where thermal decomposition events are noted between 200 ºC to 400 ºC. Pristine cellulose decomposes ~280 - 360 ºC whereas, the cross-linked polymers show slightly offset values: **C-EP-0.5** (~200 - 380 ºC), **C-EP-2** (~200 - 385 ºC) and **C-EP-4** (~200 - 370 ºC). These results reveal the major decomposition events for the **C-EP** polymers at higher temperatures relative to cellulose. The event at ~360 ºC is assigned to the decomposition of the cellulose-EP framework, while the decomposition of EP domains occurs near 280 ºC. This trend coincides with structural effects due to cross-linking such as the micropore formation and the related changes in heat capacity observed for other types of cross-linked polysaccharides.[25] **C-EP-4** was predicted to have a higher thermal event in accordance with the variation in physicochemical properties with greater cross-linking.[65]

However, **C-EP-4** displayed an opposite trend among the polymers studied and this may be related to less adhesive interactions between apolar domains of the polymer. The lower thermal events are consistent with a reduced heat capacity and inter-chain hydrogen bonding interactions between cellulose chains relative to higher temperature events attributed to covalent bond cleavage of the polymer framework. The variable thermal stability of cellulose at variable EP composition provides supporting evidence of the cross-linking reaction presented in Scheme 3.1.

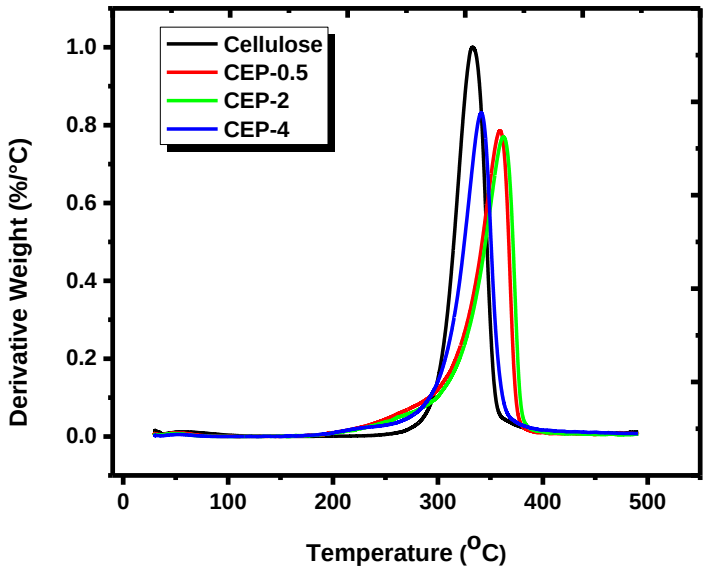

Figure 3.2: TGA of cellulose and **C-EP** polymer materials.

3.4.1.3 Point of Zero Charge (PZC)

Point of zero charge (PZC) is the pH where the net charge of a material is zero (PZC=0) and is an important parameter for interpreting interactions at material surfaces for charged species due to electrostatic effects.[50, 52, 66] The solution pH at which the sorbent material has a net zero surface charge (pHpzc) and the overall negligible adsorption reveals the importance of electrostatic interactions.[50, 52] At pH > pHzpc, the surface of the adsorbent becomes negatively charged due to

adsorption of OH^- ions and/or the deprotonation of ionisable hydrogen ions. For conditions when the pH < pHzpc, the adsorbent surface becomes positively charged due to adsorption of H^+ ions at base sites on the sorbent surface. The results obtained herein show that pHzpc of the sorbent materials is approximately 6.50 while that of cellulose is closer to 6.00 (*cf.* Figure 3.3).The foregoing implies that when the solution conditions are alkaline (e.g., pH = 9), the surface of the sorbent materials bear a negative surface charge, in agreement with studies on modified sawdust (pHpzc = 6.68) and raw sawdust (pHpzc = 7.29).[52] Elsewhere, the zeta potential of cellulose at pH 4 has been reported to be zero.[66-67] The results show that these sorbent materials may be more suitable for uptake of cationic species when pH > pHpzc when ambient pH conditions apply (pH~ 7). By contrast, anionic species are adsorbed more favorably when pH < pHpzc since the repulsive electrostatic interactions are minimized when pH conditions are acidic.

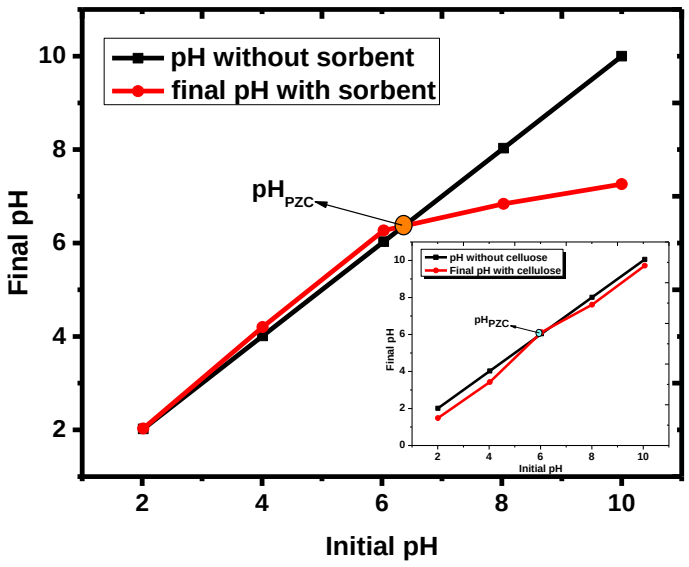

Figure 3.3: Point of zero charge of one of the copolymers (**C-EP-0.5**), where the Inset illustrates the point of zero charge for cellulose.

3.4.1.4 Surface Area (SA) of Materials

The use of dye-based adsorption methods serve as an auxiliary characterization method for estimation of textural properties of biopolymers in their hydrated states.[61] The surface area of the cellulose materials was characterized using **PNP** as the dye-based probe where its molecular surface area (SA) was 52.5 $Å^2$ when adsorption occurs in a co-planar orientation on the sorbent surface. The results in Table 3.3 show that the apparent SA at pH 9 increased for **C-EP-0.5** to **C-EP-2** but decreased for **C-EP-4**. At pH 5, the SA obtained for **C-EP-0.5** was greater relative to estimates obtained at pH 9, in agreement with the electrostatic effects outlined above. The variable pH effects on PZC are further supported by the greater sorption capacity at pH 5 according to the greater Q_m values at pH 5 relative to pH 9. Overall, the SA values in Table 3.3 range from 9.83 ± 0.49 m^2/g to 38.6 ± 1.9 m^2/g for cellulose-based materials. Estimates of SA (ca. 10^1 m^2/g to10^2 m^2/g) reported for β-cyclodextrin (β-CD) cross-linked materials[55, 61] are greater and this difference was attributed to inclusion of the dye in the β-CD cavity along with adsorption at the cross-linker sites of the polymer framework. The effects of the size of the cross-linker on the sorption capacity in starch and β-CD cross-linked sorbents was reported by Mohamed et al.,[63-64] along with other independent support elsewhere.[68]

Table 3.3: Estimated Surface Area of Polymer Materials by the Dye-Based Method.

Mole ratio (cellulose/EP)	Surface area pH 9 (m^2/g)	Surface area* pH 5 (m^2/g)	Yield (%)
1 : 0.5	9.83 ± 0.49	16.8 ± 0.8	61.4
1 : 2	38.6 ± 1.9	-	49.0
1 : 4	8.19 ± 0.41	-	40.6

*surface area at pH 5 for polymers at 1:2 and 1:4 mole ratio since it is clear from the 1:0.5 polymer that the polymers possess greater surface area at lower pH

3.4.1.5 Equilibrium Swelling in Water

The results of equilibrium swelling studies of cellulose and the cross-linked polymers are shown in Table 3.4. The results reveal that pristine cellulose had the least swelling relative to the cross linked polymers, in agreement with independent estimates.[25] The greater swelling of the cross-linked polymers compared with pristine cellulose may be due to the reduced tendency of solvent to infiltrate the fibre domains of cellulose due to hydrogen bonding effects. The cross-linking of cellulose creates defect sites and micropores in the polymer framework that corresponds to an increase in swelling and the greater SA of cross-linked cellulose. A recent report[37] outlined the formation of comparable types of micropores in cross-linked chitosan while a study of β-CD cross-linked with epichlorohydrin revealed the formation of mesopore domains with tunable dimensions[69] relevant to the results reported herein.

Table 3.4: Equilibrium swelling properties of cellulose and copolymers in water at 295 K

Copolymer	Swelling %
Cellulose	161 ± 8
C-EP-0.5	215 ± 11
C-EP-2	205 ± 10
C-EP-4	297 ± 15

3.4.1.6 *Phenolphthalein Decolorization Studies*

The decolorization of phenolphthalein (**phth**) was used to estimate the surface accessible hydroxyl groups of the cellulose materials according to the extent of the cross-linking reaction (*cf.* Scheme 3.3). Figure 4 illustrates the dependence of the decolorization of **phth** with variable mass of adsorbent. In general, the cross-linked cellulose shows greater decolorization relative to pristine cellulose. However, the dependence is not directly proportional to the EP (cross-linker) content of the cellulose polymer. The weak decolorization of **phth** by cellulose is in agreement with a recent structural study of cellulose[70] where it was reported that a large fraction of the hydroxyl groups

are surface inaccessible due to inter-/intra-molecular hydrogen bonding. According to a study by Bertau and Jorg,[71] the decolorization of **phth** was attributed to non-specific enclathration and H-bonding interactions between the saccharides and **phth**. The trends in Figure 3.4 can be attributed to a combination of effects related to the surface accessibility of the hydroxyl groups. Firstly, the increased SA of the cross-linked materials result in enhanced decolorization. Secondly, the formation of cross-links may induce structural and morphology changes of the cellulose materials which influence the dye accessibility within the micropore network (*cf*. Scheme 3.1) of the polymer framework. In any case, there is a semi quantitative dependence between the level of EP content and the level of decolorization. The molecular mechanism of the observed effect is likely a combination of factors that are the subject of future work and is beyond the scope of the present study. The results in Figure 3.4 provide additional support for the proposed cross-linking reaction shown in Scheme 3.3 and the variable level of cross-linking of cellulose. Scheme 3.3 illustrates that complete cross-linking reduces the net number of accessible hydroxyl groups by one –OH group for each mole of EP reacted, as supported by the results in Figure 3.4 and the FTIR results described above.

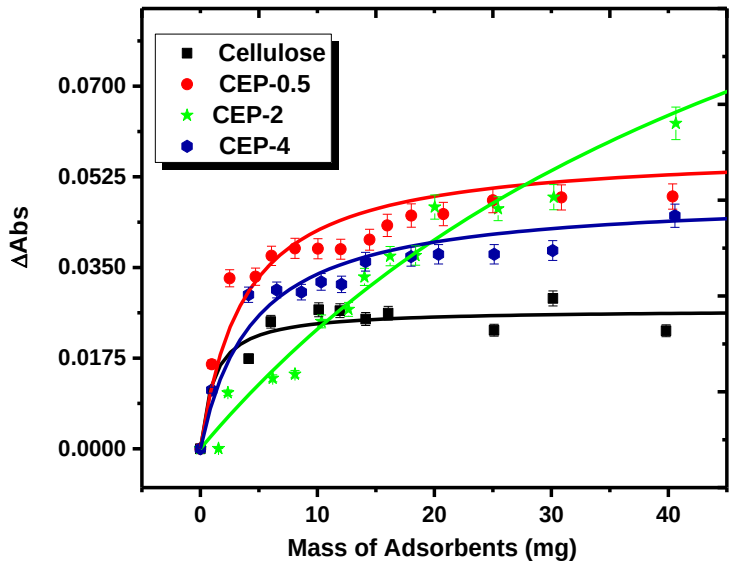

Figure 3.4: Phenolphthalein decolorization from solution using variable amounts of cellulose and copolymers at 295 K and pH 10.5

3.4.2 Sorption Studies

3.4.2.1 Sorption of p-Nitrophenol (PNP)

Batch sorption studies of cellulose and various polymers with **PNP** at variable pH conditions (pH 5 and 9) were employed to characterize the pH dependent sorption properties and to obtain estimates of the sorbent surface areas (*cf*. Table 3.3). The uptake behavior of the cellulose materials in Figure 3.5 reveal that the uptake of **PNP** increases as C_e increases until saturation occurs (*ca*. 6.00 - 10.0 mM). The best-fit solid lines shown through the data in Figure 3.5 (Q_e versus C_e) were obtained by the Sips model. The cross-linked polymers have greater dye uptake relative to cellulose (*cf.* Table 3.5). At pH 9, **C-EP-2** had the greatest sorptive affinity toward **PNP** (Q_m = 12.2 ± 1.0 $\times 10^{-2}$ mmol/g) while **C-EP-4** (Q_m = 2.59 ± 1.00 $\times 10^{-2}$ mmol/g) had the lowest. The greater affinity of **C-EP-2** (approximately complete stoichiometric cross-linking) with **PNP** may be correlated to the variable porosity and surface area of the sorbent material. Steric effects

likely play a role for **C-EP-4** due to excessive cross-linking, as described above. The large Q_m values of **PNP** (0.0981–2.03 mmol/g) reported for β-CD copolymers[55, 61] relate to the β-CD inclusion sites of such materials. By comparison, the isotherm parameters for pristine cellulose indicate the strongest binding to **PNP** followed by **C-EP-4**. The schematic structure of cross-linked cellulose reveals that the surface accessible -OH groups of these materials are anticipated to decrease with cross-linking as shown in Scheme 3.3 and described above. Variable cross-linking likely modifies the *hydrophile-lipophile* balance of the sorbent surface due to the loss of one hydroxyl group for each complete crosslinking of cellulose. Hydrophobic interactions between the phenolic moiety of **PNP** and the apolar domains of cellulose are predicted to increase with greater cross-linking of cellulose, in agreement with the sorption results herein and elsewhere for various chitosan/**PNP** systems.[17]

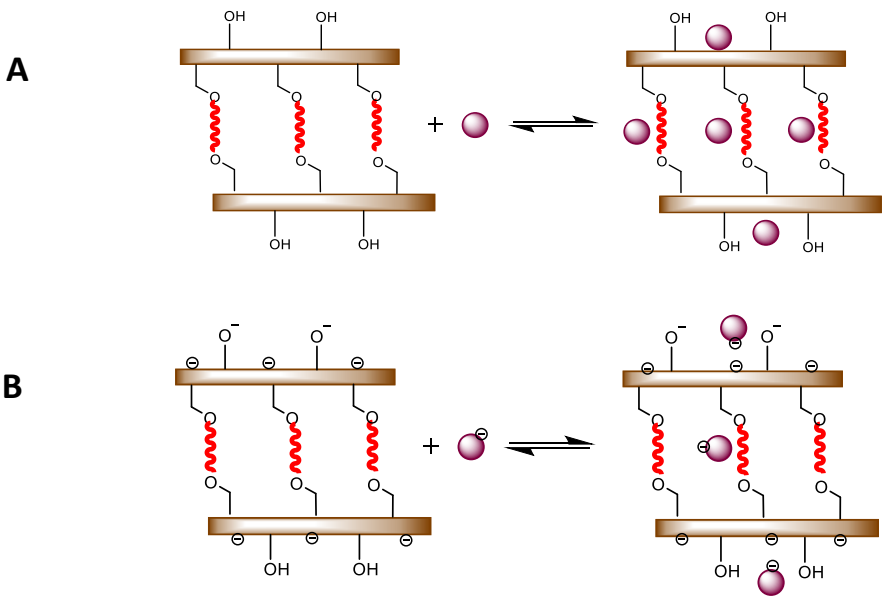

Scheme 3.4: Generalized illustration of the adsorbent-adsorbate interaction at variable pH conditions; A) pH below the PZC of the sorbent, and B) pH above the PZC of the sorbent.

Previous adsorption studies of anionic and cationic dyes by cellulose materials show that uptake was optimal at low pH for anionic dyes where the adsorbent surface was positively charged. However, at high pH uptake of cationic dyes was favored since pH_{PZC} (adsorbent) < pH which results in a negative surface charge.[50, 52, 72-73] Saxena and Jana,[35] reported a decrease in the sorption capacity of cellulose-epichlorohydrin copolymers for various dyes at variable pH, further supporting that the surface charge of the sorbent material varies with pH (*cf.* Figure 3.3). A negative surface charge for cellulose materials at pH 9 ($pH > pH_{zpc}$) is consistent with the measured value of pH_{zpc} (~6.50) herein. At pH 9, **PNP** exists as an anion ($pK_a = 7.2$) where charge repulsion occurs between the negatively charged surface of cellulose and accounts for the low uptake of anion species.[49] To confirm the greater binding affinity of these materials for neutral species, sorption studies of **PNP** at pH 5 was carried out for **C-EP-0.5** and **PNP** in Figure 3.5. At pH 5, **PNP** exists in a non-ionized form because of its greater pK_a (7.2) value. The Q_m ($5.30 \pm 0.10 \times 10^{-2}$ mmol/g) at pH 5 is approximately two-fold greater than the Q_m ($3.11 \pm 1.00 \times 10^{-2}$ mmol/g) at pH 9. The enhanced sorption capacity of an ionisable dye such as **PNP** reveals how the sorbent provides further support for the role of attractive ($pH < pK_a$) and repulsive ($pH > pK_a$) electrostatic interactions with the sorbent surface, according to its relative zeta potential.[74]

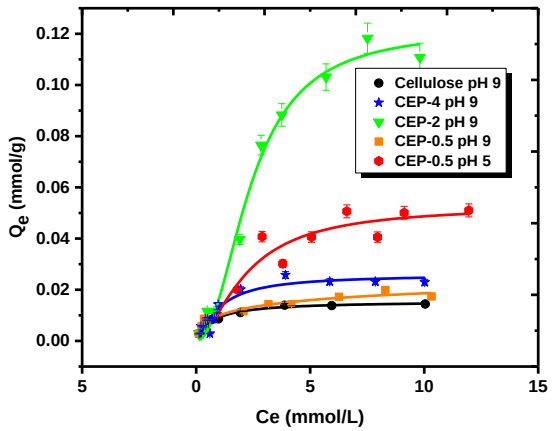

Figure 3.5. Sorption isotherms of PNP with **C-EP** copolymers at pH 5 and 9 at 295 K.

3.4.2.2 Sorption Isotherms of Single Component Carboxylates

The uptake isotherms of **S1, S2** and **S3** by the **C-EP-i** polymers are shown in Figures 3.6 and 3.7. The removal efficiency of **Si** by the cellulose materials was assessed at very low concentration of **Si** (*ca*. 1 – 80 ppm) to simulate the approximate conditions of the oil sands process water (OSPW). Figure 3.6 shows that Q_e increases with increasing C_e until saturation occurs as depicted by the plateau region of the isotherm. The Sips isotherm parameters reveal greater sorptive uptake as the linker of cellulose increases for **C-EP-0.5** and **C-EP-2**. The Sips equilibrium constant (*cf.* Table 3.5) for the **C-EP-4**/**Si** system revealed the largest value (K_s = 590 ± 2 $\times 10^{-2}$ L/mg) among the cellulose polymers studied. The effect may be attributed to the potential role of cooperative interactions due to the linker units and the adsorbate species that likely varies according to the level of cross-linking for related materials.[37] The surface area and pore structure properties amylose cross-linked materials varied in accordance with size effects of the adsorbate in an independent study.[62, 65]

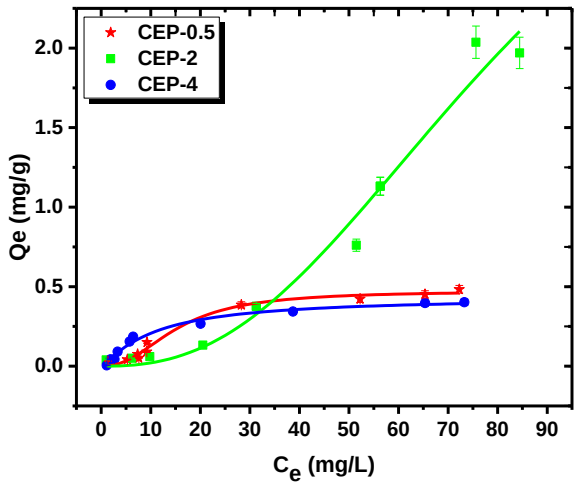

Figure 3.6. Equilibrium sorption isotherms of **S1** with **C-EP** copolymers at pH 9.00 and 295 K

The isotherm parameters in Table 3.5 reveal that **C-EP-4** possessed the greatest binding affinity with **S1** among the various surrogates (**S1**, **S2**, and **S3**), where the relative sorption capacity was observed, **S3** >**S2** >**S1**, according to Figure 3.7. By contrast, an opposite trend was reported for chitosan-glutaraldehyde polymer/**Si** systems[63] as follows: **S1** >**S2** >**S3**. The foregoing provides support of the importance of the surface accessibility of the hydroxyl groups of the sorbent, as outlined above. The trend in uptake observed (*cf.* Table 3.5) according to the adsorbate size correlates with the presence of micropores of variable size according to the level of cross-linking. The uptake of **S3** with a *z*-value of -4 was the most favored while **S2** had the strongest binding to the copolymer (*cf.* Table 3.5). Although the binding affinity is generally low, the variation in this parameter among the various surrogates according to their *z*-value is interesting. This suggests that cellulose polymers with optimized cross-linking can yield fractional separation of mixtures of such surrogates in a manner that parallels results reported elsewhere.[16, 51] The correspondingly low binding affinity reported herein further supports that hydrophobic effects are a driving force for the uptake of **Si**. Trends in binding according to the cellulose polymers are related to variable surface area, steric hindrance, and electrostatic effects at alkaline pH conditions (*cf.* Scheme 3.4b). **S2** has an alicyclic ring unit with an aliphatic hydrocarbon chain of 5 carbon atoms. The strong binding affinity of **S2** to the polymer may be due to a combination of non-specific van der Waals interactions along with hydrophobic effects *via* the cyclohexyl ring units. The n_s values (**S1** = 1.24, **S2** = 1.68, **S3** = 0.863) provide an index of the surface heterogeneity of the adsorbent. The uptake properties of **S1** and **S2** with the cross-linked polymers such as **C-EP-4** deviate from monolayer adsorption behavior. The sorption of **S3** with **C-EP-4** was homogenous in nature according to the n_s values. In Scheme 3.2, **Si** with alicyclic ring structures (variable *z*-values of **S1**, **S2**, and **S3**) likely result in variable modes of adsorption of the surrogates on the polymer surface sites.

Therefore, **S1** and **S2** may have two possible orientations on the surface of the cellulose materials, whereas **S3** with two similar rings may have a single orientation, in accordance with the relative heterogeneity of these sorption processes resulting in a lowering of the Gibbs energy of the system. Single component sorption studies of **S4** and **S5** were not performed because of the low binding affinity of these **Si** from an independent study (results not shown).

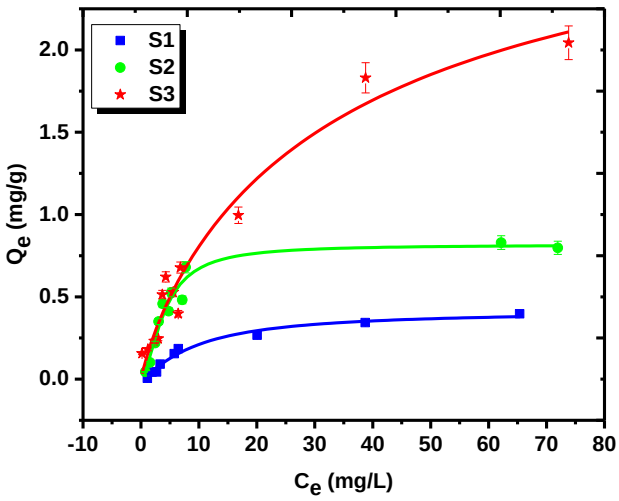

Figure 3.7. Sorption isotherms of **C-EP-4** with **S1**, **S2**, **S3** at pH 9 and 295 K.

3.4.2.3 Equilibrium Uptake of Equimolar Surrogate Mixtures

In Figure 3.8, the relative uptake of equimolar mixture of **Si** (**S1** to **S5**) by cellulose and cross-linked forms were examined at equilibrium conditions. The trend in uptake for **S1** in the mixture bears a similar trend to that observed in Figure 3.7. **C-EP-2** showed the greatest affinity for the **Si** followed by **C-EP-4** and **C-EP-0.5**. The results also show that cellulose and **C-EP-0.5** had nearly negligible uptake, in agreement with the results from uptake studies of single component **Si**. Differences in uptake for the equimolar mixtures and single component **Si** relate to the solvent activity effects due to adsorbate-adsorbate interactions that compete with the weak

polymer/**Si** adsorption process. The relative binding affinity of the individual polymer/**Si** systems are listed, as follows: **C-EP-2** (**S3 > S5 >S4 > S1 > S2)**, **C-EP-4 (S3 > S5 >S1 > S2 > S4); C-EP-0.5** (**S5>S3)** and cellulose (**S5>S3>S2)**. These results suggest that the interaction between the surrogates and the sorbent material likely involve a primary van der Waals interactions *via* the cyclohexyl ring units and secondary electrostatic attractions between the carboxylate head group of **Si** with the sorbent surface, consistent with the role of hydrophobic effects. **S1** has the largest lipophilic surface area[16, 51] but this does not correlate to the highest binding affinity with the copolymer systems. **S1** displays the lowest binding affinity (K_s = 7.40 ± 1.00 ×10^{-4} L/mg) to the sorbent materials relative to **S2** (K_s= 9.62 ± 4.00 ×10^{-2} L/mg), in agreement with the above results.

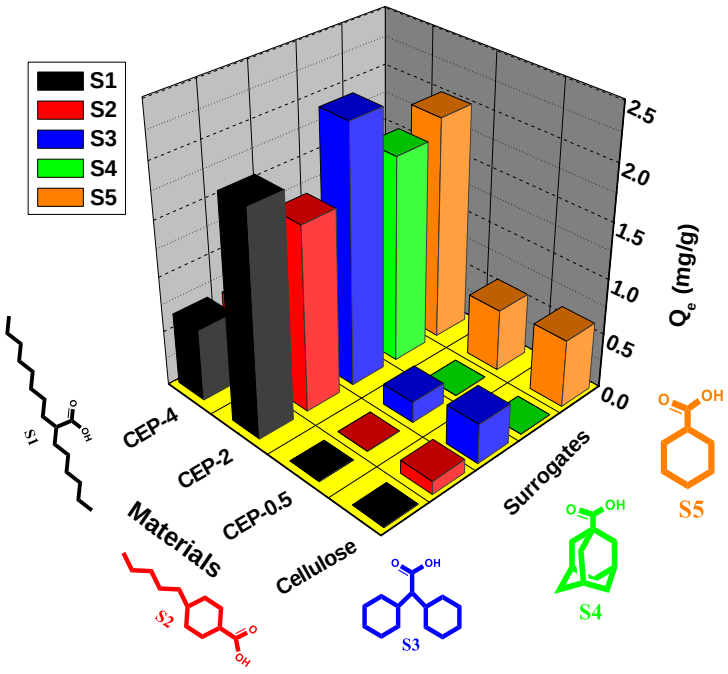

Figure 3.8. Equilibrium uptake of equimolar mixture of **S1**, **S2**, **S3, S4** and **S5** using 10 mg of pristine cellulose and the **C-EP** copolymers at pH 9.00 and 295 K. Note: the bars are color coded for each adsorbate species (**S1-S5**) and some data are not shown due to negligible uptake

Table 3.5: Sips isotherm parameters for **C-EP** polymers with the various adsorbate species at pH 5 and 9 and 295 K.

Adsorbate	Parameters	Sorbent			
		Cellulose	**C-EP-0.5**	**C-EP-2**	**C-EP-4**
PNP (pH 9.00)	$\mathbf{Q_m}$**(mmol/g)**$\times 10^{-2}$	1.56 ± 1.00	3.11 ± 1.00	12.2± 1.00	2.59 ± 1.00
	$\mathbf{K_S}$ **(L/mg)** $\times 10^{-1}$	14.3 ± 3.00	4.67 ± 1.00	1.55± 0.20	9.90 ± 0.30
	$\mathbf{n_s} \times 10^{-1}$	10.1 ±1.40	5.02 ± 1.40	21.3± 2.40	13.1 ± 3.50
PNP (pH 5.00)	$\mathbf{Q_m}$ **(mmol/g)** $\times 10^{-2}$	-	5.30 ± 0.10	-	-
	$\mathbf{K_S}$ **(L/mg)** $\times 10^{-1}$	-	2.76 ± 0.60	-	-
	$\mathbf{n_s}$	-	1.62 ±0.37	-	-
S1 (pH 9.00)	$\mathbf{Q_m}$ **(mg/g)** $\times 10^{-1}$	-	4.31± 0.30	42.7 ± 22.2	4.15 ± 0.40
	$\mathbf{K_s}$ **(L/mg)** $\times 10^{-4}$	-	7.40 ± 1.00	0.20 ± 0.10	590 ± 2.00
	$\mathbf{n_s}$	-	2.79± 0.81	2.48± 0.64	1.24 ± 0.25
S2 (pH 9.00)	$\mathbf{Q_m}$ **(mg/g)** $\times 10^{-1}$				8.16 ± 0.50
	$\mathbf{K_S}$ **(L/mg)** $\times 10^{-2}$		-	-	9.62 ± 4.00
	$\mathbf{n_s}$	-			1.68 ± 0.30
S3 (pH 9.00)	$\mathbf{Q_m}$ **(mg/g)**				3.25 ± 1.15
	$\mathbf{K_S}$ **(L/mg)** $\times 10^{-2}$	-	-	-	4.52 ± 1.00
	$\mathbf{n_s} \times 10^{-1}$				8.63 ± 2.00

(-) Denotes unreported values due to poor sorption capacity of materials

3.5. Conclusion

Synthesis and characterization of cellulose-epichlorohydrin polymers was carried out with variable cross-linking. Dye probe studies were carried out with two phenolic dyes (**PNP** and **phth**) to obtain information on the surface area and surface accessibility of the binding sites of the cellulose materials. Adsorptions isotherm of the cellulose materials with five types of carboxylate anions (**Si**) were studied at pH 5 and 9. **C-EP-2** had the highest sorptive uptake of **PNP** and **Si**, while the **C-EP-4**/**Si** systems had the strongest binding affinity. Sorption studies of **C-EP-4** with various **Si**

(**S1**, **S2** and **S3**) revealed that the relative binding affinity was in the following order: **S3**>**S2** >**S1**. The pH_{zpc} of the cellulose materials revealed that the surface was negatively charged at pH 9 resulting in an attenuated sorption capacity. At pH 5, the sorption capacity was improved by a reduction of unfavorable electrostatic repulsion between uncharged **PNP** and the sorbent surface where the pH was below its pH_{pzc}. The cross-linked materials described herein have potential application for the controlled removal of naphthenic acids in oil sands process water (OSPW) that surpass the properties of unmodified cellulose according to uptake properties with single- and multi-component component **Si** systems.

3.6 References

1. **Environment Canada** 2014 http://ec.gc.ca/inrp-npri/default.asp?lang=En&n=386BAB5A-1&offset=3&toc=show Accessed 05.09.14
2. Clemente, J. S.; Fedorak, P. M. *Chemosphere* **2005,** *60* (5), 585-600.
3. Tollefsen, K. E.; Petersen, K.; Rowland, S. J. *Environ. Sci. Technol.* **2012,** *46* (9), 5143-5150.
4. Forgacs, E.; Cserháti, T.; Oros, G. *Environ Int* **2004,** *30* (7), 953-971.
5. Robinson, T.; McMullan, G.; Marchant, R.; Nigam, P. *Bioresour. Technol.* **2001,** *77* (3), 247-255.
6. Headley, J. V.; Peru, K. M.; Mohamed, M. H.; Frank, R. A.; Martin, J. W.; Hazewinkel, R. R. O.; Humphries, D.; Gurprasad, N. P.; Hewitt, L. M.; Muir, D. C. G.; Lindeman, D.; Strub, R.; Young, R. F.; Grewer, D. M.; Whittal, R. M.; Fedorak, P. M.; Birkholz, D. A.; Hindle, R.; Reisdorph, R.; Wang, X.; Kasperski, K. L.; Hamilton, C.; Woudneh, M.; Wang, G.; Loescher, B.; Farwell, A.; Dixon, D. G.; Ross, M.; Pereira, A. D. S.; King, E.; Barrow, M. P.; Fahlman, B.; Bailey, J.; McMartin, D. W.; Borchers, C. H.; Ryan, C. H.; Toor, N. S.; Gillis, H. M.; Zuin, L.; Bickerton, G.; McMaster, M.; Sverko, E.; Shang, D.; Wilson, L. D.; Wrona, F. J. *J. Environ. Sci. Health., Part A* **2013,** *48* (10), 1145-1163.
7. Headley, J. V.; McMartin, D. W. *J Environ Sci Health, Part A* **2004,** *39* (8), 1989-2010.

8. Toor, N. S.; Franz, E. D.; Fedorak, P. M.; MacKinnon, M. D.; Liber, K. *Chemosphere* **2013,** *90* (2), 449-458.

9. Rogers, V. V. *Toxicol. Sci.* **2002,** *66* (2), 347-355.

10. Hill, A. E.; Malisoff, W. M. *J. Am. Chem. Soc.* **1926,** *48* (4), 918-927.

11. Hammam, A. M. Z., M.S.; Yousef, R.A.; Fawzi, O. *Adv Environ Biol* **2015,** *9* (8), 38 - 48.

12. Michałowicz, J. D., W. *Pol J Environ Stud* **2007,** *16* (3), 347 - 362.

13. Buikema, A. L. J. N., B.R.; Cairn, J. Jr. *Water Res.* **1982,** *16*, 239-262.

14. Schweigert, N.; Zehnder, A. J. B.; Eggen, R. I. L. *Environ. Microbiol.* **2001,** *3* (2), 81-91.

15. Wilson, L. D.; Mohamed, M. H.; Guo, R.; Pratt, D. Y.; Hyuck Kwon, J.; Mahmud, S. T. *J Agromedicine* **2010,** *15* (2), 105-116.

16. Mohamed, M. H.; Wilson, L. D.; Peru, K. M.; Headley, J. V. *J. Colloid Interface Sci.* **2013,** *395* (0), 104-110.

17. Poon, L.; Younus, S.; Wilson, L. D. *J. Colloid Interface Sci.* **2014,** *420*, 136-144.

18. Wilson, L. D.; Mohamed, M. H.; Headley, J. V. *Rev. Environ. Health* **2014**.

19. Mekonnen, T.; Mussone, P.; Khalil, H.; Bressler, D. *J Mater Chem A* **2013,** *1* (43), 13379.

20. Flieger, M.; Kantorova, M.; Prell, A.; Rezanka, T.; Votruba, J. *Folia Microbiol (Praha)* **2003,** *48* (1), 27-44.

21. Kuroda, K.; Kunimura, H.; Fukaya, Y.; Ohno, H., *Cellulose* **2014,** *21* (4), 2199-2206.

22. Xiao, P.; Zhang, J.; Feng, Y.; Wu, J.; He, J.; Zhang, J. *Cellulose* **2014,** *21* (4), 2369-2378.

23. Qiu, X.; Hu, S., "Smart" Materials Based on Cellulose: A Review of the Preparations, Properties, and Applications. *Materials* **2013,** *6* (3), 738-781.

24. Habibi, Y. *Chem. Soc. Rev.* **2014,** *43* (5), 1519-1542.

25. Dehabadi, L.; Wilson, L. D. *Carbohydr. Polym.* **2014,** *113*, 471-479.

26. Spaic, M.; Small, D. P.; Cook, J. R.; Wan, W. *Cellulose* **2014,** *21* (3), 1529-1540.

27. Li, Y.; Xiao, H.; Chen, M.; Song, Z.; Zhao, Y. *J Mater Sci* **2014,** *49* (19), 6696-6704.

28. Nada, A. M. A. A. E.-M., S.; Abd El-Sayed, E. S. *BioResources* **2009,** *4* (4), 80-93.

29. Wang, S.; Yu, Y., Bioactive Bead Type Cellulosic Adsorbent for Blood Purification. **2013**.

30. Habibi, Y.; Lucia, L. A.; Rojas, O. J. *Chem. Rev.* **2010,** *110* (6), 3479-3500.

31. Moon, R. J.; Martini, A.; Nairn, J.; Simonsen, J.; Youngblood, J. *Chem. Soc. Rev.* **2011,** *40* (7), 3941.

32. Lin, N.; Huang, J.; Dufresne, A. *Nanoscale* **2012,** *4* (11), 3274.

33. Klemm, D.; Kramer, F.; Moritz, S.; Lindström, T.; Ankerfors, M.; Gray, D.; Dorris, A., *Angew. Chem. Int. Ed.* **2011,** *50* (24), 5438-5466.

34. Eichhorn, S. J.; Dufresne, A.; Aranguren, M.; Marcovich, N. E.; Capadona, J. R.; Rowan, S. J.; Weder, C.; Thielemans, W.; Roman, M.; Renneckar, S.; Gindl, W.; Veigel, S.; Keckes, J.; Yano, H.; Abe, K.; Nogi, M.; Nakagaito, A. N.; Mangalam, A.; Simonsen, J.; Benight, A. S.; Bismarck, A.; Berglund, L. A.; Peijs, T. *J Mater Sci* **2009,** *45* (1), 1-33.

35. Saxena, S. G., S.; Jana, A.K. *J. Environ. Res. Develop.* **2012,** *6* (3), 424 - 431.

36. Lin, N.; Bruzzese, C.; Dufresne, A. *ACS Appl. Mater. Interfaces* **2012,** *4* (9), 4948-4959.

37. Xue, C.; Wilson, L. D. *Carbohydr. Polym.* **2016,** *135*, 180-186.

38. Chang, C.; Lue, A.; Zhang, L. *Macromol. Chem. Phys.* **2008,** *209* (12), 1266-1273.

39. Hu, D. W., P.; Li, J.; Wang, L. *BioResources* **2014,** *9* (4), 5951-5962.

40. Coma, V.; Sebti, I.; Pardon, P.; Pichavant, F. H.; Deschamps, A. *Carbohydr. Polym.* **2003,** *51* (3), 265-271.

41. Ibbett, R. N.; Phillips, D. A. S.; Kaenthong, S. *Dyes Pigments* **2007,** *75* (3), 624-632.

42. Kreze, T.; Jeler, S.; Strnad, S. *Mater. Res. Innovations* **2002,** *5* (6), 277-283.

43. Pradeep Sekhar, C.; Kalidhasan, S.; Rajesh, V.; Rajesh, N. *Chemosphere* **2009,** *77* (6), 842-847.

44. Ahmad, R.; Kumar, R.. *Appl. Surf. Sci.* **2010,** *257* (5), 1628-1633.

45. Acemioglu, B.; Kertmen, M.; Digrak, M.; Alma, M. H. *Afr J Biotechnol* **2010,** *9* (6), 874-881.

46. Batzias, F. A.; Sidiras, D. K. *J. Hazard. Mater.* **2004,** *114* (1-3), 167-174.

47. Batzias, F. A.; Sidiras, D. K. *Bioresour Technol* **2007,** *98* (6), 1208-1217.

48. Abdus-Salam, N. B., M. *Pac. J. Sci. Technol.* **2014,** *15* (1), 232-244.

49. Mukherjee, R.; De, S. *J. Hazard. Mater.* **2014,** *265*, 8-19.

50. Hubbe, M. A. B., K.R.; O'Neal, W.G.; Sharma, Y.C. *BioResources* **2012,** *7* (2).

51. Mohamed, M. H.; Wilson, L. D.; Headley, J. V., *J. Phys. Chem. B* **2013,** *117* (13), 3659-3666.

52. Singh, J., Mishra, Uma, N. S., Banerjee, S., & Sharma, Y. C. *BioResources* **2011,** *6* (3), 2730 - 2743.

53. Mohamed, M. H.; Wilson, L. D.; Headley, J. V. *Carbohydr. Polym.* **2010,** *80* (1), 186-196.

54. Wilson, L. D.; Mohamed, M. H.; Berhaut, C. L. *Materials* **2011,** *4* (12), 1528-1542.

55. Pratt, D. Y.; Wilson, L. D.; Kozinski, J. A.; Mohart, A. M. *J. Appl. Polym. Sci.* **2010**, 116, 2982–2989.

56. Giles, C. H.; MacEwan, T. H.; Nakhwa, S. N.; Smith, D. *J Chem Soc (Resumed)* **1960**, 3973-3993.

57. Lynam, M. M.; Kilduff, J. E.; Weber, W. J. *J. Chem. Educ.* **1995,** *72* (1), 80-84.

58. Allen, T., *Particle Size Measurement: Volume 2: Surface Area and Pore Size Determination*. Springer: London, UK, 1997; p 252.

59. Sips, R. *J. Chem. Phys.* **1948,** *16* (5), 490-495.

60. Pratt, D. Y.; Wilson, L. D.; Kozinski, J. A. *J. Colloid Interface Sci.* **2013,** *395* (0), 205-211.

61. Wilson, L. D.; Mohamed, M. H.; Headley, J. V. *J. Colloid Interface Sci.* **2011,** *357* (1), 215-222.

62. Mohamed, M. H.; Wilson, L. D.; Headley, J. V. *Carbohydr. Res.* **2011,** *346* (2), 219-229.

63. Mohamed, M. H.; Udoetok, I. A.; Wilson, L. D.; Headley, J. V. *Rsc Advances* **2015,** *5* (100), 82065-82077.

64. Mohamed, M. H.; Wilson, L. D.; Shah, J. R.; Bailey, J.; Peru, K. M.; Headley, J. V. *Chemosphere* **2015,** *136*, 252-258.

65. Mohamed, M. H.; Wilson, L. D.; Headley, J. V.; Peru, K. M. *Phys. Chem. Chem. Phys.* **2011,** *13* (3), 1112-1122.

66. Kosmulski, M. *J. Colloid Interface Sci.* **2002,** *253* (1), 77-87.

67. Zimmermann, R.; Freudenberg, U.; Schweiß, R.; Küttner, D.; Werner, C. *Curr Opin Colloid Interface Sci.* **2010,** *15* (3), 196-202.

68. Okoli, C. P.; Guo, Q. J.; Adewuyi, G. O. *Carbohydr. Polym.* **2014,** *101*, 40-49.

69. Mohamed, M. H.; Wilson, L. D.; Headley, J. V. *Microporous Mesoporous Mater.* **2015,** *214*, 23-31.

70. Chaplin, M. Water structure and science. Available from: http://www1.lsbu.ac.uk/water/martin chaplin.html. (Accessed on 05-09-2015)

71. Bertau, M.; Jörg, G. *Biorg. Med. Chem.* **2004,** *12* (11), 2973-2983.

72. Niide, T.; Shiraki, H.; Oshima, T.; Baba, Y.; Kamiya, N.; Goto, M. *Solvent Extr Res Dev, Jpn* **2010,** *17* (0), 73-81.

73. Yan, L.; Shuai, Q.; Gong, X.; Gu, Q.; Yu, H. *CLEAN - Soil, Air, Water* **2009,** *37* (4-5), 392-398.

74. Kwon, J. H.; Wilson, L. D.; Sammynaiken, R. *J. Colloid Interface Sci.* **2015,** *457*, 388-397.

Chapter 4

(Manuscript 3)

Description

In this chapter, cellulose was cross-linked with EP/aqueous ammonia using the conventional stirring/heating method versus the application of sonication. The modified **C-EP heating** and **C-EP sonication** polymers were characterized via FTIR and ^{13}C solids NMR spectroscopy, differential scanning calorimetry (DSC) and TGA studies. The results revealed variable modification of cellulose according to the synthetic procedure, where the different synthetic routes produced polymers with different morphology, equilibrium swelling and adsorption properties. **C-EP sonication** exhibited optimum sorption properties relative to the **C-EP heating**.

Authors' contribution

The experimental design was conceived by me and Lee D. Wilson. I performed all the experiments related to this project along with data analysis; Lee D. Wilson secured funding and John V. Headley contributed analysis tools; I wrote the first draft of the manuscript with extensive editing by Lee D. Wilson, where John V. Headley provided final proofreading of the final manuscript.

Relation of Manuscript 2 to Overall Objective of this Project

The goal of this project coincides with the first and fourth themes (cross-linking of chitosan and cellulose and sorption studies of NAFCs using cellulose and chitosan based polymers) of the

overall objective the thesis research. This project was designed to overcome the challenge of inefficient pillaring of cellulose due to strong inter-/intra-molecular hydrogen bonding in the biopolymer. In this project, cellulose was cross-linked with EP/ aqueous ammonia using the conventional stirring/heating method and the application of sonication.

Graphical Abstract

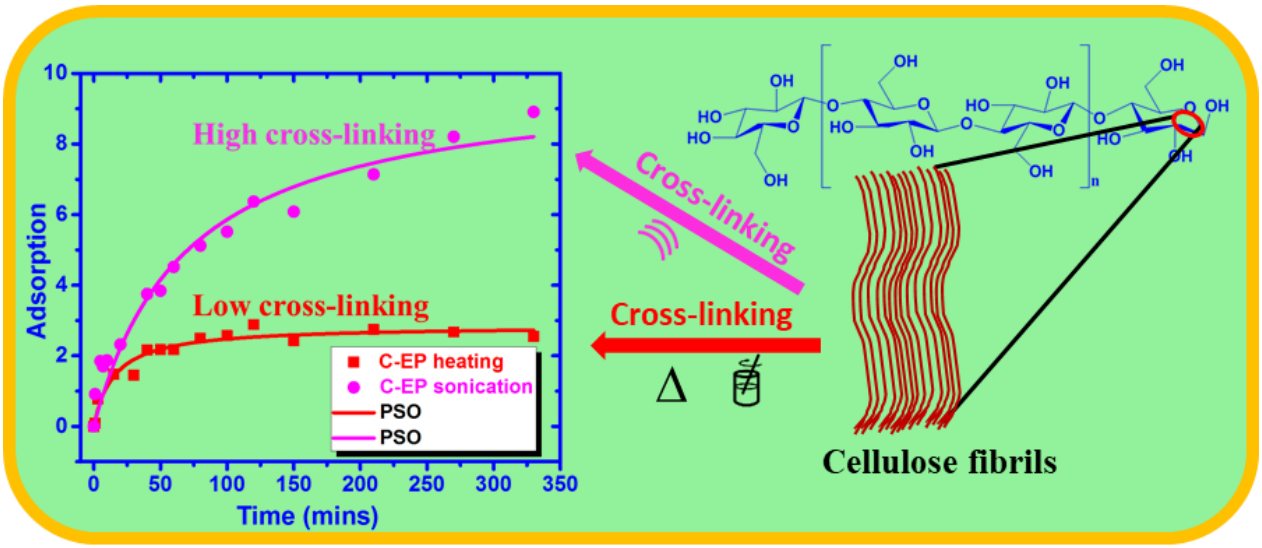

Research Highlights

- Cellulose was modified by conventional heating vs assisted sonication.
- Variable structure and adsorption properties were noted for each method.
- Sonication yielded greater cross-linking of cellulose with epichlorohydrin.
- Cross-linked cellulose has variable adsorption properties and pillared structure.
- Cross-linking assisted by sonication is a valuable synthetic tool.

4. Ultra-Sonication-Assisted Synthesis of Cross-linked Cellulose Polymers

Inimfon A. Udoetok[1]; Lee D. Wilson[1*] and John V. Headley[2]

[1]Department of Chemistry, University of Saskatchewan, 110 Science Place, Saskatoon, Saskatchewan, S7N 5C9

[2]Water Science and Technology Directorate, Environment and Climate Change Canada, 11 Innovation Boulevard, Saskatoon, Saskatchewan, S7N 3H5

***Corresponding Author**: L. D. Wilson, Tel. +1-306-966-2961, Fax. +1-306-966-4730, Email: lee.wilson@usask.ca

4.1 Abstract

Cross-linked cellulose-epichlorohydrin polymers were synthesized by a conventional heating with stirring (**C-EP heating)** and a parallel process using ultra-sonication (**C-EP sonication**) in the presence of aqueous ammonia. Structural characterization of modified cellulose was carried out using FTIR/^{13}C solid state NMR spectroscopy and thermal methods (DSC and TGA) to characterize the cross-linked products by conventional versus sonication assisted synthesis. Evidence of products with variable textural properties and morphology was supported by nitrogen gas adsorption, solvent swelling, and microscopy (SEM, TEM) results. **C-EP sonication** possess greater cross-linker content judging by the loss of the cellulose fibril structure which was facilitated by acoustic cavitation effects due to ultra-sonication. Equilibrium sorption studies in aqueous solution with 2-naphthoxy acetic acid (**S6**) revealed that **C-EP heating** had slightly greater sorption capacity than **C-EP sonication** at alkaline pH. By contrast, **C-EP sonication** had greater uptake of **S6** at acidic pH. Kinetic uptake studies at pH 3 is described by

the pseudo-second order model, where the surface sites of **C-EP heating** became saturated within ca. 75 minutes; whereas, ca. 350 minutes occurred for **C-EP sonication**. This study demonstrates that the yield of sonication assisted cross-linking of cellulose is greater with improved adsorption properties. The study also reveals the utility of sonicated assisted synthesis for the valorization and utilization of cellulose modified materials.

Keywords: Cellulose; cross-linking; epichlorohydrin; sonication; sorption isotherms

4.2 Introduction

Cellulose is one of the most abundant renewable biopolymers that is recyclable, renewable, biodegradable, and nontoxic in nature.[1-2] Cellulose is a structurally unique polysaccharide containing a repeat unit analogous to cellobiose, $(C_6H_{10}O_5)_n$; where n = 2) consisting of β-1→4-glycosidic linkages. [2] Cellulose has crystalline and amorphous domains that afford extensive intra-molecular (O3-H⟶O5' and O6⟶H-O2') and intra-strand (O6-H⟶O3') hydrogen bonding. This extensive hydrogen bonding for the tertiary structure of cellulose confers high mechanical strength and limited solubility in conventional solvents. Due to the widespread abundance of this environmentally friendly biopolymer, cellulose is the subject of continued interest. A key focus of research in this area relates to the structural modification of cellulose and improvement of its solubility properties for use in personal care products, nanocomposites, emulsion stabilizing agents, adsorbents and drug delivery agents etc.[2-13] The modification of cellulose involves esterification, cationisation, oxidation via 2,2,6,6-tetramethylpiperidinyl-1-oxyl (TEMPO), acetylation, carboxylation, etherification, silylation, cross-linking and polymer grafting.

Cross-linking is a tool that affords tuning of the physicochemical properties of cellulose[3, 11, 13] using suitable bifunctional linkers such as epichlorohydrin (EP) or glutaraldehyde (GL).

These linkers alter the surface chemical and textural properties of the polymer through *pillaring effects* on the biopolymer network.[14] Previous work has shown that cross-linking of cellulose alters the surface chemistry, morphology, and physicochemical properties such as solvent swelling, transport phenomena, adsorption, mechanical/chemical stability, and biodegradability.[3, 13, 15] A key challenge related to the modification of cellulose, especially in heterogeneous reaction media is the ability to advance reactions to a controlled extent. Limitations in this regard can be attributed to solvent accessibility due to the extensive intra/intermolecular hydrogen bonding of cellulose that limit the relative hydroxyl group accessibility for cross-linking reactions. In a previous report,[13] cellulose cross-linked with epichlorohydrin had reduced adsorption of negatively charged species due to its lower surface area and negative ζ-potential.

Unconventional solvents like ionic liquids [16-17] or NaOH/urea systems [18-19] may improve the dissolution of cellulose in homogeneous reaction media. However, such solvent systems may not be cost effective nor environmentally friendly in view of their potential toxicity. There is a need to develop improved strategies for the modification of cellulose in heterogeneous media to address the foregoing knowledge gaps. The cross-linking of cellulose in heterogeneous media may be facilitated by the application of sonochemistry to improve the accessibility of hydroxyl groups and the resulting yield of such reactions. Sonochemistry refers to the study of chemical reactions that are mediated by ultrasound radiation (20 kHz–10 MHz).[20] Ultrasonic irradiation is known to enhance reactions in both homogeneous and heterogeneous media by increasing the reaction rate and chemical selectivity. A key effect of ultrasound waves in chemical reactions relate to the role of cavitation. Cavitation refers to the nucleation, growth, oscillation and transient collapse of tiny gas or vapor bubbles due to a variation in the internal pressure generated in the medium via ultrasound radiation.[21-22] The physical effects of ultrasound and cavitation include: (*i*) improved

mass transport due to turbulent mixing and acoustic streaming, (*ii*) surface damage at liquid-solid interfaces because of shock waves and microjets, (*iii*) high-velocity interparticle collisions in slurries, and (*iv*) mechanical fragmentation of large solid particles to increase surface area.[20, 23] These processes afford favorable reaction kinetics and a consequent increase in the product yield.[24] Previous studies[25-26] on the use of sonochemistry in chemical synthesis reveal that cavitation effects in liquid-solid systems enhance chemical reactivity. For example, the accessibility and oxidative reactivity of cellulose with sodium periodate in terms of water retention value (WRV) was found to increase with longer sonication time.[27] As well, Frone et al. [28] reported that variable sized nanofibers with similar crystallinity were observed in PVA/cellulose composites prepared under different ultrasonic conditions. Wood et al. [29] and Ofori- Boateng and Lee [30] reported greater bioethanol production with applied sonication. A review of ultrasound assisted reactions for the initiation of polymerization reveal that ultrasonic irradiation aids the dispersion of inorganic nanoparticles and organo-clay, and also acts as an initiator to enhance polymerization rate for polymer nanocomposites.[31] Another report shows that sonication enhances the control of hydrogel molecular weight along with improving their swelling ratio.[24, 32] Li et al. showed that ultrasonic irradiation in the enzymatic extraction of bovine tendon collagen increased the yield (ca. 124%) of collagen while significantly reducing the extraction time compared with a conventional pepsin isolation method.[33] Wang et al. reported that lignin-*g*-poly (acrylamide-co-N-Isopropyl acrylamide) hybrid hydrogel synthesized via sonication had excellent dye removal from wastewater.[34] Yu et al. reported a 27.5% and 27.8% increase in gelatin hydrolysis rate constant and enzyme inactivation constant with ultrasonic pretreatment.[35] Islam et al. [36] reported on the effectiveness of sonication assisted transesterification over the conventional process. They demonstrated that at low molar ratio, sonication assisted transesterification led to a stoichiometric

conversion while the reaction via the conventional transesterification process was less efficient. Ahmed et al. [37] reported that ultrasonic-assisted deacetylation of cellulose acetate was faster versus conventional deacetylation, where reaction time was reduced from are 30 h to 1 h. Sonication-assisted depolymerization of plant (PC) and bacterial (BC) celluloses was reported by Wong et al. [38] The authors reported a change in the molecular weight of cellulose accompanied by a parallel drop in the polydispersity index (PDI) of PC. An unexpected increase in the PDI of BC along with a major increase in the crystalline fraction of cellulose was observed. Gadhe et al. [39] reported on the modification of the surface properties of wood fibers by the generation of free radicals using high-frequency ultrasound, that resulted in an increase in the number of non-conjugated carbonyl groups in the thermomechanical pulp fibers. They also reported an increase in the surface free energy of the fibers after sonication. The role of ultrasonic application on various carbohydrate polymers has been reported in a recent review.[40]

This study compares the physicochemical and adsorption properties of cellulose cross-linked with epichlorohydrin by conventional heating with stirring versus a sonication assisted reaction. This study contributes to the development of modified cellulose in several ways: *i*) the role of ultrasound irradiation for the cross-linking of cellulose with epichlorohydrin, *ii*) the utility of sonochemistry as an assisted method is revealed for cross-linking of cellulose in heterogeneous media, and *iii*) the valorization of cellulose as an adsorbent for chemical fractionation and environmental remediation.

4.3 Material and methods

4.3.1 Materials

Cellulose (medium fibre from cotton linters), sodium hydroxide, aqueous ammonia, 99% epichlorohydrin (EP), HCl, 2-naphthoxy acetic acid (**S6**) and ACS grade acetone were obtained from Sigma Aldrich (MO, USA). All materials were used as received without further purification. A sonication bath, JAC 4020 with an ultrasonic power of 40 kHz (KODO technical research company limited, Korea) for the cross-linking reaction.

4.3.2 Synthesis of Cross-linked cellulose Polymers

C-EP heating was synthesized according to reports from previous studies [11, 41] with slight modification as follows: 2 g of bulk cellulose was heated in 16 mL of 10% NaOH at 65 ^{o}C for 3 h, followed by drop-wise addition of 1 mL of EP and 2 mL of aqueous ammonia (14.1M). The resulting reaction mixture was stirred with heating at 65 ^{o}C for ca. 6 h followed by neutralization with 6 M HCl. The product was separated from the supernatant via vacuum filtration followed by washing with cold Millipore water and ACS grade acetone. For **C-EP sonication**, 2 g of bulk cellulose in 16 mL 10% NaOH was treated in a sonication bath for 2 h followed by drop-wise addition of 1 mL of EP and 2 mL of aqueous ammonia (14.1 M), respectively. The reaction mixture was kept under continuous sonication for 6 h (from treatment with 10% NaOH to the end of the synthesis), where the temperature of the sonication bath ranged from 25 to 60 ^{o}C. The product was isolated by vacuum filtration, followed by washing with cold Millipore water and ACS grade acetone. The product was dried at 60 ^{o}C. Soxhlet extraction for 24 h with HPLC grade acetone was used to remove unreacted/excess reagents, followed by drying in a vacuum oven at 60 ^{o}C for 12 h. The products were ground using a mortar and pestle and passed through a 40-mesh sieve.

Each material was synthesized at least 3 times during the research project and characterization results affirmed the repeatability of the synthetic procedure. The yield of the cross-linked polymers was calculated using eqn. (1) as follows

$$\%\text{Yield} = \frac{\text{dry weight of cross-linked polymers (g)}}{\text{dry weight of Cellulose (g)}} \times 100 \qquad \text{Equation 4.1}$$

4.3.3 Characterization

4.3.3.1 Fourier Transform Infrared (FTIR) Spectroscopy

The FTIR spectra of the cross-linked polymers and cellulose were obtained using A Bio-RAD FTS-40 IR spectrophotometer. Dry and powdered samples were mixed with pure spectroscopic grade KBr in a weight ratio of 1:10 with grinding in a small mortar and pestle. The DRIFT (Diffuse Reflectance Infrared Fourier Transform) spectra were obtained in reflectance mode at 295 K with a resolution of 4 cm^{-1} over a spectral range of 400–4000 cm^{-1}. Multiple scans were recorded and corrected relative to a background of pure KBr.

4.3.3.2 Solid State ^{13}C NMR Spectroscopy

Solid state ^{13}C NMR spectra of cellulose and cross-linked forms were obtained using a Bruker AVANCE III HD spectrometer furnished with a 4 mm DOTY CP-MAS (cross polarization with magic angle spinning; CP-MAS) solids probe operating at 125.8 MHz (^{1}H frequency at 500.2 MHz). The following instrumental parameters were applied: mas spinning speed (10 kHz), a ^{1}H 90^0 pulse of 3.5 µs, contact time (0.75 ms), with a ramp pulse on the ^{1}H channel. Others include a ^{13}C 90^0 pulse of 3.15 µs and a 25 kHz SPINAL-64 with ^{1}H decoupling during acquisition. 2k scans were accumulated with a recycle delay of 2 s, and all spectra were recorded using 71 kHz SPINAL-

64 decoupling during acquisition, where chemical shifts were externally referenced to the low field signal of adamantane (δ=38.48 ppm).

4.3.3.3 Thermal Gravimetric Analysis (TGA)

Thermal stability of cellulose and its cross-linked forms were determined using a TA Instruments Q50 TGA system operated with a heating rate of 5˚C min^{-1} up to 500˚C using nitrogen as the carrier gas. The results are shown as first derivative (DTG), mass loss with temperature (%/˚C) versus temperature (˚C), and TGA plots of weight loss (%) versus temperature.

4.3.3.4 Differential Scanning Calorimetry (DSC) Studies

The DSC thermograms of cellulose and its cross-linked forms were acquired using a TA Q20 thermal analyzer between 40 - 400°C. A scan rate of 5 °C /min was applied while dry nitrogen gas was used to regulate temperature and compartment purging.

4.3.3.5 Equilibrium Solvent Swelling

The equilibrium solvent swelling properties of samples were examined by adding approximately ~30 mg into a 20 mL vial followed by the addition of 15 mL of Millipore water and equilibrating for 48 h. The weight of hydrated sample (ws) was determined after tamping dry while the dry weight was obtained following further drying in an oven at 60 °C to a constant weight (wd). The swelling ratio was calculated using equation 4.2

$$Sw(\%) = \frac{\mathrm{Ws}-\mathrm{Wd}}{Wd} \times 100 \qquad \text{Equation 4.2}$$

4.3.3.6 *Scanning Electron Microscopy (SEM)*

The surface morphology of samples were studied using scanning electron microscopy (SEM; Model SU8000, HI-0867-0003). Samples were coated with 2 nm of chromium and images collected under the following instrument conditions; accelerating voltage – 5kV and 2.0 kV, working distance (WD) of 9.1, 4.3 and 4.2 mm with a magnification of × 55 k.

4.3.3.7 Transmission Electron Microscopy (TEM) Studies

Transmission electron microscope (TEM) images of samples were obtained using a Hitachi TEM system at a voltage of 80.0 k. Samples were dispersed in methanol prior to deposition onto a carbon-coated copper TEM grid.

4.3.3.8 Gas Adsorption Studies

A Micromeritics ASAP 2020 (Norcross, GA) system was used to characterize the surface area (SA) and pore structure properties of the polymers by nitrogen adsorption. Sample (ca. 1 g) degassing was carried out under the following conditions: evacuation rate of 5 mmHg s^{-1} in the sample chamber to a stable outgas rate of <10 mmHg min^{-1} and a degassing temperature of ~100 °C for 72 h. The instrumental parameters were calibrated using an alumina standard (Micromeretics). The BET SA was calculated based on the adsorption isotherm using 0.162 nm^2 as the SA for gaseous molecular nitrogen.[42] A t-plot using the de Boer method)[43] afforded estimation of the micropore SA while the Barret–Joyner–Halenda (BJH) method was used to estimate the pore volume and pore diameter from the adsorption isotherm.

4.3.4 Sorption Studies

4.3.4.1. Equilibrium Uptake Studies of Single Component Carboxylate Anions

A 100 mL stock solution of **S6** at 150 ppm was prepared in Millipore water with sonication and further stirring until **S6** completely dissolved.

Fixed amounts (~10 mg) of cellulose, **C-EP heating** and **C-EP sonication** were mixed with 5 mL of **S6** solutions in 2 dram vials at a fixed concentration of 150 ppm. The mixtures were equilibrated at 295 K on a horizontal shaker for 24 h. A double beam spectrophotometer (Varian CARY 100) was used to determine the initial concentration (C_o) and residual concentration of NAA at equilibrium (C_e) at λ=325 nm and 295 K. Centrifugation was used to separate the polymers from the sample mixture prior to UV-vis spectral analyses. The uptake of **S6** was estimated according by equation 4.3.

$$Q_e = \frac{(C_o - C_e) \times V}{m}$$ Equation 4.3

Q_e is the quantity of adsorbate bound in the solid phase at equilibrium (mg g^{-1}), C_o is initial concentration of adsorbate (mg L^{-1}) in solution, C_e is concentration of adsorbate in solution at equilibrium (mg L^{-1}), V is volume of adsorbate solution, and m is the mass (g) of sorbent.

4.3.4.2 Kinetic Uptake Studies

Kinetic studies were carried out using a one pot method [44]. In brief, ca. 100 mg of sample was added to a Whatman filter paper (55 mm diameter), that was folded and clamped at both ends to contain the added polymer. The filter paper assembly containing the sample was immersed in a fixed volume (120 mL) of **S6** solution (150 ppm). 3 mL of the **S6** solution was sampled at variable

time intervals with a double beam spectrophotometer (Varian CARY 100) to determine the residual concentration of the aliquots at 295 K. The uptake of **S6** at variable intervals (t) was estimated using equation 4.4, where C_o and C_t are concentrations at t = 0 and variable t.

$$Q_t = \frac{(C_o - C_t) \times V}{m} \qquad \text{Equation 4.4}$$

The results were analysed by plotting kinetic isotherms (Q_t vs time) according to the pseudo-first order (PFO; equation 4.5) and pseudo-second order (PSO; equation 4.6), where the rate constants are denoted as k_1 and k_2 respectively.

$$Q_t = Q_e(1 - e^{-k_1 t}) \qquad \text{Equation 4.5}$$

$$Q_t = \frac{Q_e^2 k_2 t}{1 + k_2 t Q_e} \qquad \text{Equation 4.6}$$

4.4 Results and Discussion

4.4.1 Characterization Results

4.4.1.1 FTIR Spectroscopy

Fourier transform infra-red (FTIR) spectroscopy studies was employed for structural characterization of the functional groups of cellulose after synthetic modification. The modification may result in attenuation or enhancement of characteristic functional groups as presented in Figure 4.1. The spectra (*cf.* Figure 4.1) reveal a broad IR band (~3000–3600 cm^{-1}) related to intermolecular bonded OH and NH groups, C–H stretching (~2800–3000 cm^{-1}), O–H and C–H bending (~1400–1300 cm^{-1}), and C–O–H and C–O–C asymmetric stretching (~1000–1200 cm^{-1}), in agreement with other reports. [3, 13] The spectra reveal that cross-linking of cellulose

with EP result in modification of the functionality of native cellulose, where the modified materials display a new signature (N–H band at ~1575 cm^{-1}) (*cf.* Figure 4.1B) and/or enhanced signal intensity between 3000–3600 cm^{-1} and 2800–3000 cm^{-1}, related to O–H and C–H bending vibrations, respectively. The foregoing relates to the introduction of these groups to cellulose from the linkers, in agreement with other studies.[3, 13] A notable feature from the spectra of the ultra-sonication assisted material (**C-EP sonication**) relative to **C-EP heating** and cellulose is the greater intensity and broadening of the N–H band (1575 cm^{-1}) and adsorbed water (1640 cm^{-1}) (*cf.* Fig. 1B). Sonication may contribute to improved mass transport due to turbulent mixing and acoustic streaming from the ultrasound waves, along with greater cross-linking efficiency, in agreement with other reports. [25-26] The FTIR results provide support that sonication improves the product yield of such cross-linking reactions.

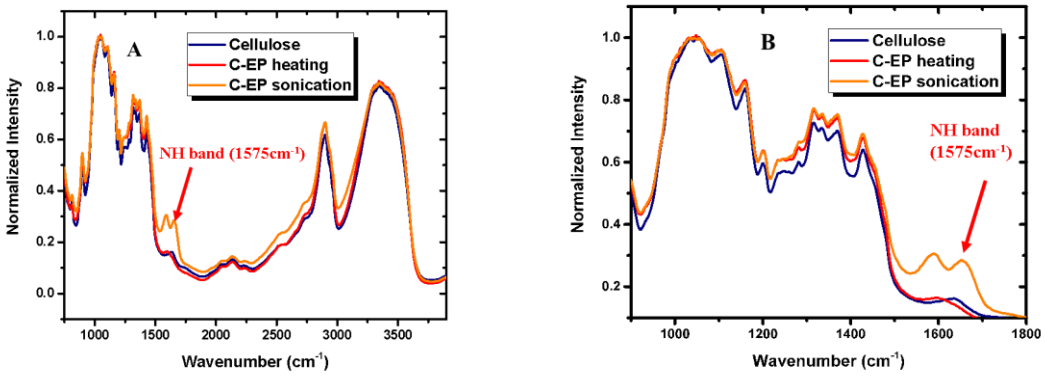

Figure 4.1A) FTIR spectra of cellulose and cross-linked polymers from 750 cm^{-1} to 4000 cm^{-1}

B) FTIR spectra of cellulose and cross-linked polymers from 800 cm^{-1} to 1800 cm^{-1}

4.4.1.2 CP-MAS Solid State ^{13}C NMR Spectroscopy

^{13}C CP-MAS solid state NMR spectroscopy provide structural information about the carbon framework of cellulose and its modified forms, as illustrated in Figure 4.2. The ^{13}C signals of cellulose and its cross-linked forms are observed between 62 to 105 ppm, in agreement with other studies on cellulose and related biopolymers. [45-48] The signals at 104.9 ppm (C1), 88.7 ppm (C4) and 64.7 ppm (C6) are attributed to ^{13}C nuclei in the crystalline (cry.) domains. By comparison, spectral signatures at 83.8 ppm (C4) and 63 ppm (C6) relate to the ^{13}C nuclei for the amorphous (Am.) domains of cellulose. The ^{13}C signals between 70 – 87 ppm are related to C2, C3 and C5 of cellulose. The similar trends in chemical shift for the ^{13}C nuclei of cellulose and its cross-linked forms affirm the preservation of the skeletal structure of the biopolymer, in agreement with previous reports.[41, 48] A noteworthy feature of the ^{13}C NMR spectra of cross-linked cellulose is the sharpness of ^{13}C NMR resonance lines and reduced intensity of the amorphous domains (83.8 and 63 ppm), especially for **C-EP sonication**, where signal splitting occurs at 104.9 ppm and 70 – 87 ppm. This reduced intensity, sharpness and splitting of the ^{13}C NMR signals suggests that the groups responsible for these signals participated in the cross-linking reaction or possess greater mobility due to *pillaring effects*.[14] Sharp spectral lines for the ^{13}C nuclei of the cross-linked materials relate to structural changes affecting the hydrogen bonded fibril structure of cellulose. Cross-linking of cellulose with EP is known to contribute *pillaring effects* that have been reported [13] for cross-linked chitosan.[14, 49] NMR studies [50-51] of materials cross-linked with EP reveal ^{13}C NMR signatures between 69 to 73 ppm for the EP linker unit, in agreement with the NMR results in Figure 4.2. The sharper NMR lines for **C-EP sonication** versus **C-EP heating** and cellulose provide support that greater cross-linking occurs via sonication, as supported by reduced thermal stability by TGA results, and a greater FTIR band intensity with broadening of the N–H signature

at ~1575 cm^{-1}.The N-H signature originates from the addition of aqueous ammonia during the cross-linking reaction. Improved reaction kinetics and product yield for reactions assisted by sonication has been previously reported. [24]

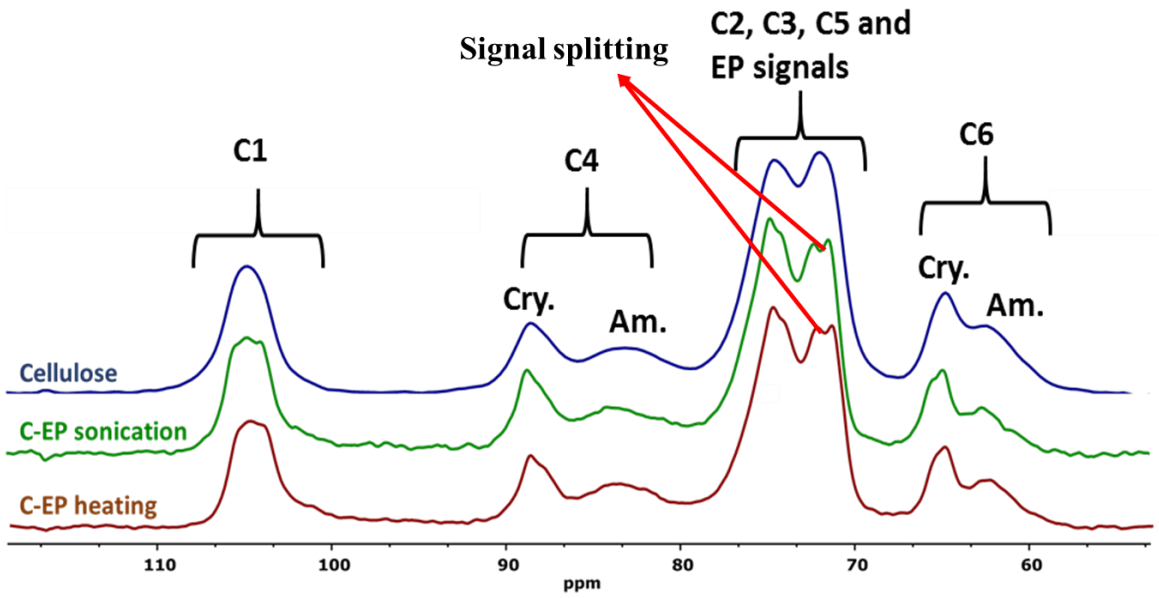

Figure 4.2. CP-MAS ^{13}C solid state NMR spectra of cellulose and its cross-linked forms

4.4.1.3 Thermogravimetric Analysis (TGA)

TGA profiles can be used to elucidate changes in the thermal properties of polymers due to cross-linking effects. Reports [3, 13, 19, 52] on the cross-linking of cellulose have shown that TGA profiles reveal variations in the thermal properties of modified cellulose versus pristine cellulose. The TGA and DTG curves of cellulose and its modified forms in Figures 4.3A-B reveal two decomposition events for cellulose, whereas; three events occur for the cross-linked polymers. The first relates to the evaporative loss of absorbed water and the second and third events relate to the decomposition of cross-linker and cellulose domains. **C-EP sonication** displayed the lowest onset degradation temperature (ca. 154 ºC) with maximum degradation occurring at 322 ºC. This was

followed by **C-EP heating** with an onset temperature of 211 ºC and maximum degradation temperature of 361 ºC. Cellulose has an onset temperature of 253 ºC and the maximum degradation temperature of 332 ºC. The TGA results provide support that cellulose cross-linking assisted by sonication affects the thermal stability of cellulose accordingly. **C-EP sonication** displayed the lowest maximum degradation temperature that may relate to mechanical stress and shock waves from cavitation on the cellulose fibrils by the ultrasonic irradiation. These unique conditions are inferred to result in defibrillation as a result of dissociation of the inter- and intramolecular hydrogen bonding of cellulose. The greater cross-linking yield agrees with FTIR results and the reduction of the crystalline order of cellulose.[53-54] Synthesis of **C-EP heating** involved conventional stirring and heating, where the thermal profiles revealed the highest maximum degradation temperature. The greater degradation temperature was related to cross-linking of the amorphous regions of cellulose with EP and minimal or no grafting of N-H groups. The presence of grafted N-H groups in cellulose leads to a more gradual thermal degradation as shown for **C-EP sonication** versus **C-EP heating** and cellulose. The degradation process will begin from the more accessible grafted N-H groups whereas the higher temperature event relates to the degradation of the non-grafted domains. Overall, the TGA and DTG results provide support that greater cross-linking occurs under sonication conditions due to acoustic cavitation effects, in agreement with the onset of degradation of **C-EP sonication** at a lower temperature and its wider temperature range of decomposition.[55] The weight loss of **C-EP sonication** (75 %) relative to **C-EP heating** (89 %) and cellulose (93 %) agrees with variable thermal stability and flame-retardant ability of the modified cellulose due to greater cross-linking and grafting driven by cavitation effects through sonication.[13, 55-58]

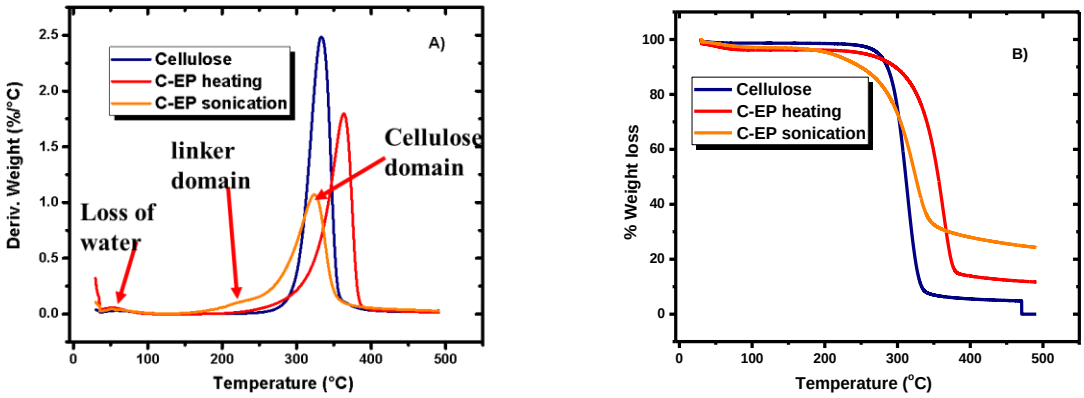

Figure 4.3. A) DTG and B) TGA thermograms of cellulose and cross-linked polymers

4.4.1.4 Differential Scanning Calorimetry (DSC) Studies

Differential scanning calorimetry (DSC) is a versatile thermal analytical tool suitable for the characterization of changes in polymers related to modification due to its sensitivity to heat flow measurements and physical or chemical transitions of materials. DSC measurements at variable temperature and their time dependence provide useful quantitative and qualitative insights about various structural and chemical changes of modified materials. The DSC profiles of cellulose and its cross-linked forms are presented in Figure 4.4. The results reveal an endothermic peak (91 – 93 °C) for all samples, where cellulose, **C-EP heating** and **C-EP sonication** have a peak maxima at 93.5 °C, 78.4 °C and 91.0 °C, respectively, in agreement with another study. [59] The enthalpy for this process relates to evaporation of bound water to the polysaccharide. The DSC profile of cellulose, and **C-EP heating** show a second endotherm at ~ 350 °C and ~ 364 °C, in accordance with the thermal degradation of the materials, in agreement with TGA results in Figure 3A–B. Cellulose has a prominent endotherm while **C-EP heating** shows a higher degradation temperature, in accord with TGA results in Figure 3A–B. Conversely, the **C-EP sonication**

material exhibits an exotherm at 356 °C that relates to degradation that is distinctive from cellulose and **C-EP heating** in Figure 4.4. The variable thermal properties of cellulose and its cross-linked forms highlight the unique structural features of these materials and the role of sonication assisted modification of cellulose via cross-linking.[60]

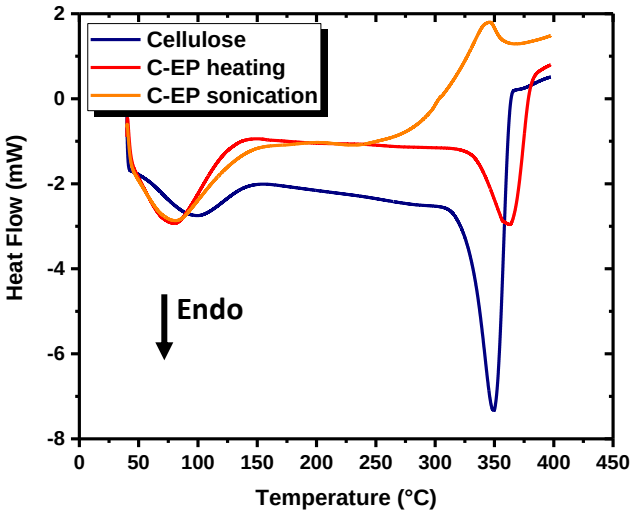

Figure 4.4 DSC profiles of cellulose and its cross-linked forms

4.4.1.5 Solvent swelling

The solvent swelling of biopolymers is related to the surface and internal polymer network structure due to the adsorption and absorption properties of the materials. The complex fibril structure and arrangement of cellulose subunits affect the solvent swelling properties due to the accessibility of micropores, and polar versus apolar domains for such biopolymers. The water swelling results of cellulose and its cross-linked forms are shown in Figure 4.5. The cross-linked polymers (**C-EP heating** and **C-EP sonication**) display greater swelling in water over cellulose, that relate to differences in the tertiary structure of the fibrils. The *pillaring* of the fibrils upon cross-linking with EP results in a greater hydrophile surface area due to increased hydroxyl group

accessibility[13] at the biopolymer surface. The water swelling results reveal that **C-EP heating** has greater swelling over the **C-EP sonication** material due to variable cross-linking via the sonication assisted route. Previous studies [25-26] report that sonication leads to improved mass transport due to turbulent mixing and acoustic streaming. Since efficient mixing is a key parameter that affects the cross-linking, sonication is inferred to enhance the process.[61] Greater cross-linking results in a reduction of free volume available for swelling of the biopolymer framework, [62-63] since *pillaring effects* introduce defects and covalent links in the network of native cellulose (*cf.* Scheme 1 in Ref. 13). As well, EP introduces defects in the case of cross-linked forms that lead to more dynamic motional processes of the cellulose framework, yielding sharper ^{13}C NMR lines. The sharper ^{13}C NMR lines and greater N-H FTIR band intensity for the **C-EP sonication** material (*cf.* Figure 4.1) are consistent with the above claims.

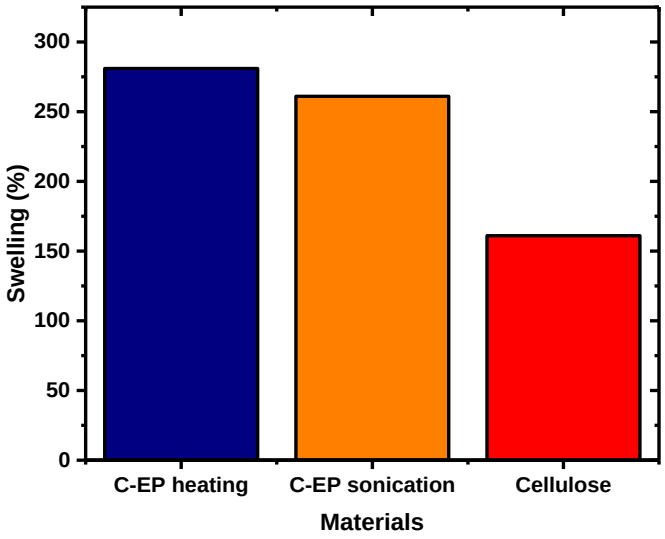

Figure 4.5: Swelling properties of cellulose and cross-linked polymers

4.4.1.6 Scanning Electron Microscopy

Scanning electron microscopy (SEM) enables a study of the surface topology and morphology of biopolymers. SEM may also provide insight on the surface modification of materials due to cross-linking, grafting and composite formation.[64] The SEM results of cellulose and its cross-linked forms (**C-EP heating** and **C-EP sonication**) are shown in Figures 4.6A–C. The micrograph for cellulose (*cf.* Figure 4.6A) reveal that the fibrils of cellulose assemble to form bundles of long fibers, in agreement with the known morphology of cellulose.[65-67] The entanglement of cellulose fibrils and resulting topology from fibrils to sheet-like forms relate to hydrogen bonding interactions. The SEM images of modified cellulose in Figures 4.6B-C show evidence of collapse and disintegration of the fibril structure where long fibers become fragmented. [57] A comparison of the SEM images show that **C-EP heating** has a smoother surface with slight collapse of the fibril structure, while **C-EP sonication** has greater fiber fragmentation with a roughened surface, in agreement with related study. [67] The cellulose fiber lengths have been reported to decrease from 80-120 μm to 30-50 μm after ultra-sonication.[67] The greater fibril disintegration and surface roughness of **C-EP sonication** may relate to acoustic cavitation effects since sound waves are known to generate micro-bubbles that collide with single fibers to enhance fibril breakdown. The foregoing agrees with the greater cross-linking as supported by TGA and ^{13}C NMR/FTIR spectral results presented above.

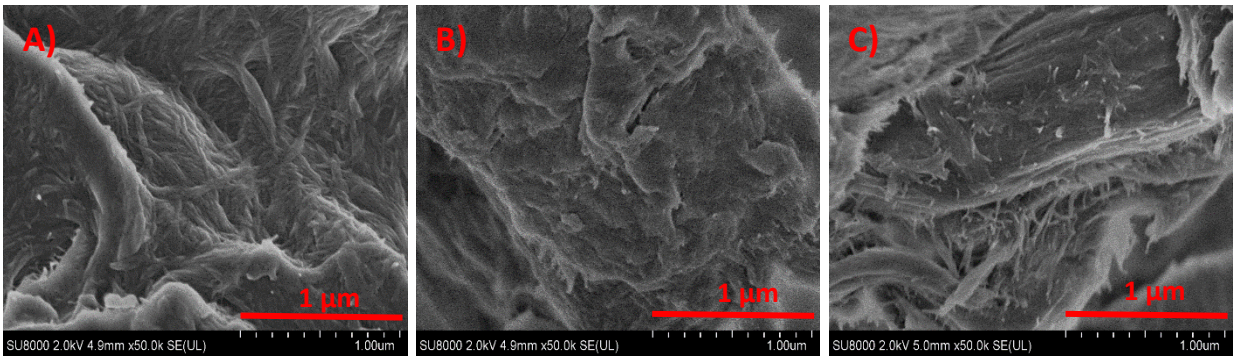

Figure 4.6. SEM micrographs of A) cellulose, B) C-EP heating and C) C-EP sonication at a magnification of 50k×, where C-EP sonication reveals fibrillation effects.

4.4.1.7 Transmission Electron Microscopy (TEM)

TEM studies provide insight on the changes in morphology of biopolymers upon synthetic modification. The greater spatial resolution of TEM provides detailed size information on the nanostructure variation of the biopolymer materials.[68] The TEM micrographs of cellulose and its modified forms are shown in Figures 4.7A–C. The TEM images of cellulose and **C-EP heating** (*cf.* Figures 4.7A and 4.7B) at a magnification of 30k× reveal the fibrillated structure of cellulose, where the appearance of large fibrils with irregular shapes are supported by the SEM results (*cf.* Figures 4.6 A - C). At a magnification of 200k× (Inset on Figures 4.7A and 4.7B), no notable changes are evident due to the large size of the fibrils. On the hand, the TEM image for **C-EP sonication** at a magnification of 30k× shows a collapse of the cellulose fibril structure, where particles with irregular size and shape are observed, in agreement with the SEM results. Furthermore, the TEM image at 200k× magnification (*cf.* Inset of Figure 4.7C) display rod-like particles with irregular size and shape. The TEM results provide additional evidence of greater *pillaring effects* of the cellulose fibrils due to the sonication assisted synthesis. Rohaizu and Wanrosli [58] reported that sono-assisted TEMPO-oxidation and a subsequent sonication process for the isolation of nanocrystalline (NCC) cellulose from oil palm empty fruit bunch led to the

formation of rod-like NCC particles. Acid hydrolysis of cellulose was reported to result in the production of NCC with rod-like shapes due to the hydrolysis of the amorphous domains of cellulose. [58, 67, 69-70] It can be inferred from these studies that the presence of these rod-like particles with irregular size and shape (*cf.* insert on Figure 4.7C) is a result of greater cross-linking of the amorphous domain of cellulose with EP and a subsequent a decrease in the particle size of **C-EP sonication** polymer due to sonication effects. [67, 69-71]

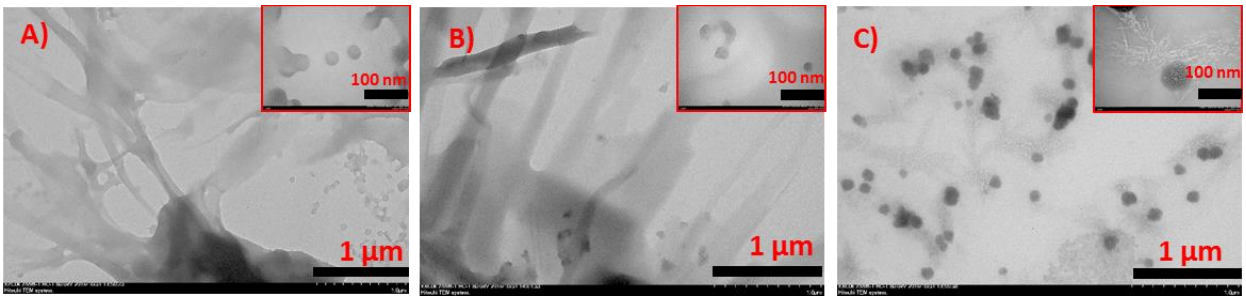

Figure 4.7. TEM micrographs of A) cellulose, B) C-EP heating and C) C-EP sonication at 30k× (Inset images were taken at 200k×)

4.4.1.8 Gas Adsorption Studies

Nitrogen adsorption/desorption isotherms enable characterization of the surface and textural properties of biopolymers. The nitrogen adsorption/desorption isotherms for modified cellulose materials are shown in Figures 4.8A and 4.8B. The isotherm result shows a behavior typical of type II isotherm according to the IUPAC classification system of adsorption isotherms. The adsorption results show completion of the monolayer saturation profile at a low relative pressure (p/p^o) near 0.2. Greater adsorption of nitrogen gas occurs p/p^o at 0.8, in agreement with previous results.[14] At higher p/p^o values, nitrogen can access the grain boundaries and surface sites of the modified materials, in accordance with a higher gas uptake at such conditions[11]. The estimated BET SA and average pore size of **C-EP heating** were 1.18 ± 0.002 $m^2\ g^{-1}$ and 9.15 ± 0.01 nm. By contrast, the values for **C-EP sonication** was 0.871 ± 0.001 $m^2\ g^{-1}$ and 10.0 ± 0.02

nm, respectively. The lower SA of **C-EP sonication** may be due to differences in cross-linking that affect the textural properties of the polymers. However, the greater average pore-size of **C-EP sonication** indicates a loss of the cellulose fibril structure according to the SEM and TEM results.

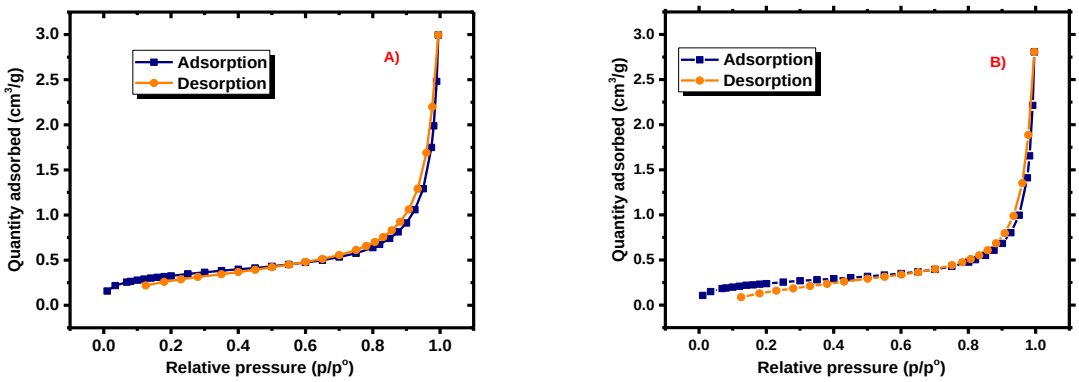

Figure 4.8. Nitrogen adsorption/desorption isotherms: A) C-EP heating and B) C-EP sonication

4.4.2 Effects of Reaction Conditions on Cellulose Cross-Linking

The synthetic yield of any reaction provides a response factor to assess the efficiency of a reaction. The yield (%) of modified cellulose was evaluated by two synthetic routes for cross-linking: i) conventional stirring/heating and ii) sonication assisted cross-linking (*cf*. Figure 4.9). The results show that **C-EP sonication** prepared with the aid of ultra-sonication had greater yield relative to **C-EP heating**. This result correlates with the greater intensity of the N-H band from FTIR studies and parallels the greater cross-linking by the sonication assisted synthesis. The greater cross-linking via the sonication assisted route is understood by the acoustic cavitation that aids in breakdown of the hydrogen bonding between the hydroxyl groups of cellulose, and improving the functional group accessibility for cross-linking. [72]

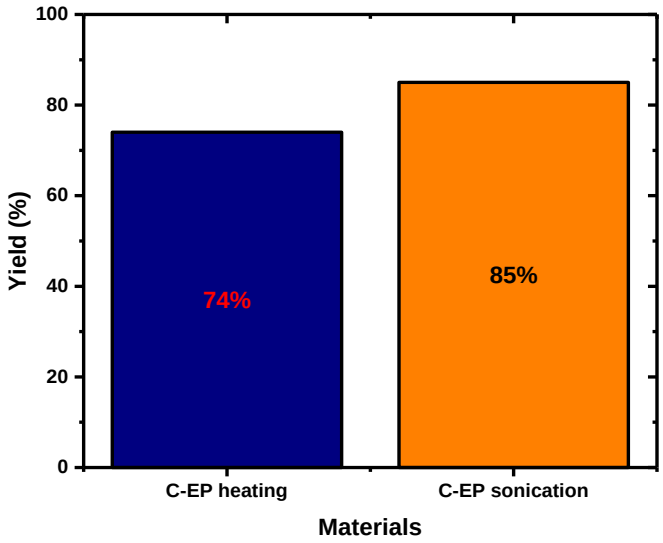

Figure 4.9: Synthetic yield (%) of the cross-linked cellulose

4.4.3. Sorption Studies

4.4.3.1 Single-point Adsorption Study

Equilibrium sorption properties provide a useful tool for probing variations in the morphology and surface functionality of biopolymers. [3, 11, 13-14, 73-74] Single point equilibrium sorption studies of cellulose and its cross-linked forms was carried out with **S6** at variable pH values (pH 3 and 9), as shown in Figure 4.10. The adsorption results also affirm that modification of cellulose by each method had a notable influence on the properties of cellulose, in agreement with the structural characterization results above. For example at pH 3, the sorption capacity (mg/g) of cellulose and the cross-linked forms for **S6** was in the following descending order **C-EP sonication** > **C-EP heating** > cellulose (17.2 > 6.59 > 0.074). At pH 9, the polymers had attenuated sorption capacity (mg/g) for the adsorbate relative to pH 3 as follows: **C-EP heating** > **C-EP sonication** > cellulose (1.85 > 0.82 > 0.23). The above results show that unmodified cellulose consistently displayed the lowest sorption for the adsorbate at each tested pH value. The attenuated

sorption properties of cellulose relate to its limited functional groups' accessibility and lower SA due to its hydrogen bonded fibril structure. The greater sorption of **C-EP sonication** material relative to **C-EP heating** material at pH 3 may relate to cross-linking effects and the role of amine groups, especially at pH 3 due to protonation. Favorable electrostatic interactions between the protonated amines on the polymer surface and the Lewis base sites of the adsorbate favors sorptive uptake. [75] On the contrary, as the pH increases, the level of amine protonation decreases, and concur with a lower uptake of **S6** by **C-EP sonication** at alkaline pH. By contrast, **C-EP heating** has slightly higher uptake and it can be inferred that the uptake of **S6** is strongly influenced by electrostatic and hydrophobic interactions especially at pH 3. By contrast, hydrophobic effects may play a greater role according to the reduced sorption capacity of the biopolymers. At alkaline pH, **S6** is negatively charged along with the surface of the polymers, in agreement with the reported negative ζ-potential of cellulose. [13, 76] The attendant electrostatic repulsion may be offset by adsorption between the apolar sites of the biopolymer and **S6**, in accordance with hydrophobic association processes, especially when the pH lies below the pK_a of **S6**, as observed in Figure 4.10.[77]

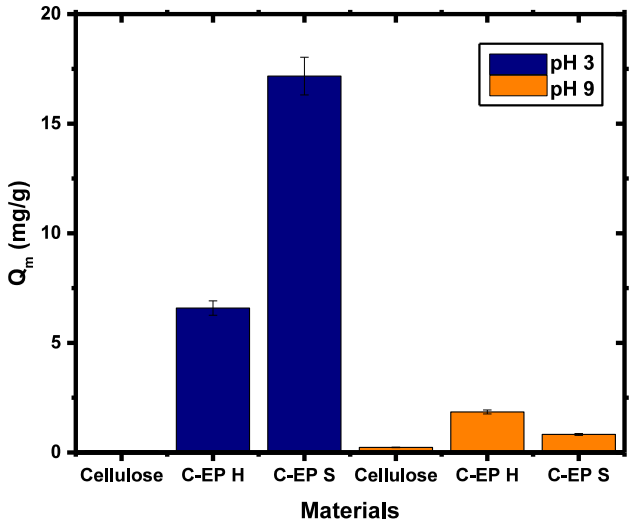

Figure 4.10. Equilibrium uptake of **S6** by cellulose and its modified forms, where C-EP H represent **C-EP heating** and C-EP S represents **C-EP sonication**

4.4.3.2 Kinetic Uptake Studies

Kinetic uptake studies of adsorbent-adsorbate systems provide insight on the level of biopolymer modification. Structural effects via cross-linking are likely to influence the change in surface functionality and textural properties. It follows that the rate of diffusion of the adsorbates are altered in an incremental manner, [44, 78] as shown by the kinetic uptake profiles of **C-EP heating** and **C-EP sonication** with **S6** at pH 3 in Figure 4.11. The trend in uptake reveals that the pseudo-second order kinetic (PSO) model had the best-fit according to favorable R^2 values. The Q_t values (mg/g) for **C-EP heating** and **C-EP sonication** materials are 2.85 ± 0.12 and 9.94 ± 0.69, respectively. The corresponding k_2 (mg/*g*.min) values for **C-EP heating** and **C-EP sonication** were estimated as 0.023 ± 0.006 and 0.00144 ± 0.0004, respectively. The kinetic uptake results show that **C-EP heating** was saturated after ca. 75 minutes versus ca. 350 minutes for the **C-EP sonication** material. The kinetic results reveal that **C-EP sonication** had greater sorption capacity with **S6** at equilibrium while **C-EP heating** displayed a faster kinetic uptake. The greater cross-

linking density of **C-EP sonication** over **C-EP heating** is consistent with the structure and equilibrium sorption results described above. The greater kinetic uptake of **S6** by **C-EP sonication** is correlated with the greater cross-linking of this polymer, along with the presence of surface grafted amine groups on the cellulose material. The results concur with the presence of ammonium cation species and the enhanced electrostatic interaction with **S6** at pH 3.[75] The kinetic results provide additional support that sonication assisted synthesis provide enhanced (ca. four-fold) sorption properties, in agreement with the equilibrium uptake results above (*cf*. Figure 4.10).

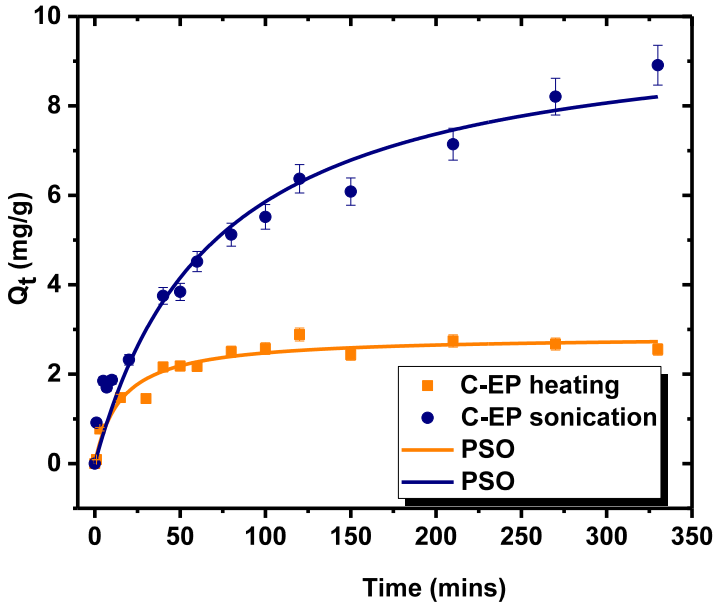

Figure 4.11. Kinetic uptake profiles for **C-EP heating** and **C-EP sonication** at pH 3 and 298 K

4.5 Conclusions

Cellulose was cross-linked with EP/ aqueous ammonia by two routes: i) conventional heating and stirring with heating at 65 ^{o}C and ii) assistance by ultra-sonication. Cross-linking of cellulose by these routes afforded materials with variable structure and physicochemical

properties. Evidence of structural variation through cross-linking was supported by FTIR/^{13}C solids NMR spectroscopy, TGA, DSC, and SEM/ TEM results. Solvent swelling and adsorption properties with **S6** under equilibrium and kinetic conditions provided further support for differences in the structural, surface chemical and textural properties according to the method of synthesis. Cross-linking is inferred to alter the fibril structure of cellulose by changing its surface area and functional group accessibility. The kinetic uptake profiles of modified cellulose/**S6** systems reveal greater adsorption at kinetic and equilibrium conditions. **C-EP sonication** exhibited greater sorption capacity for **S6** at pH 3 whereas **C-EP heating** displayed slightly higher uptake at pH 9. In general, the properties of modified cellulose were improved by sonication assisted synthesis in agreement with the greater yield (ca. 15%) over conventional cross-linking without sonication. This study presents the first example of the comparison of the differences of cross-linked cellulose by two different routes. Furthermore, this study contributes to a greater understanding of assisted ultra-sonication for improving the reaction efficiency and structural modification of cross-linked biopolymers. The unique structure, morphology and adsorption properties of cellulose materials are demonstrated by the assisted sonication method reported herein.

References

1. Yamazawa, A.; Iikura, T.; Shino, A.; Date, Y.; Kikuchi, J. *Molecules* **2013,** *18* (8), 9021-9033.
2. Qiu, X.; Hu, S. *Materials* **2013,** *6* (3), 738-781.
3. Udoetok, I. A.; Wilson, L. D.; Headley, J.V. *Materials* **2016,** *9* (8), 645-660.
4. Habibi, Y. *Chem Soc Rev* **2014,** *43* (5), 1519-1542.
5. Habibi, Y.; Lucia, L. A.; Rojas, O. J. *Chem Rev* **2010,** *110* (6), 3479-3500.

6. Wang, S.; Yu, Y. **2013**. Bioactive Bead Type Cellulosic Adsorbent for Blood Purification, Cellulose - Medical, Pharmaceutical and Electronic Applications, Dr. Theo G.M. Van De Ven (Ed.), InTech, DOI: 10.5772/56223. Available from: https://www.intechopen.com/books/cellulose-medical-pharmaceutical-and-electronic-applications/bioactive-bead-type-cellulosic-adsorbent-for-blood-purification.

7. Moon, R. J.; Martini, A.; Nairn, J.; Simonsen, J.; Youngblood, J. *Chem Soc Rev* **2011,** *40* (7), 3941-3994.

8. Lin, N.; Huang, J.; Dufresne, A. *Nanoscale* **2012,** *4* (11), 3274-3294.

9. Klemm, D.; Kramer, F.; Moritz, S.; Lindström, T.; Ankerfors, M.; Gray, D.; Dorris, A *Angew Chem Int Ed* **2011,** *50* (24), 5438-5466.

10. Eichhorn, S. J.; Dufresne, A.; Aranguren, M.; Marcovich, N. E.; Capadona, J. R.; Rowan, S. J.; Weder, C.; Thielemans, W.; Roman, M.; Renneckar, S.; Gindl, W.; Veigel, S.; Keckes, J.; Yano, H.; Abe, K.; Nogi, M.; Nakagaito, A. N.; Mangalam, A.; Simonsen, J.; Benight, A. S.; Bismarck, A.; Berglund, L. A.; Peijs, T. *J Mater Sci* **2009,** *45* (1), 1-33.

11. Dehabadi, L.; Wilson, L. D. *Carbohydr Polym* **2014,** *113*, 471-479.

12. Li, Y.; Xiao, H.; Chen, M.; Song, Z.; Zhao, Y. *J Mater Sci*, 49 (2014) 6696-6704.

13. Udoetok, I. A.; Dimmick, R. M.; Wilson, L. D.; Headley, J. V. *Carbohydr Polym* **2016,** *136*, 329-340.

14. Mohamed, M. H.; Udoetok, I. A.; Wilson, L. D.; Headley, J. V. *RSC Adv* **2015,** *5* (100), 82065-82077.

15. Rimdusit, S.; Somsaeng, K.; Kewsuwan, P.; Jubsilp, C.; Tiptipakorn, S. *Eng J* **2012,** *16* (4), 15-28.

16. Ingildeev, D.; Hermanutz, F.; Bredereck, K.; Effenberger, F. *Macromol Mater Eng* **2012,** *297* (6), 585-594.

17. Kimura, A.; Nagasawa, N.; Taguchi, M. *Rad Phys Chem* **2014,** *103*, 216-221.

18. Chang, C.; Lue, A.; Zhang, L. *Macromol Chem Phys* **2008,** *209* (12), 1266-1273.

19. Navarra, M.; Dal Bosco, C.; Serra Moreno, J.; Vitucci, F.; Paolone, A.; Panero, S. *Membranes* **2015,** *5* (4), 810-823.

20. Mojtabazade, F.; Mirtamizdoust, B.; Morsali, A.; Talemi, P. *Ultrason Sonochem* **2018,** *42*, 134-140.

21. Hashemi, H.; Namazi, H. *Ultrason Sonochem* **2018,** *42*, 124-133.

22. Singh, S.; Agarwal, M.; Sarma, S.; Goyal, A.; Moholkar, V. S. *Ultrason Sonochem* **2015,** *26*, 249-256.

23. Pinjari, D. V.; Pandit, A. B. *Ultrason Sonochem* **2010,** *17* (5), 845-852.

24. Koutsianitis, D.; Mitani, C.; Giagli, K.; Tsalagkas, D.; Halász, K.; Kolonics, O.; Gallis, C.; Csóka, L. *Ultrason Sonochem* **2015,** *23*, 148-155.

25. Suslick, K. S.; Price, G. J. *Annu Rev Mater Sci* **1999,** *29*, 295-326.

26. Suslick, K. S.; Fang, M. M.; Hyeon, T.; Mdleleni, M. M. *Nato Adv Sci I C-Mat* **1999,** *524*, 291-320.

27. Aimin, T.; Hongwei, Z.; Gang, C.; Guohui, X.; Wenzhi, L. *Ultrason Sonochem* **2005,** *12* (6), 467-472.

28. Frone, A. N.; Panaitescu, D. M.; Donescu, D.; Spataru, C. I.; Radovici, C.; Trusca, R.; Somoghi, R. *Bioresources* **2011,** *6* (1), 487-512.

29. Wood, B. E.; Aldrich, H. C.; Ingram, L. O. *Biotechnol Prog* **1997,** *13* (3), 232-237.

30. Ofori-Boateng, C.; Lee, K. T. *Fuel.* **2014,** *119*, 285-291.

31. Bhanvase, B. A.; Sonawane, S. H. *Chem Eng Process.* **2014,** *85*, 86-107.

32. Bhanvase, B. A.; Sonawane, S. H.; Pinjari, D. V.; Gogate, P. R.; Pandit, A. B. *Chem Eng Process.* **2014,** *85*, 168-177.

33. Li, D.; Mu, C.; Cai, S.; Lin, W. *Ultrason Sonochem.* **2009,** *16* (5), 605-609.

34. Wang, Y.; Xiong, Y.; Wang, J.; Zhang, X. *Colloids Surf. A* **2017,** *520*, 903-913.

35. Yu, Z.-L.; Zeng, W.-C.; Zhang, W.-H.; Liao, X.-P.; Shi, B. *Ultrason Sonochem* **2016,** *29*, 495-501.

36. Janajreh, I.; Hussain, M. N.; El Samad, T. *IOP Conference Series: Mater Sci Eng* **2015,** *92*, 012016.

37. Ahmed, F.; Ayoub Arbab, A.; Jatoi, A. W.; Khatri, M.; Memon, N.; Khatri, Z.; Kim, I. S. *Ultrason Sonochem* **2017,** *36*, 319-325.

38. Wong, S.-S.; Kasapis, S.; Tan, Y. M. *Carbohydr Polym* **2009,** *77* (2), 280-287.

39. Gadhe, J. B.; Gupta, R. B.; Elder, T. *Cellulose* **2006,** *13* (1), 9-22.

40. Ogutu, F. O. Mu, T.; Elahi, R.; Zhang, M.; Sun, H. *J Food Process Technol.* **2015,** 6(5), 446-453

41. Pratt, D. Y.; Wilson, L. D.; Kozinski, J. A.; Mohart, A. M. *J Appl Polym Sci* **2010**, 2983-2989.

42. Sing, K. *Colloids Surf. A* **2001,** *187-188*, 3-9.

43. Broekhoff, J. *J Catal* **1968,** *10* (2), 153-165.

44. Mohamed, M.; Wilson, L. *Nanomaterials* **2015,** *5* (2), 969-980.

45. Aloulou, F.; Boufi, S.; Labidi, J. *Sep Purif Technol* **2006,** *52* (2), 332-342.

46. Moulthrop, J. S.; Swatloski, R. P.; Moyna, G.; Rogers, R. D. *Chem Commun* **2005,** (12), 1557.

47. Tran, C. D.; Duri, S.; Delneri, A.; Franko, M. *J Hazard Mater* **2013,** *252*, 355-366.

48. Tang, L. R.; Huang, B.; Lu, Q. L.; Wang, S. Q.; Ou, W.; Lin, W. Y.; Chen, X. R. *Bioresource Technol* **2013,** *127*, 100-105.

49. Tang, L. R.; Zhuang, S. Y.; Lu, Q. L.; Lin, S.; Li, P. F.; Liao, Y. N.; Huang, B. *J Biobased Mater Bio* **2016,** *10* (1), 27-33.

50. Crini, G.; Cosentino, C.; Bertini, S.; Naggi, A.; Torri, G.; Vecchi, C.; Janus, L.; Morcellet, M. *Carbohyd Res* **1998,** *308* (1-2), 37-45.

51. Renard, E.; Deratani, A.; Volet, G.; Sebille, B. *Eur Polym J* **1997,** *33* (1), 49-57.

52. Dantas, P. A.; Botaro, V. R. *Open J Polym Chem* **2012,** *02* (04), 144-151.

53. Zhang, Q.; Benoit, M.; De Oliveira Vigier, K.; Barrault, J.; Jégou, G.; Philippe, M.; Jérôme, F. *Green Chem* **2013,** *15* (4), 963.

54. SriBala, G.; Chennuru, R.; Mahapatra, S.; Vinu, R. *Cellulose* **2016,** *23* (3), 1725-1740.

55. Roman, M.; Winter, W. T. *Biomacromolecules* **2004,** *5* (5), 1671-1677.

56. Xu, B.; Malik, N. S.; Ahmad, M.; Minhas, M. U. *PloS One* **2017,** *12* (2), e0172727.

57. Li, W.; Wang, R.; Liu, S. X. *Bioresources* **2011,** *6* (4), 4271-4281.

58. Rohaizu, R.; Wanrosli, W. D. *Ultrason Sonochem* **2017,** *34*, 631-639.

59. Veeramachineni, A.; Sathasivam, T.; Muniyandy, S.; Janarthanan, P.; Langford, S.; Yan, L. *Appl Sci* **2016,** *6* (6), 170.

60. Karoyo, A. H.; Sidhu, P. S.; Wilson, L. D.; Hazendonk, P.; Borisov, A. *J Phys Chem C* **2015,** *119* (38), 22225-22243.

61. Morin-Crini, N.; Winterton, P.; Fourmentin, S.; Wilson, L. D.; Fenyvesi, É.; Crini, G. *Prog Polym Sci* **2017,** *117* (22), 13461-13501.

62. Wong, R.; Ashton, M.; Dodou, K. *Pharmaceutics* **2015,** *7* (3), 305-319.

63. Chavda, H. V.; Patel, C. N. *Int J Pharm Investig* **2011,** *1* (1), 17-21.

64. Mahaninia, M. H.; Wilson, L. D. *J Appl Polym Sci* **2016,** *133* (5), 42949-42959.

65. Chinga-Carrasco, G. *Nanoscale Res Lett* **2011,** *6* (1), 417-423.

66. Ding, S.-Y.; Zhao, S.; Zeng, Y. *Cellulose* **2013,** *21* (2), 863-871.

67. Sumari, S.; Roesyadi, A.; Sumarno, S. *Scientific Study & Research. Chemistry & Chemical Engineering, Biotechnology, Food Industry* **2013,** *14* (4), 229–239.

68. Dolatkhah, A.; Wilson, L. D. *ACS Appl Mater Interfaces* **2016,** *8* (8), 5595-5607.

69. Csiszar, E.; Kalic, P.; Kobol, A.; Ferreira, E. d. P. *Ultrason Sonochem* **2016,** *31*, 473-480.

70. Hamid, S. B. A.; Chowdhury, Z. Z.; Karim, M. Z.; Ali, M. E. *Bioresources* **2016,** *11* (2), 3840-3855.

71. Tang, L.; Huang, B.; Lu, Q.; Wang, S.; Ou, W.; Lin, W.; Chen, X. *Bioresource Technol* **2013,** *127*, 100-105.

72. Huang, W.; Lin, Y.; Taylor, S.; Gaillard, J.; Rao, A. M.; Sun, Y.-P. *Nano Lett* **2002,** *2* (3), 231-234.

73. Astrini, N.; Anah, L.; Haryono, A. *Procedia Chem* **2012,** *4*, 275-281.

74. Chen, X.; Zhou, S.; Zhang, L.; You, T.; Xu, F. *Materials* **2016,** *9* (7), 582.

75. Morrow, B. H.; Payne, G. F.; Shen, J. *J Am Chem Soc* **2015,** *137* (40), 13024-13030.

76. Singh, J.; Mishra, N. S.; Uma; Banerjee, S.; Sharma, Y. C. *Bioresources* **2011,** *6* (3), 2732-2743.

77. Blokzijl, W.; Engberts, J. B. F. N. *Angew Chemie Int Ed* **1993,** *32* (11), 1545-1579.

78. Mohamed, M. H.; Wilson, L. D.; Headley, J. V. *Carbohydr Polym* **2010,** *80* (1), 186-196.

Chapter 5

(Manuscript 4)

Description

This study reports the modification of cellulose via surface functionalization using aqueous ammonia and glycidyl trimethyl ammonium chloride (GTAC) as the grafting agents. The modified biopolymers reported in chapters 2 and 3 were optimized by grafting quaternary ammonium groups unto their surface to afford hydrogels with enhanced sorption properties. The hydrogels were characterized via CHN analysis, TGA, FTIR/ and ^{13}C solids NMR spectroscopy.

Authors' contribution

Lee D. Wilson and I conceived and designed the experiments; I performed all experiments and analyzed the data; Lee D. Wilson secured funding and John V. Headley contributed analysis tools; I wrote the first draft of the paper with extensive editing by Lee D. Wilson, where John V. Headley provided final proofreading.

Relation of Manuscript 4 to Overall Objective of this Project

This chapter discusses the modification of cellulose through surface functionalization with glycidyl trimethyl ammonium chloride. It addresses the second and fourth themes (surface functionalization of cellulose and sorption studies of NAFCs using cellulose and chitosan based polymers) of the objectives of my thesis research.

Graphical Abstract

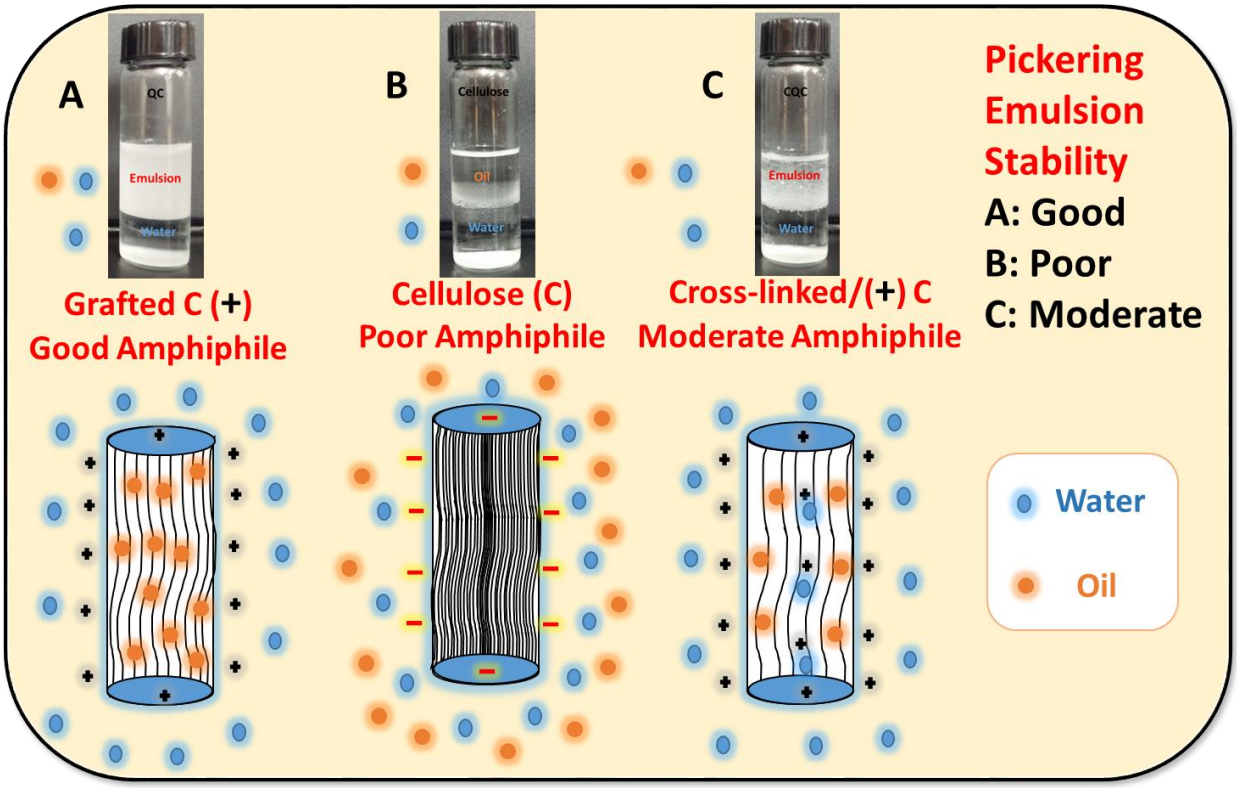

Research Highlights

- Cellulose hydrogels were prepared through cross-linking with EP and/ or surface functionalization with GTAC.
- The hydrogels were more thermally stable than cellulose.
- The hydrogels had greater sorption affinity for naphthenates anions relative to cellulose.
- **C-EP-G** displayed greater sorption capacity than **C-G**.
- The hydrogels exhibited little or no discrimination for NAFC species.
- pH had minor effects on the sorption properties of the hydrogels.

5. Quaternized Cellulose Hydrogels as Sorbent Materials and Pickering Emulsion Stabilizing Agents

Inimfon A. Udoetok[1]; Lee D. Wilson[1*] and John V. Headley[2]

[1] Department of Chemistry, University of Saskatchewan, 110 Science Place, Saskatoon, Saskatchewan, S7N 5C9; Inimfon.udoetok@usask.ca, lee.wilson@usask.ca

[2] Water Science and Technology Directorate, Environment Canada, 11 Innovation Boulevard, Saskatoon, Saskatchewan, S7N 3H5; john.headley@canada.ca

*****Correspondence: lee.wilson@usask.ca; Tel. +1-306-966-2961, Fax. +1-306-966-4730,

5.1 Abstract

Cross-linked/quaternized (**C-EP-G**) and quaternized (**C-G**) cellulose hydrogels were prepared by cross-linking native cellulose with epichlorohydrin (EP), with subsequent grafting of glycidyl trimethyl ammonium chloride (GTAC). Materials characterization via CHN analysis, TGA, and FTIR/ ^{13}C solids NMR spectroscopy provided supportive evidence of the hydrogel synthesis. Enhanced thermal stability of the hydrogels were observed relative to native cellulose. Colloidal stability of hexane and water mixtures revealed that **C-G** induces greater stabilization over **C-EP-G**, as evidenced by the formation of a hexane-water Pickering emulsion system. Equilibrium sorption studies with naphthenates from oil sands process water (**OSPW**) and 2-naphthoxy acetic acid (**S6**) in aqueous solution revealed that **C-EP-G** possess higher affinity relative to **C-G** with the naphthenates. According to the Langmuir isotherm model, the sorption capacity of **C-EP-G** for **OSPW** naphthenates was 33.0 ± 2.8 mg/g and **S6** was 69.5 ± 4.3 mg/g. **C-EP-G** displays similar affinity for the various **OSPW** naphthenate component species in aqueous solution. Kinetic uptake of **S6** at variable temperature, pH and adsorbent dosage showed

that increased temperature favored the uptake process, where Q_m at 303 K = 76.7 ± 4.3 mg/g. Solution conditions at pH 3 or 9 had a minor effect on the sorption process, while equilibrium was achieved in a shorter time at lower dosage (ca. three-fold lower) of hydrogel (100 mg *versus* 30 mg). The estimated activation parameters are based on temperature dependent rate constants, k_1, which reveal contributions from enthalpy-driven electrostatic interactions. The kinetic results indicate an ion-based associative sorption mechanism, where this study contributes to a greater understanding of the adsorption and physicochemical properties of cellulose-based hydrogels.

Keywords: Cellulose; hydrogel; sorption; cross-linking; quaternization; hydrophile-lipophile balance; cooperative interactions

5.2 Introduction

Hydrogels are three-dimensional macromolecular polymer networks capable of absorbing and retaining significant water content due to its hydrophilic nature and network structure.[1-3] Hydrogels are usually prepared by various methods such as chemical cross-linking[4] and physical entanglement. [5] Biopolymer hydrogels derived from polysaccharides are very promising as carrier systems for drug delivery, stabilizers for Pickering emulsions, and adsorbents for pollutant removal. Biopolymer hydrogels are advantageous due to their abundance, low toxicity, biocompatibility, biodegradability, and tunable functionality.[3, 6-8] Cellulose is an abundant and renewable biomaterial that has a white coloration and is odorless, and nontoxic in nature. Cellulose also has unique properties such as mechanical strength, hydrophilicity, relative thermal stability and tunable functionality.[6] The superior mechanical strength of cellulose over other polysaccharides with similar chemical structure and functionality relate to the strong versatile hydrogen bonding within and between biopolymer strands. This structural arrangement allows for

segregation of hydrophobic and hydrophilic regions of the polymer to interact favorably with other components.[9-11]

The synthesis of cellulose-based hydrogels was reported using insoluble cellulose derivatives with bifunctional linkers such as epichlorohydrin,[12] epichlorohydrin with aqueous ammonia,[13] and divinylsulfone (DVS).[14] As well, water soluble forms of cellulose containing quaternary ammonium salt derivatives[15-16] have also been explored. Previous reports [12, 17] indicate that the point of zero charge (PZC) of cellulose-based hydrogels range from 6 to 8, thus affording suitable uptake properties towards both anionic and cationic adsorbates according to the pH conditions. However, the use of these hydrogels for the sorption of anions such as naphthenic acid fraction components (NAFCs) found in oil sands process water (OSPW) is limited due their surface chemistry. At pH conditions above the zeta potential of the hydrogel, adsorptive uptake is attenuated due to electrostatic repulsion between the negatively charged hydrogel surface and the ionized naphthenates. However, the presence of hydrophilic moieties on the hydrogel surface may enhance the uptake affinity with amphiphilic naphthenate species, according to the "law of matching water affinities".[18] OSPW is reported to display toxicity [19-24] due to the water soluble organic fraction that contains the major persistent toxic constituent, referred to as the NAFCs. NAFCs exhibit chemical stability, surfactant-like properties, and persistence in the environment, non-volatility and high viscosity, especially at pH values above the pK_a of NAFCs. The growth in the oil sands extraction industries and the zero-discharge policy of the Government of Canada indicate the need for the development of low cost and sustainable technology for the treatment of the process-affected water. Biopolymer sorbents and their modified hydrogel forms may serve to address this need by subsequent reclamation of the vast area of land used for the storage of these tailings and process-affected water.[25-26]

One approach to improve the affinity of cellulose hydrogels for contaminants like NAFCs at pH values above their point of zero charge (PZC) is to cross-link with bifunctional units such as EP before further grafting with quaternary ammonium salts such as glycidyl trimethyl ammonium chloride (GTAC). Cross-linking with EP may enhance the surface area, porosity and hydrophobic character of the hydrogel, [12] while grafting with quaternary ammonium groups will alter the hydrophile-lipophile balance (HLB) of the system. The shift of the PZC to higher pH values through the introduction of the quaternary ammonium groups afford charge stabilization of the hydrogel over a wider range of pH conditions.[27]

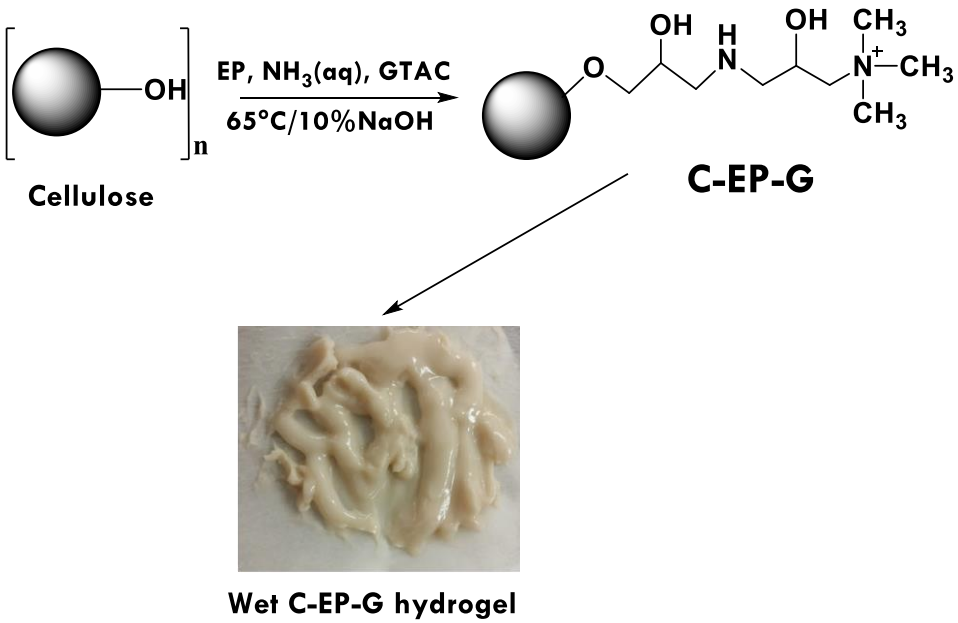

Scheme 5.1. Synthetic scheme for the preparation of **C-EP-G**

The aim of this research focuses on understanding the role of cross-linking of cellulose with EP and surface modification via grafting with aqueous ammonia and GTAC, along with a study of the uptake properties of hydrogel materials with NAFCs. This research work will contribute to the development of low cost and sustainable materials for the treatment of tailing ponds in several ways: *i*) to provide a greater understanding of the chemistry of cellulose hydrogels

by studying the effect of cooperative interactions for hydrogel/adsorbate systems, *ii*) to study the effect of cellulose cross-linking before the introduction of quaternary ammonium ions on the adsorption properties of such hydrogel systems, , *iii*) to evaluate the utility of cellulose hydrogels as Pickering emulsion stabilizers and as sorbent materials for the uptake of NAFCs.

5.3 Materials and Methods

5.3.1 Materials

Cellulose (medium fibre from cotton linters), sodium hydroxide, aqueous ammonia, sodium chloride, 99% epichlorohydrin (EP), glycidyl trimethyl ammonium chloride (GTAC), HCl, 2 naphthoxy acetic acid (**S6**) and ACS grade acetone and octanol were obtained from Sigma Aldrich (MO, USA). All materials were used as received without further purification.

5.3.2 Synthesis of Cellulose Hydrogels

Synthesis of a cellulose hydrogel (**C-EP-G**) was carried out using 2 g of bulk cellulose with heating in 15 mL of 10% NaOH at 65 ^{o}C for 3 h. 1 mL of EP followed by 1 mL of aqueous ammonia was added to the NaOH-cellulose mixture in a drop-wise manner over a one-minute period, where the reaction mixture was stirred at 65 ^{o}C for ca. 16 h. The resulting reaction mixture was neutralized using 6 M HCl and the product separated from the supernatant via vacuum filtration followed by washing with cold Millipore water and ACS grade acetone. The resulting product was added to another round bottom flask and heated in 15 mL of 10% NaOH 65 ^{o}C for 1 h followed by the drop-wise addition of 10 mL GTAC. The reaction mixture was allowed to stir for at least 6 h before separation of the final products via vacuum filtration, followed by washing with cold Millipore water and ACS grade acetone with drying at 60 ^{o}C. Soxhlet extraction for 24 h with HPLC grade acetone was used to remove unreacted/excess reagents, followed by drying in

a vacuum oven at 60ºC for 12 h. The resulting polymer was ground in a mortar and pestle and sieved with a 40-mesh sieve. Another hydrogel (**C-G**) was also synthesized via the same method but without the EP and aqueous ammonia cross-linking step. Each material was synthesized at least 3 times during the research project and characterization results affirmed the repeatability of the synthetic procedure.

5.3.3 Characterization

5.3.3.1 Fourier Transform Infrared (FTIR) Spectroscopy

The FTIR spectra of the hydrogels and cellulose were obtained using A Bio-RAD FTS-40 IR spectrophotometer. Dry and powdered samples were mixed with pure spectroscopic grade KBr in a weight ratio of 1:10 with grinding in a small mortar and pestle. The DRIFT (Diffuse Reflectance Infrared Fourier Transform) spectra were obtained in reflectance mode at room temperature with a resolution of 4 cm^{-1} over the 400–4000 cm^{-1} spectral range. Multiple scans were recorded and corrected relative to a background of pure KBr.

5.3.3.2 Thermal Gravimetric Analysis (TGA)

Thermal stability of the hydrogels and cellulose were determined using a TA Instruments Q50 TGA system operated with a heating rate of 5˚C min^{-1} up to 500˚C using nitrogen as the carrier gas. The results obtained are shown as first derivative (DTG) plots of weight with temperature (%/˚C) against temperature (˚C).

5.3.3.3 Carbon, Hydrogen and Nitrogen (CHN) Analyses

The C, H, and N composition of the hydrogels and cellulose were obtained using a Perkin Elmer 2400 CHN Elemental Analyzer with the following instrument conditions: combustion oven temperature (above 925 °C) and reduction oven temperature (above 640 °C). The instrument was purged with a mixture of pure oxygen and helium gas, where acetanilide was used as the calibration standard. Elemental analyses was obtained in triplicate with an estimated precision of ±0.3%.

5.3.3.4 Hydrophile-Lipophile Balance (HLB) of the Hydrogels

The hydrophile-lipophile balance (HLB) of the hydrogels was estimated via swelling in Millipore water and octanol, respectively. This was done by shaking approximately 30 mg of the materials in 15 mL of Millipore water and octanol in a horizontal shaker for ~ 48 h. The weight of swollen hydrogels (w_s) were determined after tamping dry with filter paper. The dry weight (w_d) was obtained after drying in an oven at 65°C to a constant mass. The swelling ratio was calculated for each neat solvent system using Eq. (5.1):

$$Sw(\%) = \frac{Ws\text{-}Wd}{Wd} \times 100 \qquad \text{Equation 5.1}$$

5.3.3.5 Solids State ^{13}C NMR Spectroscopy

A Bruker AVANCE III HD spectrometer furnished with a 4 mm DOTY CP-MAS (cross polarization with magic angle spinning) solids probe operating at 125.8 MHz (^1H frequency at 500.2 MHz) was use to acquire the ^{13}C solids NMR spectra of the hydrogels and cellulose. The experimental conditions were as follows: spinning speed of 10 kHz, a ^1H 90^0 pulse of 3.5 µs, a contact time of 0.75 ms, with a ramp pulse on the ^1H channel. Others are MAS rate of 10 kHz, a

^{13}C 90^0 pulse of 3.15 µs and a 25 kHz SPINAL-64 ^1H decoupling during acquisition. For different samples, 600 – 5000 scans were accumulated, with a recycle delay of 2 s. All experiments were recorded using 71 kHz SPINAL-64 decoupling during acquisition. Chemical shifts were referenced to adamantane at 38.48 ppm (low field signal).

5.3.4 Sorption Studies

5.3.4.1 Sorption of OSPW Naphthenates and Single Component Carboxylate Anions

A 100 mL stock solution at 100 ppm was prepared for the OSPW and 150 ppm for 2 naphthoxy acetic acid (**S6**), respectively. An appropriate amount of **S6** was dissolved in a 0.1 M aqueous NH_3 solution with sonication and further stirring until the resulting solution was clear, while 2800 ppm OSPW was diluted using Millipore water and stirred overnight. Solutions with variable concentration (1 – 150 ppm) were prepared by dilution of the stock with Millipore water.

Fixed amounts (10 mg) of the hydrogels were mixed with 5 mL of **S6** and OSPW solutions in 2 dram vials at variable concentration. The mixtures were equilibrated at room temperature on a horizontal shaker table for 24 h. The initial concentration (C_o) and residual concentration at equilibrium (C_e) of OSPW naphthenates and **S6** were determined using an electrospray ionization high resolution mass spectrometer and a double beam spectrophotometer (Varian CARY 100) at room temperature (293 ± 0.5 K). The samples were centrifuged prior to ESI-MS and UV-vis spectroscopy analyses. Uptake of **S6** and NAFCs in OSPW was determined from the difference between C_o and C_e values described by Eq. (5.2).

$$Q_e = \frac{(C_o - C_e) \times V}{m} \qquad \text{Equation 5.2}$$

Q_e is the quantity of adsorbate uptake in the solid phase at equilibrium (mg g^{-1}), C_o is initial concentration of adsorbate (mg L^{-1}) in solution, C_e is concentration of adsorbate at equilibrium (mg L^{-1}) in solution, V is volume of adsorbate solution, and m is the mass (g) of sorbent.

5.3.4.2 High Resolution Electrospray Ionization Mass Spectrometric (HR ESI-MS) Analysis

The residual (C_e) and initial (C_o) concentration of the NAFCs was estimated using a ThermoScientific LTQ Orbitrap high resolution Elite Electrospray ionization mass spectrometer (HR ESI-MS). The resolution setting of the spectrometer was 30,000 while a full-scan mass spectrum was collected between *m/z* 100 and 600. Quantification of samples was achieved by extracting the mass range of the analyte of interest. The electrospray ionization (ESI) interface was set to negative-ion mode. Mass spectrometer conditions were optimized by the transmission of *m/z* 112.98563. The heated ESI interface (HESI) parameters were as follows: source heater temperature (53 °C); spray voltage (2.86 kV); capillary temperature (275 °C); sheath gas flow rate (25 L h^{-1}); auxiliary gas flow rate (5 L h^{-1}); and spray current (5.25 μA).

5.3.4.3 Sorption Isotherms and Modeling

Sorption isotherms were obtained by plotting Q_e *vs* C_e (*cf*. Equation 5.2). The isotherms were subsequently analyzed using Langmuir [28] Freundlich [29] and the Sips [30] models (*cf*. Equations 5.3 – 5.5). The "best fit" for the data was obtained by minimizing the SSE (*cf*. Equation 5.6) for all data across the range of conditions. Q_{ei} is the experimental value, Q_{ef} is the calculated value from data fitting and N is the number of Q_e data points.

$$Q_e = \frac{K_L Q_m C_e}{1 + K_L C_e} \qquad \text{Equation 5.3}$$

$$Q_e = K_F C_e^{1/n_f}$$ Equation 5.4

$$Q_e = \frac{Q_m (K_S C_e)^{n_s}}{1 + (K_S C_e)^{n_s}}$$ Equation 5.5

$$SSE = \sqrt{\frac{(Q_{ei} - Q_{ef})^2}{N}}$$ Equation 5.6

5.3.5 Kinetic and Thermodynamic Studies

5.3.5.1 Kinetic Studies

Kinetic studies were carried out using a one pot method [31] as follows: variable amounts (~100 mg or 30 mg) of the hydrogel were added to a folded Whatman filter paper (55 mm diameter), where both ends were clamped after encasing the polymer. The clamped filter paper containing the sample was immersed in a fixed volume (120 mL) of a 150 ppm **S6** solution. 3 mL of the **S6** solution were sampled after designated time intervals. The residual concentration of the aliquots was determined using a double beam spectrophotometer (Varian CARY 100) at 293 ± 0.5 K. Uptake of **S6** at each sampling time interval (t) was estimated according to Equation 5.7, where C_o and C_t refer to the surrogate concentration at t = 0 and variable t.

$$Q_t = \frac{(C_o - C_t) \times V}{m}$$ Equation 5.7

Kinetic isotherms were obtained by plotting Q_t vs time according to the pseudo-first order (PFO kinetic model (*cf.* Equation 5.8).

$$Q_t = Q_e (1 - e^{-k_1 t})$$ Equation 5.8

5.3.5.2 Thermodynamic Studies

The standard enthalpy of activation (ΔH*), entropy of activation (ΔS*), and free energy of activation (ΔG*) in the adsorption process were calculated from a plot of ln k_1/T versus 1/T according to the Eyring equation (Equation 5.9),

$$\frac{\ln k}{T} = \ln\frac{k_B}{h} + \frac{\Delta S^*}{R} - \frac{\Delta H^*}{RT} \qquad \text{Equation 5.9}$$

where k is the adsorption rate constant, k_B is the Boltzmann constant (1.3807×10^{-23} J K^{-1}), h is Planck's constant (6.6261×10^{-34} J s), R is the ideal gas constant (8.314 $J.mol^{-1}K^{-1}$), and T is the temperature (K). The values of ΔH* and ΔS* were determined from the slope and intercept of a plot of ln k/T versus 1/T. The values obtained were used to compute ΔG* from equation 5.10 below:

$$\Delta G^* = \Delta H^* - T\Delta S^* \qquad \text{Equation 5.10}$$

The activation energy (E_a) of the process was obtained by plotting *ln* k_1 versus 1/T according to the Arrhenius equation 5.11,

$$\ln k = \ln A + \frac{E_a}{R}\left(\frac{1}{T}\right) \qquad \text{Equation 5.11}$$

where k is the rate constant, A is the pre-exponential factor, E_a is the activation energy, R is the gas constant and T is the temperature (K).

5.4 Results and Discussion

5.4.1 Characterization of Cellulose Hydrogels

5.4.1.1 FTIR Studies

The FTIR spectra of the cellulose hydrogels and native cellulose are displayed in Figure 5.1a. The salient features of the spectra include a broad band (~3000 – 3600 cm^{-1}) attributed to intermolecular bonded OH and NH groups, C–H stretching (~2800–3000 cm^{-1}), O–H and C–H bending (~1400 – 1300 cm^{-1}), and C–O–H and C–O–C asymmetric stretching (~1000 – 1200 cm^{-1}), in agreement with a study on cross-linked cellulose.[12] The spectra reveal differences between native cellulose and the hydrogels, where the introduction of methylene, methyl and quaternary ammonium groups occur due to cross-linking and/or quaternization reactions, in agreement with reported studies.[32-33] The different features include IR bands at 1485 cm^{-1}, ~1000 – 1200 cm^{-1} and ~2934 cm^{-1} which display greater intensity relative to native cellulose, along with attenuation of the bands at ~1300 - 1400 cm^{-1}. The new IR bands relate to the methyl groups from the quaternary ammonium ion, ether linkage from cross-linking with epichlorohydrin, as well as the methylene groups due to cross-linking/ or quaternization reactions, in agreement with other reports.[34-35] An increased intensity and broadening of the band at ~1640 cm^{-1} relates to adsorbed water molecules and the C – N band at ~1450 cm^{-1} for the hydrogels provide further evidence for the introduction of quaternary ammonium groups onto the surface sites of cellulose.[17, 34]

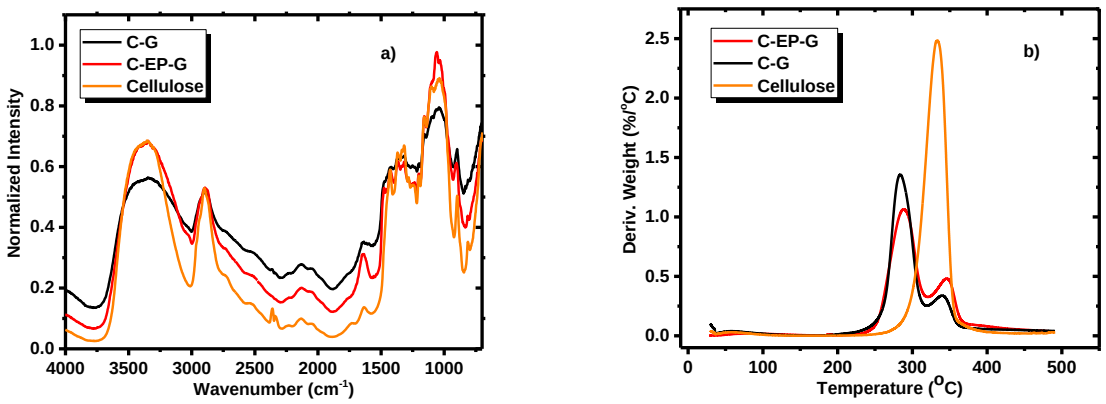

Figure 5.1 a) FTIR spectra, and b) DTG plot of cellulose and the hydrogels.

5.4.1.2 Thermogravimetry Studies

The thermal stability of native cellulose and the hydrogels are inferred from the plots of derivative weight (%/°C) *versus* temperature (°C) in Figure 5.1b. The TGA results show a single thermal event for cellulose relative to two thermal events for the hydrogels, in agreement with an independent report. [36] The maximum decomposition temperature for pristine cellulose occurs at ~320 °C; whereas, the hydrogels display maximum decomposition at ~260 °C and ~360 °C. The two thermal events for the hydrogels differ as compared to cellulose which shows a single thermal event. The TGA results of the hydrogels relate to cross-linking and/or quaternization of cellulose, in agreement with the IR band at 1485 cm^{-1} in Figure 5.1a. The lower thermal event (~260 °C) for the hydrogels correspond to the cross-linker and quaternary ammonium groups, whereas; the event at ~360 °C relates to the decomposition of cellulose.[36] The thermogravimetry profiles also reveal that the intensity of the thermal event due to the decomposition of the cross-linker and quaternary ammonium groups of the hydrogel differ from the profile of cellulose. The foregoing provides support that cellulose is modified via cross-linking and quaternization. The profile also reveals that

the cross-linked and quaternized hydrogel (**C-EP-G**) has greater thermal stability over the quaternized hydrogel (**C-G**). This greater stability of the cross-linked and quaternized hydrogel may be due to cross-linking effects as noted for cellulose in another study.[12]

5.4.1.3 Carbon, Hydrogen and Nitrogen (CHN) Composition of Hydrogels

The CHN results of the hydrogel composition is compared with cellulose in Table 5.1. The hydrogel contains greater C, H, and N content than unmodified cellulose. The presence of nitrogen in the hydrogels confirms the grafting of quaternary ammonium groups, in agreement with the above FTIR and TGA results, along with a related study.[37] The results reveal that **C-EP-G** contains more nitrogen than **C-G** and may be a consequence of the cross-linking of cellulose with EP and aqueous ammonia before the quaternization process. The effect corresponds with a related study for the cross-linking of hydroxypropyl cellulose with EP and aqueous ammonia.[13]

Table 5.1 CHN content (%) and solvent swelling results of cellulose and its modified forms.

Material	% C	% H	% N	Swelling (Water)%	Swelling (Octanol)%	HLB*
Cellulose	41.0 ± 2.1	6.27± 0.31	NA	125 ± 5	NA	NA
C-EP-G	42.4 ± 2.1	6.48± 0.32	1.17 ± 0.06	292 ± 9	211 ± 8	0.720
C-G	42.8 ± 2.1	7.43± 0.37	0.80 ± 0.04	415 ± 11	260 ± 9	0.625

*HLB is estimated by proxy as the ratio of swelling in octanol: water

5.4.1.4 Hydrophile-Lipophile Balance (HLB) of Cellulose Hydrogels

The relative HLB of the cellulose materials was estimated by proxy according to results obtained for solvent swelling in octanol and water (*cf*. Table 5.1). The swelling results reveal that **C-G** synthesized without cross-linking with EP/aqueous ammonia displayed greater swelling in water and octanol relative to its cross-linked form (**C-EP-G**). The ratio of the swelling in octanol

and water reveal that **C-G** has measureable differences in HLB over **C-EP-G** (**C-EP-G** = 0.720; **C-G** = 0.625). The HLB results are affirmed by **C-G** which displays the greatest stabilization of a hexane in water emulsion Pickering emulsion system (*cf.* Figure 5.2a), exceeding four weeks. The colloidal stabilization of the emulsion by **C-G** is due to its greater wetting properties and ability to reduce the interfacial energy by adsorption at the oil/water interface. The foregoing also reveals that **C-EP-G** is a more hydrophobic hydrogel as evidenced by its HLB value, in agreement with the greater sorptive uptake of **S6** (*cf.* Figure 5.2b), an amphiphilic adsorbate.[38-39]

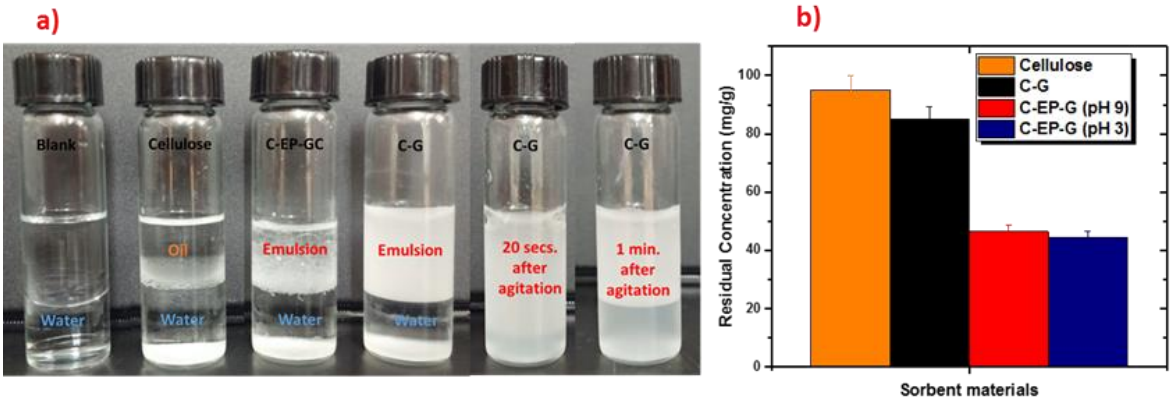

Figure 5.2 Stabilization of oil/water emulsions by cellulose and hydrogels, and b) Uptake of **S6** by cellulose and the hydrogels at pH 3 and 9 at 293 K.

5.4.1.5 ^{13}C NMR Studies of Cellulose Hydrogels

The ^{13}C solids NMR spectra of native cellulose and the hydrogels are presented in Figure 5.3. Unmodified cellulose display the following ^{13}C resonances: C1 (~105 ppm), C2/C3/C5 (~68 - 78 ppm), C4 (88.4 and 83.3 ppm), and C6 (64.7 and 62.7 ppm), in agreement with a previous report. [40] The ^{13}C spectra of the hydrogels possess features resembling the native cellulose, in agreement with the preservation of the cellulose biopolymer structure. The hydrogels reveal new ^{13}C NMR resonance lines, band broadening, and chemical shift variations. These features are

absent in the spectra of cellulose, in accordance with the TGA and FTIR results above. For example, new resonance lines at ~55.0 ppm for $(CH_3)_3N^+$ and ~77 ppm relate to CH_2 groups from EP and GTAC, respectively, in agreement with other reports.[41-42] The resonance lines for EP and GTAC may overlap with the spectral features (*cf.* ~62 - 65 ppm and ~68 - 78 ppm) of native cellulose, in accordance with the line broadening related to quaternization.[42] The shoulder at ~103 ppm may be due to C3 which bears substituted or non-substituted hydroxyl groups.[43] The difference between **C-EP-G** and **C-G** in the ^{13}C NMR spectra relate to the well resolved and increased spectral intensity of the lines ~68 – 78 ppm from EP and GTAC, related to their similar chemical environments. **C-G** was synthesized via grafting cellulose with GTAC without cross-linking. The ^{13}C NMR results provide support that cross-linking occurs between cellulose and EP as well as quaternization with GTAC, in agreement with the TGA results reported above.

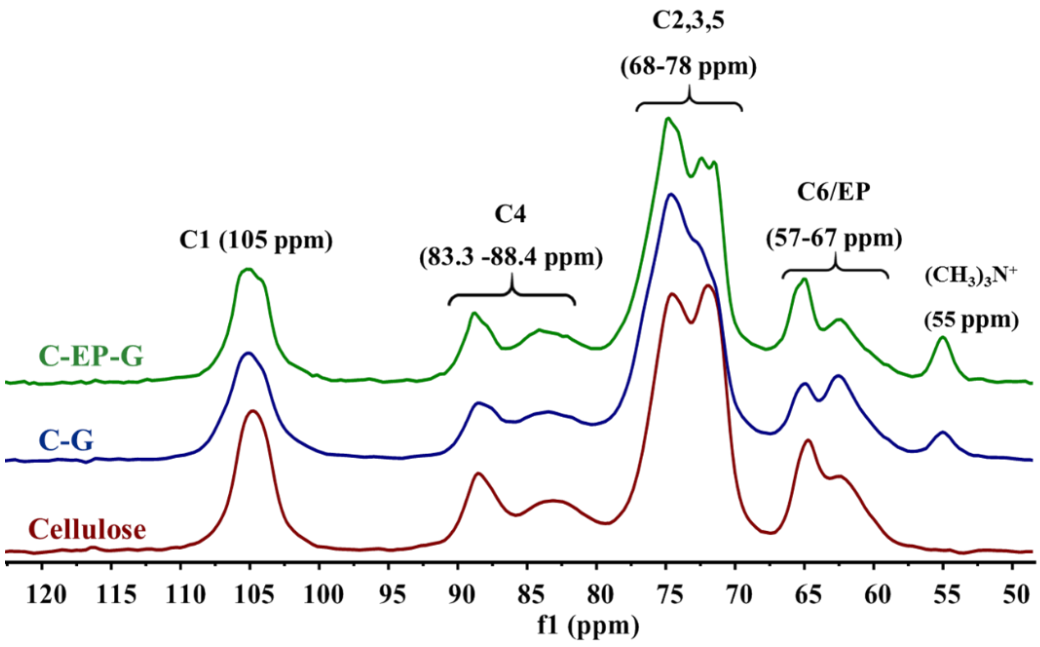

Figure 5.3 CP-MAS ^{13}C solid state NMR spectra of cellulose, **C-G** and **C-EP-G** obtained at 125.8 MHz with MAS at 10 kHz and 293 K.

5.4.2 Sorption Studies

5.4.2.1 Comparative Uptake of Single Component Carboxylate Anion

Sorption results for the uptake affinity of cellulose and the hydrogels with **S6** in aqueous solution are shown in Figure 5.2b. The results reveal that **C-EP-G** displays greater affinity for the uptake of **S6** relative to cellulose and **C-G**. The greater affinity of **C-EP-G** with **S6** likely relate to the surfactant-like properties of **S6**, in accordance with the HLB results presented above for **C-EP-G**. Cross-linking of cellulose with EP results in reduced water solubility; whereas, grafting with GTAC further enhances the hydrophile character due to the introduction of quaternary ammonium groups into the structure of the hydrogels. Thus, the uptake of **S6** by **C-EP-G** is a result of cooperative interactions. The uptake results in Figure 5.2b show that pH has a minor effect on the equilibrium uptake of **S6** by **C-EP-G** due to the grafting of the quaternary ammonium ions onto cellulose. Previous reports on the uptake properties[12] of anions with cellulose materials indicate that low anion affinity occurs at alkaline pH as a result of the negative zeta potential on the sorbent surface.[44] The introduction of quaternary ammonium groups offsets the low anion affinity in the case of unmodified cellulose through the introduction of a positive zeta-potential, as for the case of **C-G** or **C-EP-G**.

5.4.2.2 Equilibrium Studies of S6 and OSPW Naphthenates

The uptake isotherms of the sorbents with **S6** and OSPW naphthenates are presented as plots of Q_e versus C_e in Figure 5.4a. The isotherms display a non-linear increase for Q_e as C_e increases. The Langmuir model provides a reasonable "best-fit" to the experimental results and reveal that the sorbent surface has homogenous sorption sites (*cf.* Table 5.2). The proposed structure of **C-EP-G** in Scheme 5.1 agrees with the ^{13}C solids NMR and FTIR spectral results,

where two possible sorption sites exist in such sorbent materials. These include the quaternary ammonium sites and the hydrophobic domains of cellulose even though the isotherm results are described by the Langmuir model. Evidence of a singular type of sorption site for these materials can be understood on the basis of a large offset in the binding affinity of each respective site. The uptake of **S6** and **OSPW** naphthenates by **C-EP-G** is likely dominated by the ion-ion electrostatic attractions, along with cooperative hydrophobic effects. The Langmuir isotherm data shows that **C-EP-G** displayed a two-fold greater uptake of **S6** (Q_m = 69.5 ± 4.3 mg/g) over **OSPW** naphthenates (Q_m = 33.0 ± 2.8 mg/g). The variable uptake of **S6** by **C-EP-G** may be due to the mixed composition of **OSPW**, where certain congeners have reduced uptake due to steric effects or variable HLB that limit the binding with **C-EP-G**. The variable lipophilicity profile of **OSPW** relates to the *z*-value of the naphthenates, where the *z*-value denotes the "hydrogen deficiency", as reported elsewhere. [45-49] Naphthenates with *z*-values less than 2 in the **OSPW** display enhanced binding affinity with **C-EP-G**, as follows: **OSPW** (0.0333 ± 0.006 L/mg) and **S6** (0.0260 ± 0.003 L/mg). The hydrogel reported herein has favorable uptake relative to activated carbon (AC) and nickel- based alumina (Ni-Al_2O_3); 20 mg/g and chemically treated AC; 35 mg/g, for OSPW naphthenates. [50-51]

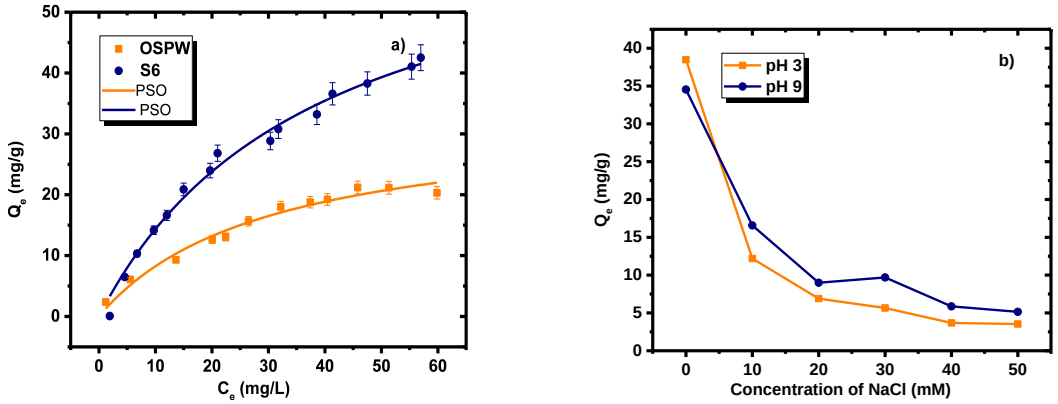

Figure 5.4.a) Sorption isotherm of **C-EP-G** with **S6** at pH 9 and OSPW at pH 10.5 and 293 K, and b) Effect of ion concentration on the sorption isotherm of **S6** by **C-EP-G** with at pH 3 and 9 and 293 K.

Table 5.2 Sorption isotherm parameters obtained from the Langmuir, Sips, and Freundlich models for **C-EP-G** with **OSPW** naphthenates (pH 10.5) and **S6** (pH 9) at 295 K.

Adsorbates	Isotherm model	Parameters	Sorbent (C-EP-G)
OSPW	Langmuir	**Q_m (mg g^{-1})**	33.0 ± 2.8
		K_L (L mg^{-1})	0.0333 ± 0.006
		SSE	0.921
	Sips	**Q_m (mg g^{-1})**	36.9 ± 11.8
		K_S (L mg^{-1})	0.0370 ± 0.009
		n_s	0.904 ± 0.20
		SSE	2.73
	Freundlich	**K_F (L mg g^{-1})**	2.63 ± 0.44
		$1/n_f$	1.89 ± 0.05
		SSE	2.75×10^{3}
S6	Langmuir	**Q_m (mg g^{-1})**	69.5 ± 4.3
		K_L (L mg^{-1})	0.0260 ± 0.003
		SSE	0.994
	Sips	**Q_m (mg g^{-1})**	60.5 ± 8.4
		K_S (L mg^{-1})	0.0234 ± 0.005
		n_s	1.12 ± 0.14
		SSE	4.10
	Freundlich	**K_F (L mg g^{-1})**	3.47 ± 0.48
		$1/n_f$	2.09 ± 0.04
		SSE	1.13×10^{6}

5.4.2.3 Effects of Ion Concentration on the Uptake of S6

The concentration effect of NaCl on the sorption of **S6** with **C-EP-G** is presented in Figure 5.4b. The results reveal that an increase in the level of NaCl in the **S6** solution results in a reduced uptake of **S6** with **C-EP-G**, in agreement with other reports.[50, 52] The uptake of **S6** decreased from 38.0 ± 0.12 mg/g to 5.00 ± 0.05 mg/g at pH 3, and 35.0 ± 0.11 mg/g to 6.00 ± 0.05 mg/g at pH 9 as the concentration of NaCl increased to 50.0 mM. The attenuated uptake of **S6** in the presence of electrolyte may be due to charge screening effects at the sorption sites between the carboxylate anions and the quaternary ammonium groups, in agreement with enhanced ion-ion binding contributions, as outlined above.

5.4.2.4 Sorption of OSPW Naphthenates by Cellulose Hydrogels

The HR ESI-MS speciation profile of OSPW before and after sorption with **C-EP-G** is presented in Figures 5.5a-b. Figure 5.5a displays the class distribution plots for OSPW and shows that O_2H species are the most prominent; whereas, the O_2S species are of secondary abundance. The results demonstrate a significant attenuation of the concentration of the O_2H species after sorption with the **C-EP-G** hydrogel. The foregoing shows that the **C-EP-G** hydrogel has favorable uptake affinity and removal of these **OSPW** fractions at equilibrium.

Figure 5.5b presents a distribution profile of double bond equivalent (DBE) species in **OSPW** as a function of the normalized concentration of O_2H species. The DBE accounts for the hydrogen deficiency due to ring formation or double bonds of the naphthenate systems.[53] The results show that the O_2H species are comprised of naphthenates with DBE values in the range of 1 to 10. As well, the more prominent species in the OSPW mixture have DBE values between 2 and 8. The uptake results show that **C-EP-G** has little or no selectivity toward the carboxylate

anion species in the mixture, in agreement with the electrostatic driven binding for the hydrogel/**OSPW** systems. The removal efficiency ranged from 38% (DBE = 4) to 69% (DBE = 8). While Mohamed et al. [54] reported an increase in removal efficiency with increasing DBE due to hydrophobic effects, the results reported in chapter 3 revealed a greater uptake of model naphthenates as the number of rings increased for cellulose and its cross-linked forms. The foregoing shows that **C-EP-G** has appreciable fractionation efficacy for **OSPW** naphthenates that may be attributed to cooperative electrostatic and hydrophobic effects, as noted above.

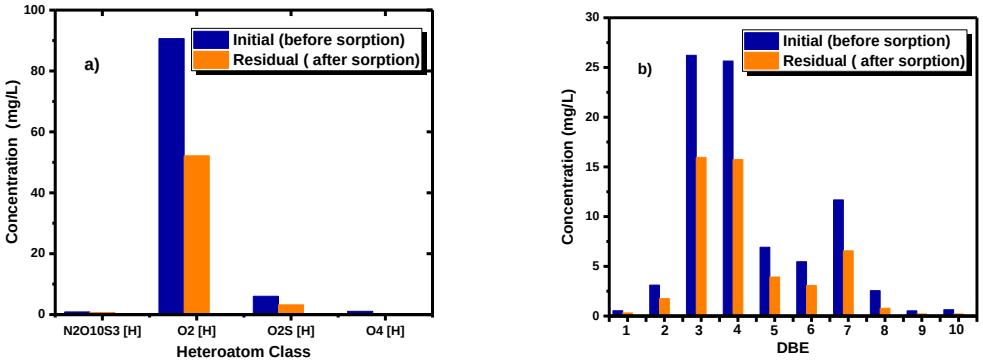

Figure 5.5 a) HR ESI-MS speciation profile of OSPW, and b) Double bond equivalents (DBE) distribution of OSPW as a function of normalized concentration for the O_2 species before and after sorption with **C-EP-G** at pH 10.5 and 293 K.

5.4.3 Kinetic Uptake Studies

5.4.3.1 Effects of Temperature and Sorbent dosage

Figure 5.6 illustrates the effects of temperature on the kinetic uptake of **S6** from aqueous solution by **C-EP-G** *via* the one-pot kinetic system. The uptake profile is well described by the pseudo-first order (PFO) kinetic model, in agreement with a single type of sorption site. The results show an increase in Q_t values with increasing time, where saturation occurs at t > 400 s. In Figure 5.6a, the kinetic profile reveals that Q_e (mg/g) and the PFO rate constant, k_1 (s^{-1}) increase with

temperature at a low dosage (30 mg) of **C-EP-G** (*cf.* Table 5.3), where dynamic equilibrium is reached after 460 mins. At higher hydrogel dosage (100 mg) in Figure 5.6b, the rate becomes attenuated as temperature increases, due to the fact that the monolayer saturation of the biopolymer was not achieved after 400 mins. A comparison of the Q_t values for each adsorbent dosage (*cf.* Table 5.4) reveal that uptake of **C-EP-G** (30 mg dosage) at 303 K was higher relative to uptake at 100 mg hydrogel dosage, in support of the claim that monolayer saturation was not achieved after 400 s. Figure 5.6b shows that the uptake profile at 303 K converged with the results at 298 K, supporting the claim that longer time is required to achieve dynamic equilibrium. The increase of Q_e and k_1 values as temperature increases indicate that increased temperature provides the required energy to activate the adsorption process, in agreement with other results.[55]

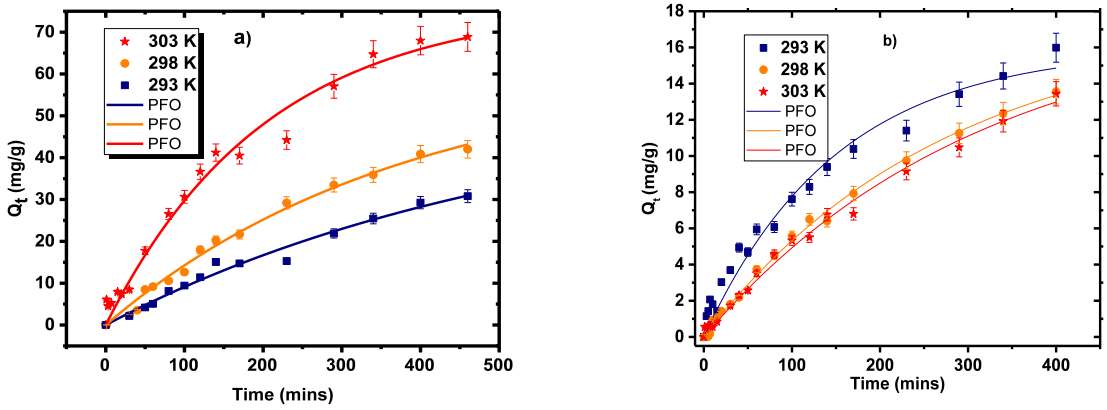

Figure 5.6. Uptake kinetic profile of **S6** by a) low dosage (30 mg), and b) high dosage (100 mg) of **C-EP-G** at pH 9 and 293 K, 298 K and 303 K. The fitted lines correspond to the PFO model.

5.4.3.2 Effects of pH

A study of pH effects on the uptake kinetics of **S6** by **C-EP-G** hydrogel is shown in Figure 5.7. The results reveal an increase for Q_t as time increases that agree with general effects of

temperature and sorbent dosage. The kinetic uptake results at pH 3 (Q_t) and the PFO rate constant (k_1) are greater relative to conditions at pH 9 (*cf.* Table 5.3). These results do not agree with those herein for the comparative equilibrium uptake of **S6** by cellulose and the hydrogels at pH values at 3 and 9. The slight disparity in the uptake capacity between the equilibrium and kinetic studies likely relate to the earlier claim that 400 mins is insufficient for achieving isotherm saturation as well as the faster rate of the uptake at pH 3. The greater PFO rate constant obtained for the kinetic uptake at pH 3 may relate to the reduced role of counter ion binding with the quaternary ammonium ions at acidic pH relative to pH 9, where greater charge screening effects are anticipated as the level of OH^- increases.

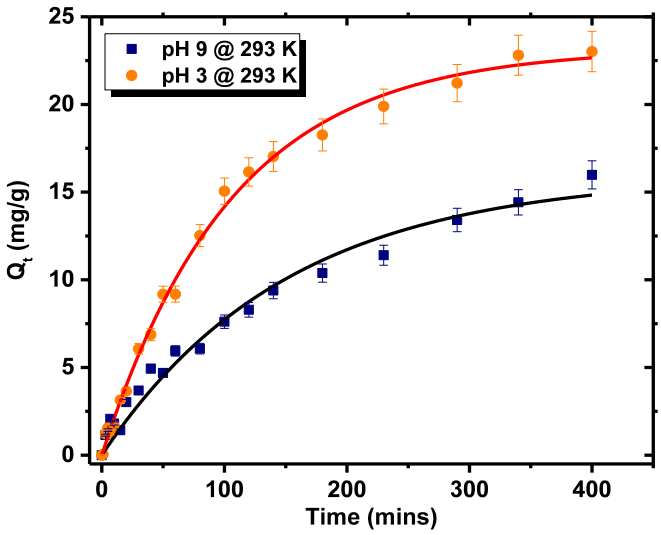

Figure 5.7. Kinetic uptake profile of **S6** with a 0.833 mg/mL dosage of **C-EP-G** at pH 9 and 3 and 293K, where the fitted lines correspond to the PFO model.

Table 5.3: Pseudo-first order (PFO) kinetic uptake results of **S6** by **C-EP-G** hydrogel at 293 K, 298 K and 303 K and pH 3 and 9.

Weight of adsorbent (mg)	Temperature (K)	pH	Parameters Q_m (mg/g)	K_1 (s^{-1})	R^2
30	293	9	54.2 ± 10.0	0.00184 ± 0.0005	0.980
	298		61.3 ± 4.7	0.00265 ± 0.0003	0.992
	303		76.7 ± 4.3	0.00491 ± 0.0006	0.982
100	293		16.0 ± 0.8	0.00666 ± 0.0007	0.974
	298		17.4 ± 0.7	0.00634 ± 0.0002	0.997
	303		18.0 ± 1.2	0.00319 ± 0.0003	0.992
	293	3	23.2 ± 0.4	0.00943 ± 0.0004	0.996

5.4.3.3 Activation Parameters

The calculated activation parameters such as the change in Gibbs energy *(ΔG*), enthalpy change *(ΔH),* entropy change *(ΔS),* and activation energy *(E_a),* were based on the trend in PFO rate constants (k_1) with temperature. The activation parameters were calculated from a plot of $\ln k_1/T$ versus 1/T (*cf.* Figure 5.8a) by the Eyring equation (Equation 5.9). The positive value of *ΔG** (*cf.* Table 5.4) at variable temperature shows a decrease with increasing temperature, indicating that the sorption process is exergonic. The endothermic nature of Δ*H** of the sorption process is anticipated for electrostatic driven processes. The *ΔS** values inferred an associative sorption mechanism which proceeds via the formation of an activated complex for the hydrogel system. [56] The E_a value in Table 5.4 derived from the plot of ln k_1 versus 1/T (*cf.* Figure 5.8b) by the Arrhenius equation (Equation. 5.11) is 72 ± 1 kJ/mol. The result agrees with the E_a values for other ion exchange systems reported elsewhere.[57] The foregoing along with the Langmuir-based description for the adsorption process supports the claim that electrostatic interactions are predominant with evidence of cooperative hydrophobic effects for the uptake of **S6** by **C-EP-G** hydrogel.

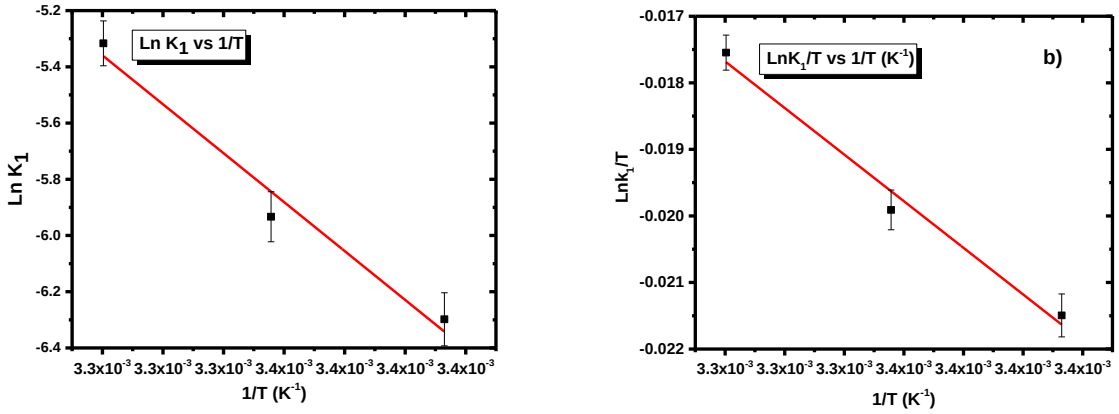

Figure 5.8 a) Plot of *ln* k_1 versus 1/T for the determination of activation energy (E_a), b) Plot of *ln* k_1 /T versus 1/T for the determination of activation parameters of adsorption for the **S6**/**C-EP-G** hydrogel system.

Table 5.4 Thermodynamic parameters for the uptake of **S6** by **C-EP-G** hydrogel.

Temp. (K)	**E_a (kJ/mol)**	**Activation parameters**		
		ΔH^* (kJ/mol)	**ΔS^* (J/Kmol)**	**ΔG^* (kJ/mol)**
293	72 ± 1	0.291 ± 0.001	-196 ± 3	57.9 ± 0.2
298				58.9 ± 0.2
303				59.8 ± 0.5

5.5 Conclusions

Quaternized and cross-linked cellulose hydrogel (**C-EP-G)** and the non-cross-linked form (**C-G**) were prepared. The grafting of GTAC with cellulose results in the presence of quaternary ammonium groups, according to structural support via FTIR, CHN analysis, ^{13}C NMR and TGA. The hydrogels possess enhanced network structure and variable hydrophobic character due to cross-linking and grafting of quaternary ammonium groups. The TGA results indicate enhanced thermal stability of the hydrogels relative to cellulose, while solvent swelling studies in octanol and water indicate that **C-G** has variable hydrophile-lipophile balance (HLB) relative to **C-EP-G**.

C-G in hexane-water mixtures afford the formation of stable oil/water Pickering emulsions. The sorption of **OSPW** naphthenates and **S6** by the hydrogels revealed that **C-EP-G** has greater affinity over **C-G**, where the uptake is favored by cooperative hydrophobic and electrostatic interactions. **C-EP-G** displays similar affinity for the component species of **OSPW** naphthenates, where the PFO model provides best fit for the experimental kinetic uptake results. The kinetic uptake process is favored by increased temperature while pH has a minor effect. The activation parameters were derived from temperature dependent variations of the rate constants, k_1, where an enthalpy- driven sorption process appears to follow an associative ion-based driven sorption mechanism. This study contributes to a greater understanding of the structure-function properties of cellulose hydrogels and their uptake properties with carboxylate anions. This study will catalyze further development of low-cost and versatile biopolymer materials for tunable Pickering emulsions, chemical fractionation, and diverse adsorption-based processes.

5.6 References and Notes[¥]

1. Chang, C.; Zhang, L. *Carbohyd Polym* **2011**, *84*, 40-53.
2. Chang, C.; Zhang, L.; Zhou, J.; Zhang, L. *Carbohyd Polym* **2010**, *82*, 122-127.
3. Sannino, A.; Demitri, C.; Madaghiele, M. *Materials* **2009**, *2*, 353.
4. Molina, M.J.; Gómez-Antón, M.R.; Piérola, I.F. *J. Phys Chem B* **2007**, *111*, 12066-12074.
5. Wong, J.E.; Díez-Pascual, A.M.; Richtering, W. *Macromolecules* **2009**, *42*, 1229-1238.
6. Qiu, X.; Hu, S. *Materials* **2013**, *6*, 738-781.
7. Cavalieri, F.; Chiessi, E.; Finelli, I.; Natali, F.; Paradossi, G.; Telling, M.F. *Macromol Biosci* **2006**, *6*, 579-589.
8. Zoppe, J.O.; Venditti, R.A.; Rojas, O.J. *J Colloid Interf Sci* **2012**, *369*, 202-209.
9. Luo, X.; Zhang, L. *Food Res Int* **2013**, *52*, 387-400.

10. Bergenstråhle, M.; Wohlert, J.; Himmel, M.E.; Brady, J.W. *Carbohyd Res* **2010**, *345*, 2060-2066.

11. Chaplin, M. Water structure and science: Cellulose. http://www1.lsbu.ac.uk/water/cellulose.html (assessed on June 20, 2016)

12. Udoetok, I.A.; Dimmick, R.M.; Wilson, L.D.; Headley, J.V. *Carbohyd Polym* **2016**, *136*, 329-340.

13. Yan, L.; Shuai, Q.; Gong, X.; Gu, Q.; Yu, H. *CLEAN - Soil, Air, Water* **2009**, *37*, 392-398.

14. Marc, G.; Mele, G.; Palmisano, L.; Pulito, P.; Sannino, A. *Green Chem* **2006**, *8*, 439.

15. Chen, J.C.; Yeh, J.T.; Chen, C.C. *J Appl Polym Sci* **2003**, *90*, 1662-1669.

16. Yang, S.P.; Fu, S.Y.; Li, X.Y.; Zhou, Y.M.; Zhan, H.Y. *Bioresources* **2010**, *5*, 1114-1125.

17. Hu, D.Y.; Wang, P.; Li, J.; Wang, L.J. *Bioresources* **2014**, *9*, 5951-5962.

18. Vlachy, N.; Jagoda-Cwiklik, B.; Vácha, R.; Touraud, D.; Jungwirth, P.; Kunz, W. *Adv Colloid Interface Sci* **2009**, *146*, 42-47.

19. Leishman, C.; Widdup, E.E.; Quesnel, D.M.; Chua, G.; Gieg, L.M.; Samuel, M.A.; Muench, D.G. *Chemosphere* **2013**, *93*, 380-387.

20. Lengger, S.K.; Scarlett, A.G.; West, C.E.; Rowland, S.J. *Rapid Commun. Mass Spectrom.* **2013**, *27*, 2648-2654.

21. Reinardy, H.C.; Scarlett, A.G.; Henry, T.B.; West, C.E.; Hewitt, L.M.; Frank, R.A.; Rowland, S.J. *Environ. Sci. Technol.* **2013**, *47*, 12, 6614-6620.

22. Yue, S.; Ramsay, B.A.; Wang, J.; Ramsay, J. *Sci. Total Environ* **2015**, *538*, 573-582.

23. Wiseman, S.B.; Anderson, J.C.; Liber, K.; Giesy, J.P. *Aquat. Toxicol* **2013**, *142-143*, 414-421.

24. He, Y.; Patterson, S.; Wang, N.; Hecker, M.; Martin, J.W.; El-Din, M.G.; Giesy, J.P.; Wiseman, S.B. *Water Res* **2012**, *46*, 6359-6368.

25. Wilson, L.D.; Mohamed, M.H.; Headley, J.V. *Rev. Environ Health* **2014**, *29*, (1-2), 5-8.

26. Tang, J.; Quinlan, P.J.; Tam, K.C. *Soft Matter* **2015**, *11*, 3512-3529.

27. Oyanedel-Craver, V.A.; Smith, J.A. *J Hazard Mater* **2006**, *137*, 1102-1114.

28. Langmuir, I. The adsorption of gases on plane surfaces of glass, mica and platinum. *J Am Chem Soc* **1918**, *40*, 1361-1403.

29. Freundlich, H.M.F. Over the adsorption in solution. *J Phys Chem* **1906**, *57A*, 385-470.

30. Sips, R. Structure of a catalyst surface. *J Chem Phys* **1948**, *16*, 490-495.

31. Mohamed, M.; Wilson, L. *Nanomaterials* **2015**, *5*, 969-980.

32. Song, Y.; Zhou, J.; Li, Q.; Guo, Y.; Zhang, L. *Macromol Biosci* **2009**, *9*, 857-863.

33. Oh, S.Y.; Yoo, D.I.; Shin, Y.; Seo, G. *Carbohyd Res* **2005**, *340*, 417-428.

34. Pei, A.; Butchosa, N.; Berglund, L.A.; Zhou, Q. *Soft Matter* **2013**, *9*, 2047.

35. Song, Y.; Zhou, J.; Li, Q.; Guo, Y.; Zhang, L. *Macromol Biosci* **2009**, *9*, 857-863.

36. Li, G.B.; Fu, Y.J.; Shao, Z.Y.; Zhang, F.S.; Qin, M.H. *Bioresources* **2015**, *10*, 7782-7794.

37. Song, Y.; Zhang, L.; Gan, W.; Zhou, J.; Zhang, L. *Colloids Surf B* **2011**, *83*, 313-320.

38. Kalashnikova, I.; Bizot, H.; Cathala, B.; Capron, I. *Langmuir* **2011**, *27*, 7471-7479.

39. Andresen, M.; Stenius, P. *J Disper Sci Technol* **2007**, *28*, 837-844.

40. Okushita, K.; Komatsu, T.; Chikayama, E.; Kikuchi, J. *Polym J* **2012**, *44*, 895-900.

41. Chaker, A.; Boufi, S. *Carbohyd Polym* **2015**, *131*, 224-232.

42. Song, Y.; Sun, Y.; Zhang, X.; Zhou, J.; Zhang, L. *Biomacromolecules* **2008**, *9*, 2259-2264.

43. Yan, L.; Tao, H.; Bangal, P.R. *CLEAN - Soil, Air, Water* **2009**, *37*, 39-44.

44. Stenstad, P.; Andresen, M.; Tanem, B.S.; Stenius, P. *Cellulose* **2008**, *15*, 35-45.

45. Dzidic, I.; Somerville, A.C.; Raia, J.C.; Hart, H.V. *Anal Chem* **1988**, *60*, 1318-1323.

46. Fan, T.P. *Energy Fuels* **1991**, *5*, 371-375.

47. Wong, D.C.L.; van Compernolle, R.; Nowlin, J.G.; O'Neal, D.L.; Johnson, G.M. *Chemosphere* **1996**, *32*, 1669-1679.

48. St. John, W.P.; Rughani, J.; Green, S.A.; McGinnis, G.D. *J Chromatogr A* **1998**, *807*, 241-251.

49. Hsu, C.S.; Dechert, G.J.; Robbins, W.K.; Fukuda, E.K. *Energy Fuels* **1999**, *14*, 217-223.

50. Azad, F.S.; Abedi, J.; Iranmanesh, S. *J Environ Sci and Health, Part A* **2013**, *48*, 1649-1654.

51. Iranmanesh, S.; Harding, T.; Abedi, J.; Seyedeyn-Azad, F.; Layzell, D.B. *J. Environ. Sci. Heal. A* **2014**, *49*, 913-922.

52. Kushwaha, A.K.; Gupta, N.; Chattopadhyaya, M.C. *J. Saudi Chem. Soc.* **2014**, *18*, 200-207.

53. Marshall, A.G.; Rodgers, R.P. *PNAS* **2008**, *105*, 18090-18095.

54. Mohamed, M.H.; Wilson, L.D.; Shah, J.R.; Bailey, J.; Peru, K.M.; Headley, J.V. *Chemosphere* **2015**, *136*, 252-258.

55. Mufazzal Saeed, M.; Ahmed, M. *Separ Sci Technol* **2006**, *41*, 705-722.

56. Saha, P.; Chowdhury, S. In Insight into Adsorption Thermodynamics, Thermodynamics, Tadashi, M. (Ed.), InTech: China 2011. pp. 349–365. DOI: 10.5772/13474. Available from:http://www.intechopen.com/books/thermodynamics/insight-into-adsorption-thermodynamics

57. Inglezakis, V.J.; Zorpas, A.A. *Desalin Water Treat* **2012**, *39*, 149-157.

¥Disclaimer: As there is a lack of representative analytical standard methodologies related to the analysis of total NAs or NAFCs, the results presented in this manuscript should be considered internally consistent, but may not be directly comparable to other results. For further information on the methods and analytical procedures used in this study, please contact the corresponding author.

Chapter 6

(Manuscript 5)

Description

In this chapter, chitosan-cellulose composite materials were cross-linked using glutaraldehyde (GL) at incremental cross-linker ratios. The preparation of the composite materials was informed by the outcome of the studies reported in chapters 2 and 3, where the collapse of the pore structure of cross-linked chitosan and inefficient pillaring of cellulose attenuated the sorption properties of the **CH-GL** and **C-EP** polymers. The results from the study indicated that the composite materials displayed variable morphological and adsorption properties according to the cross-linker feed ratios, where the composite with highest feed ratio (**CH-GL3-C**) had the optimum sorption properties.

Authors' contribution

The entire experimental design was conceptualized by me and Lee D. Wilson, where I executed all synthesis, characterization of the polymers and data analysis. Lee D. Wilson secured funding and John V. Headley contributed analysis tools. I also wrote the first draft of the manuscript with extensive editing by Lee D. Wilson, while John V. Headley provided final proofreading of the manuscript before submission for publication.

Relation of Manuscript 4 to Overall Objective of this Project

Cross-linked chitosan/cellulose glutaraldehyde composite materials (**CH-GL-C**) were prepared and characterized using physicochemical methods related to adsorption properties. The study reported in this chapter relates to the third and fourth themes (composite formation between

cellulose and chitosan based biopolymers and sorption studies of NAFCs using cellulose and chitosan based polymers) of the thesis research.

Graphical Abstract

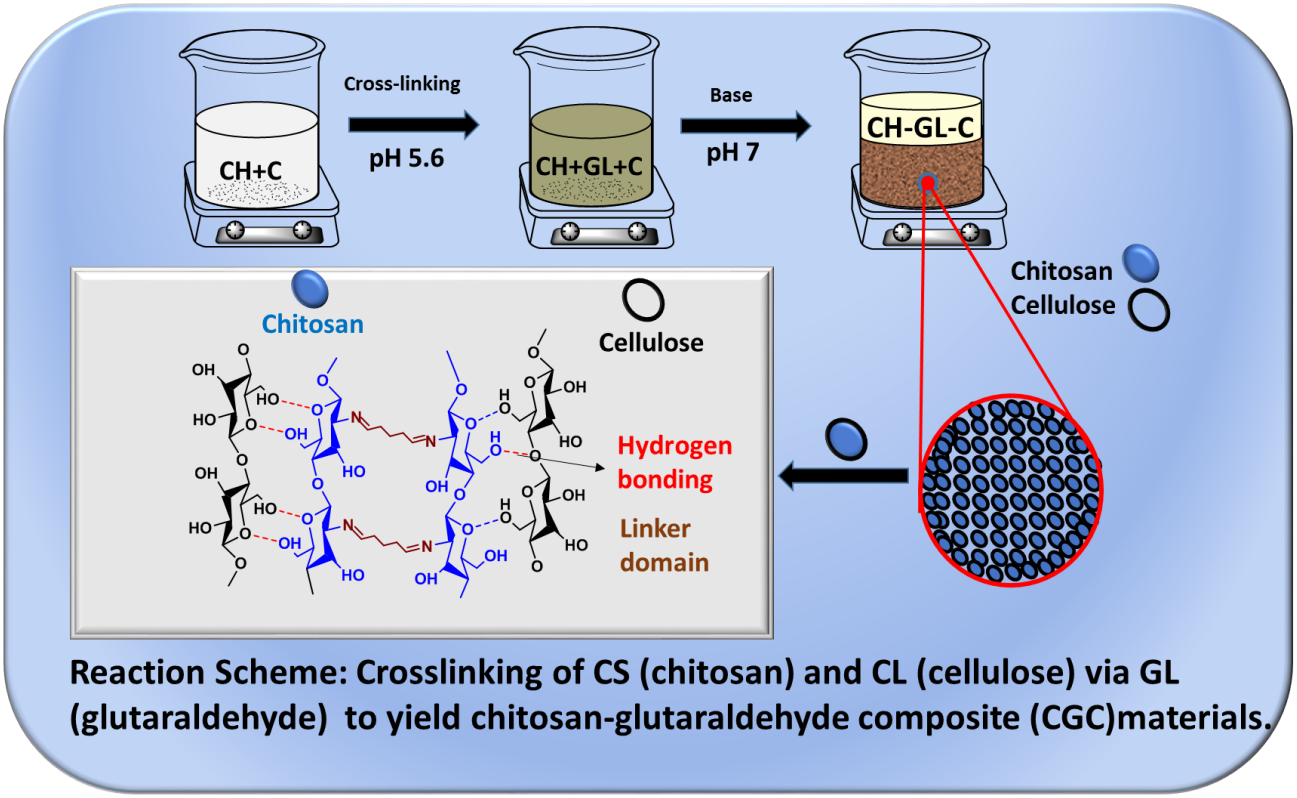

Research Highlights

- Cross-linked chitosan-cellulose composite materials (**CH-GL-C**) were prepared at incremental GL ratios.
- The composite materials were more thermally stable than their precursors.
- The sorption affinity of the composites for naphthenate anions was greater than that of the precursors.
- **CH-GL3-C** with the highest GL feed ratio had the best anion recognition properties.

6. Self-Assembled and Cross-linked Animal and Plant-Based Polysaccharides: Chitosan-Cellulose Composites and their Anion Sorption Properties

Inimfon A. Udoetok[1]; Lee D. Wilson[1*] and John V. Headley[2]

[1]Department of Chemistry, University of Saskatchewan, 110 Science Place, Saskatoon, Saskatchewan, S7N 5C9

[2]Water Science and Technology Directorate, Environment Canada, 11 Innovation Boulevard, Saskatoon, Saskatchewan, S7N 3H5

***Corresponding Author**: L. D. Wilson, Tel. +1-306-966-2961, Fax. +1-306-966-4730,

Email: lee.wilson@usask.ca

6.1 Abstract

Self-assembled and cross-linked chitosan/cellulose glutaraldehyde composite materials (**CH-GL-C**) were prepared with enhanced surface area and variable morphology. FTIR, CHN and ^{13}C solid state NMR studies provided support for the crosslinking reaction between the amine groups of chitosan and glutaraldehyde; whereas, XRD and TGA studies provided evidence of cellulose-chitosan interactions in the composites. SEM, equilibrium swelling and nitrogen adsorption studies corroborate the enhanced surface area and variable morphology of the cross-linked polymers. Equilibrium sorption studies at alkaline conditions with phenolic dyes, single component and mixed naphthenates in aqueous solution revealed variable affinity of the composites for these anion species. According to the Freundlich isotherm model, **CH-GL3-C** had the highest affinity for phenolphthalein (**phth**) followed by *ortho*-nitrophenyl acetic acid (**ONPAA**) and *para*-nitro phenol (**PNP**) respectively (**Phth**: $5.03 \pm 1.40 \times 10^{-1}$ L mmol g^{-1}, **PNP**: $8.49 \pm 0.40 \times 10^{-2}$ L mmol g^{-1}, and **ONPAA**: $2.28 \pm 0.30 \times 10^{-1}$ L mmol g^{-1}). The Sips isotherm model provided a good description of the sorption of single component and OSPW naphthenates. The monolayer uptake capacity (Q_m) was in the order; 2 hexyldecanoic acid (**S1;** 115 ± 15 mg g^{-}

^{1}) > 2 naphthoxyacetic acid **(S6;** 40.5 ± 4.0 mg g^{-1}) > *trans*-4-pentylcyclohexylcarboxylic acid (**S2;** 13.7 ± 1.1 mg g^{-1}). The sorption capacity of **CH-GL3-C** for naphthenate mixtures was 24.1± 0.9 mg/g via UV spectroscopy and 27.4 ± 1.4 mg g^{-1} via high resolution electrospray ionization mass spectroscopy (HR ESI-MS), with the sorbent material showing greater affinity for naphthenates with low double bond equivalence (DBE). Kinetic studies revealed that the sorption of **phth** followed the pseudo-second order (PSO) model whereas the pseudo-first order (PFO) model gave a good description of the kinetic uptake of **S6** and naphthenate mixtures. This study therefore contributes to a greater understanding of the chemistry of the two most abundant biopolymers on the earth by bringing to light, the importance of the interaction between them in composites materials, and revealed the role of hydrophobic interactions as the primary driving force in the sorptive uptake process.

Keywords: Cellulose, Chitosan, Cross-linking, Carboxylates, Adsorption, Composite.

6.2 Introduction

The rapid growth and development of the oil sands extraction industry in north-eastern Alberta, Canada has been a source of environmental concern due to increased process-affected wastewater produced during bitumen extraction via the Clark caustic hot water extraction method.[1-4] The oil sands process-affected water (OSPW) produced during this process is made up of sand, clay, unrecoverable bitumen and hydrocarbons.[1] The zero-discharge policy of the government stipulates that tailings and OSPW must be stored on site within tailing ponds or integrated into a reclaimed landscape.[5-7] In 2010, the Athabasca oil sands industry in northern Alberta had accumulated just under 840 million m^3 of tailings and process-affected water[5]; whereas, the total volume of fine fluid tailings reported by the mine operators in 2013 was 975.6 million m^3, where

a total liquid surface area of the ponds was estimated at 88 km^2.[8] Toxicity studies of OSPW [9-14] relate the toxicity to the water soluble organic fraction, where the major persistent constituent are the naphthenic acid fraction components (NAFCs). NAFCs exhibit chemical stability, persistence in the environment, non-volatility, high viscosity and surfactant-like properties, especially at pH conditions above their pK_a. The environmental concerns raised by the toxicity of NAFCs has prompted several studies on their sequestration and/or removal from OSPW. [3, 15-20] Contaminants such as phenolic dyes are highly mobile in aquatic environments as evidenced by the high water solubility of phenol.[21] Phenolic dyes which often originate from textile and chemical industries are ubiquitous contaminants in the environment and are a source of concern due to their carcinogenic and mutagenic properties.[22, 23] Other toxic effects of exposure to phenolic dyes include skin irritation, necrosis, and damage to kidneys, liver, muscle and eyes. Their toxicity in aquatic environments at ppb levels may be ascribed to their organoleptic properties. The fate and transport of such phenolic compounds can be modified by the adsorptive removal using cross-linked polysaccharide materials such as cellulose and chitosan.[24] Sorption-based removal of phenolic dyes and NAFCs from wastewater using organic polymer materials is a feasible treatment technology due to the synthetic versatility and relatively low cost of biopolymers.[25]

Cellulose and chitosan are the two most abundant bio-renewable biopolymers on the earth.[26] An interesting feature of these polysaccharides is the extensive network of intra/intermolecular hydrogen bonds which yield ordered structures, where variation of the functional groups occur at C-2 of each respective monomer unit. Previous studies with these materials[3, 15, 27-29] report that cross-linking enhances their sorption capacity via surface accessibility of groups due to "*pillaring effects*".[3, 15] However, the challenge with enhancing the sorption capacity of these cross-linked materials relate to the swelling phenomena and disruption of intra-

molecular hydrogen bonding with a consequent collapse of the pore structure of chitosan.[3, 30] On the other hand, the superior mechanical strength of cellulose limits the porosity of its native and crosslinked forms.[15] To address this challenge, the preparation of binary composite containing self-assembled and cross-linked cellulose and chitosan is proposed. The versatile reactivity of chitosan due to the presence of NH_2 groups favor cross-linking reaction with linkers like glutaraldehyde. While the toxicity of glutaraldehyde is well established[31], cross-linking with biopolymers such as chitosan may offset its overall toxicity. The superior mechanical properties of cellulose as well as their similar chemical structures suggest that blending and cross-linking of these two biopolymers could be a prospective way to improve and modify the properties of the final products.[32] Studies of related composite materials [30, 32-45] indicate an improvement in the sorption capacity, microstructure, mechanical, swelling, and surface chemical properties for such materials. Binary blends of cellulose and chitosan are promising systems for creating new polymer architectures such as films, fibers, and sponges due to their low cost, low density, renewable resource origin, biodegradability and unique properties such as porosity and surface area.[34] In particular, composite materials may serve to address the need for the development of low cost and sustainable sorbent materials. For example, a previous[43] study on chitosan-cellulose composite material show that it displays efficient cation recognition and reusability, while other studies[44, 45] revealed greater tensile strength of the composites relative to the precursors. Keungputpong et al.[42] reported that the addition of starch resulted in decreased cross-linking between chitosan and glutaraldehyde with an increased structural stability, as evidenced by thermal and swelling properties of the system. While the formation of composite materials that incorporate chitosan and a second component are known,[42-45] the present study differs from other reports by the nature of the composites and their application as tunable adsorbents for anion recognition.

To the best of our knowledge the effects of self-assembly of cellulose with chitosan, along with the effects of pH on cross-linking via glutaraldehyde have not been reported in terms of the morphological, textural, surface and anion recognition properties of such composite materials. Herein, we report on the self-assembly and cross-linking effects of cellulose/chitosan composites and their anion recognition properties for OSPW, single component naphthenic acids and phenolic dyes. This study reports on several contributions to the field of advanced materials; *i*) the development of valorized biopolymer composites derived from plant and animal polysaccharides, *ii*) composites with variable morphology due to self-assembly and cross-linking effects, and *iii*) tunable biopolymer sorbents for anion recognition properties in chemical mixtures for the controlled removal of waterborne contaminants such as OSPW and phenolic dyes.

6.3 Experimental

6.3.1 Materials

Low molecular weight chitosan (~75%-85% deacetylation), cellulose (medium fibre from cotton linters), sodium hydroxide, aqueous ammonia, glutaraldehyde, phenolphthalein (phth), *ortho*-nitrophenyl acetic acid (**ONPAA**), *para*-nitro phenol (**PNP**), 2-hexyldecanoic acid (**S1**), *trans*-4-pentylcyclohexylcarboxylic acid (**S2**) and 2 naphthoxyacetic acid (**S6**) were obtained from Sigma-Aldrich Canada Ltd. (Oakville, ON). HPLC grade methanol was obtained from Fisher scientific, NJ, USA, whereas, ACS grade glacial acetic acid was obtained from EMD chemicals, NJ, USA. Samples were stored in 2 mL HPLC amber vials with screw-cap perforated Teflon-lined septa from Canadian Life Sciences. All materials were used as received without further purification.

6.3.2 Synthesis of Cellulose Supported Cross-linked Chitosan Composite Materials

Synthesis of the composite materials (**CH-GL1-C**, **CH-GL2-C**, and **CH-GL3-C**) was carried out as follows: 2 g of low molecular weight chitosan was stirred in 400 mL of 5% v/v glacial acetic acid in a 1 L beaker until complete dissolution was achieved. 2 g of cellulose was added to the resulting light-yellow chitosan solution with continuous stirring for about 4 hours. The pH of the mixture was raised to 5.60 using 1 M NaOH, before the desired volume of glutaraldehyde (*cf.* Table 6.1) was added drop-wise over a one-minute period with stirring at 550 rpm and the mixture allowed to continue stirring for 12 h. 6 M NaOH solution was added gradually to the mixture with vigorous magnetic stirring, until pH 7 and a dark yellow coloured precipitate was formed (*cf.* Scheme 6.1).

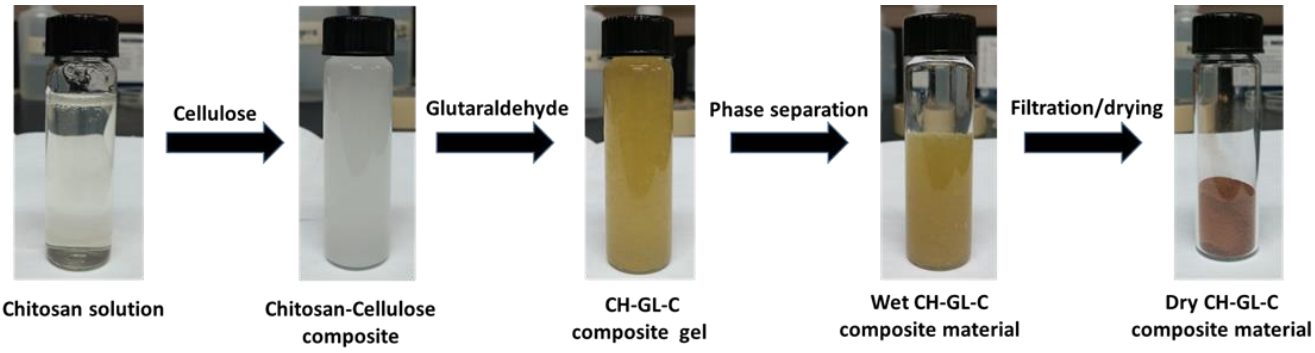

Scheme 6.1: Synthetic procedure for **CH-GL-C** composite materials

The precipitate was separated from the supernatant via vacuum filtration followed by washing with cold Millipore water and drying at ~50 ^{o}C. Soxhlet extraction for 24 h using HPLC grade methanol was used to remove unreacted/excess reagents followed by drying in a vacuum oven at 56 ^{o}C for 12 h. The resulting polymer was ground in a mortar and pestle and sieved using a 40-mesh sieve. A composite material (**CH-C**) was also synthesized via the same method but without the cross-

linking step. Each material was synthesized at least 3 times during the research project and characterization results affirmed the repeatability of the synthetic procedure.

Table 6.1 Mass of precursors versus volume of glutaraldehyde in cross-linked **CH-GL-C** materials

Reaction Conditions	CH-C	CH-GL1-C	CH-GL2-C	CH-GL3-C
Glutaraldehyde content (mL)	0	2.17	4.35	6.52
Mass of chitosan (g)	2.00	2.00	2.00	2.00
Mass of cellulose (g)	2.00	2.00	2.00	2.00

6.3.3 Characterization of CH-GL-C Composite Materials

6.3.3.1 Thermal Gravimetric Analysis (TGA)

Thermal stability of the composite materials were measured using a TA Instruments Q50 TGA system operated with a heating rate of 5˚C min^{-1} to a maximum temperature of 500˚C using nitrogen as the carrier gas. The results obtained were displayed as first derivative (DTG) plots of weight with temperature (%/˚C) against temperature (˚C).

6.3.3.2 Fourier Transform Infrared (FTIR) Spectroscopy

A Bio-RAD FTS-40 IR spectrophotometer was used to obtain the IR spectra of the cross-linked composite materials. Powdered samples were mixed with pure spectroscopic grade KBr in a weight ratio of 1:10 followed by grinding in a small mortar and pestle. The DRIFT (Diffuse Reflectance Infrared Fourier Transform) spectra was obtained in reflectance mode at room temperature with a resolution of 4 cm^{-1} over the 400–4000 cm^{-1} spectral range. Multiple scans were recorded and corrected relative to a background of pure KBr.

6.3.3.3 Carbon, Hydrogen and Nitrogen (CHN) Analyses

A Perkin Elmer 2400 CHN Elemental Analyzer with the following instrument conditions; combustion oven temperature (> 925 °C) and reduction oven temperature (> 640 °C) was used to determine the CHN composition of the samples. The instrument was purged with a mixture of pure oxygen and helium gas and acetanilide was used as the calibration standard. Elemental analyses results of samples were obtained in triplicate with an estimated precision within ±0.3%. Degree of substitution (DS) was calculated using the following equation 6.1,

$$DS = \frac{(C/N)p - (C/N)c}{n} \qquad \text{Equation 6.1}$$

where $(C/N)p$ and $(C/N)c$ are the ratio of carbon to nitrogen in the composites and pristine chitosan and n is the number of carbon atoms from the glutaraldehyde feed ratio.

6.3.3.4 SEM

The surface morphology of non-crosslinked and cross-linked composite materials were studied using scanning electron microscopy (SEM; Model SU8000, HI-0867-0003). Images from gold coated samples were collected under the following instrument conditions; accelerating voltage – 5kV, working distance (WD) - 8.7 mm and magnification - ×50,000.

6.3.3.5 Powder X-ray Diffraction (PXRD)

The X-ray diffraction patterns of non-crosslinked and cross-linked composite materials were obtained using a PANalytical Empyrean powder X-ray diffractometer. A monochromatic Co-Kα1 radiation was used while applied voltage and current were set to 40 kV and 45 mA, respectively. The samples were mounted in a horizontal configuration after evaporation of

methanol films. The PXRD patterns were measured in continuous mode over a 2θ range, where 2θ = 7–50° with a scan rate of 3.2° min^{-1}. The crystallinity index (CrI) was calculated from the height ratio between the intensity of the crystalline peak (I_{cr}) and amorphous peak (I_{AM}).

6.3.3.6 Equilibrium Swelling Properties of Composite Materials

The swelling properties of the precursors and composites were determined by shaking approximately 50 mg of the materials in 12 mL of Millipore water in a horizontal shaker for ~ 48 h. The weight of swollen precursors and composites (w_s) were determined by weighing after tamping dry with filter paper, whereas the dry weight (w_d) was obtained after drying in an oven at 65ºC to a constant weight. The swelling ratio was calculated using equation 6.2:

$$Sw(\%) = \frac{Ws\text{-}Wd}{Wd} \times 100 \qquad \text{Equation 6.2}$$

6.3.3.7 Gas Adsorption Studies

Surface area and pore structure properties of one of the cross-linked composite material (**CH-GL3-C**) was obtained via nitrogen adsorption measurements using a Micromeritics ASAP 2020 (Norcross, GA) with an accuracy of ±5%. Briefly, a 1.0 g sample was degassed at an evacuation rate of 5 mm Hg/s and degassing temperature maintained at ~ 100°C for ~48 h. Stabilization of the outgas rate at <10 μmHg/min indicated the completion of degassing. Alumina (Micromeretics) was used to calibrate the instrumental parameters. The BET surface area was determined from the adsorption isotherm using 0.162 nm^2 as the surface area for gaseous molecular nitrogen.[46, 47] The Barret–Joyner–Halenda (BJH) method and a t-plot (de Boer method)[48] were used to estimate the pore volume/pore diameter and micropore surface area respectively.

6.3.3.8 ^{13}C Solids State NMR Spectroscopy

^{13}C solids state NMR spectra were obtained with a Bruker AVANCE III HD spectrometer equipped with a 4 mm DOTY CP-MAS (cross polarization with magic angle spinning) solids state probe operating at 125.77 MHz (^{1}H frequency at 500.23MHz). The ^{13}C CP-MAS (Cross Polarization with Magic Angle Spinning) experiments were carried out at a spinning speed of 10 kHz, a ^{1}H 90^{0} pulse of 3.5 µs, and a contact time of 0.75 ms with a ramp pulse on the ^{1}H channel. For different samples, 600 – 1200 scans were accumulated, with a recycle delay of 2 s. All experiments were recorded using 71 kHz SPINAL-64 decoupling during acquisition. The spectra were referenced externally to adamantane at 38.48 ppm (low field signal).

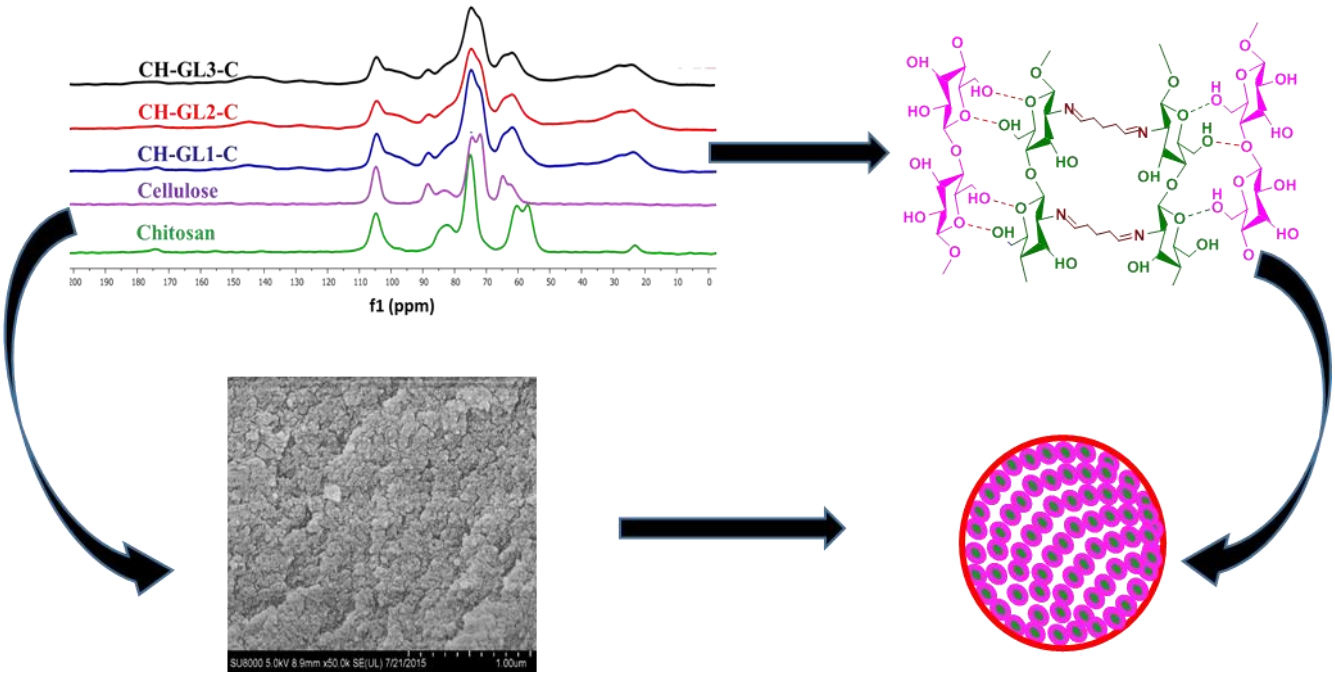

Scheme 6.2: Structure morphology relationship of **CH-GL-C** composite materials where purple (cellulose) outline on green spheres (chitosan) represent support of chitosan pore structure by cellulose)

6.3.4 Sorption studies

6.3.4.1 Sorption of Phenolic Dyes

A 50 mM stock solution of phenolphthalein (**phth**) in ethanol was prepared followed by 33 μM solution by diluting 66 μL of the stock solution to 100 mL using sodium bicarbonate buffer (pH 10.5). 10 mM *para*-nitro phenol (**PNP**) and 0.55 mM *o*-nitrophenyl acetic acid (**ONPAA**) solutions at pH 9 were prepared by dissolving appropriate amount in sodium bicarbonate buffer. Absorption measurements were carried out at λ_{max}=552 nm (**phth**), 400 nm (**PNP)** and 271nm (ONPAA) respectively. 7 mL of aqueous solution containing the phenolic dyes were added to vials containing 10 mg of the sorbent materials. The mixtures were shaken for 24 h, centrifuged (Precision Micro-Semi Micro Centricone, Precision Scientific Co.) at 1550 rpm, and the absorbance of the supernatant was measured using a double beam UV-vis spectrophotometer (Varian CARY 100) at room temperature (295 ± 0.5 K)

6.3.4.2. Sorption of OSPW Naphthenates and Single Component Carboxylate Anions

A 100 mL stock solution at 100 ppm was prepared for the OSPW and single component carboxylic acids (**S1**, **S2**, and **S6**) respectively. This was done by dissolving appropriate amounts of the surrogates in a 0.1 M aqueous NH_3 solution under sonication until the resulting mixture was dissolved, where a 2800 ppm OSPW was diluted using aqueous NH_3 solution (0.1 M). The mixture was stirred overnight and different concentrations (1 – 100 ppm) of the surrogates were prepared by dilution of the stock solution with Millipore water.

Fixed amounts (10 mg) of the cross-linked composites were mixed with 5 mL of surrogates and OSPW solutions in 2 dram vials at variable concentration. The mixtures were equilibrated at 295 K on a horizontal shaker table for 24 h. The initial concentration (C_o) and residual

concentration at equilibrium (C_e) of the surrogates and OSPW napththenates was determined using a ThermoScientific LTQ Orbitrap Elite mass spectrophotometer and a double beam UV-vis spectrophotometer (Varian CARY 100) at 295 ± 0.5 K. The samples were centrifuged prior to HR ESI-MS and UV spectral analyses. Uptake of **S1**, **S2** and **S6** was determined from the difference between C_o and C_e values described by equation 6. 3.

$$Q_e = \frac{(C_o - C_e) \times V}{m} \qquad \text{Equation 6.3}$$

Q_e is the quantity of adsorbate in the solid phase adsorbed at equilibrium (mg g^{-1}), C_o is initial concentration of adsorbate (mg L^{-1}) in solution, C_e is concentration of adsorbate at equilibrium (mg L^{-1}) in solution, V is volume of adsorbate solution, and m is mass (g) of sorbent material.

6.3.4.3. Kinetic Studies

Kinetic uptake studies were carried out using a one pot method[49] for **phth**; whereas, a batch method was used for OSPW and **S6** uptake studies as follows: ~100 mg of the polymer was added to a folded Ahlstrom filter paper (Grade 613, 7.5 cm), where both ends were clamped after addition of the polymer. The folded and clamped filter paper containing the composite was immersed in a fixed volume (120 mL) of a 33 μM phth solution. Aliquots of the phth solution were pipetted (3 mL) out after each designated time interval and quantified by UV-vis absorption. For the batch kinetics studies, ~10 mg of cross-linked composite material (**CH-GL3-C**) was placed in 2 dram vials followed by addition of 5 mL of OSPW. Each vial was shaken for specific time intervals (2, 5, 10, 15, 20, 30, 40, 50, 60, 70 and 100 min). The aliquots were quantified using a double beam UV-vis spectrophotometer (Varian CARY 100) at 295 ± 0.5 K after phase separation of the solid composite material, as described for equilibrium studies. The above batch procedure was repeated

for **S6**. Uptake of OSPW and **S6** at each sampling time interval (t) where C_o and C_t refer to the surrogate concentration at t = 0 and variable t values, according to equation 6.4.

$$Q_t = \frac{(C_o - C_t) \times V}{m} \qquad \text{Equation 6.4}$$

6.3.4.4. Electrospray Ionization Mass Spectrometry Analysis

A ThermoScientific LTQ Orbitrap Elite mass spectrometer was used to monitor the electrospray ionization mass spectra (ESI-MS) and estimate the concentration of the surrogates in aqueous solutions. The resolution setting of the spectrometer was 30,000 while a full-scan mass spectrum was collected between *m/z* 100 and 600. Samples were quantified by extracting the mass of the analyte of interest. The electrospray ionization (ESI) interface was set to negative ionization mode. Mass spectrometer conditions were optimized by the transmission of *m/z* 112.98563. The heated ESI interface (HESI) parameters were as follows: source heater temperature (53 °C); spray voltage (2.86 kV); capillary temperature (275 °C); sheath gas flow rate (25 L h^{-1}); auxiliary gas flow rate (5 L h^{-1}); and spray current (5.25 μA).

6.3.4.5. Sorption Isotherms and Modeling

Sorption isotherms were obtained by plotting Q_e *vs* C_e (*cf.* Equation 6.3). The isotherms were subsequently analyzed using Freundlich [50] and Sips [51] isotherm models (*cf.* Equations 6.5-6.6). The Freundlich and Sips models additionally account for surface heterogeneities. The binding constant is represented by an equilibrium parameter (K_i).

$$Q_e = K_F C_e^{1/n_f} \qquad \text{Equation 6.5}$$

$$Q_e = \frac{Q_m (K_S C_e)^{n_s}}{1 + (K_S C_e)^{n_s}}$$ Equation 6.6

Kinetic isotherms were obtained by plotting Q_t vs t (*cf*. Equation 6.4). The pseudo-first order (PFO) and the pseudo-second order (PSO) kinetics models (*cf*. Equations 6.7-6.8) were used to analyze the isotherms.

$$Q_t = Q_e (1 - e^{-k_1 t})$$ Equation 6.7

$$Q_t = \frac{Q_e^{\,2} k_2 t}{1 + k_2 t Q_e}$$ Equation 6.8

6.4. Results and Discussion

6.4.1 Characterization of Composite Materials

6.4.1.1 FTIR Spectroscopy

The FTIR spectra of the cross-linked composite materials and the precursors are shown in Figure 6.1. The salient features of the spectra include broad bands at ~3000–3700 cm^{-1} ascribed to the stretching of hydrogen bonded O–H and N–H groups, ~2800–3000 cm^{-1} attributed to C–H stretching, and ~1550–1680 cm^{-1} corresponding to N–H bending, imine and ethylenic groups, respectively.[52] These bands for the composites are absent and/ or are broader when compared to similar bands for the precursors and the non-cross-linked polymer. This may be due to hydrogen bonding between O–H and N–H groups of cellulose and chitosan[53] and/or crosslinking reaction between chitosan and the glutaraldehyde linker. The decreased intensity of the O–H and N–H bands at ~3000–3700 cm^{-1} and sharpness/increased intensity of the N–H band at 1574 cm^{-1} for the non-cross-linked composite material support such interactions in agreement with a reported study.[53] Other features are methyl deformation (1395 cm^{-1}), amide III (1340 cm^{-1}), and several

bands ~1000–1200 cm^{-1} indicative of C–O–H, C–O–C and C–N–H asymmetric stretching. These bands attenuate as linker content increases and may be explained by greater steric hindrance in the polymer network due to crosslinking and/ or hydrogen bonding effects.[41] Band broadening at ~3000–3700 cm^{-1} and ~1560–1670 cm^{-1} affirm this claim. The most supportive evidence of the formation of **CH-GL-C** polymers is the appearance of a new band at ~1710 cm^{-1} which is attributed to vibrations of aldehyde groups. The carbonyl band increases in intensity as the cross-linker content increases and appears uniquely in the spectra of cross-linked polymers, in agreement with previous studies.[29, 52] The preservation of the basic structural properties of the precursors of these materials is supported by the similarities in the respective spectral signatures of crosslinked chitosan and cellulose materials.[3, 15]

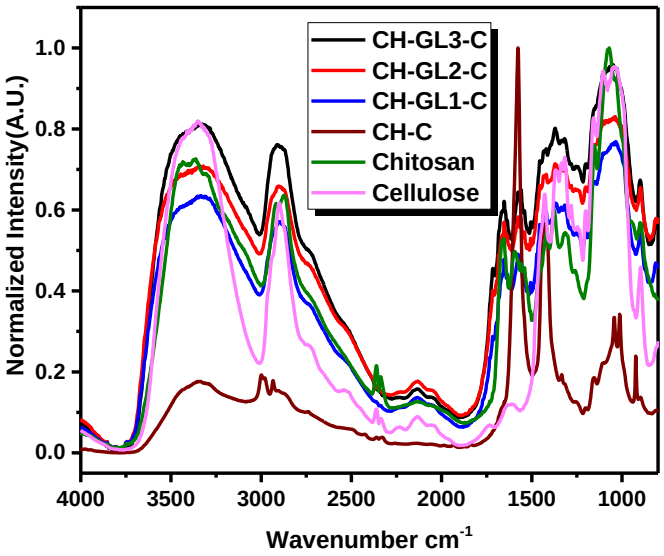

Figure 6.1. FTIR spectra of the precursors and **CH-GL-C** composite materials

6.4.1.2 Thermal Gravimetric Analysis (TGA)

Thermogravimetric studies of the cross-linked composite materials and precursors are shown in Figure 6. 2. A single thermal event occurs ca. ~295 ºC (chitosan) and ~335 ºC (cellulose) for the precursors, two for the non-crosslinked material (~260 ºC for the chitosan domain and ~450 ºC for cellulose domain). The cross-linked materials display three thermal events at ~239 ºC, ~350 ºC, and ~426 ºC. The thermal events for the **CH-GL-C** composite materials correspond to decomposition of chitosan, cellulose and linker domains of the materials. The TGA results affirm that the basic structural properties of the precursors are preserved in accordance with FTIR studies and previous work.[15] A shift in the thermal events of chitosan/cellulose domains for the **CH-GL-C** composites occur relative to the precursors, indicative of the greater thermal stability for the composites. The observed shift in thermal events for the **CH-GL-C** materials may be due to hydrogen bonding and/ or cross-linking with glutaraldehyde as affirmed by changes in the FTIR bands related to such interactions. Previous studies[30, 32] on similar composite materials reveal enhanced mechanical and thermal properties relative to the unmodified polysaccharides.

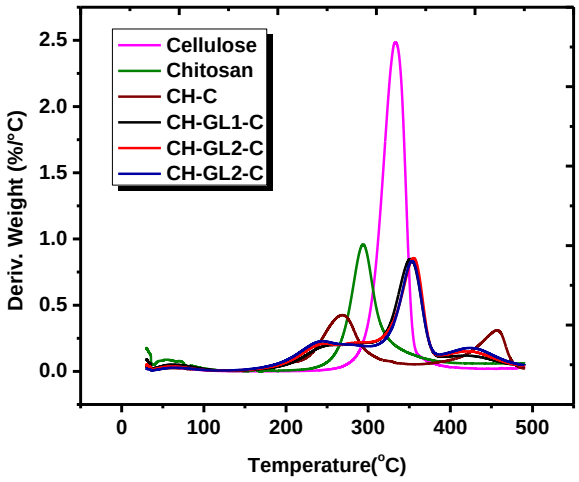

Figure 6.2. DTG profiles of chitosan, cellulose and **CH-GL-C** composite materials

6.4.1.3 CHN Analyses

The results obtained from CHN analyses of the samples and precursors are shown in Table 6.2. The C-content of the composites increased with greater cross-linking; whereas, nitrogen and hydrogen levels decreased in agreement with previous studies.[54, 55] This may be due to the increased carbon content via composite formation between cellulose and chitosan with glutaraldehyde cross-linking. The increase in the C/N ratio and degree of substitution with increasing level of linker content (*cf.* Table 6.2) supports the observation where the C/N ratio for the composites far exceeds the level for chitosan. The increase in DS and C/N values are in agreement with increased thermal stability from TGA studies and the presence of an imine bond in the FTIR spectra and ^{13}C NMR spectra of these materials.

Table 6.2 CHN composition of precursors and cross-linked **CH-GL-C** composite materials

Material	% C	% H	% N	C/N	DS**	% CrI*
Chitosan	41.6 ± 2.1 (44.7)	7.46 ± 0.37 (7.45)	7.67 ± 0.38 (8.70)	5.42 ± 0.27 (5.14)	NA	40.0 ± 2.0
Cellulose	41.0 ± 2.1 (44.4)	6.27 ± 0.34 (7.41)	NA (NA)	NA (NA)	NA	70.0 ± 3.5
CH-C	35.1 ± 1.8	5.42 ± 0.27	1.71 ± 0.09	20.5 ± 1.0	NA	NA
CH-GL1-C	43.9 ± 2.2	7.00 ± 0.35	2.79 ± 0.14	15.7 ± 0.8	2.06 ± 0.10	21.0 ± 1.1
CH-GL2-C	45.0 ± 2.3	6.97± 0.35	2.59 ± 0.13	17.4 ± 0.9	2.40 ± 0.12	18.0 ± 0.9
CH-GL3-C	46.2 ± 2.3	6.87± 0.34	2.40 ± 0.12	19.3 ± 1.0	2.78 ± 0.14	11.0 ± 0.6

*CrI – Crystallinity index, **DS – Degree of substitution (*cf.* Equation 6.1), NA – Not applicable, values in parentheses are theoretical values for the starting materials

6.4.1.4 SEM

Figure 6.3 shows the SEM micrographs of the non-crosslinked and cross-linked composite materials. The images show that the starting materials and non-cross-linked composite (**CH-C**) are made up of large and dense fibre bundles with multiple layers. By comparison, the cross-linked **CH-GL-C** composites display reduced particle sizes with a reduction in the layered structure as the level of cross-linking increases. The micrographs reveal that cross-linking of the starting materials show changes in the morphology and structure of the polymers according to the level of linker content. As well, changes in the surface chemistry of the materials parallel changes in roughness and porosity as the linker content increases, as reported for related materials.[54] Results obtained from this study reveal that composite materials possess higher porosity, roughness and surface area when compared with pristine cellulose or chitosan, and cross-linked chitosan.[3] These improved textural and morphological properties may be due to the support provided for the porous composite materials as a result of the interaction between cellulose and chitosan.

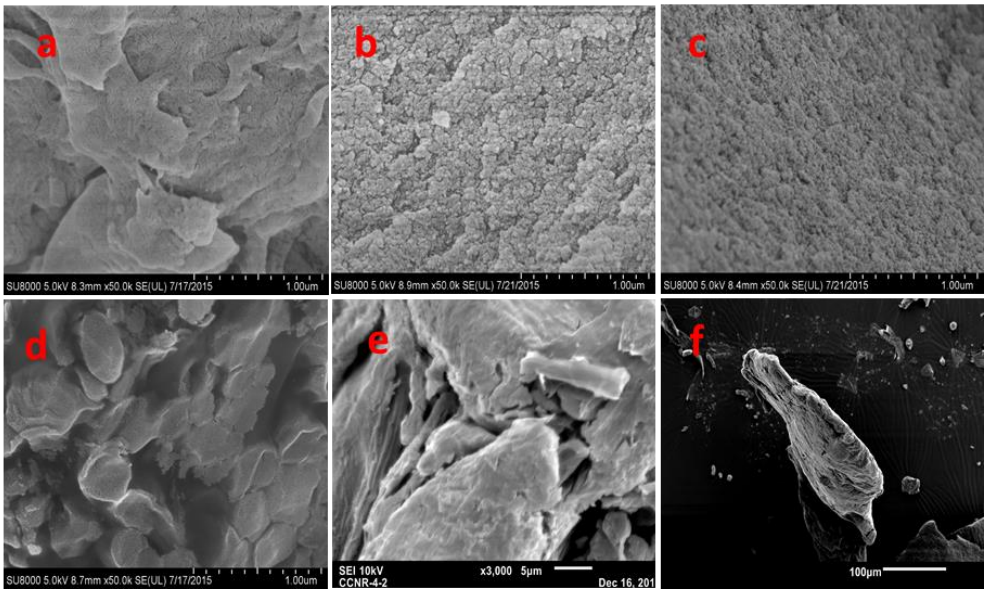

Figure 6.3. SEM micrographs of a) **CH-GL1-C**, b) **CH-GL2-C**, c) **CH-GL3-C**, d) **CH-C**, e) cellulose and f) chitosan

6.4.1.5 Powder X-ray Diffraction (PXRD)

The PXRD patterns of chitosan, cellulose, non-crosslinked and crosslinked composite materials are displayed in Figure 6.4. The salient feature of the diffraction patterns are peaks at ~16º, ~19 º, ~24 º, ~26 º and ~40 º which is typical of cellulose I and peaks at ~10 º and ~20 º from chitosan. The patterns also reveal several sharp peaks through the range of 2θ values for the non-crosslinked composite. These patterns confirm the preservation of the basic structural properties of the starting materials, in agreement with the FTIR and TGA results. The presence of sharp features for the non-cross-linked composite may result from increased crystallinity of this material due to strong hydrogen bonding between the amino group of chitosan and OH groups of cellulose. The sharp band due to the protonation of NH groups of chitosan at 1574 cm^{-1} and the attenuation of the N–H/ O–H (~3000–3700 cm^{-1}) and C–H stretching bands at ~2800–3000 cm^{-1} in the FTIR spectra of the non-cross-linked composite concur with the PXRD results. The diffraction patterns of the cross-linked composite materials show a sharp decrease in the intensity of the PXRD peaks from their precursors, and is consistent with relevant study.[55] This decrease in peak intensity with greater glutaraldehyde content of the composites may relate to a decrease in the crystallinity of the composite materials due to crosslinking reaction. The latter was affirmed by the presence of an imine bond in the FTIR and ^{13}C spectra of the composites as well as the crystallinity index obtained from the crystalline and amorphous peak ratios.

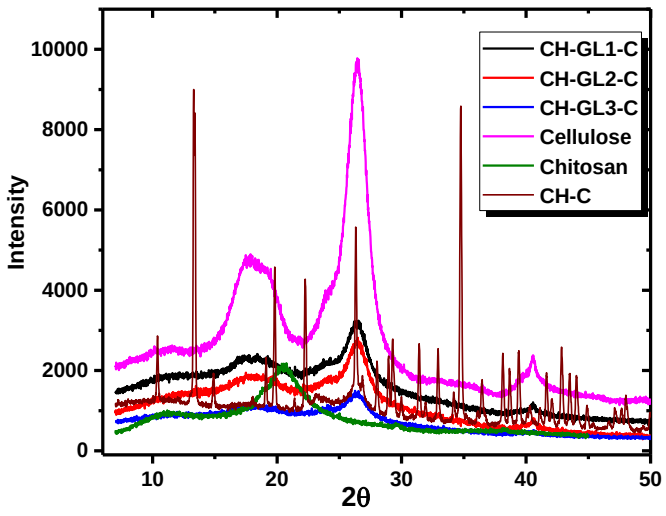

Figure 6.4. PXRD patterns of chitosan, cellulose and **CH-GL-C** composite materials

6.4.1.6 Gas Adsorption Studies

Figure 6.5 illustrates the results for the nitrogen adsorption/desorption for one of the composite materials (**CH-GL3-C**). The isotherm resembles a type II isotherm according to the International Union of Pure and Applied Chemistry (IUPAC) classification,[56] where isotherms of this type describe adsorption on non-porous powders or on powders with pore diameter exceeding that of micropore domains.[57] The isotherm indicates monolayer adsorption coverage at a relative pressure (p/p^o) of 0.5 and a BET surface area of 0.947 ± 0.001 m^2g^{-1} as well as an average pore-width of 8.16 nm. The nitrogen adsorption agrees with the SEM results which reveal greater porosity and surface area; whereas, the PXRD results indicate decreased crystallinity of the composites. A low uptake of nitrogen up to a greater relative pressure (p/p^o 0.8) and greater adsorption at higher p/p^o (>0.8) is evident from the nitrogen uptake isotherm. The trend in gas uptake may be due to adsorption at the outer surface and/or grain boundaries of the composite

materials at lower pressure and within the macro-pores at elevated pressure.[58, 59] The foregoing illustrate that the cross-linked composites possess higher surface area, porosity and strength than cross-linked chitosan-glutaraldehyde (**CH-GL**) polymers reported previously in chapter 2, and may relate to the interaction between cellulose and chitosan.[34, 60]

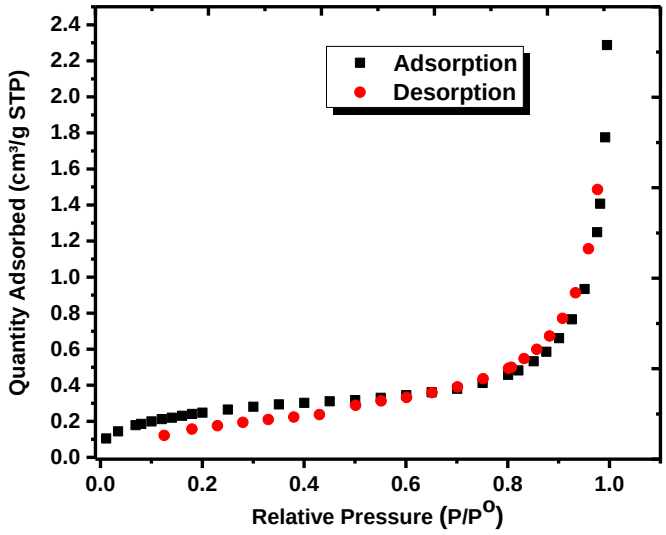

Figure 6.5. Nitrogen adsorption and desorption isotherm at 77 K for **CH-GL3-C**

6.4.1.7 Equilibrium Swelling Properties of Composite Materials

The swelling properties of the composite materials and their precursors are presented in Table 6.3. The results indicate that the non-cross-linked composites showed the least swelling; whereas composites with greater glutaraldehyde content displayed the greatest swelling in water, in agreement with the PXRD results. PXRD indicates an increased crystallinity due to composite formation and reduced crystallinity after cross-linking. The results obtained herein reveal that cross-linking of the composite materials lead to increased porosity and surface area, in agreement with the SEM and nitrogen adsorption study above.

Table 6.3 Swelling properties of composite materials and precursors

Materials	Swelling%
Cellulose	125 ± 6
Chitosan	355 ± 18
CH-C	49 ± 2
CH-GL1-C	179 ± 9
CH-GL2-C	245 ± 12
CH-GL3-C	524 ± 26

6.4.1.8 ^{13}C Solid State NMR Spectroscopy

The ^{13}C solid state NMR spectra of the precursors and cross-linked composite materials are presented in Figure 6.6. The spectra of unmodified chitosan shows ^{13}C resonances for C1 (~105 ppm), C2 (~56.8 ppm), C3, 5 (~75.0 ppm), C4 (~82.4 ppm), C6 (~60.6 ppm), C=O (~174 ppm), and CH_3 (~23.1 ppm), in agreement with other NMR reports.[30, 61] By comparison, native cellulose displays resonances for C1 (~105 ppm), C2/C3/C5 (74.5 ppm), C4 (88.4 and 83.3 ppm), and C6 (64.7 and 62.7 ppm). The spectra of the composites bear similar features to ^{13}C NMR results for each single component, indicating that the structural character of the starting materials are preserved, in agreement with the FTIR, TGA and PXRD studies. The spectral differences between these composites and their precursors relate to the broadening and shift variations in the ^{13}C signatures, along with the appearance of new resonances at ~28.0 and 41.0 ppm, ~100 ppm, ~129/125 ppm, ~142/144 ppm, and ~180ppm. The high field signatures relate to the methylene groups of glutaraldehyde with different chemical environments (~28.0 and 41.0 ppm), conjugated ethylenic bond (~100, 125 – 144 ppm) and an imine bond (~ 180 ppm). The occurrence of cross-linking agrees with FTIR bands at 2800–3000 cm^{-1}(CH_2 groups), ~1550–1680 cm^{-1} (ethylenic group) and ~1710 cm^{-1} (C=O) along with previous studies.[52, 55, 61, 62] The new resonance lines has an increased intensity according the level of crosslinking, in agreement with previous studies.[3] The

^{13}C line intensity of the peaks at ~28.0 and ~ 180 ppm increase for **CH-GL1-C** to **CH-GL3-C**, where they approach similar magnitude with the spectral signatures of the precursors.

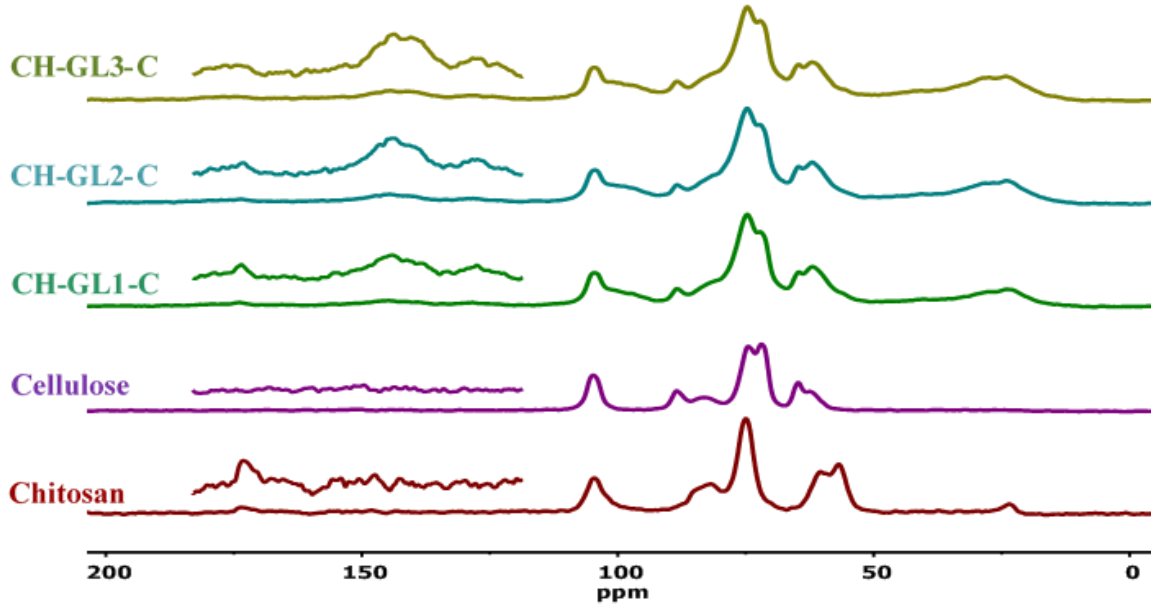

Figure 6.6. CP-MAS ^{13}C solid state NMR spectra of cellulose, chitosan and CH-GL-C composite materials at 295 K, with 10 kHz MAS and 125 MHz field strength.

6.4.2 Sorption studies

6.4.2.1 Sorption of Phenolic Dyes

The adsorption isotherms of several phenolic dyes [phenolphthalein (**phth**), *p*-nitrophenol (**PNP**) and *o*-nitrophenyl acetic acid (**ONPAA**)] are shown in Figures (6.7a - c). The best-fit sorption parameters of the Freundlich and Sips models are listed in Table 6.5. The results illustrate that the sorbent materials possess variable affinity for the uptake of different phenolic dyes, where an increase in uptake occurs as the cross-linker content increases, in agreement with results reported in chapter 2. **CH-GL3-C** had the highest uptake of **phth** and was used for subsequent studies.

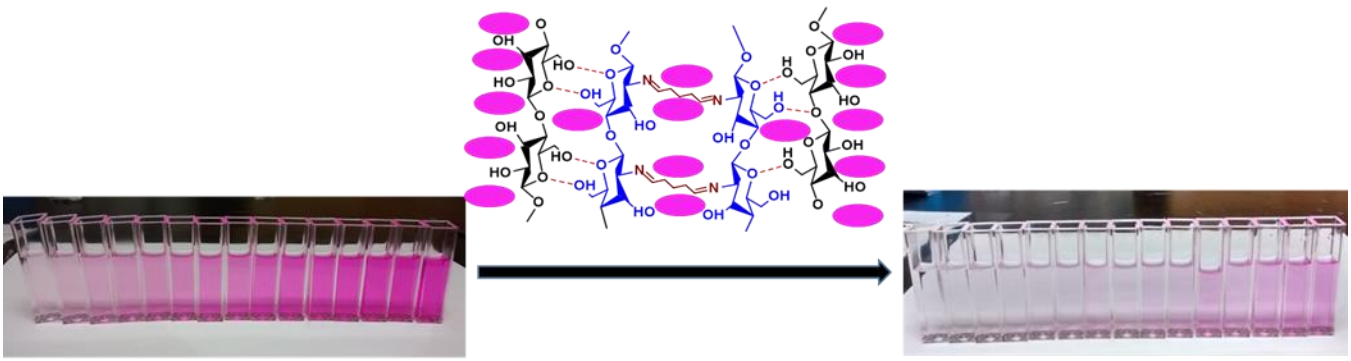

Scheme 6.3: Uptake of phenolphthalein dianion species by **CH-GL-C** composite materials

According to the Freundlich isotherm model, uptake of the dyes by **CH-GL3-C** was in the following order: **Phth** ($5.03 \pm 1.40 \times 10^{-1}$ L mmol g^{-1}), **ONPAA** ($2.28 \pm 0.30 \times 10^{-1}$ L mmol g^{-1}) and **PNP** ($8.49 \pm 0.40 \times 10^{-2}$ L mmol g^{-1}). These results suggest that hydrophobic interactions contribute as the primary driving force for the uptake of these phenolic dyes by the sorbent materials. **PNP** is among one of the more hydrophilic dyes as evidenced by its water solubility. The 1/n parameter in the Freundlich equation is a measure of the feasibility of the sorption process. Greater 1/n values signify an unfavourable sorption process. Based on the 1/n values obtained for the three phenolic dyes, the feasibility of the sorption process increased in the following order: **ONPAA** (1.15 ± 0.05) < **phth** (1.40 ± 0.04) < **PNP** (1.92 ± 0.03).

Table 6.4. Selected physicochemical properties of the phenolic dyes

Properties	*p*-nitrophenol (PNP)	Phenolphthalein (Phth)	*o*-nitrophenylacetic acid (ONPAA)
Structure	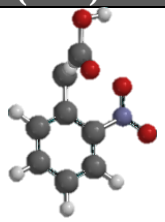	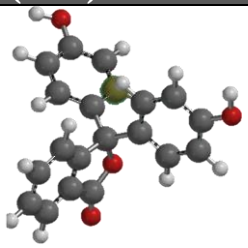	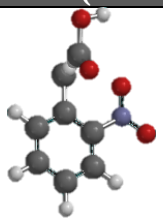
pK_a @ 25ºC[a]	7.15	9.70	4.00
Log P[a]	1.91	2.41	NA
Solubility in water @ 20ºC (mg L^{-1})[a]	11600	400	NA

NA: Not available, [a] Adapted from http://www.drugbank.ca/drugs.[63]

The trend in **PNP** uptake relates to its hydrophilic character when compared to other dyes with greater hydrophobicity (**phth** and **ONPAA**). This greater hydrophobicity of **phth** and **ONPAA** enable strong binding to the pores of the composite materials (*cf.* Table 6.4). Results obtained herein compare the uptake of **PNP** by the single component and composite materials (Cellulose[15]: 1.56×10^{-2} mmol g^{-1}, Chitosan[64]: 9.00×10^{-3} mmol g^{-1}), where the composites show higher uptake affinity. A comparison of the uptake of **phth** by these composites with other sorbent materials show that they possess superior uptake relative to activated carbon and β-cyclodextrin polymers (0.114 – 0.262 mmol g^{-1}).[65]

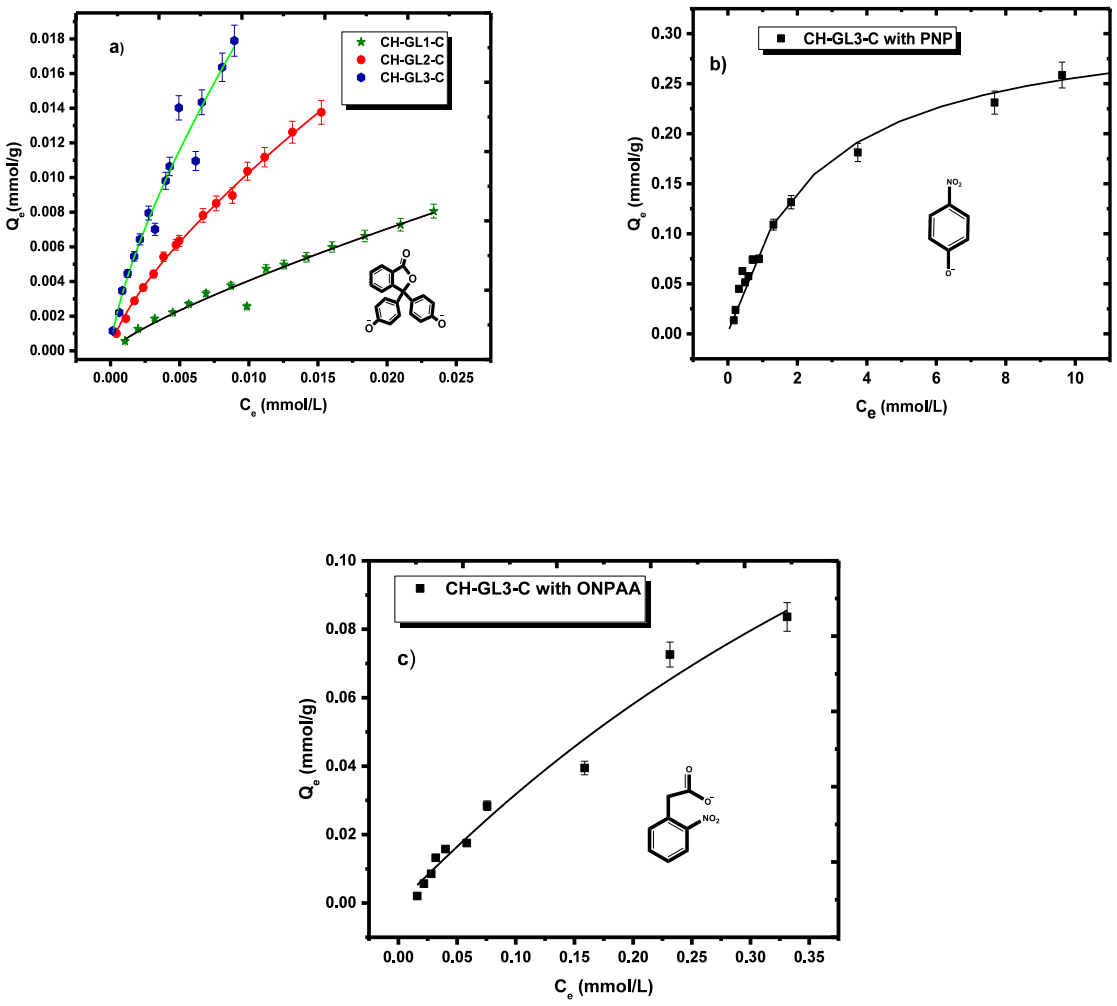

Figure 6.7. Sorption isotherms of **CH-GL-C** composite material with phenolic dyes; a) **phth**, b) **PNP** and c) **ONPAA** at 295 K.

6.4.2.2. Sorption of Single Component Carboxylate Anions

The experimental sorption results plotted as Q_e vs C_e for OSPW and single component carboxylate anions (**S1, S2** and **S6**) are shown in Figure 6.8. The isotherms reveal a monotonic increase observed for Q_e vs C_e as the total concentration of the species in solution increases. The isotherm parameters are well-described according to the Sips model, where **CH-GL3-C** shows

greater affinity for carboxylate anions with $z = 0$, in agreement with previous studies.[3, 65] According to the data obtained from the Sips isotherm model (Table 6.5), **S1** ($z = 0$) had the highest uptake ($Q_m = 115 \pm 15$ mg/g) with **CH-GL3-C**, followed by **S6** ($z = -4$) and **S2** with $z = -2$, in agreement with previous results for the single component biopolymer.[15] These result suggest that the number of ring systems for the carboxylates affect the adsorptive uptake properties. As well, the critical micelle concentrations (CMCs) play an important role in the sorptive uptake since the CMC is a measure of hydrophobic character.[66] For example, **S6** ($Q_m = 40.5 \pm 4.0$ mg/g) displays greater **uptake** for **CH-GL3-C** than **S2** ($Q_m = 13.7 \pm 1.1$ mg/g), and may relate to the different solubility profile of **S2** and **S6** according to differences in the CMC. A comparison of the uptake for **S1** and **S2** by crosslinked chitosan glutaraldehyde (**CH-GL**) polymers[3] and with **CH-GL-C** composite materials shows that the latter display greater uptake of these two surrogates than the **CH-GL** polymers. The offset in sorption properties affirm the synergistic role of the interactions between chitosan and cellulose and the role of the pore structure in such composite materials.

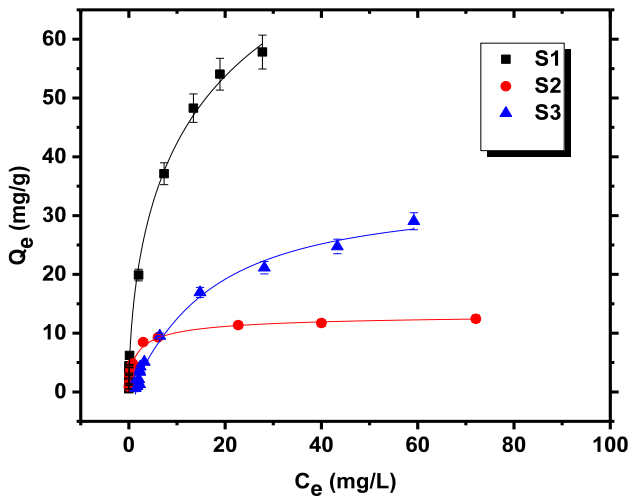

Figure 6.8. Equilibrium sorption isotherms of **CH-GL3-C** composite material with carboxylates (**S1**, **S2**, and **S6**) at pH 9 and 295 K.

6.4.2.3. Sorption of OSPW NAFCs

Sorption studies of **CH-GL3-C** with naphthenates from OSPW is presented in Figure 6.9. The data obtained according to the Sips isotherm model show that there is a monotonic increase in the uptake of **OSPW** naphthenates from aqueous solution until the saturation was achieved, where the sorption capacity of **CH-GL3-C** is 24.1± 0.9 mg/g.

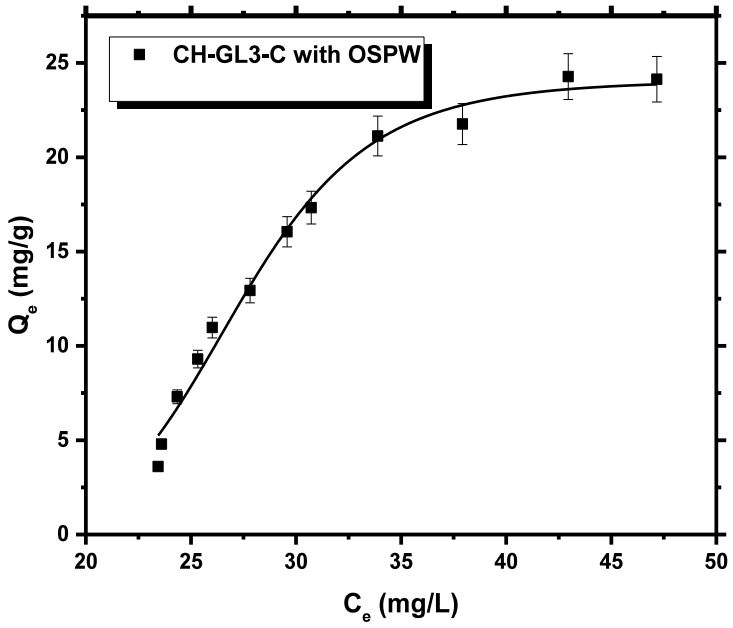

Figure 6.9. Sorption isotherm of **CH-GL3-C** composite material with OSPW naphthenates at pH 9 and 295 K.

OSPW contains a variety of naphthenates ranging from straight chain to cyclic aliphatic and/or aromatic, as well as oxyacids, nitrogen and oxygen containing heteroatom compounds, according to high resolution mass spectrometry.[17, 67, 68] The OSPW components with variable carbon number or hydrogen deficiency possess variable affinity for sorbent materials as revealed by Mohamed et al. 2015,[17] where activated carbon (AC - 92%) had better removal efficiency than **CH-GL3-C** (53%). Other sorbents reported by Mohamed et al.[17] include biochar samples (BC-1:

24%, BC-2 and BC-3: 15%), goethite: 15%, PANI: 9.5% while cellulose and magnetite showed negligible removal efficacy of NAFCs. A detailed study of cellulose and its cross-linked forms with single component carboxylate anions reveal lower uptake by an order of magnitude (*cf*. Figure 3.7 in chapter 3) and measurably higher uptake for cross-linked chitosan materials (*cf*. Figure 2.7 in chapter 2). This study reveals that chitosan and cellulose biopolymers can be transformed into composite materials with unique adsorption properties, that suggest synergistic effects due to variable textural and surface chemistry properties via self-assembly and cross-linking.

Table 6.5. Sorption isotherm parameters obtained from the Freundlich and Sips models for **CH-GL-C** composite materials with phenolphthalein (pH 10.5) and carboxylate anions (pH 9) at 295 K.

Adsorbates	Parameters	Sorbents		
		CH-GL-C1	**CH-GL-C 2**	**CH-GL-C 3**
Phenolphthalein (phth)	$\mathbf{K_F}$ **(L mmol g^{-1})** $\times 10^{-1}$	1.60 ± 0.40	2.76 ± 0.20	5.03 ± 1.40
	$\mathbf{1/n_F}$	1.25 ± 0.06	1.40 ± 0.01	1.40 ± 0.04
***p*-nitrophenol (PNP)**	$\mathbf{K_F}$ **(L mmol g^{-1})** $\times 10^{-2}$	-	-	8.49 ± 0.40
	$\mathbf{1/n_F}$	-	-	1.92 ± 0.03
***o*-nitrophenyl acetic acid (ONPAA)**	$\mathbf{K_F}$ **(L mmol g^{-1})** $\times 10^{-1}$	-	-	2.28 ± 0.30
	$\mathbf{1/n_F}$	-	-	1.15 ± 0.05
S1	$\mathbf{Q_m}$ **(mg g^{-1})**	-	-	115 ± 15
	$\mathbf{K_S}$ **(L mg^{-1})** $\times 10^{-2}$	-	-	3.96 ± 0.20
	$\mathbf{n_s} \times 10^{-1}$	-	-	5.86 ± 0.30
S2	$\mathbf{Q_m}$ **(mg g^{-1})**	-	-	13.7 ± 0.5
	$\mathbf{K_S}$ **(L mg^{-1})** $\times 10^{-1}$	-	-	4.90 ± 0.35
	$\mathbf{n_s} \times 10^{-1}$	-	-	6.56 ± 0.50
S6	$\mathbf{Q_m}$ **(mg g^{-1})**	-	-	40.5 ± 1.1
	$\mathbf{K_S}$ **(L mg^{-1})** $\times 10^{-2}$	-	-	4.20 ± 1.00
	$\mathbf{n_s}$	-	-	1.03 ± 0.09
OSPW	$\mathbf{Q_m}$ **(mg g^{-1})**	-	-	24.1 ± 0.9
	$\mathbf{K_S}$ **(L mg^{-1})** $\times 10^{-12}$	-	-	0.47 ± 0.04
	$\mathbf{n_s}$	-	-	8.59 ± 0.64

6.4.2.4 Selective Sorption of OSPW NAFCs by CH-GL3-C

The HR ESI-MS speciation profile of OSPW before and after sorption with the **CH-GL3-C** composite material is shown in Figures 6.10a and b. The sorption capacity (Q_m) of **CH-GL-C** materials for OSPW naphthenates was 27.4 ± 1.4 mg/g, in good agreement with results from kinetic and equilibrium studies. The class distribution plots in Figure 6.10a indicate that O_2H species were the most abundant component followed by the O_2S species. A significant reduction in the concentration of these species is noted after sorption by **CH-GL-C** composite materials. Thus, **CH-GL-C** materials possess good affinity for the uptake of these **OSPW** fractions from aqueous solution in agreement with kinetic and equilibrium studies.

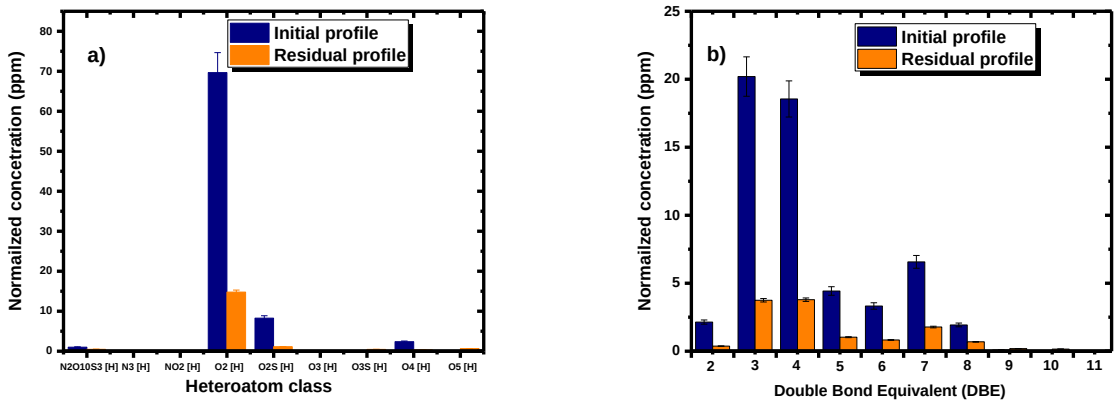

Figure 6.10 a) HR ESI-MS speciation profile of OSPW, b) Double bond equivalents (DBE) distribution of OSPW as a function of normalized concentration for the O_2 species

In Figure 6.10b, the double bond equivalents (DBE) distribution of OSPW is presented as a function of the normalized concentration of O_2 species, where DBE refers to the hydrogen deficiency of the naphthenate systems. DBE relates to the number of rings plus double bonds involving carbon, since each ring or double bond results in a loss of two hydrogen atoms.[69] The results show that the DBE of the naphthenates ranged from 2 to 11. It also reveals congeners that

possess DBE of 3 and 4 as the most abundant fraction within the OSPW mixture. The uptake results show an increased removal efficiency for OSPW with decreasing DBE, in agreement with equilibrium and kinetic studies. The **CH-GL-C** composite materials show uptake selectivity for NAFCs with low DBEs by the greater uptake for **S1** (DBE= 0) relative to **S2** (DBE = 1) and **S6** (DBE = 8).

6.4.3. Kinetic studies

6.4.3.1 Kinetic Uptake Studies of Phenolphthalein

Kinetic uptake profiles of **phth** with the cross-linked materials were obtained using the one-pot method.[49] Figure 6.11 shows the kinetic profile for the composites with **phth** over a 400 min. interval, where the pseudo-second order (PSO) kinetic model (Equation 6.8) provided the best fit results. According to the kinetic parameters, the sorbent materials displayed variable trends in uptake capacity for **phth** that relates to the level of cross-linking, in agreement with the equilibrium uptake results described above. The Q_t values (mmol g^{-1}) for the three sorbent materials increase with an increasing level of cross-linker as follows: **CH-GL1-C** (0.00531 ± 0.0002) < **CH-GL2-C** (0.00771 ± 0.0004) < **CH-GL3-C** (0.0093 ± 0.0007) whereas the PSO rate constant (k_2; g/mmol.min) decreased with greater cross-linker content, as follows: **CH-GL1-C** (1.01 ± 0.11) > **CH-GL2-C** (0.425 ± 0.06) > **CH-GL3-C** (0.198 ± 0.04). These trends are in agreement with the characterization results (FTIR, TGA, CHN, XRD, and ^{13}C NMR) provided and with other reports on the precursor polysaccharides.[3, 70] The foregoing results suggest that the linker and precursor domains may have been the active adsorption sites by increasing Q_t values as the linker content increases that parallel reports from other independent studies.[3, 49] The k_2 values decrease as the cross-linking ratio increases. The trend in kinetic results may relate to an increased

steric hindrance which limit the diffusion of **phth** through the pore network of the sorbent materials.

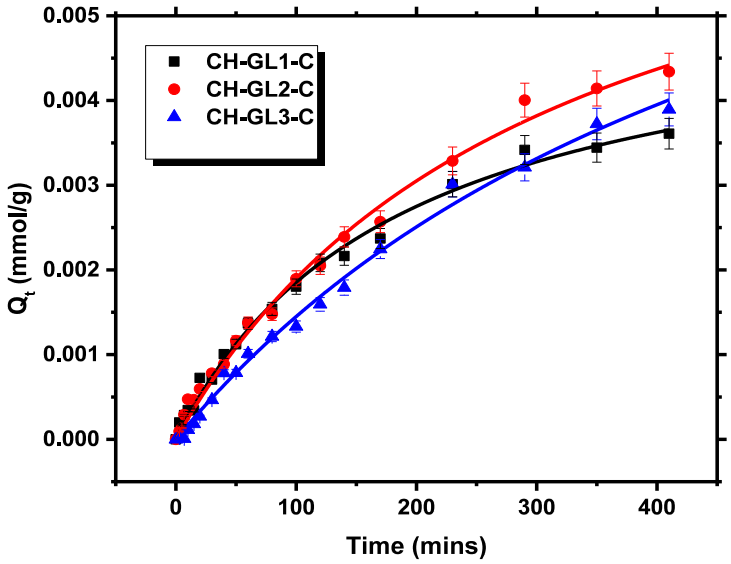

Figure 6.11. Uptake kinetic profile of phth by **CH-GL-C** composite materials at pH 10.5 and 295K, where the fitted lines correspond to the pseudo-second order model.

6.4.3.2 Batch Kinetics Studies of OSPW and S6

The batch kinetic profile of the uptake of **OSPW** and **S6** by **CH-GL3-C** is shown in Figure 6.12. The PFO model describes the adsorption of single sorption sites for the adsorbent and provided the best fit for the experimental data. The difference in the best fit model for the one-pot versus batch systems relates to the different sensitivities of the two systems. The batch system affords a highly dispersed adsorption process; whereas, the one-pot system may be subject to mass transfer effects for the adsorbate molecules to access the sorbent material via the barrier which the sorbent material in enclosed.[44] The Q_t and k_1 values for OSPW was 22.6 ± 0.5 mg/g and 0.378 ± 0.05 s^{-1}, while the values for **S6** were 19.6 ± 0.3 mg/g and 0.407 ± 0.04 s^{-1}. The results reveal the

attainment of equilibrium within the first 10 minutes of the kinetic process with **S6** displaying a greater PFO rate constant. The greater kinetic rate displayed by **S6** is consistent with the greater equilibrium uptake toward **S6**. The kinetic profiles provide support that these cross-linked composite materials are versatile adsorbents for the uptake of OSPW naphthenates from aqueous solution that extend the field of application of chitosan and cellulose biopolymers reported elsewhere.[3,15,71]

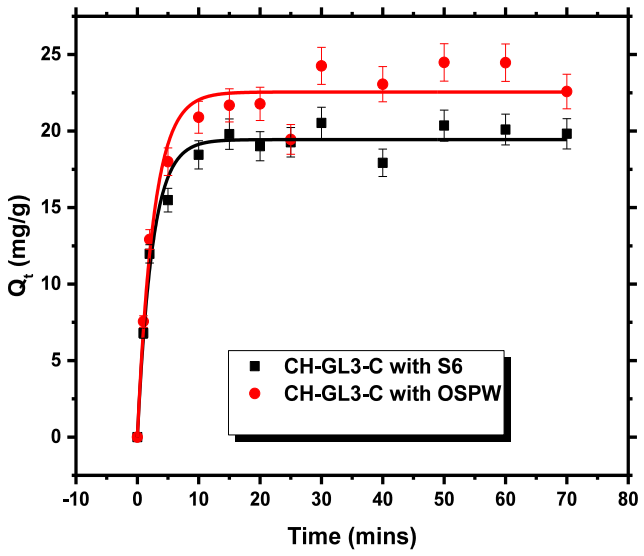

Figure 6.12. Batch kinetic uptake profile of **CH-GL3-C** with **OSPW** (pH 10.5) and **S6** (pH 9) at 295 K, where the best-fit curve corresponds to the pseudo-first order model.

6.5 Conclusions

Chitosan/cellulose glutaraldehyde composite materials were prepared with variable morphology and surface properties due to reinforcement of the interactions between biopolymer components at variable levels of self-assembly and cross-linking. Evidence of cross-linking of the composite materials *via* glutaraldehyde is supported by spectral characterization (FTIR and ^{13}C NMR). The characterization results provide support of imine bond formation (^{13}C resonance at

180 ppm and FTIR signature at ~1550–1680cm^{-1}). PXRD and TGA studies of the composites provide support of cellulose-chitosan interactions as evidenced by increased crystallinity and thermal stability of the non-crosslinked material. The greater pore structure and surface area of the composite materials are supported by variable morphology and surface properties obtained through SEM and nitrogen adsorption studies. The enhanced anion recognition properties of **CH-GL-C** composite materials relative to **CH-GL** polymers reported previously reveal that crosslinked chitosan-cellulose composites display greater sorption affinity toward phenolic dyes, single component naphthenates as well as OSPW naphthenates. This study therefore contributes to a greater understanding of the structure and synergistic adsorption properties of cellulose-chitosan composites. This work will contribute to the utilization of abundant biopolymers and highlight the unique adsorption properties of such ternary composite materials for technological applications such as advanced water treatment, nanomedicine and drug delivery.

6.7 References

1. Frank, R. A.; Kavanagh, R.; Kent Burnison, B.; Arsenault, G.; Headley, J. V.; Peru, K. M.; Van Der Kraak, G.; Solomon, K. R. *Chemosphere* **2008**, 72, 1309-1314.

2. Chastko, P. A. *Developing Alberta's Oil Sands: From Karl Clark to Kyoto*. University of Calgary Press: Calgary, 2004.

3. Mohamed, M. H.; Udoetok, I. A.; Wilson, L. D.; Headley, J. V. *RSC Adv* **2015**, 5, 82065-82077.

4. Romanova, U. G.; Valinasab, M.; Stasiuk, E. N.; Yarranton, H. W. *J Can Petrol Technol* **2006**, 45, 36-45.

5. Leclair, L. A.; Pohler, L.; Wiseman, S. B.; He, Y.; Arens, C. J.; Giesy, J. P.; Scully, S.; Wagner, B. D.; van den Heuvel, M. R.; Hogan, N. S. Water. *Environ Sci Technol* **2015**, 49, 5743-5752.

6. Madill, R. E. A.; Orzechowski, M. T.; Chen, G. S.; Brownlee, B. G.; Bunce, N. J. *Environ Toxicol* **2001**, 16, 197-208.

7. Giesy, J. P.; Anderson, J. C.; Wiseman, S. B. *PNAS* **2010**, 107, 951-952.

8. Alberta Oil Sands: Energy, Industry and the Environment. *Dev Environm Sci* **2012**, 11, 1-496.

9. Leishman, C.; Widdup, E. E.; Quesnel, D. M.; Chua, G.; Gieg, L. M.; Samuel, M. A.; Muench, D. G. *Chemosphere* **2013**, 93, 380-387.

10. Lengger, S. K.; Scarlett, A. G.; West, C. E.; Rowland, S. J. *Rapid Commun Mass Spectrom* **2013**, 27, 2648-2654.

11. Reinardy, H. C.; Scarlett, A. G.; Henry, T. B.; West, C. E.; Hewitt, L. M.; Frank, R. A.; Rowland, S. J. *Environ Sci Technol* **2013**, *47*, 12, 6614-6620.

12. Yue, S.; Ramsay, B. A.; Wang, J.; Ramsay, J. *Sci Total Environ* **2015**, 538, 573-582.

13. Wiseman, S. B.; Anderson, J. C.; Liber, K.; Giesy, J. P. *Aquat Toxicol* **2013**, 142-143, 414-421.

14. He, Y.; Patterson, S.; Wang, N.; Hecker, M.; Martin, J. W.; El-Din, M. G.; Giesy, J. P.; Wiseman, S. B. *Wat. Res.* **2012**, 46, 6359-6368.

15. Udoetok, I. A.; Dimmick, R. M.; Wilson, L. D.; Headley, J. V. *Carbohyd Polym* **2016**, 136, 329-340.

16. Mohamed, M. H.; Wilson, L. D.; Headley, J. V. *J Phys Chem B* **2013**, 117, 3659-3666.

17. Mohamed, M. H.; Wilson, L. D.; Shah, J. R.; Bailey, J.; Peru, K. M.; Headley, J. V. *Chemosphere* **2015**, 136, 252-258.

18. Gamal El-Din, M.; Fu, H.; Wang, N.; Chelme-Ayala, P.; Pérez-Estrada, L.; Drzewicz, P.; Martin, J. W.; Zubot, W.; Smith, D. W. *Sci Total Environ* **2011**, 409, 5119-5125.

19. Azad, F. S.; Abedi, J.; Iranmanesh, S. *J Environ Sci and Heal A* **2013**, 48, 1649-1654.

20. Frank, R. A.; Kavanagh, R.; Burnison, B. K.; Headley, J. V.; Peru, K. M.; Der Kraak, G. V.; Solomon, K. R. *Chemosphere* **2006**, 64, 1346-1352.

21. Hill, A. E.; Malisoff, W. M. *J Am Chem Soc* **1926**, 48, 918-927.

22. Schweigert, N.; Zehnder, A. J. B.; Eggen, R. I. L. *Environ Microbiol* **2001**, 3, 81-91.

23. Chang, Y.; Tai, K.; Huang, F.; Huang, M. *J Endodont* **2000**, 26, 440-443.

24. Wilson, L. D.; Mohamed, M. H.; Guo, R.; Pratt, D. Y.; Hyuck Kwon, J.; Mahmud, S. T. *J Agromedicine* **2010**, 15, 105-116.

25. Dumitriu, S. *Polysaccharides: Structural Diversity and Functional Versatility, Second Edition*. CRC Press: 2004.

26. Duri, S.; Tran, C. D. *Langmuir* **2013**, 29, 5037-5049.

27. Wilson, L. D.; Xue, C. *J Appl Polym Sci* **2013**, 128, 667-675.

28. Wilson, L. D.; Pratt, D. Y.; Kozinski, J. A. *J Colloid Interf Sci* **2013**, 393, 271-277.

29. Poon, L.; Wilson, L. D.; Headley, J. V. *Carbohyd Polym* **2014**, 109, 92-101.

30. Tran, C. D.; Duri, S.; Delneri, A.; Franko, M. *J hazard mater* **2013**, 252-253, 355-366.

31. Leung, H.-W. *Ecotoxicol Environ Saf* **2001**, 49, 26-39.

32. Kuzmina, O.; Heinze, T.; Wawro, D. *ISRN Polym Sci* **2012**, 2012, 1-9.

33. Ostadhossein, F.; Mahmoudi, N.; Morales-Cid, G.; Tamjid, E.; Navas-Martos, F.; Soriano-Cuadrado, B.; Paniza, J.; Simchi, A. *Materials* **2015**, 8, 6401-6418.

34. Lee, K.-Y.; Aitomäki, Y.; Berglund, L. A.; Oksman, K.; Bismarck, A. *Compos Sci and Technol* **2014**, 105, 15-27.

35. Ristić, T.; Mohan, T.; Kargl, R.; Hribernik, S.; Doliška, A.; Stana-Kleinschek, K.; Fras, L. *Cellulose* **2014**, 21, 2315-2325.

36. Liuyun, J.; Yubao, L.; Chengdong, X. *J Mater Sci- Mater M* **2009**, 20, 1645-1652.

37. Azeredo, H. M. C.; Mattoso, L. H. C.; Avena-Bustillos, R. J.; Filho, G. C.; Munford, M. L.; Wood, D.; McHugh, T. H. *J Food Sci* **2010**, 75, N1-N7.

38. Rogovina, S. Z.; Akopova, T. A.; Vikhoreva, G. A.; Gorbacheva, I. N.; Zharov, A. A.; Zelenetskii, A. N. *Vysokomol Soedin* **2000**, 42, 10-15.

39. Vikhoreva, G. A.; Kil'deeva, N. R.; Gorbacheva, I. N.; Shablykova, E. A.; Rogovina, S. Z.; Akopova, T. A. *Fibre Chem* **2000**, 32, 402-406.

40. Wan Ngah, W. S.; Teong, L. C.; Hanafiah, M. A. K. M. *Carbohyd Polym* **2011**, 83, 1446-1456.

41. Wang, Z.; Hu, Q.; Dai, X.; Wu, H.; Wang, Y.; Shen, J. *Polym Composites* **2009**, 30, 1517-1522.

42. Keungputpong, N.; Matchariyakul, N.; Tiptipakorn, S. *Adv Mat Res* **2014**, 989-994, 697-700.

43. Peng, S.; Meng, H.; Ouyang, Y.; Chang, J. *Ind Eng Chem Res* **2014**, 53, 2106-2113.

44. Wu, T.; Du, Y.; Yan, N.; Farnood, R. *J Appl Polym Sci* **2015**, 132, (33), 42375/1-42375/8

45. Wu, T.; Farnood, R. *Cellulose* **2015**, 22, 1955-1961.

46. Allen, T. *Particle Size Measurement: Volume 2: Surface Area and Pore Size Determination*. Springer: London, UK, 1997; p 252.

47. Sing, K. *Colloids Surfaces A* **2001**, 187–188, 3-9.

48. Broekhoff, J. C. P.; De Boer, J. H. *J Catal* **1968**, 10, 153-165.

49. Mohamed, M.; Wilson, L. *Nanomaterials* **2015**, 5, 969-980.

50. Freundlich, H. M. F. Over the adsorption in solution. *J Phy Chem* **1906**, 57A, 385-470.

51. Sips, R. Structure of a catalyst surface. *J Chem Phys* **1948**, 16, 490-495.

52. Kildeeva, N. R.; Perminov, P. A.; Vladimirov, L. V.; Novikov, V. V.; Mikhailov, S. N. *R J Bioorganic Chem* **2009**, 35, 360-369.

53. Chaudhary, J. P.; Vadodariya, N.; Nataraj, S. K.; Meena, R. *ACS Applied Mater Interfaces* **2015**, 7, 24957-24962.

54. Li, B.; Shan, C.-L.; Zhou, Q.; Fang, Y.; Wang, Y.-L.; Xu, F.; Han, L.-R.; Ibrahim, M.; Guo, L.-B.; Xie, G.-L.; Sun, G.-C. *Mar Drugs* **2013**, 11, 1534-1552.

55. Monteiro, O. A. C.; Airoldi, C. *Int J Biol Macromol* **1999**, 26, 119-128.

56. Sing, K. S. W. *Pure Appl Chem* **1985**, 57, (4), 603–619.

57. Karoyo, A. H.; Sidhu, P.; Wilson, L. D.; Hazendonk, P. *J Phys Chem B* **2013**, 117, 8269-8282.

58. Lowell, S.; Shields, J. E.; Thomas, M. A.; Thommes, M. *Characterization of Porous Solids and Powders: Surface Area, Pore Size and Density*. Springer Netherlands: 2012.

59. Dehabadi, L.; Wilson, L. D. *Carbohyd Polym* **2014**, 113, 471-479.

60. Borysiak, S.; Grząbka-Zasadzińska, A. *J Appl Polym Sci* **2016**, 133, 42864.

61. Wang, K.; Yuan, X.; Guo, Z.; Xu, J.; Chen, Y. *Carbohyd Polym* **2014**, 102, 699-707.

62. Migneault, I.; Dartiguenave, C.; Bertrand, M. J.; Waldron, K. C. *Biotechniques* **2004**, 37, 790-6, 798-802.

63. Drugbank drugs page. http://drugbank.ca/drugs (Assessed March 24, 2016).

64. Poon, L.; Younus, S.; Wilson, L. D. *J Colloid Interf Sci* **2014**, 420, 136-144.
65. Mohamed, M. H.; Wilson, L. D.; Headley, J. V.; Peru, K. M. *J Colloid Interf Sci* **2011**, 356, 217-226.

66. Mohamed, M. H.; Wilson, L. D.; Peru, K. M.; Headley, J. V. *J Colloid Interf Sci* **2013**, 395, 104-110.

67. Huang, R.; Sun, N.; Chelme-Ayala, P.; McPhedran, K. N.; Changalov, M.; Gamal El-Din, M. *Chemosphere* **2015**, 127, 291-296.

68. Brown, L. D.; Ulrich, A. C. *Chemosphere* **2015**, 127, 276-290.

69. Marshall, A. G.; Rodgers, R. P. Petroleomics: Chemistry of the underworld. *PNAS* **2008**, 105, 18090-18095.

70. Chiou, M.-S.; Li, H.-Y. *J Hazard Mater* **2002**, 93, 233-248.

71. Kyzas, G. Z.; Bikiaris, D. N. Review. *Mar. Drugs* **2015**, 13, 312-337.

Chapter 7

(Manuscript 6)

Description

This chapter discusses the preparation and adsorption properties of quaternary and ternary composite materials made from chitosan (CH), carboxymethyl cellulose (CC), glutaraldehyde (GL) and iron III species. The composite materials were designed to optimize the sorption properties of the biopolymer composite materials discussed in chapter 6, where charge screening at alkaline pH conditions may have attenuated the sorption properties of the composites.

Authors' contribution

Author's contribution: I and Lee D. Wilson conceived and designed the experiments; I performed all the experiments, analyzed the data and wrote the first draft of the manuscript with extensive editing by Lee D. Wilson, along with securing funding for this project. John V. Headley contributed analysis tools as well as final proofreading of the manuscript.

Relation of Manuscript 6 to Overall Objective of this Project

This project satisfies the third and fourth themes (composite formation between cellulose and chitosan based biopolymers and sorption studies of NAFCs using cellulose and chitosan based biopolymers) of the thesis research.

Graphical Abstract

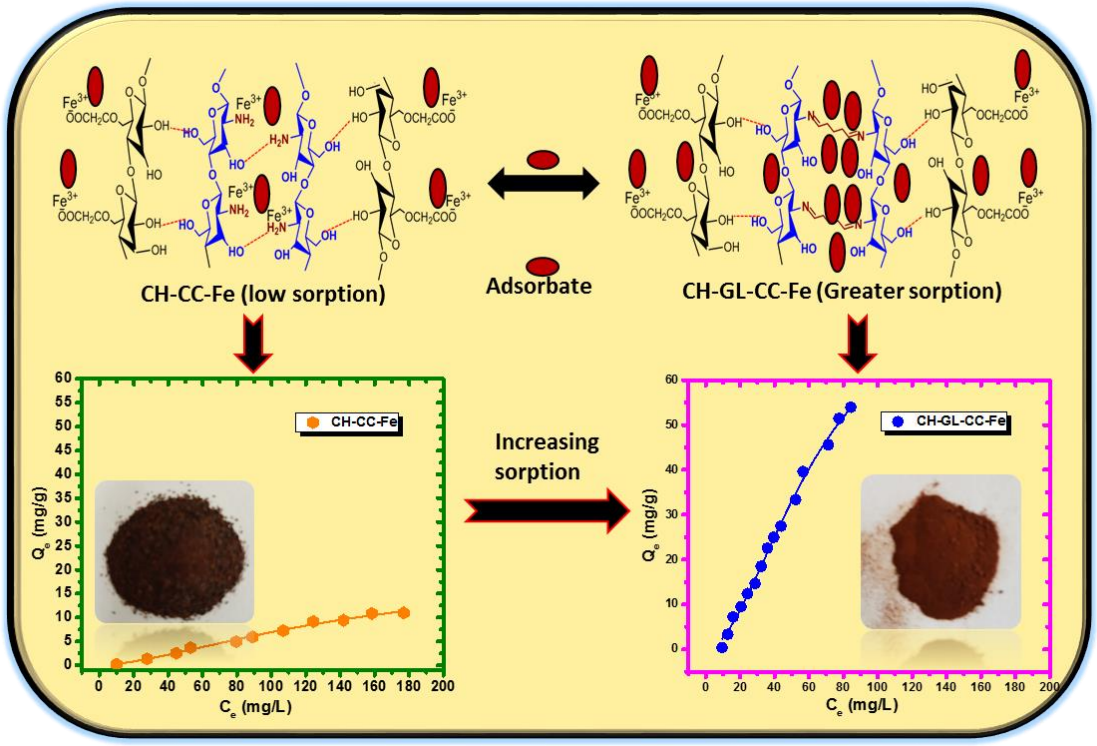

Research Highlights

- Quaternary and ternary composite materials were prepared.
- The composite materials display variable texture and morphology.
- The quaternary composite materials displayed greater sorption capacity relative to the ternary composite.
- Cross-linking with GL increased the sorption capacity of the quaternary composite.
- Doping of iron III species supported the uptake of anions by the composite materials.

7. Amphiphilic Iron Doped Chitosan- Carboxymethyl Cellulose Composites for Anion Uptake.

Inimfon A. Udoetok[1]; Lee D. Wilson[1*] and John V. Headley[2]

[1]Department of Chemistry, University of Saskatchewan, 110 Science Place, Saskatoon, Saskatchewan, S7N 5C9

[2]Water Science and Technology Directorate, Environment Canada, 11 Innovation Boulevard, Saskatoon, Saskatchewan, S7N 3H5

***Corresponding Author**: L. D. Wilson, Tel. +1-306-966-2961, Fax. +1-306-966-4730, Email: lee.wilson@usask.ca

7.1 Abstract

Quaternary (**CH-GL-CC-Fe**) and ternary (**CH-CC-Fe**) composite materials with variable morphology and anion recognition properties were prepared from carboxymethyl cellulose (CC), chitosan, glutaraldehyde as cross-linker while iron (III) (Fe^{3+}) species served as Lewis acid sites. FTIR study supported successful cross-linking between the amine groups of chitosan and glutaraldehyde to yield composite formation between the anionic and cationic polysaccharides. ICP-OES provided evidence of a variable level of iron doping in the materials, while SEM results reveal that composites possess variable morphology. The results of equilibrium uptake studies indicate that **CH-GL-CC-Fe** surpassed the sorption capacity of **CH-CC-Fe**, where a 200 % increase in adsorbate concentration revealed a (204 %) increase in the sorption capacity of **CH-GL-CC-Fe**. An increase in temperature of 283 – 303 K adversely affected the sorption process. The Sips and Langmuir isotherm models provided the best-fit for the sorption profile of 2-naphthoxy acetic acid (**S6**) at alkaline and acidic pH conditions respectively. The monolayer

sorption capacity (Q_m; mg g^{-1}) of **CH-GL-CC-Fe** for **S6** was 263 ± 85 mg/g and 484 ± 76 mg/g at alkaline and acidic pH conditions, respectively. The composite materials show limited or no discrimination of the various naphthenate congeners in OSPW, according to the DBE or molecular weight. This study advances the design of polysaccharide composite sorbents and an understanding of the role of Fe III species and cross-linking on the anion recognition properties in aqueous solution.

Keywords: Carboxymethyl cellulose; Chitosan; Iron (III); Cross-linking; Anion; Composites

7.2 Introduction

Tailings ponds are temporary storage facilities for the accumulation of oil sands process affected water (OSPW) with the aim of recovering water for reuse. The components of tailings include water, sand, fine silts, clay, residual bitumen and lighter hydrocarbons, inorganic salts and water-soluble organic compounds[1]. The fine silts in the tailing ponds tend to entrap large volumes of water, thus making pond reclamation very challenging. As well, the water-soluble organic fraction of OSPW contains naphthenic acid fraction components (NAFCs) [2-5] which pose a concern to ecosystem health.

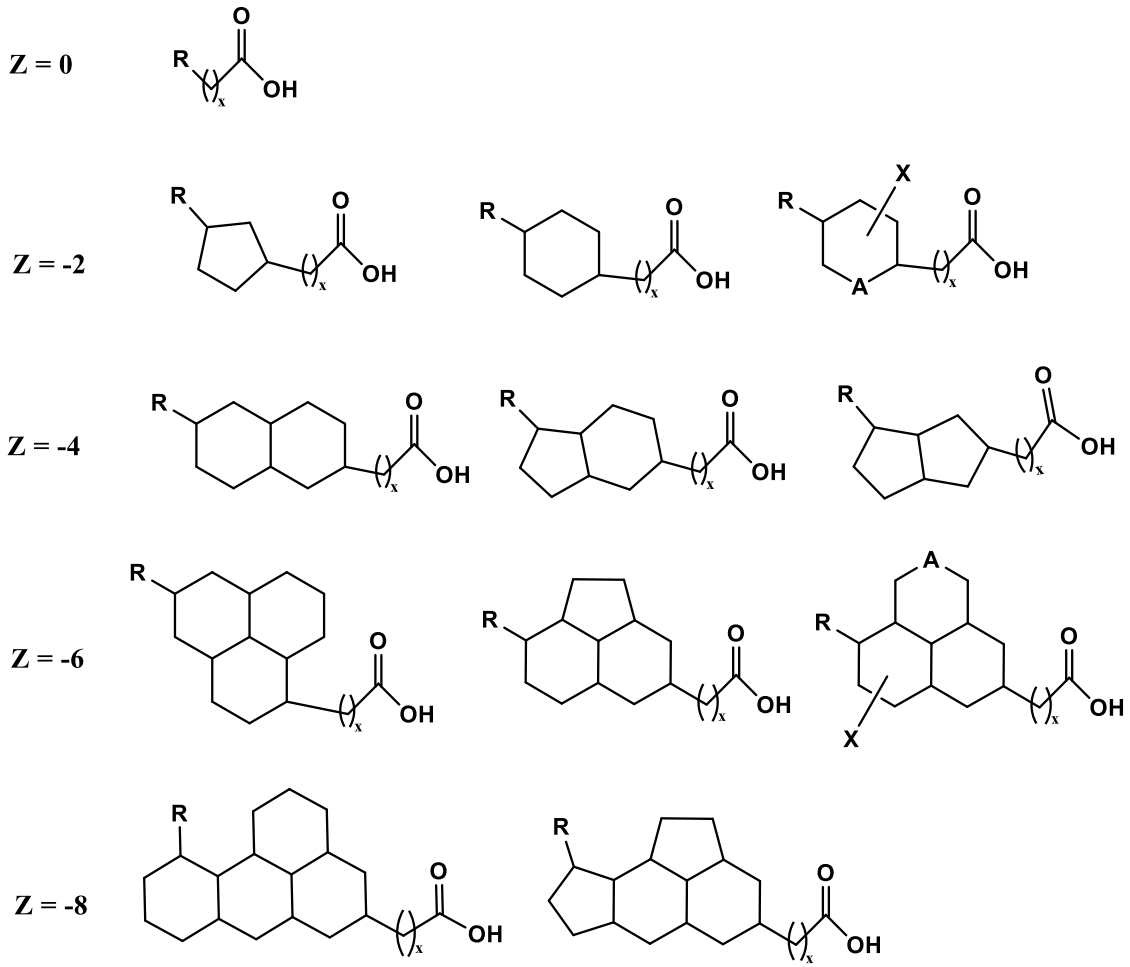

Scheme 7.1: Example structure of NAFCs in OSPW showing Z values (0, -2, -4, -6 and -8) and heteroatoms. *R* = alkyl group, *X* = COOH, R, OH, SO_x, NO_x, SH and *A* = C, S, N(where x is a variable integer value) .

NAFCs are a broad range of polar organic compounds defined by the conventional formula, $C_nH_{2n+z}O_2$, where "z" represents the "hydrogen deficiency" and is a negative even integer [6-10] (*cf.* scheme 7.1). The term double bond equivalents (DBE) is also used to represent *z*, where DBE refers to the hydrogen deficiency of the NAFCs. DBE relates to the number of rings plus double bonds involving carbon, since each ring or double bond results in a loss of two hydrogen atoms.[11] The toxicity of NAFCs relate to their chemical stability, persistence in the environment, low volatility, high viscosity, and surfactant-like properties, especially at pH conditions above their

pK_a. To address aspects of toxicity, government regulations stipulate the reduction of the tailings volume in the ponds as well as reclamation not later than five years after ponds are no longer in use.[2, 12]

Challenges related to tailing pond reclamation reveals an urgent need for the development of treatment options for timely and effective removal of NAFCs in OSPW as part of reclamation strategies. Thus, the development of low-cost, sustainable, and efficient sorbent materials for controlled removal of the toxic water-soluble organic components in OSPW is a potential strategy. The merits of sorption-based technologies using modified biopolymers for the removal of NAFCs is supported by the research activity of various international research groups.[13-21] The modification of biopolymers to enhance the removal of NAFCs is an area of continued research, where methods such as cross-linking and grafting have led to improved sorbents with greater surface area and surface modification of the biopolymers.[14-16] Composite formation between two or more biopolymers is another approach that affords materials with variable surface area and surface functionalization.[22]

Cellulose and chitosan are among the two most abundant biopolymers[23] that have attracted much attention due to their low toxicity, low cost, high availability, biodegradability, and synthetic versatility. These biopolymers differ due to their chemical functionalization at the C-2 of their respective pyranosyl units, where chitosan is a cationic biopolymer that is soluble in acidic media. By contrast, cellulose requires harsh solvents like ionic liquids or NaOH/urea systems at low temperature for dissolution. Previous studies on the use of cross-linked cellulose,[16] chitosan[14] and cross-linked chitosan-cellulose composites[22] for the removal of NAFCs from aqueous solution have been reported in the literature. The authors revealed that composite materials have greater uptake capacity for the naphthenates relative to the single component biopolymers. In some cases,

reduced sorption affinity may occur due to charge repulsion between the carboxylate anions and the negatively charged polymer surface, especially at alkaline pH conditions. Chitosan and cellulose-based composite materials adopt positive or negative charge that relates to their chemical functionalization.[24] Charge repulsion in composite materials at alkaline pH values can be controlled by replacing cellulose with carboxymethyl cellulose (CC). As well, the introduction of Lewis acid sites on the composites via introduction of iron III species may attenuate the charge repulsion. Chitosan and CC possess opposite electrostatic charge, where complex formation results in greater biocompatibility.[25-28] Ahmed and Ramadan[29] reported on the complexation of metal ions with vitamin B9 and glycine that revealed Fe^{3+} had stronger binding affinity with carboxylate and amine groups versus divalent iron (Fe^{2+}), zinc (Zn^{2+}) and calcium (Ca^{2+}) species. Therefore, a composite material derived from CC/chitosan/Fe III species may possess better anion recognition properties relative to a recently developed series of **CH-GL-C** composites.[22] Polysaccharide composites may be sustainable and low-cost sorbent materials for the removal of anionic and cationic pollutants from water due to their enhanced porosity, surface area and amphoteric nature.[22] For example, previous studies on similar CC-chitosan composite materials reveal that they are efficient polyelectrolyte membranes, [25, 26] exhibit efficient cation recognition,[30, 31] and are useful in biomedical applications.[26, 27, 32] The present study relates to the preparation of Fe III species doped CC/chitosan composites, and the elucidation of their anion recognition properties as well as an assessment of the effects of cross-linking with glutaraldehyde on the sorption properties of the composite materials.

To the best of our knowledge, the introduction of Lewis acid sites in conjunction with cross-linking to prepare CC/chitosan composites with unique anion recognition properties has not yet been reported in the literature. Herein, we present a study on the design of composite materials

targeted at addressing the aforementioned knowledge gaps on cellulose/chitosan composite materials. This study will further contribute to the development of low-cost sorbent materials that combines self-assembly with chemical modification for advanced water treatment technology relevant to OSPW remediation.

7.3 Experimental

7.3.1 Materials

Low molecular weight chitosan (~75%-85% deacetylation), sodium carboxymethyl cellulose (Mw: 250,000), glutaraldehyde, sodium hydroxide, aqueous ammonia, six model naphthenic acid compounds [2-hexyldecanoic acid (**S1**), *trans*-4-pentylcyclohexylcarboxylic acid (**S2**), 2, 2-dicyclohexylacetic acid (**S3**), adamantane carboxylic acid (**S4**), cyclohexane carboxylic acid (**S5**), and 2-naphthoxy acetic acid (**S6**)], HPLC grade acetone and iron (III) sulfate hydrate were purchased from Sigma-Aldrich Canada Ltd. (Oakville, ON). Glacial acetic acid (ACS grade) was obtained from EMD Chemicals, NJ, USA while methanol (HPLC grade) was acquired from Fisher Scientific, NJ, USA. All materials were used as received without further purification unless specified otherwise.

7.3.2 Synthesis of Iron Doped Chitosan-CC Composite Materials

The quaternary composite material (**CH-GL-CC-Fe**) was synthesized as follows: ~2 g of low molecular weight chitosan was dissolved in 200 mL 5% v/v glacial acetic acid with stirring. ~1.62 g of sodium carboxymethyl cellulose (CC) was dissolved in 160 mL of Millipore water with the aid of sonication. The light-yellow chitosan solution was titrated drop-wise into the CC solution with stirring over a 5-minute period. The mixture was allowed to stir for 3 h and the pH was raised

to pH 5.60 using 6 M NaOH, followed by addition of 6.52 mL of glutaraldehyde drop-wise over a 1-minute time (*cf.* Table 7.1), followed by continuous stirring for ~12 h.

Table 7.1: Amount of components for the preparation of composite materials

Reaction Conditions	CH-CCFe	CH-GL-CC-Fe
Glutaraldehyde content (mL)	0	6.52
Mass of chitosan (g)	2.00	2.00
Mass of CC (g)	1.62	1.62
Mass of $Fe_2(SO_4)_3$ (g)	2.50	2.50

The reaction mixture was neutralized using 6 M NaOH solution and HPLC acetone was added, followed by isolation of the product by vacuum filtration. The product was further heated in 50 mL of 5% $Fe_2(SO_4)_3$ solution at 80 ºC for 3 h. The resulting reaction mixture was filtered and the products were extensively washed using Millipore water and methanol. Residual reactants were removed via Soxhlet extraction with methanol over a 24 h period. The final composite material was dried in a vacuum oven at 60 ºC, ground in a mortar and pestle and sieved through a 40-mesh sieve. A ternary composite material (**CH-CC-Fe**) was also prepared via the same method with minor changes as follows: 50 mL of 5% $Fe_2(SO_4)_3$ added directly to the CC-chitosan system without the cross-linking and heating step. (*cf.* Scheme 7.2). Each material was synthesized at least 3 times during the research project and characterization results affirmed the repeatability of the synthetic procedure.

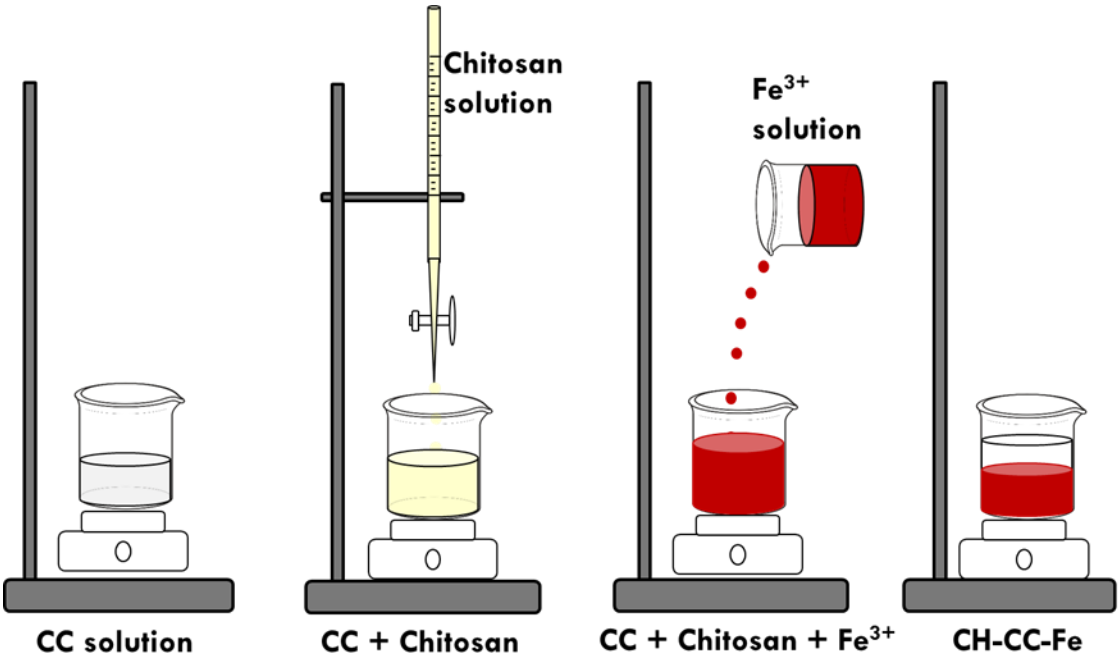

Scheme 7.2: Step-wise procedure (left to right) for the design of a ternary composite material (**CH-CC-Fe**)

7.3.3 Characterization

7.3.3.1 Thermal Gravimetric Analysis (TGA)

A TA Instruments Q50 TGA was used to determine the thermal stability profile of the composite materials. The analysis was done under the following instrumental conditions: heating rate of 5°C min^{-1} to a maximum temperature of 500°C using nitrogen as the carrier gas. A DTG plot of weight with temperature (%/°C) against temperature (°C) was used to illustrate the results.

7.3.3.2 Fourier Transform Infrared (FTIR) Spectroscopy

The FTIR spectra of the composite materials were obtained using a Bio-RAD FTS-40 IR spectrophotometer. A mixture of the composites and pure spectroscopic grade KBr in a weight ratio of 1:10 were co-ground in a small mortar and pestle prior to FTIR analyses. The DRIFT (Diffuse Reflectance Infrared Fourier Transform) spectra were obtained over the 400–4000 cm^{-1}

spectral range in reflectance mode at 295 K with a resolution of 4 cm^{-1}.16 scans were recorded and corrected relative to a background of pure KBr.

7.3.3.3 SEM

The surface morphology of the composite materials was studied using scanning electron microscopy (SEM; Model SU8000, HI-0867-0003). Images from 2nm chromium coated samples were collected under the following instrument conditions; accelerating voltage (2 kV), working distance (4.9 – 5.0 mm), and fixed magnification (50,000×).

7.3.3.4 Inductively Coupled Plasma-Optical Emission Spectrometry (ICP-OES)

ICP-OES was used to estimate the iron content in the composites. The composites were digested in aqua regia (1:3 HNO_3/HCl) and the undissolved particles removed via filtration. A 1000 ppm Fe cocktail standard was prepared. The instrument was calibrated using variable concentrations prepared from the standard mixture. The following instrument conditions were applied: The flush pump rate (100 L/min), analysis pump rate (40 L/min with a 5 s stabilization time), RF power (1150 W), auxiliary gas flow rate (0.5 L/min) and nebulizer gas flow (0.50 L/min).

7.3.4 Sorption studies

7.3.4.1. Sorption of OSPW Naphthenates and S6.

150 ppm, 200 ppm and 350 ppm stock solutions of **S6** (pH 9), 350 ppm at pH 3 and 100 ppm of **OSPW** extract were prepared, respectively. **S6** was prepared by dissolution of an appropriate mass in water with stirring, while 2800 ppm **OSPW** was diluted to 100 ppm using Millipore water. The pH of the resulting **S6** solution was 3 and an aqueous NH_3 solution was used to adjust to pH 9. The resulting solutions were stirred overnight to ensure complete dissolution

followed by a serial dilution over the range of 10 – 350 ppm for **S6**. Fixed dosages (5 and 10 mg) of the composite materials were mixed with 5 mL of **S6** in 2-dram vials according to variable concentrations by serial dilution. 10 mg of the materials were added to 5 mL of 100 ppm OSPW extract where equilibration of the samples was done at 295 K for 24 h using a horizontal shaker with a mixing rate of ~180 rpm. Molar concentration of **S6** before (C_o) and after sorption (C_e) was determined using a double beam UV-vis spectrophotometer (Varian CARY 100). High resolution electrospray ionization high-resolution mass spectrometer (HR ESI-MS) was used for determination of **OSPW** naphthenate concentration at 295 ± 0.5 K. The samples were centrifuged prior to UV and ESI-HRMS analyses. Uptake of **S6** and OSPW naphthenates were determined using equation 7.1.

$$Q_e = \frac{(C_o - C_e) \times V}{m} \qquad \text{Equation 7.1}$$

Q_e is the uptake quantity (mg g^{-1}) of **S6** and **OSPW** naphthenates removed from the solution at equilibrium, C_o is the concentration of adsorbate (mg L^{-1}) in solution before adsorption, C_e is concentration of adsorbate in solution at equilibrium (mg L^{-1}) after adsorption, V is volume of adsorbate solution, and m is mass (g) of composite material.

7.3.4.2 Equilibrium Sorption Studies at Variable Temperatures

A one pot system was used to carry out equilibrium sorption studies at variable temperature, where ca. 30 mg of the **CH-GL-CC-Fe** was added to 100 mL of 30 ppm **S6** at pH 3 in a vessel connected to a heating/cooling bath. The composite/**S6** mixture was allowed to stir continuously for 24 h prior to sampling 10 mL of the mixture, followed by centrifuging where the initial concentration (C_o) and concentration after sorption (C_e) was determined via UV spectral

analyses. The quantity of **S6** removed from the solution by **CH-GL-CC-Fe** was calculated according to equation 7.1.

7.3.4.3 Sorption of Equimolar Concentration of Mixed Surrogates

An equimolar mixture containing the surrogates (**S1** to **S6**) was prepared by dissolving appropriate amounts of the surrogates in aqueous NH_3 solution with sonication for ~5 mins and stirring overnight. Fixed dosages (~20 mg) of the composites were added to 6-dram vials and 20 mL of the equimolar surrogate solution. The sorbent/adsorbate mixture was equilibrated at 295 K on a horizontal shaker table (180 rpm) for 24 h. HR ESI-MS was used for the quantification of the surrogate concentration before (C_o) and after sorption (C_e).

7.3.4.4. Electrospray Ionization Mass Spectrometric Analysis

The concentration of surrogates and OSPW naphthenates was estimated using a ThermoScientific LTQ Orbitrap high resolution elite mass spectrometer. A full-scan mass spectrum was collected between *m/z* 100 and 600 with a resolution of 30,000. Quantification of the samples was done by extracting the mass of the analyte of interest and the external standard method with the ESI interface set to negative ionization mode. The mass spectrometer conditions were optimized by the transmission of *m/z* 112.98563 fragment ion. The heated ESI interface (HESI) parameters were as follows: source heater temperature (53 °C); spray voltage (2.86 kV); capillary temperature (275 °C); sheath gas flow rate (25 L h^{-1}); auxiliary gas flow rate (5 L h^{-1}); and spray current (5.25 μA).

7.3.4.5. Sorption Isotherms and Modeling

Sorption isotherms were obtained by plotting Q_e *vs* C_e (*cf.* Equation 7.1). The Sips[33] and Langmuir[34] isotherm models account for heterogeneous and homogeneous surface sites, by equations 7.2 – 7.3.

$$Q_e = \frac{Q_m (K_S C_e)^{n_s}}{1 + (K_S C_e)^{n_s}} \qquad \text{Equation 7.2}$$

$$Q_e = \frac{K_L Q_m C_e}{1 + K_L C_e} \qquad \text{Equation 7.3}$$

7.4 Results and Discussion

7.4.1 Characterization of Composite Materials

7.4.1.1 *FTIR Spectroscopy*

The FTIR spectra of the quaternary (**CH-GL-CC-Fe**) and ternary (**CH-CC-Fe**) composite materials including that of chitosan and CC are presented in Figure 7.1. The spectra display broad bands at ~3000–3700 cm^{-1} which relate to the stretching of hydrogen bonded O–H and N–H groups, ~2800–3000 cm^{-1} attributed to C–H stretching. Others are bands at ~1550–1710 cm^{-1} due to N–H bending, imine, carbonyl groups, and ~1000–1200 cm^{-1} ascribed to C–O–H, C–O–C and C–N–H asymmetric stretching, respectively.[35] An interesting feature of the composite materials is the merging and broadening of the bands related to the COO^- and NH_3^+ groups respectively, in agreement with electrostatic interactions between these groups and other reports.[36-38] Also the attenuation of the bands related to C=O, C–O–C and C–N–H asymmetric stretching support the trend that increasing steric hindrance occurs in the composites, along with interaction with Fe III

species and cross-linking between the amine groups of chitosan and glutaraldehyde. Further IR evidence of the formation of the quaternary composite material (**CH-GL-CC-Fe**) relates to the appearance of a new vibrational band at ~1717 cm^{-1} for the carbonyl group of glutaraldehyde, along with increased intensity/broadening of the C-H stretching band at ~2800–3000 cm^{-1}. In the case of the ternary composite, a broad shoulder at ~1749 cm^{-1} also supports that interactions occur between the COO^- and NH_3^+ groups. The enhanced intensity/broadening for the C=O and the C-H stretching band at ~2800–3000 only appear in the spectra of **CH-GL-CC-Fe**, while the broad shoulder at ~1749 cm^{-1} appears only in the spectra of **CH-CC-Fe**, in agreement with other reports.[35-38] The relative similarity of the spectra supports the preservation of the basic structure of chitosan and CC in the composites, in agreement with related studies on modified polysaccharide materials.[14, 16]

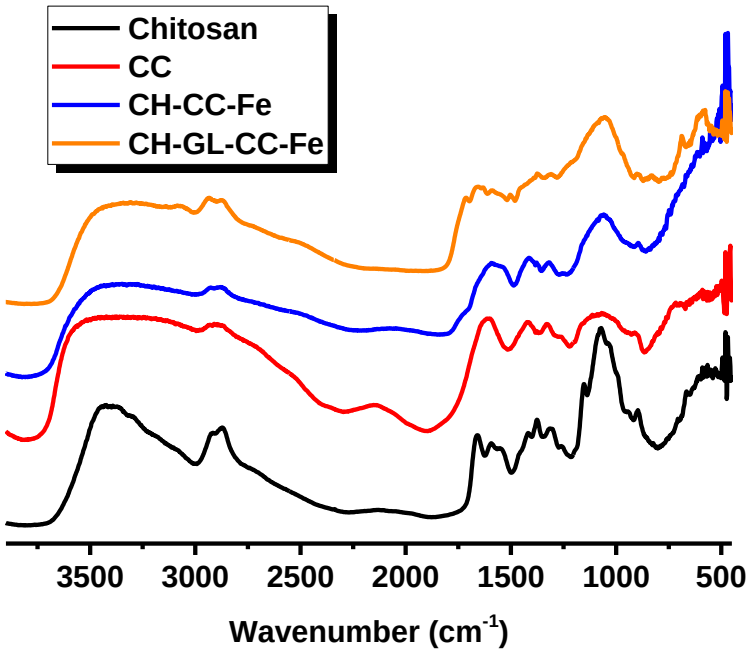

Figure 7.1. FTIR spectra of the precursors and the composite materials.

7.4.1.2 Thermogravimetric Analysis (TGA)

The thermal stability of the composite materials and their precursors were studied using thermogravimetry and the results are shown in Figure 7.2. Two thermal events occur for the precursors (chitosan: ~ 60, 295 ºC and CC: ~ 60, 288ºC), in agreement with other related systems.[22, 39] These two thermal events relate to the loss of bound water and the decomposition of the biopolymer. On the contrary, **CH-CC-Fe** reveals three thermal events at ~60 ºC, ~278 ºC and ~340 ºC, while **CH-GL-CC-Fe** shows four thermal events at ~60 ºC, ~237 ºC, ~308 ºC and ~471 ºC that concur with other related systems.[22] The thermal events relate to the evaporation of bound water, decomposition of chitosan, CC and cross-linker domains of the composites. A salient feature of the thermal profile of the composites relate to a wider temperature decomposition range versus the biopolymer precursors. A noteworthy observation is the lower decomposition temperature of the quaternary composite relative to the ternary system. These effects may be related to the variable heat capacity of the composites due to cross-linking effects.[14, 40]

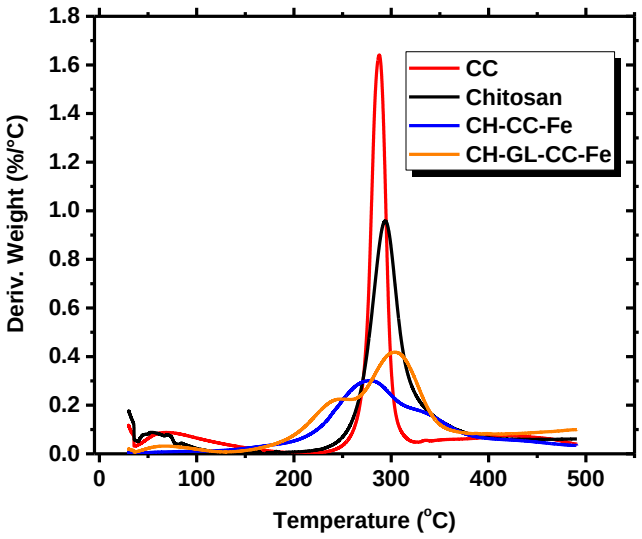

Figure 7.2. DTG curves of chitosan, carboxymethyl cellulose, and the composite materials.

7.4.1.3 Iron Content of Composites

The iron content of the composites was determined using ICP-OES studies and the results are listed in Table 7.2, where **CH-CC-Fe** has greater iron content relative to **CH-GL-CC-Fe**. This greater level for **CH-CC-Fe** is in agreement with greater attenuation of the COO^- and C–N–H asymmetric stretching bands for the FTIR results and higher degradation temperature from the TGA profiles. Greater binding of Fe (III) species to **CH-CC-Fe** results in greater steric hindrance and stronger electrostatic interactions with the binding sites of the composite. This results in the attenuation of the stretching vibrations of such functional groups as well as greater thermal energy required for the cleavage of such bonds. The lower iron content of **CH-GL-CC-Fe** relates to competition for binding sites between the glutaraldehyde linker and Fe (III) species in agreement with the role of the amine sites of chitosan in metal-ion chelation.[41-43]

Table 7.2: Iron content of the composite materials

Composite materials	CH-GL-CC-Fe	CH-CC-Fe
Iron Content (mg/g)	1.07 ± 0.05	185 ± 9

7.4.1.4 SEM

The SEM micrographs of the non-cross-linked (ternary) and cross-linked (quaternary) composites, along with the precursors are presented in Figure 7.3. The micrographs reveal that the precursors are comprised of large and dense fibre bundles, multiple layers and smooth surfaces relative to the composite materials. On the contrary, the SEM micrograph of **CH-CC-Fe** show a more roughened surface, a complete collapse of the fibril structure inherent in the precursors, greater porosity and no evidence of aggregation of Fe (III) species. This may be due to composite formation and greater binding of Fe (III) species, as inferred from the FTIR and iron content results.[26, 32] Equally, the SEM image of **CH-GL-CC-Fe** display smaller and smooth fibre structure

which form an interwoven network. Similar to **CH-CC-Fe**, the micrograph of **CH-GL-CC-Fe** shows greater porosity and a homogenous texture with no evidence of aggregation of Fe (III) species and provides further support of composite formation. The formation of an interwoven network of the fibers is consistent with greater cross-linking, in agreement with cross-linked cellulose.[16]

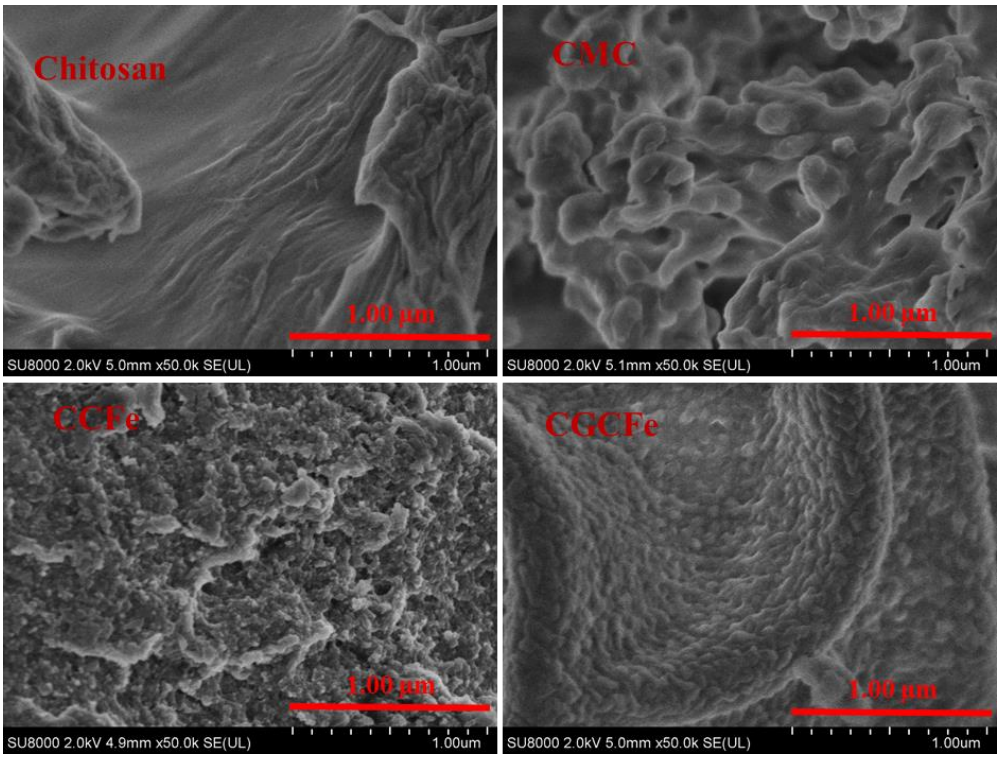

Figure 7.3. SEM micrographs of chitosan, CC, **CHCC-Fe** and **CH-GL-CC-Fe**

7.4.2 Sorption Studies

7.4.2.1. Sorption of Single Component Carboxylate Ion (S6)

The results for the uptake of **S6** at pH 9 by the composite materials are shown in Figure 7.4. The sorption isotherms were plotted as Q_e vs C_e and shows a monotonic increase in sorption as C_e for **S6** increases, where **CH-GL-CC-Fe** displayed the greater monolayer sorption capacity (Q_m; 263 ± 85 mg/g) versus **CH-CC-Fe** (Q_m; 21.1 ± 2.7 mg/g). The greater Q_m for **CH-GL-CC-**

Fe relative to **CH-CC-Fe** may be due to cross-linking effects, in agreement with previous studies.[14, 16, 22] These reports indicate that cross-linking enhances *pillaring* of the fibril structure of biopolymers which results in greater surface area. The Sips isotherm model provided the best fit parameters, where this model accounts for surface heterogeneity and the presence of multi-sorption sites for such materials. The presence of Fe (III) sites in the composites suggest that at alkaline pH values, sorption of anions may take place at both the doped Fe (III) sites via electrostatic interactions as well as biopolymer sites via hydrophobic interaction. Based on the greater uptake properties of **CH-GL-CC-Fe**, further studies were only carried out on this composite material.

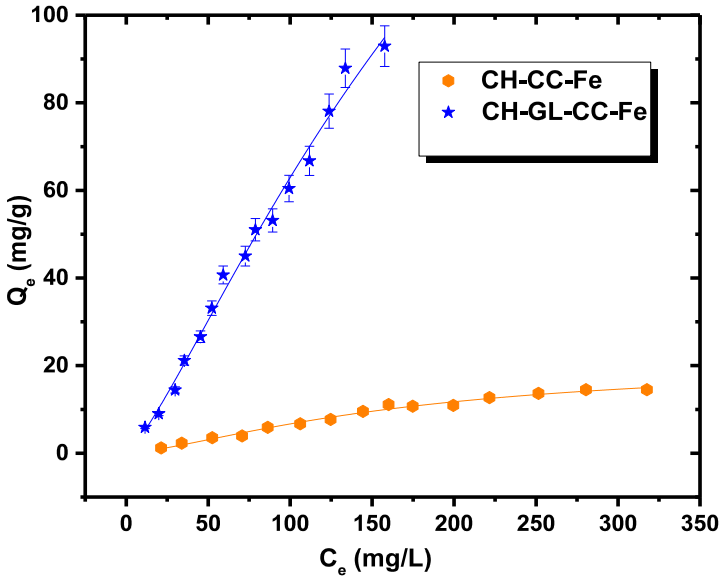

Figure 7.4. Sorption isotherms of **CH-CC-Fe** and **CH-GL-CC-Fe** composite material with **S6** at pH 9 and 295K**.**

7.4.2.2. Effects of pH on the Sorption of S6

The effect of pH on the sorption of **S6** by **CH-GL-CC-Fe** is shown in Figure 7.5, as illustrated by isotherms at pHs 3 and 9. These pH values were selected to ensure the protonation/deprotonation of the -COOH groups of CC and the -NRH groups (R = H or acetyl) of

chitosan. The Sips isotherm model provided the best fit for the isotherm results at alkaline pH, while the Langmuir model provided the best fit at pH 3. The results reveal that **CH-GL-CC-Fe** had greater sorption capacity at pH 3 (Q_m = 484 ± 76 mg/g) versus pH 9 (Q_m = 263 ± 85 mg/g). The foregoing provide further support for hydrophobic association of **S6** with the biopolymer sites at pH 9, while electrostatic interactions are secondary in nature. This occurrence of hydrophobic and electrostatic interactions between **S6** and **CH-GL-CC-Fe** is further affirmed by the greater uptake of **S6** by **CH-GL-CC-Fe** at pH 9 relative to **CH-GL3-C** composite.[22] At pH 3, electrostatic interactions/ hydrogen bonding between NRH_2^+/ Fe (III) species and the -COOH group of **S6** may have been the main driving force for the sorption process as inferred from the Langmuir best fit parameter. Uptake of **S6** by the **CH-GL-CC-Fe** composite and other sorbent materials reveal its superior uptake (484 ± 76 mg/g), as compared with quaternized chitosan beads (315 mg/g).[44]

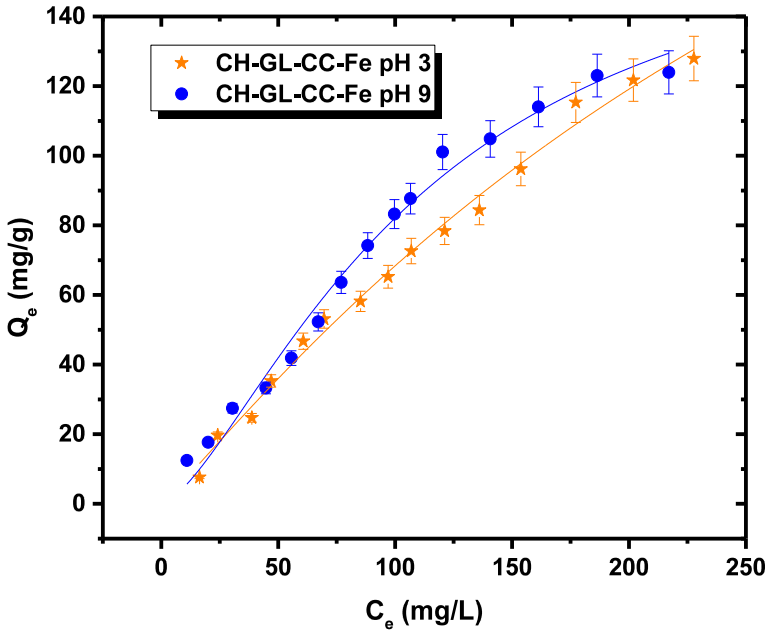

Figure 7.5. Sorption isotherms showing the effect of pH on the uptake of **S6** by **CH-GL-CC-Fe** at 295 K**.**

7.4.2.3. Effects of Adsorbent Dosage on the Sorption of S6

The effect of variable sorbent dosage for **CH-GL-CC-Fe** on the equilibrium uptake of **S6** is presented in Figure 7.6. The results show that the sorption capacity of the composite for **S6** was 263 ± 85 mg/g for a 5 mg dosage of **CH-GL-CC-Fe**. Lower uptake (177 ± 20 mg/g) was observed when a 10 mg dosage of the composite material was used. At lower adsorbent dosage, the number of sorption sites is lower, resulting in a greater saturation of the adsorbent surface, as shown by greater sorption capacity and isotherm saturation (*cf.* Figure 7.6).[15] The use of a 10 mg dosage of **CH-GL-CC-Fe** led to a greater reduction in the level of **S6** from 350 ppm to ~ 160 ppm. The lower sorption capacity is in consonant with incomplete isotherm saturation at the surface of the composite materials, as observed in Figure 7.6. These results are in agreement with a similar study where adsorbate removal efficiency increased from 71.5 % to 85.5 % at higher adsorbent dosages.[44]

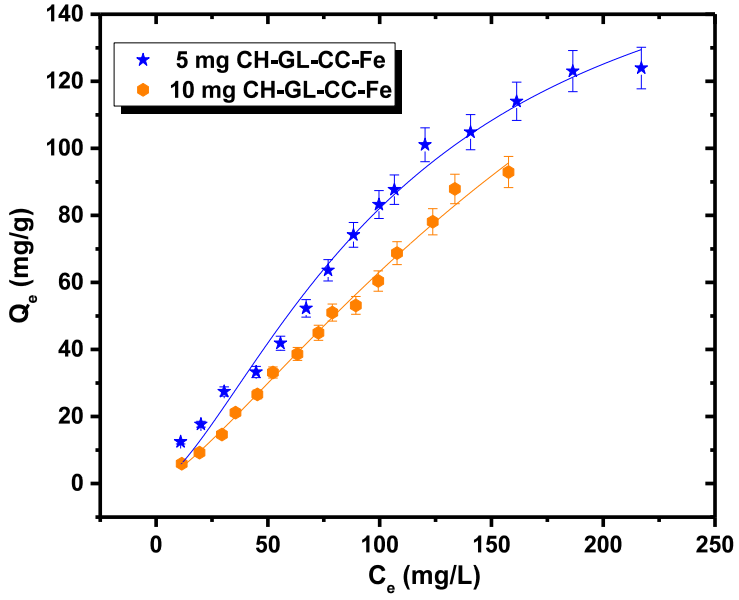

Figure 7.6. Sorption isotherms showing effect of sorbent dosage on the uptake of **S6** by **CH-GL-CC-Fe** at 295 K**.**

7.4.2.4. Effects of Adsorbate Concentration on the Sorption of S6

Variable concentrations (150 ppm, 200 ppm and 350 ppm) of **S6** was used to assess the role of adsorbate concentration on the uptake capacity of **CH-GL-CC-Fe.** Figure 7.7 reveals that the uptake capacity of the composite material increased as C_o for **S6** increased. The sorption capacity (Q_m; mg/g) are given in parentheses: 150 ppm (86.4 ± 20.4), 200 ppm (87.2 ± 9.5) and 350 ppm (263 ± 85). The results show a slight increase in Q_m values as the adsorbate level varied from 150 ppm to 200 ppm, where a 204 % increase was accomplished at 350 ppm. The trend observed for the isotherms in Figure 7.7 correspond to the filling of one or more types of vacant adsorption sites with increasing adsorbate concentration. This isotherm results for the **CH-GL-CC-Fe/ S6** system indicates that this composite may be suitable for the general removal of naphthenic acids judging by its favorable sorption capacity (484 ± 76 mg/g), as reported in section 7.4.2.2.

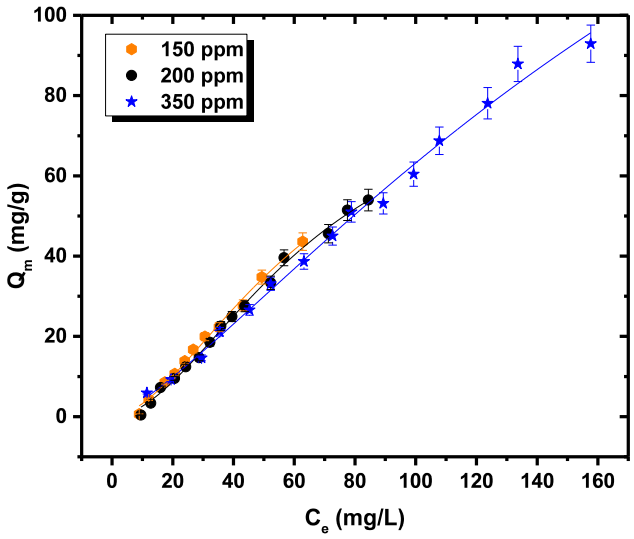

Figure 7.7. Sorption isotherms of the uptake of **S6** by **CH-GL-CC-Fe** at variable initial stock concentrations and 295 K.

7.4.2.5. Effects of Temperature

Adsorption studies were performed at 283 K, 293 K, and 303 K to evaluate temperature effects on the uptake of **S6** by **CH-GL-CC-Fe.** In Figure 7.8, a slight attenuation in the uptake of **S6** by **CH-GL-CC-Fe** is observed (30.9 ± 1.5 mg/g to 26.4 ± 1.3 mg/g) with an increase in temperature (283 K to 303 K), in agreement with a related study.[44] This slight decrease in uptake observed may relate to more favourable solvation at higher temperatures due to destabilization of the bound state for the **CH-GL-CC-Fe** /**S6** system,[45-47] and possible kinetic effects as reported elsewhere.[47, 48]

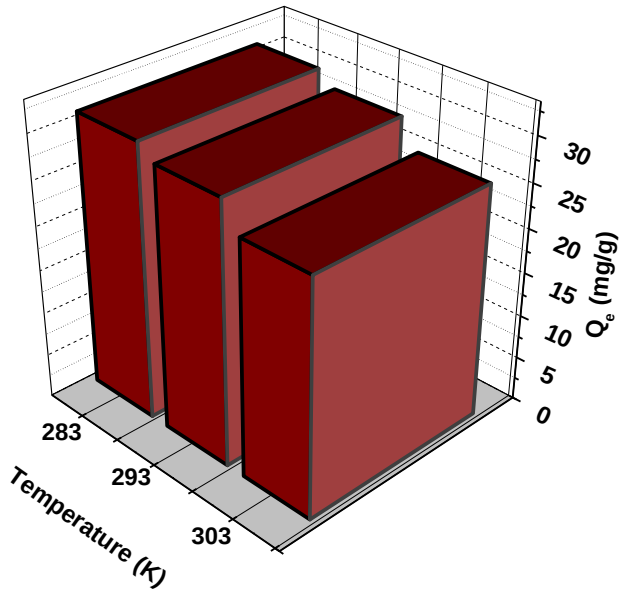

Figure 7.8. Sorptive uptake of **S6** by **CH-GL-CC-Fe** at variable temperature

7.4.2.6 Equilibrium Uptake of Equimolar Mixtures of Surrogates

The relative affinity of **CH-GL-CC-Fe** for a mixture of various surrogates (**S1** to **S6)** was elucidated at equilibrium conditions (*cf.* Figure 7.9). The **CH-GL-CC-Fe** composite exhibited

slight selectivity for the surrogates according to their respective *z* values or double bond equivalents (DBE), where **S1** was more favorably adsorbed over other surrogates (**S2-S6**).

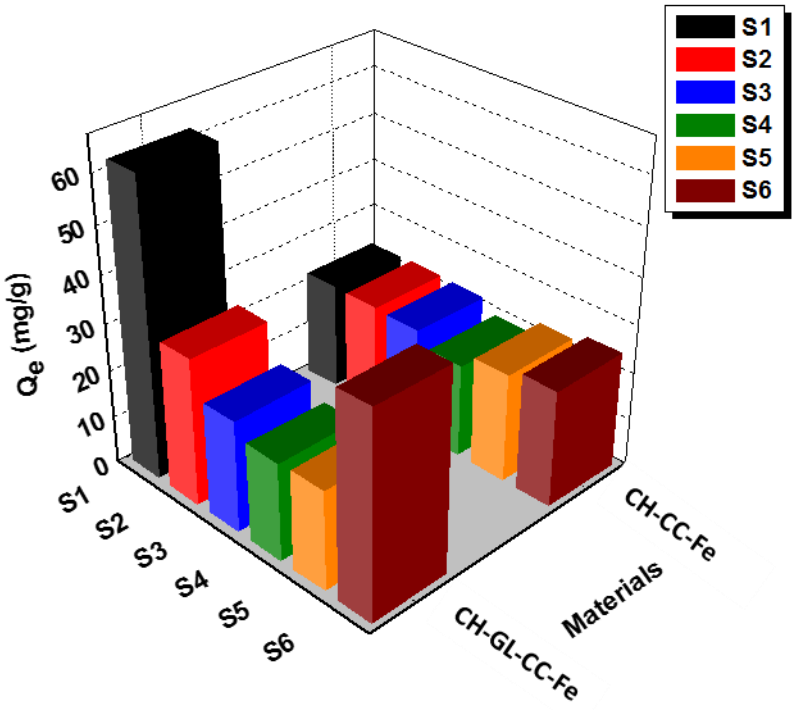

Figure 7.9. Sorptive uptake of equimolar surrogate mixture by **CH-GL-CC-Fe** and **CH-CC-Fe** composite materials at ambient conditions (pH 9 and 295 K)

However, **CH-CC-Fe** displayed no selectivity for the surrogates as affirmed by similar binding affinity irrespective of the *z* or DBE values (*cf.* Scheme 7.3). The relative sorption affinity of the **CH-GL-CC-Fe** composite with the surrogates increased in the following order: **S1 > S6 > S2 > S3 > S4 > S5**. The trend suggests that the interaction between the surrogates and the composite material involve electrostatic and hydrophobic interactions. This assertion is supported by the study at variable pH conditions and the study reported in chapter 6. The greater affinity for the **CH-GL-CC-Fe/S1** system may relate to the relatively high lipophilic surface area of **S1**,[49] as well as minimal steric hindrance that resulted in enhanced adsorption.

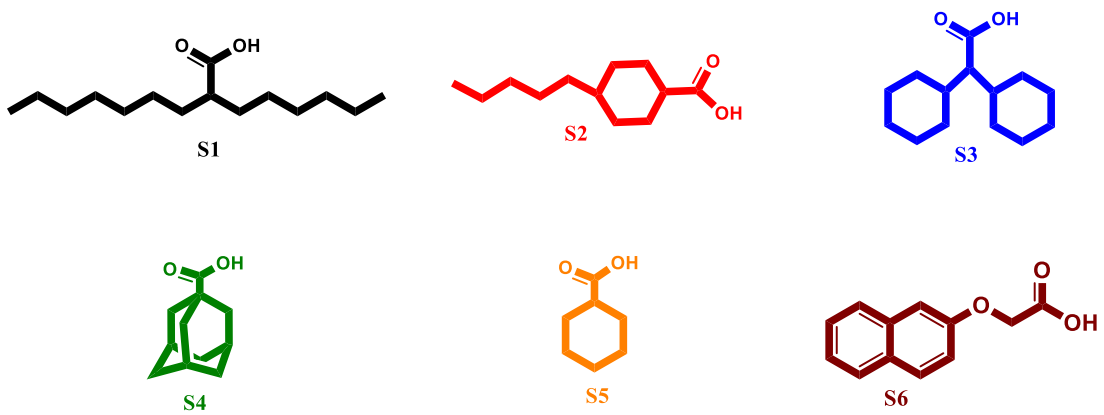

Scheme 7.3: Structure of single component carboxylic acids (**S1** – **S6**)

7.4.2.7 Effects of z-Values on the Sorption of OSPW Naphthenates by the Composite Materials

The adsorption properties of the composite materials for OSPW naphthenates with variable z-values was studied using HR ESI-MS. The corresponding speciation profiles before and after sorption are presented Figures 7.10a and b. The sorption capacity (Q_m; mg/g) for the composites with **OSPW** naphthenates are given in parentheses; **CH-GL-CC-Fe** (35.1 ± 1.8) and **CH-CC-Fe** (19.3 ± 1.0). The greater uptake displayed by **CH-GL-CC-Fe** over **CH-CC-Fe** agrees with results obtained from equilibrium uptake studies and exceeds that obtained for cellulose-chitosan (**CH-GL-C**) composite materials (Q_m; 24.7 ± 1.4 mg/g) reported in chapter 6. The greater sorption capacity of **CH-GL-CC-Fe** relative to **CH-GL-C** material is related to the effects of doping Fe (III) species onto **CH-GL-CC-Fe**. The most abundant OSPW naphthenate species were the O_2H fraction according to the class distribution plots in Figure 7.10a. Treatment of the OSPW extract with **CH-GL-CC-Fe** caused a ~50 – 60 % reduction in the total level of NAFC species in the extract.

Figure 7.10b displays a plot of the double bond equivalents (DBE) distribution of OSPW extracts versus the normalized concentration of O_2H species before and after adsorption with the

composites. The naphthenates present in the OSPW extract consist of those with DBE in the range of 2 to 10, while DBE values of 3 to 4 represented the most abundant species. The results reveal greater uptake (~20 %) for the OSPW extract treated with **CH-GL-CC-Fe** relative to **CH-CC-Fe** in agreement with other equilibrium uptake results reported herein. Interestingly, the composite materials display little or no selectivity for the various naphthenate species with different DBE values, in agreement with equilibrium results for equimolar mixtures reported in section 7.4.2.6. The observed effect may relate to the presence of Fe (III) species in the composites, where a previous study[15] revealed no selectivity for OSPW naphthenates by quaternized cellulose hydrogels.

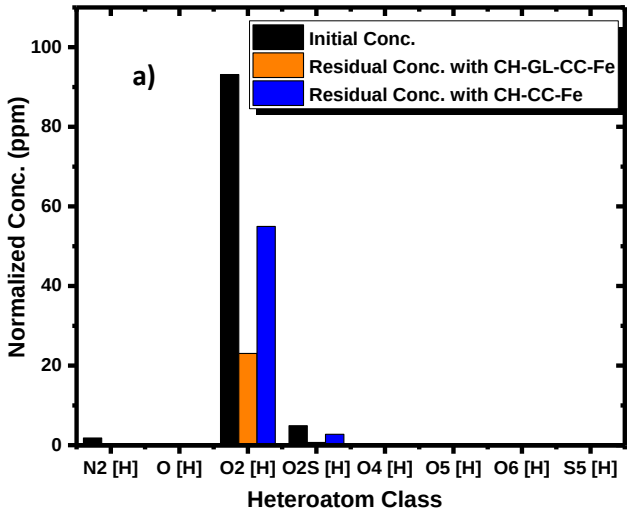

Figure 7.10. a) HR ESI-MS speciation profile of OSPW as a function of normalized concentration for the O_2 species.

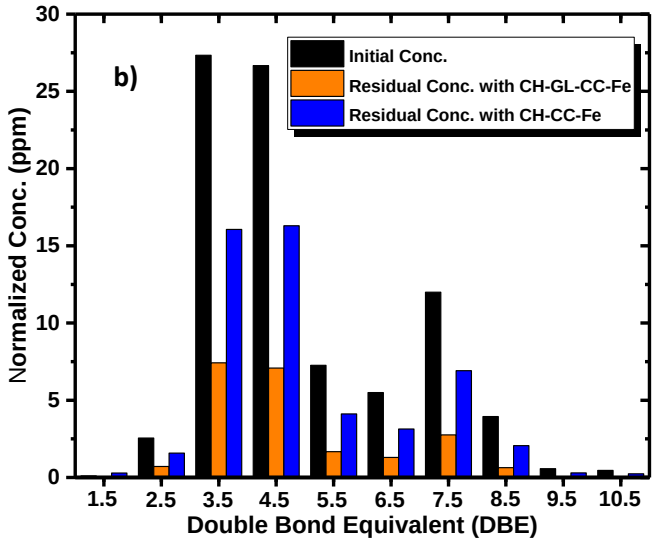

Figure 7.10. b) Double bond equivalents (DBE) distribution of OSPW as a function of normalized concentration for the O_2 species.

7.4.2.8 Effects of Carbon Number on the Sorption of OSPW Naphthenates by the Composite Materials

HR ESI-MS was used to classify the species of naphthenates present in the OSPW according to the carbon number and the DBE values, as shown in Figures 7.11a and b. The speciation results reveal that naphthenates with 13-18 carbon atoms and DBE values of 3 to 4 were the most prominent congeners, in agreement with the profile displayed in Figure 7.10b. The results confirm the greater affinity of **CH-GL-CC-Fe** for the **OSPW** naphthenates (*cf.* Figure 7.11a) as observed from equilibrium uptake results reported in sections 7.4.2.1 and 7.4.2.6.

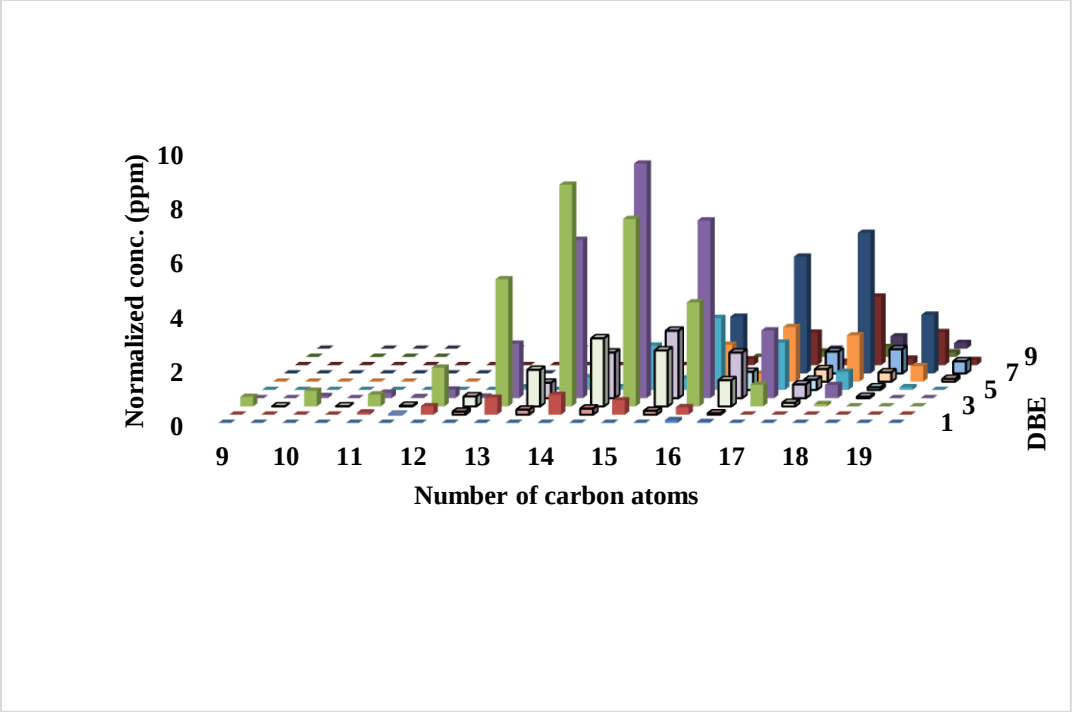

Figure 7.11. a) HR ESI-MS speciation profile of **OSPW** showing effects of carbon number on the sorption capacity of **CH-GL-CC-Fe** at ambient conditions.

CH-GL-CC-Fe and **CH-CC-Fe** display a removal efficiency of ~50 – 60% (*cf.* Figure 7.11a) and ~30 – 40 % (*cf.* Figure 7.11b) across all carbon numbers and DBE values, respectively. This study shows agreement with the effects of *z* values on the uptake affinity of the composite materials. Previous studies[50, 51] reported that naphthenates with high DBEs and carbon number are the most persistent in the environment. Results obtained from this study shows that these composite materials may be useful in the removal of the persistent NAFC classes from aqueous solution.

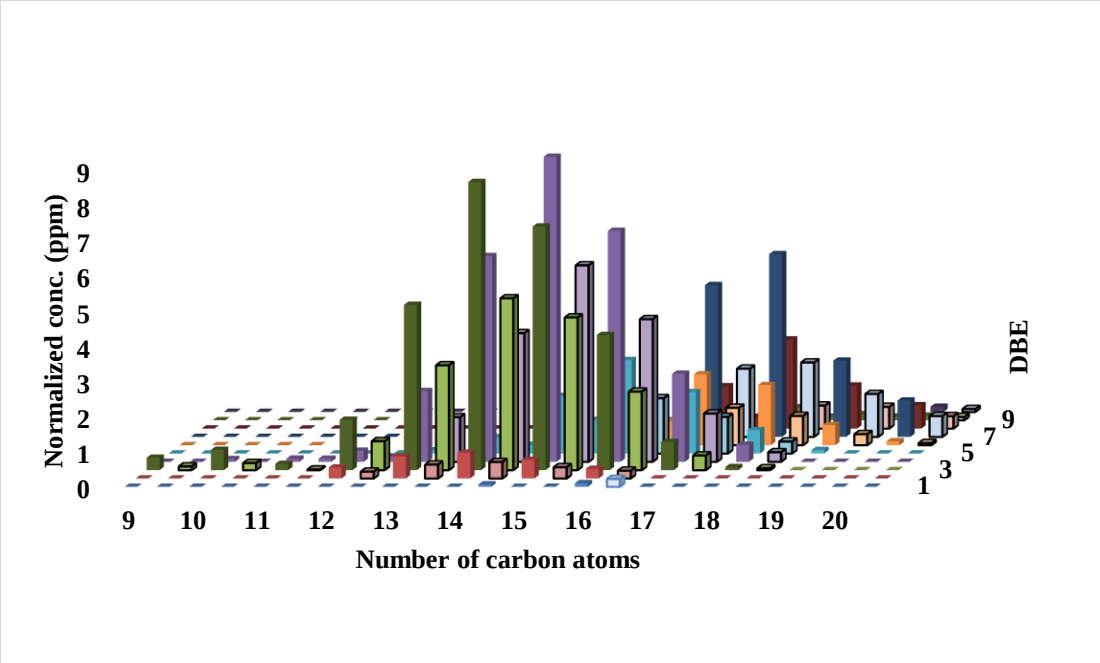

Figure 7.11. b) HR ESI-MS speciation profile of OSPW showing effects of carbon number on the sorption capacity of **CH-CC-Fe** at ambient conditions**.**

7.5 Conclusions

Quaternary (cross-linked) and ternary (non-cross-linked) carboxymethyl cellulose/chitosan composite materials (**CH-GL-CC-Fe** and **CH-CC-Fe**) were prepared with the aim of assessing the role of iron doping, along with cross-linking with glutaraldehyde, on the anion recognition properties of such composites. FTIR studies support cross-linking between the amine groups of chitosan and the carbonyl groups of glutaraldehyde. The iron content studies provide evidence of variable levels of Fe (III) species in the composite materials. SEM, TGA and sorption studies provided evidence of cross-linking effects in the composite materials, where the ternary and quaternary composites reveal unique morphology, thermal degradation profile, and sorption capacity. Isotherm sorption studies at variable pH and temperature conditions reveal that the composite materials favor uptake at lower pH and temperature. The uptake selectivity of an equimolar surrogate mixtures or OSPW naphthenates at equilibrium reveal limited selectivity for

anion species with variable DBE and carbon number. This study provides further understanding of the structural and functional compatibility between a cationic and anionic polysaccharide, with the use of Fe (III) species as a Lewis acid dopant in composite materials to improve the anion recognition properties. This study contributes to the development of low-cost sorbent materials for the reclamation of tailing ponds as well as other water treatment applications, where the anion recognition properties of **CH-GL-CC-Fe** surpass that of **CH-GL-C** composites[22] and quaternized cellulose beads reported recently.[44]

7.7 References

1. Nix, P. G.; Martin, R. W. *Environ Toxic Water* **1992**, 7, 171-188.
2. Giesy, J. P.; Anderson, J. C.; Wiseman, S. B. *PNAS **2010**, 107, 951-952.*
3. Leishman, C.; Widdup, E. E.; Quesnel, D. M.; Chua, G.; Gieg, L. M.; Samuel, M. A.; Muench, D. G. *Chemosphere* **2013**, 93, 380-387.
4. Bartlett, A. J.; Frank, R. A.; Gillis, P. L.; Parrott, J. L.; Marentette, J. R.; Brown, L. R.; Hooey, T.; Vanderveen, R.; McInnis, R.; Brunswick, P.; Shang, D.; Headley, J. V.; Peru, K. M.; Hewitt, L. M. *Environ Pollut* **2017**, 227, 271-279.
5. Scarlett, A. G.; West, C. E.; Jones, D.; Galloway, T. S.; Rowland, S. J. *Sci Total Environ* **2012**, 425, 119-127.
6. Dzidic, I.; Somerville, A. C.; Raia, J. C.; Hart, H. V. *Anal Chem* **1988**, 60, 1318-1323.
7. Fan, T. P. *Energy Fuel* **1991**, 5, 371-375.
8. Wong, D. C. L.; van Compernolle, R.; Nowlin, J. G.; O'Neal, D. L.; Johnson, G. M. *Chemosphere* **1996**, 32, 1669-1679.
9. St. John, W. P.; Rughani, J.; Green, S. A.; McGinnis, G. D. *J Chromatogr A* **1998**, 807, 241-251.
10. Hsu, C. S.; Dechert, G. J.; Robbins, W. K.; Fukuda, E. K. *Energy Fuel* **1999**, 14, 217-223.
11. Marshall, A. G.; Rodgers, R. P. *PNAS* **2008**, 105, 18090-18095.

12. Leclair, L. A.; Pohler, L.; Wiseman, S. B.; He, Y.; Arens, C. J.; Giesy, J. P.; Scully, S.; Wagner, B. D.; van den Heuvel, M. R.; Hogan, N. S. *Environ Sci Technol* **2015**, 49, 5743-5752.

13. Mohamed, M.; Wilson, L. *Nanomaterials* **2015**, 5, 969-980.

14. Mohamed, M. H.; Udoetok, I. A.; Wilson, L. D.; Headley, J. V. *RSC Adv.* **2015**, 5, 82065-82077.

15. Udoetok, I. A. ; Wilson, L. D.; Headley, J. V. *Materials* **2016**, 9, 645-660.

16. Udoetok, I. A.; Dimmick, R. M.; Wilson, L. D.; Headley, J. V. *Carbohyd Polym* **2016**, 136, 329-340.

17. Frankel, M. L.; Bhuiyan, T. I.; Veksha, A.; Demeter, M. A.; Layzell, D. B.; Helleur, R. J.; Hill, J. M.; Turner, R. J. *Bioresource Technol* **2016**, 216, 352-361.

18. Islam, M. S.; Zhang, Y.; McPhedran, K. N.; Liu, Y.; Gamal El-Din, M. *J Environ Manage* **2015**, 152, 49-57.

19. Arshad, M.; Khosa, M. A.; Siddique, T.; Ullah, A. *Chemosphere* **2016**, 163, 334-341.

20. Mohamed, M. H.; Wilson, L. D.; Shah, J. R.; Bailey, J.; Peru, K. M.; Headley, J. V. *Chemosphere* **2015**, 136, 252-258.

21. Mohamed, M. H.; Wilson, L. D.; Headley, J. V.; Peru, K. M. *Energy Fuel* **2015**, 29, 3591-3600.

22. Udoetok, I. A.; Wilson, L. D.; Headley, J. V. *ACS Appl Mater Interface* **2016**, 8, 33197-33209.

23. Duri, S.; Tran, C. D. *Langmuir* **2013**, 29, 5037-5049.

24. Peng, S.; Meng, H.; Ouyang, Y.; Chang, J. *Ind Eng Chem Res* **2014**, 53, 2106-2113.

25. Shang, J.; Shao, Z. Z.; Chen, X. *Biomacromolecules* **2008**, 9, 1208-1213.

26. Liuyun, J.; Yubao, L.; Chengdong, X. *J Mater Sci-Mater M* **2009**, 20, 1645-1652.

27. Chen, H.; Fan, M. *J Bioact Compat Pol* **2007**, 22, 475-491.

28. Chen, X.; Liu, J.; Feng, Z.; Shao, Z. *J Appl Polym Sci* **2005**, 96, 1267-1274.

29. Fazary, A. E.; Ramadan, A. M. *Complex Met* **2014**, 1, 139-148.

30. He, X.; Xu, H.; Li, H. *World Eng Technol* **2015**, 03, 234-240.

31. Seyed Dorraji, M. S.; Mirmohseni, A.; Tasselli, F.; Criscuoli, A.; Carraro, M.; Gross, S.; Figoli, A. *J Polym Res* **2014**, 21.

32. Ghasemzadeh, H.; Mahboubi, A.; Karimi, K.; Hassani, S. *Polymer Adv Tech* **2016**, 27, 1204-1210.

33. Sips, R. *J Chem Phys* **1948**, 16, 490-495.

34. Langmuir, I. *J Am Chem Soc* **1918**, 40, 1361-1402.

35. Kildeeva, N. R.; Perminov, P. A.; Vladimirov, L. V.; Novikov, V. V.; Mikhailov, S. N. *R J Bioorganic Chem* **2009**, *35*, *360-369.*

36. Liuyun, J.; Yubao, L.; Chengdong, X J Biomed Sci **2009**, 16, 1–10

37. Smitha, B.; Sridhar, S.; Khan, A. A. *Eur Polym J* **2005**, 41, 1859-1866.

38. Rosca, C.; Popa, M. I.; Lisa, G.; Chitanu, G. C. *Carbohyd Polym* **2005**, 62, 35-41.

39. Thomas, S.; Soloman, P. A.; Rejini, V. O. *Procedia Technol* **2016**, 24, 721-726.

40. Krumova, M.; López, D.; Benavente, R.; Mijangos, C.; Pereña, J. M. *Polymer* **2000**, 41, 9265-9272.

41. Varma, A. J.; Deshpande, S. V.; Kennedy, J. F. *Carbohyd Polym* **2004**, 55, 77-93.

42. Webster, A.; Halling, M. D.; Grant, D. M. *Carbohyd Res* **2007**, 342, 1189-1201.

43. Hsien, T.-Y.; Rorrer, G. L. *Ind Eng Chem Res* **1997**, 36, 3631-3638.

44. Quinlan, P. J.; Grishkewich, N.; Tam, K. C. *Can J Chem Eng* **2017**, 95, 21-32.

45. Zhou, L.; Jin, J.; Liu, Z.; Liang, X.; Shang, C. *J Hazard Mater* **2011**, 185, 1045-1052.

46. Dotto, G. L.; Lima, E. C.; Pinto, L. A. A. *Bioresource Technol* **2012**, 103, 123-130.

47. Aljeboree, A. M.; Alshirifi, A. N.; Alkaim, A. F. *Arab J Chem* **2017**, 10, S3381-S3393.

48. Li, H.; Huang, G.; An, C.; Hu, J.; Yang, S. *Ind Eng Chem Res* **2013**, 52, 15923-15931.

49. Mohamed, M. H.; Wilson, L. D.; Peru, K. M.; Headley, J. V. *J Colloid Interface Sci* **2013**, 395, 104-110.

50. Toor, N. S.; Han, X.; Franz, E.; MacKinnon, M. D.; Martin, J. W.; Liber, K. *Environ Toxicol Chem* **2013**, 32, 2207-2216.

51. Mishra, S.; Meda, V.; Dalai, A. K.; McMartin, D. W.; Headley, J. V.; Peru, K. M. *J Water Resource Prot* **2010**, 02, 644-650.

Chapter 8

8. Integrated Discussion of Manuscript Chapters, Concluding Remarks and Proposed Future Research Work

8.1 Integrated Discussion of Manuscript Chapters

This chapter provides an overview of the findings of the thesis research and provides support that address the general objectives of the thesis. As illustrated in Scheme 8.1, the manuscript chapters cover four thematic areas, where three are related to materials design of modified biopolymers to address the objectives of this PhD thesis, as described below.

1. Theme 1 relates to cross-linking of biopolymers such as cellulose and chitosan
2. Theme 2 relates to surface functionalization of cellulose
3. Theme 3 relates to composite formation between cellulose and chitosan based biopolymers

The overall objective of the thesis research relates to the development of modified biopolymer sorbent materials containing cellulose and chitosan for the uptake of NAFCs from aqueous solution according to four themes. Themes 1 to 3 are listed above, whereas the fourth theme relates to the strategy for assessing the sorption properties of the modified biopolymers with NAFCs.

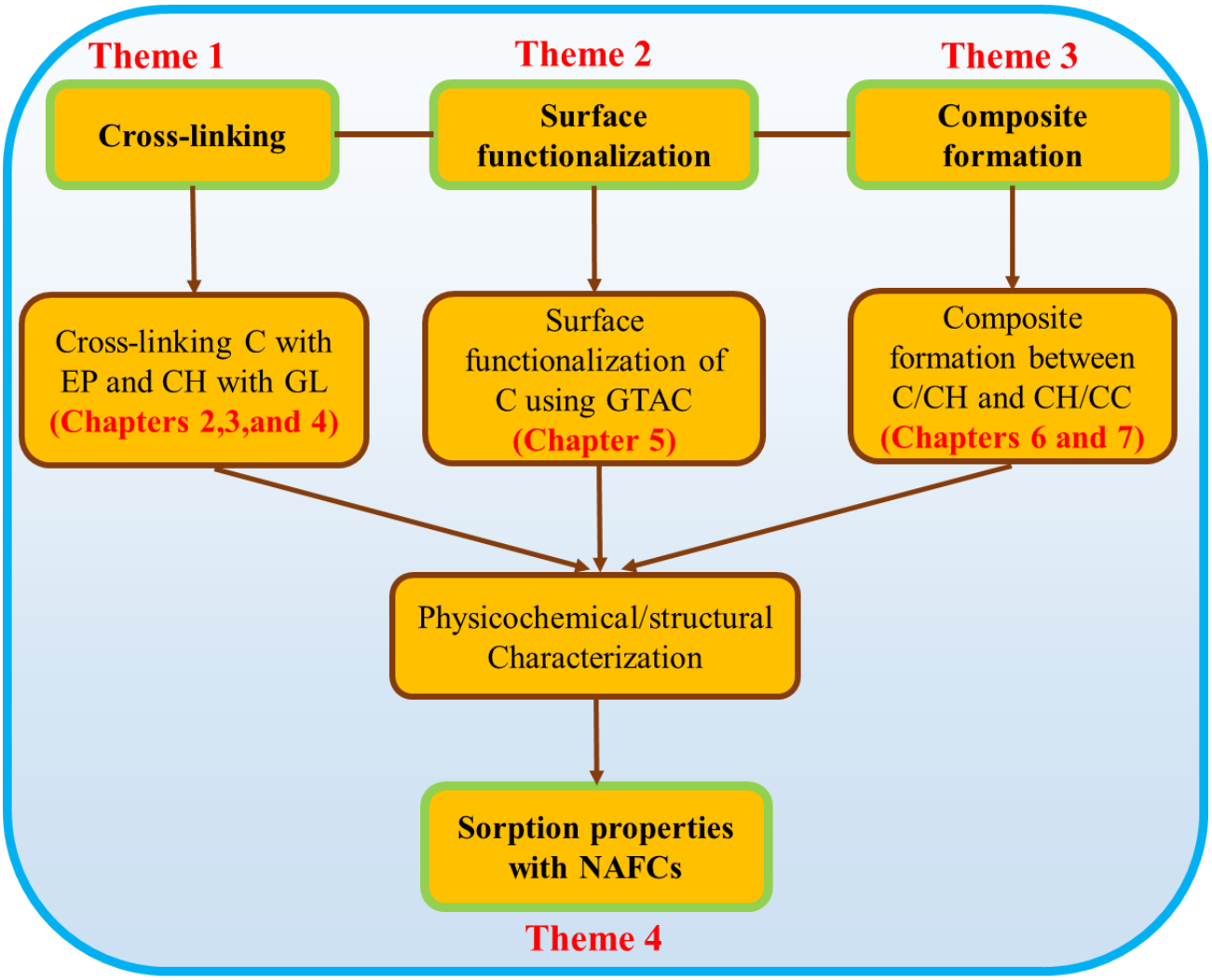

Scheme 8.1 Organization of the PhD Thesis, where the boxes with **Bold** font represent the **Four Research Themes** of this study.

In chapters 2 and 3, chitosan and cellulose were cross-linked with glutaraldehyde and epichlorohydrin, respectively. The structural and physicochemical properties of the pristine and modified biopolymers (**CH-GL** and **C-EP**) were studied using spectroscopic and thermal analyses methods along with dye and gas adsorption studies. The modification of these biopolymers via cross-linking at incremental reactant ratios yielded polymers with tunable properties in agreement with previous studies.[1-4] Cross-linking led to *pillaring* of the fibril structure of the biopolymers where the monolayer adsorption capacity of the polymers in aqueous solution was greater than that

of the pristine biopolymers according to the level of cross-linking. Mohamed et al.[3] and Quinlan et al.[2] reported variable uptake of adsorbates by cross-linked β-cyclodextrin and chitosan according to the level of cross-linking of the biopolymers that show parallel trends to the results reported in this thesis. The polymers exhibited selectivity for the model NAFCs according to their respective z values,[5] where the negative surface charge of the polymers led to attenuated sorption capacity at alkaline pH conditions. The trends observed for the adsorption properties of cellulose materials with NAFCs is supported by studies for the PZC of cellulose materials.[6-8] Chitosan polymers (**CH-GL**) exhibited greater sorption affinity for the naphthenates relative to cellulose polymers (**CE-P**), due to inefficient *pillaring* of cellulose via cross-linking (*cf.* Table 3.5).

In chapter 4, the role of *pillaring* of cellulose and its dependence on the adsorption properties was studied. Further increases to the level of cross-linking was achieved by application of a sonication assisted cross-linking process that affected the yield and adsorption properties of the cross-linked polymers (**CE-P sonication** and **CE-P heating**). The relationship of cross-linking and physicochemical properties was evaluated using spectroscopic and thermal analyses methods, along with its effect on the adsorption studies. The results revealed that the application of sonication resulted in greater cross-linking of cellulose. Consequently, the textural and adsorption properties of the sonication assisted cross-linked polymer was greater relative to the cellulose (**C-EP**) polymers reported in chapter 3 (*cf.* Table 3.5). Previous reports[9-12] on the influence of sonochemical conditions on the synthesis reveal that cavitation effects in liquid-solid systems improved the reaction kinetics and enhanced chemical reactivity, in agreement with the structural results related to cross-linking.

The study reported in chapter 5 was conceived to bridge the knowledge gaps (see section 1.1.1 of chapter 1,) of chapters 3 and 4, where the negative surface charge of the cross-linked

cellulose lowered the uptake of anions at alkaline pH conditions.[13-14] Cellulose was modified by cross-linking with and/or functionalization with GTAC. The synthesized hydrogels (**C-EP-G** and **C-G**) were characterized by CHN analysis, TGA, FTIR and ^{13}C solids NMR spectroscopy. The appearance of new resonance lines in the ^{13}C solids NMR spectra of the hydrogels at ~55.0 ppm for $(CH_3)_3N^+$ and ~77 ppm for CH_2 groups from EP and GTAC affirmed the synthesis of the hydrogels. Cross-linking of biopolymers with EP and further grafting with GTAC results in the introduction of $(CH_3)_3N^+$ and CH_2 groups onto cellulose in agreement with relevant studies and results reported in this thesis.[15-17] Furthermore, adsorption studies in aqueous solution using the hydrogels affirmed an increase in surface area (SA) due to cross-linking as observed from the results in chapters 2, 3 and 4 for modified chitosan and cellulose. The trends observed in Chapters 2-4 are supported by results from other independent studies.[4, 18-19] The attenuation of anion uptake due to the negative surface charge of the **C-EP** polymers at alkaline pH conditions was also observed. The aforementioned claims were supported by the cross-linked/surface functionalized hydrogel (**C-EP-G**) exhibiting greater anion recognition relative to the surface functionalized hydrogel (**C-G**). These results further affirm the important role of surface area and charge in sorption processes. Studies on the effects of surface area on adsorption shows that adsorption capacity increases with increasing surface area of the sorbent material.[20-22] Liu et al.[23] demonstrated that the greater binding affinity and adsorption capacity of plant roots of *indica* species for Cu and Cd cations was due to the negatively charged surface and functional groups of the sorbent material. Also, Wang et. al.[24] showed that the complexation of lignin with Cu^{2+} resulted in an increased sorption affinity of lignin for phenanthrene. The hydrogels had greater sorption capacity for the naphthenates than all the sorbents reported in chapters 2 – 4. The results in Table

8.1 provide support for the effects of surface area and charge on the adsorption capacity of adsorbents.

In chapter 6, glutaraldehyde cross-linked chitosan/cellulose composite materials (**CH-GL-C**) were prepared using incremental levels of glutaraldehyde. The textural, morphological, and adsorption properties of the composite materials were studied by spectroscopy, microscopy, thermal and dye adsorption methods. The results further affirmed the tunable nature of the adsorption properties of biopolymers according to variable cross-linker content as earlier reported in chapters 2 and 3. The chapter further revealed that composite formation between cellulose and chitosan resulted in greater anion recognition (*cf.* Table 6.5) and limited selectivity toward the adsorption of OSPW naphthenates. These results are in contrast relative to the single component chitosan (**CH-GL)** and cellulose (**C-EP**) biopolymers reported in chapters 2 and 3. The results reported in chapter 6 are in agreement with relevant studies on chitosan-cellulose composite materials where efficient cation recognition and reusability[25], greater tensile strength, [26-27] and structural stability [28] were reported.

Chapter 7 reports the synthesis and characterization of quaternary (**CH-GL-CC-Fe**) and ternary (**CH-CC-Fe**) composite materials from carboxymethyl cellulose, chitosan, glutaraldehyde and Fe (III) species. The project bridges the knowledge gaps reported in chapter 6, where charge screening at alkaline pH may have attenuated the sorption of anions by the **CH-GL-C** composite materials. Cellulose was replaced with carboxymethyl cellulose and Fe (III) species were introduced as Lewis acid sites via complexation at surface accessible sites of carboxymethyl groups of cellulose and the amine groups of chitosan. The composite materials were characterized through spectroscopy, microscopy and a thermal analysis. The characterization results affirmed that the quaternary and ternary composite materials contained variable content of Fe (III) species,

with variable morphology and textural properties. The trends for the composite materials were in good agreement with the favorable compatibility of CC and chitosan reported elsewhere.[29-32] Adsorption studies with **S6** and OSPW naphthenates show that **CH-GL-CC-Fe** displayed greater sorption affinity for the naphthenates than other sorbent materials reported in this thesis (*cf.* Table 8.1). The improvement in sorption properties for composite materials are supported by the observed efficiency of chitosan-CC composite materials as polyelectrolyte membranes[29-30] and adsorbents for cationic adsorbates.[33-34]

The sorption results further affirm the role of cross-linking and surface charge in enhancement of the sorption affinity and capacity of biopolymers in agreement with studies reported in chapters 2 – 7 and previous reports. [20-24]

Table 8.1. Summary of the sorption capacity of some sorbents reported in this thesis

Chapter	Sorbent materials	Sorbates					
		S1	**S2**	**S3**	**S6**	**S7**	**OSPW**
2	**CH-GL3**	6.65‡	9.50‡	9.25‡	NA	28.4‡/33.5†	NA
3	**C-EP**	4.27‡	0.0962‡	0.0452‡	NA	NA	NA
4	**C-EP sonication**	NA	NA	NA	17.5*/0.82	NA	NA
5	**C-EP-G**	NA	NA	NA	60.5‡	NA	33.0‡
6	**CH-GL3-C**	115‡	13.7‡	NA	40.5‡	NA	24.1‡
7	**CH-GL-CC-Fe**	NA	NA	NA	**484*/263‡**	NA	35.1‡

* Represent uptake values obtained at pH 3, † Represent uptake values obtained at pH 6 and ‡Represent uptake values obtained at pH 9

8.2 Concluding Remarks

In conclusion, the overall objective of this thesis research related to the development of sustainable biopolymer materials as sorbents for the controlled uptake of NAFCs from aqueous solution. The materials design approach to achieve this overall goal of biopolymer design was divided into three strategies described by Themes 1-3 while Theme 4 concerns the assessment of the suitability of the modified biopolymers for the uptake of NAFCs from aqueous solution. (*cf.* Scheme 8.1).

In Theme 1, biopolymers were modified through cross-linking with bifunctional agents such as glutaraldehyde (**CH-GL**)[35] and epichlorohydrin (**C-EP**)[14] at incremental cross-linker ratios, as described in chapters 2 – 4. The results obtained address hypotheses 1 to 3 (see section 1.1.1 of chapter 1) of the thesis research. Structural and physicochemical characterization studies using FTIR/NMR spectroscopy, and TGA revealed tunable morphology and adsorption properties for the modified biopolymers according to the cross-linker content and mode of cross-linking.[14, 35] In general, cross-linking affects the crystallinity of the biopolymer, in agreement with other related studies.[1-4] Greater *pillaring* of the biopolymers occurred at the highest cross-linker ratio that was further enhanced by variable synthetic conditions such as sonication assisted synthesis. The application of ultrasound irradiation has been reported to enhance reaction kinetics and yield due to acoustic cavitation effects.[9-12] Evidence of such synthetic modification and tunability of the physicochemical properties was further affirmed by improvement of the sorption capacities toward single component and equimolar mixtures of NAFC model compounds (**S1** – **S7**) and OSPW naphthenates. Optimal sorption properties of the modified biopolymers was observed at the highest cross-linker feed ratio (*cf.* Figures 2.9 and 3.8) and for the material (**C-EP sonication**) obtained by sonication assisted cross-linking (*cf.* Figure 4.9). One exception to the above trend was reported

in chapter 3 where hydrolysis of epichlorohydrin occurred at alkaline pH conditions.[14] Competitive hydrolysis of EP over cross-linking with cellulose (*cf.* Scheme 3.3b) offsets the anticipated effects of *pillaring* of cellulose. **CH-GL** polymers displayed greater sorption properties over **C-EP** polymers, where both types of modified biopolymer had variable selectivity for the different NAFC congeners with different DBE values. The OSPW used in the study consisted of naphthenates with DBE values that ranged from 2 – 10 and are known to influence the apolar character of such adsorbates and their relative solvent accessibility.[36-37] In this study, the limitations of cross-linking cellulose and chitosan in the case of flexible aliphatic cross-linkers such as glutaraldehyde (GL) and epichlorohydrin (EP) were noted.[14, 35] The limitations were related to the following effects: *i*) collapse of the pore structure of the modified biopolymers due to the flexibility and/or conformational entropy of the cross-linkers used, especially for cross-linkers with greater *n*-akyl chain length such as glutaraldehyde, and *ii*) negative zeta-potential of the modified biopolymers at alkaline pH conditions.

The results related to the second theme was reported in chapter 5 that addresses the fourth hypothesis of the thesis research; to determine if cross-linking and/or surface functionalization of cellulose can increase the sorption affinity of cellulose for NAFCs. In chapter 5, surface functionalization of cellulose with quaternary ammonium groups was presented, where the quaternary ammonium groups were introduced to overcome the negative surface charge of the polymers at alkaline pH conditions due to the presence of surface –OH groups. The study presented in chapter 5 also reports the adsorption properties of the surface functionalized cellulose with a model NAFC compound (**S6**). Structural and physicochemical characterization studies using ^{13}C NMR /FTIR spectroscopy and TGA provide complementary support for the functionalization of cellulose with quaternary ammonium groups (*cf.* Figure 5.3).[17] Adsorption

studies revealed greater anion uptake properties for the surface functionalized cellulose hydrogels, where the cross-linked/surface functionalized hydrogel (**C-EP-G**) had optimum sorption capacity relative to the surface functionalized (**C-G**) hydrogel and the other modified biopolymers (**CH-GL**, **C-EP** and **C-EP sonication**) reported in chapters 2-4. The hydrogels displayed no selectivity for the various NAFC congeners, irrespective of carbon number or the DBE value contrary to the results for **CH-GL** and **C-EP** polymers. The variable uptake affinity of these polymers may relate to the nature of their interactions with the naphthenate anions. In the case of the **CH-GL** and **C-EP** polymers, the uptake selectivity provide support for the role of hydrophobic effects, in agreement with the changes in the SA and HLB of the biopolymer network. On the other hand, the lack of selectivity exhibited by the hydrogels may be afforded by presence of ion-exchange sites (quaternary ammonium groups) of the hydrogel with the naphthenate anions. This study further affirms the role of cross-linking and surface chemistry in adsorption processes.

The studies reported in chapters 6 and 7 are based on the third theme of the thesis objective that address hypotheses 5 and 6 (see section 1.1.2 of chapter 1). In chapter 6, studies on composite formation between chitosan and cellulose based biopolymers were reported. This study was carried out to optimize the adsorption properties of **CH-GL** polymers, where collapse of the biopolymer pore structure in aqueous media may have lowered the sorption capacity. It was hypothesized that the greater mechanical strength of cellulose relative to chitosan may help create permanent pore structure in the composites, along with *pillaring* of the fibrils introduced by cross-linking. A composite material of chitosan and cellulose with further cross-linking by glutaraldehyde was achieved at incremental cross-linker ratios (**CH-GL-C**). The composite materials were characterized using various structural and physicochemical methods such as ^{13}C NMR /FTIR spectroscopy, TGA and SEM. The characterization and sorption results (*cf.* Section 6.4) reveal

that the composite materials exhibited tunable sorption properties according to the cross-linker feed ratio. The results for the composite materials provided support that tunable sorption properties for **CH-GL** and **C-EP** resulted due to the synthetic modification as reported in chapters 2 and 3. The sorption results for **phth**, **S6,** and OSPW naphthenates showed that **CH-GL3-C** displayed optimum sorption capacity amongst the various NAFC congeners. Minor selectivity for the different congeners in OSPW was observed, contrary to the results for the single component **CH-GL** and **C-EP** polymers reported in chapters 2 and 3. The variable uptake capacity for these composite materials confirmed the tunable sorption properties of the composite materials in relation to the cross-linker feed ratio. The greater uptake capacity (*cf.* Table 8.1) of **CH-GL-C** composite materials affirmed the role of collapsed pore structure for the **CH-GL** polymers in aqueous media. This further supports the hypothesis that composite formation between cellulose and chitosan can stabilize the pore structure of chitosan following *pillaring effects* due to the cross-linking.

The study reported in chapter 7 was aimed at optimizing the sorption properties of the **CH-GL-C** composites. It was hypothesized that the **CH-GL-C** composite materials may possess a net negative zeta potential at alkaline pH conditions. The effect may relate to charge screening between the surface of the composites and the negatively charged carboxylate groups of NAFCs. In chapter 7, a quaternary composite material (**CH-GL-CC-Fe**) was prepared with carboxymethyl cellulose and chitosan followed by cross-linking with glutaraldehyde and the introduction of iron (III) species. A ternary composite material (**CH-CC-Fe**) (*cf.* Scheme 7.2) was also prepared but without the cross-linking step. The introduction of iron (III) species afforded chelation with the carboxylate groups of CC. The result of metal ion coordination serves to neutralize the negative surface charge of the anion groups and changes the zeta potential according to the extent of

chelation. FTIR spectroscopy, TGA, SEM and ICP-OES results supported the formation of the composite materials and the doping of iron III species. Adsorption studies with model NAFCs and OSPW naphthenates revealed that the **CH-GL-CC-Fe** composite materials had greater anion uptake relative to **CH-CC-Fe**, in agreement with the role of *pillaring effects* due to cross-linking, reported in chapters 2 – 6. Unlike the **CH-GL-C** composites, the **CH-GL-CC-Fe** and **CH-CC-Fe** composites showed no selectivity with the various OSPW congeners. This research highlights the role of ion-exchange on the sorption of NAFCs, in agreement with results reported in chapter 5. The composite materials reported in chapter 7 had the greatest sorption affinity for NAFCs relative to the cross-linked and surface functionalized polymers reported overall in this thesis (*cf.* Table 8.1) and shows a comparative advantage over other sorbent materials reported in the literature in terms of cost (*cf.* Table 8.2). These results therefore support the hypothesis that the **CH-GL-C** composites adopt a negative surface charge at alkaline pH conditions.

Table 8.2. Summary of the sorption capacity of various sorbents with OSPW naphthenates

Sorbent Materials		% Removal of NAFCs from water	References
CMC-Chitosan Composite	CHGL3CCFe	**59.2**	This thesis
Cellulose-chitosan Composite	CHGL3C	**51.3**	This thesis
Quaternized cellulose	C-EP-G	**40.8**	This thesis
GAC biofilm + Sodium Azide		27.9 (Raw OSPW) 49.8 (Ozonated OSPW)	Islama et al.[60]
Modified Keratin Fibre	GMKB PMKB	66.1 64.6	Arshad et al.[61]
Activated Carbon from Biomass	N1	59.0	Iranmanesh et al.[62]
Geothite		15	Mohamed et. al.[63]
Activated Carbon		95	
Biochar	BC1 BC2 BC3	24 15 15	
Cellulose		0	

This thesis reports novel findings on the role of various structural modification of biopolymers on the sorption properties of the modified biopolymers with carboxylate anions possessing variable DBE values (aliphatic to aromatic). These results are supported by the physicochemical properties related to adsorption (swelling, dye uptake, isotherm results) and structural characterization. The results obtained herein provide support that cross-linking enhances the biopolymer SA through *pillaring effects*. However, the enhancement of the sorption properties of biopolymers are limited especially at alkaline pH conditions since less favorable electrostatic interactions occur due to the buildup of negative zeta-potential on the sorbent surface. Greater uptake capacity can be achieved at alkaline pH conditions through combined effects of synthetic modification; cross-linking/surface functionalization or cross-linking/composite formation. The studies reported herein provide a greater understanding of the structure-property relationship for polymer-adsorption phenomena. The results highlight molecular selectivity for adsorbates by single component cross-linked (**CH-GL** and **C-EP**) polymers relative to the surface functionalized (**C-EP-G**) and composite (**CH-GL-C**, **CH-GL-CC-Fe**) materials. Studies that report the structure-property relationship of NAFCs-biopolymer systems are limited in the literature.[38-39]

The studies reported in this thesis will contribute to the design of modified biopolymer adsorbent materials with improved and tunable physicochemical properties, especially for applications involving adsorption processes such as chemical separations and environmental remediation of waterborne contaminants.

8.3 Proposed Future Research Work

Further studies that detail the effects of drying conditions[40] on the structural framework of biopolymers modified with rigid cross-linkers are required. Conventional oven drying versus freeze drying is known to alter the morphology of polymer materials.[40] In turn, materials with such structural variability is likely to influence the nature of interactions between the modified polymers and NAFCs, and the sorption mechanism due to the role of textural properties on the thermodynamics and kinetics of the sorption processes.[41-43]

To achieve the above, single component cross-linked biopolymers and cross-linked composite materials shall be prepared using more rigid cross-linkers[43] such as terephthalaldehyde[44] and genipin[45-47] at incremental cross-linker ratios. Rigid cross-linkers have been reported to afford permanent porosity in sorbent materials.[43] The use of rigid versus flexible cross-linkers will afford studies relating to the determination the role of intermolecular versus intramolecular cross-linking. Flexible cross-linkers may tend to favor intramolecular cross-linking relative to rigid cross-linkers due to the differences in their conformational entropy. The synthetic procedure for these materials shall be similar to the ones reported in this thesis, in order to provide a good basis for the proposed study. The effects of drying conditions on the pore structure of the modified biopolymers shall be evaluated by the use oven drying versus freeze-drying processes.[40] The modified polymers prepared by different strategies shall be characterized to illustrate the variations in their structural physicochemical properties. In turn, such variations can be evaluated by examining the sorption isotherms with NAFCs at equilibrium and kinetic conditions to illustrate differences in uptake and selectivity toward congeners that vary by DBE, and carbon number.

The study reported by Alsbaiee et al.[43] showed that the use of rigid cross-linkers such as tetrafluoroterephthalonitrile (TFP) afforded polymers with high surface area and permanent

porosity that enabled the rapid removal of organic contaminants from water. The study revealed approximately 50 % difference in the removal efficiency of bisphenol A when β-cyclodextrin was cross-linked with TFP relative to the more flexible cross-linker epichlorohydrin. A kinetic uptake study on the removal of bisphenol A with the TFP cross-linked β-cyclodextrin showed that 95 % of bisphenol A was removed within 10 seconds of the kinetic profile. In view of the above, equilibrium and kinetic uptake studies will be performed with oven dried and freeze-dried polymers, and their sorption capacity will be compared with those of similar materials reported in this thesis project. Thermodynamic parameters of the adsorption process such as the standard Gibbs energy change ($\Delta_{ads}G^o$), enthalpy change ($\Delta_{ads}H^o$) and entropy change ($\Delta_{ads}S^o$) can also be obtained from equilibrium sorption parameters.[48-50] The magnitude of $\Delta_{ads}H^o$ values provide information on the nature of interaction between the modified biopolymers and NAFCs.[51] These parameters are usually obtained according to the van't Hoff relationship between the sorption equilibrium constant (K_{ads}) and temperature as expressed in the equations 8.1 and 8.2

$$\Delta_{ads}G^\circ = -RT\ln K_{ads} \qquad \text{Equation 8.1}$$

$$\ln K_{ads} = -\frac{\Delta_{ads}H^\circ}{RT} + \frac{\Delta_{ads}S^\circ}{R} \qquad \text{Equation 8.2}$$

Where K_{ads} is the adsorption equilibrium constant, obtained from the sorption isotherm, R is the gas constant (8.314 J/ (mol K), and T is absolute temperature (K).

To provide a greater understanding of the sorption mechanism of the modified biopolymers with NAFCs, kinetic studies at variable temperature are required with single component model NAFCs (surrogates) as well as an equimolar surrogate mixture. The concentration of the adsorbates before after the sorption process will be quantified using HR ESI-MS, where information on molecular selectivity of the sorbent materials towards NAFC congeners with

variable DBE and carbon number will be obtained.[52] The kinetic parameters (uptake rate constants) will provide information on the sorption mechanism along with the relative rate profiles for the uptake processes. The information on adsorption rates will complement earlier results obtained from equilibrium studies on the pore properties, since a more porous sorbent material will display a faster adsorption rate relative to a material with lower porosity.[43]

Molecular docking studies using Chem3D software and ^{13}C solids NMR spectroscopy are required to provide complementary information on the nature of interactions between the polymers and NAFCs.[53-55] A proposed structure of the modified polymers and a model NAFC of interest will be used to simulate the point of interaction at a potential binding site.[56] In combination with the $\Delta_{ads}H^{o}$ values deduced from equilibrium studies with mixtures containing adsorbates with variable size and structure such as NAFCs, molecular docking studies and thermodynamic parameters will provide information on the prominent nature of interaction in the sorption process ^{13}C solids NMR spectroscopy shall be used to complement the results obtained from the simulation and equilibrium adsorption studies. To achieve this, ^{13}C solids NMR spectra of the polymers in the absence and presence of bound adsorbate at variable loadings are proposed to assess the presence of single- or multiple binding sites of the biopolymer materials. The attenuation or enhancement of some signals in the NMR spectra of the polymers will provide complementary information on the adsorption site and the modes of interaction for the adsorption process.[57-59]

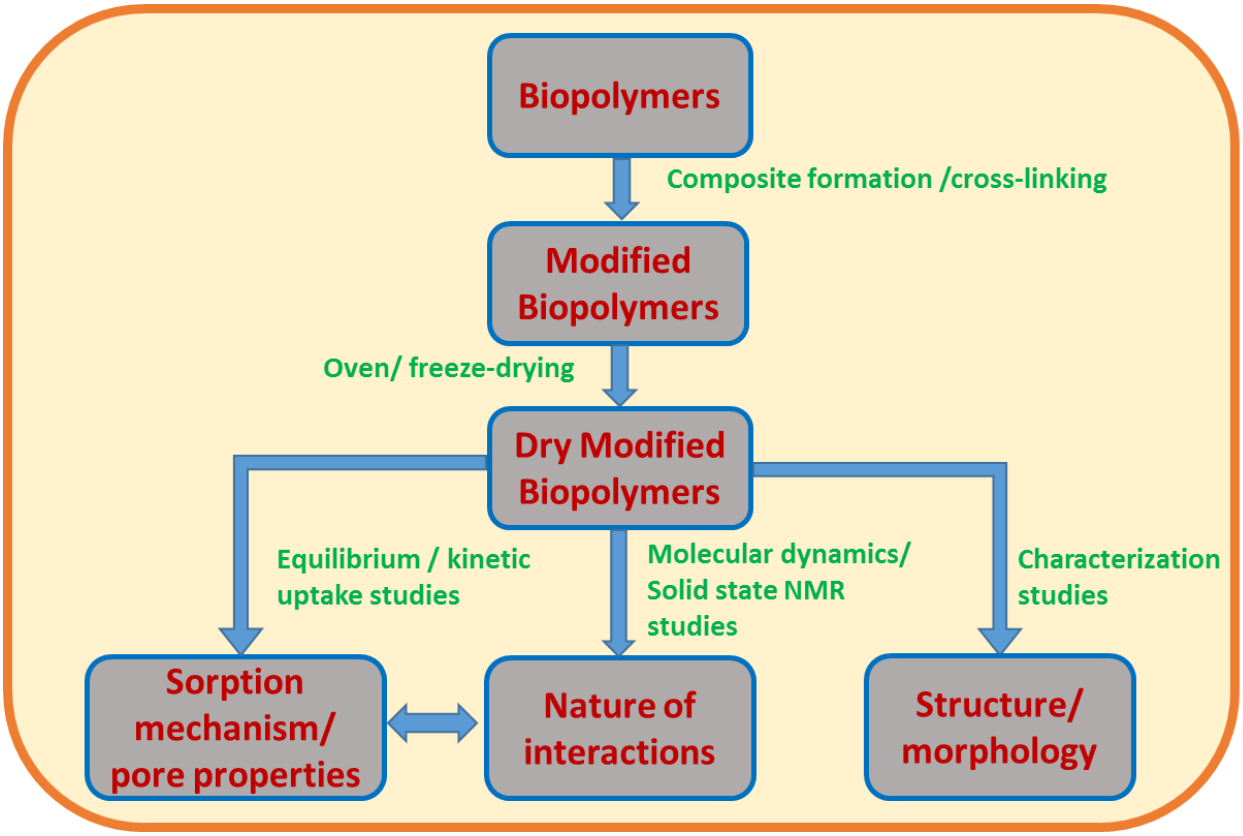

Scheme 8.2: Flow chart outlining the proposed future work

8.4 References

1. Lee, S.; Tong, X.; Yang, F. *Acta Biomaterialia* **2014,** *10* (10), 4167-4174.
2. Quinlan, P. J.; Grishkewich, N.; Tam, K. C. *Can J Chem Eng* **2017,** *95* (1), 21-32.
3. Mohamed, M. H.; Wilson, L. D.; Headley, J. V. *Microporous and Mesoporous Mater* **2015,** *214*, 23-31.
4. Liu, Q.; Li, Y.; Shen, S.; Xiao, Q.; Chen, L.; Liao, B.; Ou, B.; Ding, Y. *J Appl Polym Sci* **2011,** *121* (2), 654-659.
5. Mohamed, M. H.; Wilson, L. D.; Headley, J. V. *J Phys Chem B* **2013,** *117* (13), 3659-3666.
6. Singh, J., Mishra, Uma, N. S., Banerjee, S., & Sharma, Y. C. *BioResources* **2011,** *6* (3), 2730 - 2743.
7. Kosmulski, M. *J Colloid Interface Sci* **2002,** *253* (1), 77-87.

8. Zimmermann, R.; Freudenberg, U.; Schweiß, R.; Küttner, D.; Werner, C. *Curr Opin Colloid Interface Sci* **2010,** *15* (3), 196-202.
9. Suslick, K. S.; Price, G. J. *Annu Rev Mater Sci* **1999,** *29*, 295-326.
10. Suslick, K. S.; Fang, M. M.; Hyeon, T.; Mdleleni, M. M. *Sonochem Sonoluminescence* **1999,** *524*, 291-320.
11. Ogutu, F. O. *J Food Process Technol* **2015,** *06* (05).
12. Koutsianitis, D.; Mitani, C.; Giagli, K.; Tsalagkas, D.; Halász, K.; Kolonics, O.; Gallis, C.; Csóka, L. *Ultrason Sonochem* **2015,** *23*, 148-155.
13. Udoetok, I. A.; Wilson, L. D.; Headley, J. V. *Ultrason Sonochem* **2017**.
14. Udoetok, I. A.; Dimmick, R. M.; Wilson, L. D.; Headley, J. V. *Carbohydr Polym* **2016,** *136*, 329-340.
15. Chaker, A.; Boufi, S. *Carbohydr Polym* **2015,** *131*, 224-232.
16. Song, Y.; Sun, Y.; Zhang, X.; Zhou, J.; Zhang, L. *Biomacromolecules* **2008,** *9* (8), 2259-2264.
17. Udoetok, I. A.; Wilson, L. D.; Headley, J. V. *Materials* **2016,** *9* (8), 645-660.
18. Mane, S.; Ponrathnam, S.; Chavan, N. *Can Chem Trans* **2016**, 473-485.
19. Abbott, L. J.; Colina, C. M. *Macromolecules* **2014,** *47* (15), 5409-5415.
20. Kopac, T.; Bozgeyik, K. *Colloids Surf B* **2010,** *76* (1), 265-271.
21. Müller, B. R. *Carbon* **2010,** *48* (12), 3607-3615.
22. Tureli, F. C.; Ok, S. S.; Goldberg, S. *Soil Sediment Contam* **2014,** *24* (1), 64-75.
23. Liu, Z.-D.; Zhou, Q.; Hong, Z.-N.; Xu, R.-K. *Front Plant Sci* **2017,** *8*.
24. Wang, X.; Yang, K.; Tao, S.; Xing, B. *Environ Sci Technol* **2007,** *41* (1), 185-91.
25. Peng, S.; Meng, H.; Ouyang, Y.; Chang, J. *Ind Eng Chem Res* **2014,** *53* (6), 2106-2113.
26. Wu, T.; Du, Y.; Yan, N.; Farnood, R. *J Appl Polym Sci* **2015,** *132* (33), 42375.
27. Wu, T.; Farnood, R. *Cellulose* **2015,** *22* (3), 1955-1961.
28. Keungputpong, N.; Matchariyakul, N.; Tiptipakorn, S. *Adv Mat Res* **2014,** *989-994*, 697-700.
29. Shang, J.; Shao, Z. Z.; Chen, X. *Biomacromolecules* **2008,** *9* (4), 1208-1213.
30. Liuyun, J.; Yubao, L.; Chengdong, X. *J Mater Sci Mater Med* **2009,** *20* (8), 1645-1652.
31. Chen, H.; Fan, M. *J Bioact Compat Polym* **2007,** *22* (5), 475-491.
32. Chen, X.; Liu, J.; Feng, Z.; Shao, Z. *J Appl Polym Sci* **2005,** *96* (4), 1267-1274.

33. He, X.; Xu, H.; Li, H. *World J Eng Technol* **2015,** *03* (03), 234-240.
34. Seyed Dorraji, M. S.; Mirmohseni, A.; Tasselli, F.; Criscuoli, A.; Carraro, M.; Gross, S.; Figoli, A. *J Polym Res* **2014,** *21* (4).
35. Mohamed, M. H.; Udoetok, I. A.; Wilson, L. D.; Headley, J. V. *RSC Adv* **2015,** *5* (100), 82065-82077.
36. Jones, D.; Scarlett, A. G.; West, C. E.; Rowland, S. J. *Environ Sci Technol* **2011,** *45* (22), 9776-9782.
37. Afzal, A.; Drzewicz, P.; Pérez-Estrada, L. A.; Chen, Y.; Martin, J. W. *Environ Sci Technol* **2012,** *46* (19), 10727-10734.
38. Iranmanesh, S.; Harding, T.; Abedi, J.; Seyedeyn-Azad, F.; Layzell, D. B. *J Environ Sci Health A Tox Hazard Subst Environ Eng* **2014,** *49* (8), 913-922.
39. Azad, F. S.; Abedi, J.; Iranmanesh, S *J Environ Sci Health A Tox Hazard Subst Environ Eng* **2013,** *48* (13), 1649-1654.
40. Wang, Z.; Tang, Z.; Han, Z.; Shen, S.; Zhao, B.; Yang, J. *RSC Adv.* **2015,** *5* (26), 19838-19843.40.
41. Strachowski, P.; Bystrzejewski, M *Colloids Surf. A* **2015,** *467*, 113-123.
42. Lee, M.-S.; Park, M.; Kim, H. Y.; Park, S.-J *Sci Rep* **2016,** *6* (1).
43. Alsbaiee, A.; Smith, B. J.; Xiao, L.; Ling, Y.; Helbling, D. E.; Dichtel, W. R. *Nature* **2015,** *529* (7585), 190-194.
44. Liu, L.; Yang, J.-P.; Ju, X.-J.; Xie, R.; Liu, Y.-M.; Wang, W.; Zhang, J.-J.; Niu, C. H.; Chu, L.-Y. *Soft Matter* **2011,** *7* (10), 4821.
45. Fernandes, M.; Gonçalves, I. C.; Nardecchia, S.; Amaral, I. F.; Barbosa, M. A.; Martins, M. C. L. *Int J Pharm* **2013,** *454* (1), 116-124.
46. Lins, L. C.; Bazzo, G. C.; Barreto, P. L. M.; Pires, A. T. N. *J Braz Chem Soc* **2014** *8, 1462-1471*.
47. Zhang, Y.; Yang, Y.; Guo, T. *Carbohydr Polym* **2011,** *83* (4), 2016-2021.
48. Liu, X.; Lee, D.-J. *Bioresour Technol* **2014,** *160*, 24-31.
49. Raja, S.; Yaccone, F. S.; Ravikrishna, R.; Valsaraj, K. T. *J Chem Eng Data* **2002,** *47* (5), 1213-1219.
50. Ata, S.; Imran Din, M.; Rasool, A.; Qasim, I.; Ul Mohsin, I. *J Anal Methods Chem* **2012,** *2012*, 1-8.

51. Liu, T.; Li, Y.; Du, Q.; Sun, J.; Jiao, Y.; Yang, G.; Wang, Z.; Xia, Y.; Zhang, W.; Wang, K.; Zhu, H.; Wu, D. *Colloids Surf B* **2012,** *90*, 197-203.

52. Headley, J. V.; Peru, K. M.; Mohamed, M. H.; Wilson, L.; McMartin, D. W.; Mapolelo, M. M.; Lobodin, V. V.; Rodgers, R. P.; Marshall, A. G. *Energy Fuels* **2013,** *28* (3), 1611-1616.

53. Yeh, I.-C.; Lenhart, J. L.; Rinderspacher, B. C. *J Phys Chem C* **2015,** *119* (14), 7721-7731.

54. Teklebrhan, R. B.; Jian, C.; Choi, P.; Xu, Z.; Sjöblom, J. *J Phys Chem B* **2016,** *120* (50), 12901-12910.

55. Teklebrhan, R. B.; Jian, C.; Choi, P.; Xu, Z.; Sjöblom, J. *J Phys Chem B* **2016,** *120* (14), 3516-3526.

56. Okoli, C. P.; Guo, Q. J.; Adewuyi, G. O. *Carbohydr Polym* **2014,** *101*, 40-49.

57. Poorghorban, M.; Karoyo, A. H.; Grochulski, P.; Verrall, R. E.; Wilson, L. D.; Badea, I. *Mol Pharm* **2015,** *12* (8), 2993-3006.

58. Karoyo, A. H.; Wilson, L. D. *Langmuir* **2016,** *32* (12), 3066-3078.

59. Lubach, J. W.; Padden, B. E.; Winslow, S. L.; Salsbury, J. S.; Masters, D. B.; Topp, E. M.; Munson, E. J. *Anal Bioanal Chem* **2004,** *378* (6), 1504-1510.

60. Islam, M. S.; Zhang, Y.; McPhedran, K. N.; Liu, Y.; Gamal El-Din, M. *J Environ Manage* **2015**, 152, 49-57.

61. Arshad, M.; Khosa, M. A.; Siddique, T.; Ullah, A. *Chemosphere* **2016**, 163, 334-341.

62. Iranmanesh, S.; Harding, T.; Abedi, J.; Seyedeyn-Azad, F.; Layzell, D. B *J. Environ. Sci. Health A Tox. Hazard Subst. Environ. Eng.* **2014,** *49* (8), 913-922.

63. Mohamed, M. H.; Wilson, L. D.; Headley, J. V.; Peru, K. M. *Chemosphere* **2015,** *136*, 252-258.

Appendix (Copyright permissions)

CONTRACTS-COPYRIGHT (shared) <Contracts-Copyright@rsc.org>
Thu 11/2/2017 2:22 AM
To: Udoetok, Inimfon;

Dear Inimfon

The Royal Society of Chemistry (RSC) hereby grants permission for the use of your paper(s) specified below in the printed and microfilm version of your thesis. You may also make available the PDF version of your paper(s) that the RSC sent to the corresponding author(s) of your paper(s) upon publication of the paper(s) in the following ways: in your thesis via any website that your university may have for the deposition of theses, via your university's Intranet or via your own personal website. We are however unable to grant you permission to include the PDF version of the paper(s) on its own in your institutional repository. The Royal Society of Chemistry is a signatory to the STM Guidelines on Permissions (available on request).

Please note that if the material specified below or any part of it appears with credit or acknowledgement to a third party then you must also secure permission from that third party before reproducing that material.

Please ensure that the thesis states the following:

Reproduced by permission of The Royal Society of Chemistry

and include a link to the paper on the Royal Society of Chemistry's website.

Please ensure that your co-authors are aware that you are including the paper in your thesis.

Regards

Gill Cockhead
Publishing Contracts & Copyright Executive

Gill Cockhead
Publishing Contracts & Copyright Executive
Royal Society of Chemistry,
Thomas Graham House,
Science Park, Milton Road,
Cambridge, CB4 0WF, UK
Tel +44 (0) 1223 432134

Follow the Royal Society of Chemistry:
www.rsc.org/follow

Winner of The Queen's Award for Enterprise, International Trade 2013

Title: Self-Assembled and Cross-Linked Animal and Plant-Based Polysaccharides: Chitosan–Cellulose Composites and Their Anion Uptake Properties

Author: Inimfon A. Udoetok, Lee D. Wilson, John V. Headley

Publication: Applied Materials

Publisher: American Chemical Society

Date: Dec 1, 2016

Logged in as:
Inimfon Udoetok
Account #:
3001050631

LOGOUT

PERMISSION/LICENSE IS GRANTED FOR YOUR ORDER AT NO CHARGE

This type of permission/license, instead of the standard Terms & Conditions, is sent to you because no fee is being charged for your order. Please note the following:

- Permission is granted for your request in both print and electronic formats, and translations.
- If figures and/or tables were requested, they may be adapted or used in part.
- Please print this page for your records and send a copy of it to your publisher/graduate school.
- Appropriate credit for the requested material should be given as follows: "Reprinted (adapted) with permission from (COMPLETE REFERENCE CITATION). Copyright (YEAR) American Chemical Society." Insert appropriate information in place of the capitalized words.
- One-time permission is granted only for the use specified in your request. No additional uses are granted (such as derivative works or other editions). For any other uses, please submit a new request.

BACK CLOSE WINDOW